





Universitatea POLITEHNICA din București
Facultatea Ingineria și Managementul Sistemelor
Tehnologice



Journal of Industrial Engineering and Robotics

2022, Volume 6, Issue 2

Comitetul Științific al Revistei de Inginerie Industrială

Prof.dr.ing.	AMZA Catalin
Conf.dr.ing.	BACIU Florin
Conf.dr.ing.	CATANA Madalin-Gabriel
S.l.dr.ing.	DIJMARESCU Manuela-Roxana
S.l.dr.ing.	NICULAE Elisabeta
Conf.dr.ing.	POPA Laurentiu
S.l.dr.ing.	POPESCU Adrian
Prof.dr.ing.	SEVERIN Irina
S.l.dr.ing.	TUDOSE Daniela Ioana
Conf.dr.ing.	UNGUREANU Liviu Marian

Comitetul de Redacție al Revistei de Inginerie Industrială

Prof.dr.ing.	DUMITRESCU Andrei
S.l.dr.ing.	PARPALA Radu
S.l.dr.ing.	RADU Constantin
S.l.dr.ing.	ROTARU Alexandra
S.l.dr.ing.	TUDOSE Virgil

Editori

Prof.dr.ing.ec.	DOICIN Cristian
Conf.dr.ing.	VLĂSCLEANU Daniel
As.dr.ing.	CIOLCĂ Miruna

Cuprins

Assistive equipment for monitoring people with Alzheimer. COSTACHE Iulia	1
Research regarding smart devices for diabetic. PANAITE Andreea Lăcramioara	9
Assistance equipment used in spine diseases. SAVU Elena Andrada	15
Use of static converters in logistics systems. ROMAȘCANU Dragoș-Mircea, POPESCU Constantin-Adrian	22
Experimental researches about designing and realization of an educational stand with automated guided vehicle for transport and transfer of pallets. STAICU Mihai Laurențiu, POPESCU Constantin-Adrian	29
Study on the use of smart sensors to monitor environmental factors in greenhouses. SCARLAT Andrei Daniel, ȘTEFAN Theodora-Mihaela, POPESCU Adrian	35
Experimental research on the design and construction of an educational stand with automatic guided vehicle for the transport and transfer of pallets. SCARLAT Andrei Daniel, ȘTEFAN Theodora-Mihaela, POPESCU Constantin-Adrian	39
Study on the implementation of wireless charging solutions for AGVS. DRĂGAN Alin-Leonard, Popescu Adrian Constantin	43
Optimizing the logistic flow of manufacturing KN95 masks by using mathematical calculation methods. SEILEANU Floarea-Loredana	49
Experimental research on the control of a CNC axis actuated through a step engine. ROTARU Dragos, ENACHE George, COCIAȘU Cosmin	57
Color analysis and pigments technology identified for printing romanian postal stamps. PĂUNESCU Mihai	61
Aerodynamic analysis of the fuselage of a fixed wing aircraft type UAV using the finite element method. CUCU Cătălin	69
Recherche sur la fabrication de lentilles assistées par ordinateur. BENDIC Honoriu Eduard	77
Access metro solution et ingenierie WDM (serie OSN 1800). GARBAYA Joulia	85
Explicit dynamic analysis of disposable plastic trays considering an effector programming error. MARCU Rareș-Ionuț	94
Explicit dynamic simulation of the fluid behavior in manipulated bottles considering an accidental stop of the conveyor. GIURCAN Andreea-Loredana	100
Simulation of a tactile testing system operation based on the transient structural dynamic analysis. GEAMĂNU Mihai-Bogdan	108
Robotic cell for video inspection, with four workstations, integrating an industrial articulated arm robot on track motion platform and four peripheral robotic systems. CHISCOCIU Violeta-Georgiana	116

The design and fabrication of an industrial robot scale model, with position control via a web interface. DATCU Tudor-Răzvan	121
Robotized palletization cell with two inputs and two outputs, for cardboard boxes, integrating an industrial articulated arm robot. STOICA Raluca-Georgiana	127
Development of a modular axis structure for the purpose of attaining several robotic architectures. MUREȘAN Ștefan-Claudiu, MOROȘAN Teodor, CRISTOIU Cozmin Adrian, IVAN Andrei Mario	147
Numerical control machine tool for milling and 3D printing. TURTUREA Petre-Gabriel, CULA Ștefan, IVAN Andrei Mario, CRISTOIU Cozmin	152
Carton box palletization cell, integrating an industrial articulated arm robot. COTOILĂ Mihail-Constantin, IVAN Andrei Mario	156
Development of control and image processing firmware for articulated robot arm equipped with additional translation axis. ANASTASIU Alexandru-Ioan	162
Designing a small scale funcționabil articulated robot Motoman model. GUȚU Marius, NICOLESCU Adrian	167
Programming and simulation of a robotic cell for depalletizing support trays with chocolate products. MARIN Roxana-Ioana	174
Automation of a manufacturing process using RSLogix 5000 and Factory Talk View. ICĂ Sebastian-Ionuț, NICOLESCU Adrian	181

ASSISTIVE EQUIPMENT FOR MONITORING PEOPLE WITH ALZHEIMER

COSTACHE Iulia

Faculty: Industrial Engineering and Robotics, Specialization: Equipments for recovery therapies,
Year of study: 2021-2022, e-mail: iulia.costache97@yahoo.com

Scientific supervisor: Prof.dr.eng. **Cristina MOHORA**

ABSTRACT: Alzheimer's disease is a progressive neurological disorder that causes a slow deterioration of memory, logical thinking, behavioral and social skills. Systems designed for cognitive degradation play a key role in structuring daily activities within the home. Automated healthcare devices allow people with Alzheimer's disease to live partially independent in their own homes for a longer period of time. The aim of this research is to develop an assistive patient monitoring unit in their own home, equipped with a drug dose distribution system and a caregiver alert system in case of refusal / failure of the pill dose.

KEYWORDS: Alzheimer's disease, assistive equipment, intelligent system, pill distribution, sensors.

1. General aspects

The increasing costs associated with specific aging healthcare services such as health monitoring, prevention of worsening health problems, rehabilitation services or palliative care, together with a lack of qualified staff in the field, have increased investments in the development of smart technology, supporting the current health needs of users, thus improving their quality of life and safety.

The aim is also to maintain a level of independence as high as possible in their own house, which can be seen in the avoidance of transfers to medical units or nursing homes, thus preserving the ability of older people to care for themselves and carry out activities in their homes.

Alzheimer's disease is a progressive degenerative disorder of the brain that occurs mainly among elderly people, producing an increasingly severe deterioration of the brain's cognition functions, with loss of the individual's intellectual abilities and social value of his or her personality, associated with behavioural disorders.

When a person's ability to perform daily activities is impaired, their independence becomes limited and they may require assistance from elderly care services. For example, patients may have trouble managing medication, maintaining a routine, scheduling daily and essential activities or getting help in case of an emergency. These difficulties can be a burden for both the patient and their family/caregiver.

The treatment of Alzheimer's disease consists of slowing down the progression and reducing or stopping the already existing symptoms of the disease. The sooner therapy begins, the longer it is possible to maintain cognitive brain function. Unfortunately, there are no medications that lead to a full recovery, however, some pills have been proposed, which aim to improve memory and intellectual capacity, as well as eliminate the symptoms that accompany the disease (depression, anxiety, hallucinations).

Assistive systems dedicated to cognitive impairment have a fundamental role to structure routines in the home. Automated medical assistive devices allow those diagnosed with Alzheimer's disease to live more in partial independence in their own homes. An assistive robot is an ideal technology for monitoring a person's physical and/or psychological condition, enhancing quality of life, ensuring safety and reducing potential cognitive or physical decline.

This paper focuses on modeling, designing and 3D printing an equipment to assist and support people diagnosed with Alzheimer's disease.

2. Designing and modelling an assistive monitoring system for people with Alzheimer's disease

Patients diagnosed with Alzheimer's require a higher level of care compared to other age-specific diseases. In order to monitor these people, I have created a concept, where I have integrated technological mechanisms and systems, facilitating their self-care at home. The operational mechanical system is interconnected with accessories designed to provide a modern monitoring and assistance solution.

Figure 1 shows the system, modelled and animated in 3ds Max software for aided design.



Fig. 1 Isometric view of animation

The functions of the systems implemented in the animation allow:

- Constant communication with a healthcare professional/patient's family
- Permanent location of the patient
- Follow-up of the patient's vital functions
- Automatic movement of the robot in the home
- Delivery of water and pills at a predefined time
- Avoidance of possible obstacles encountered in the home
- Energy autonomy of the system
- Storage of medicines, water and glasses

The assistive robot in the presented concept is able to locate and track the patient in a restricted environment. It is equipped with mechanisms, sensors and systems developed for continuous monitoring, administration of the correct dose of medication and alerting the caregiver in case of rejected/missed dose of pills. Control of the system is handled by several digital processors that make possible the reception of information generated by environmental sensors. The robot is also equipped with proximity sensors for detecting and avoiding obstacles that may appear in its path. (see figure 2)

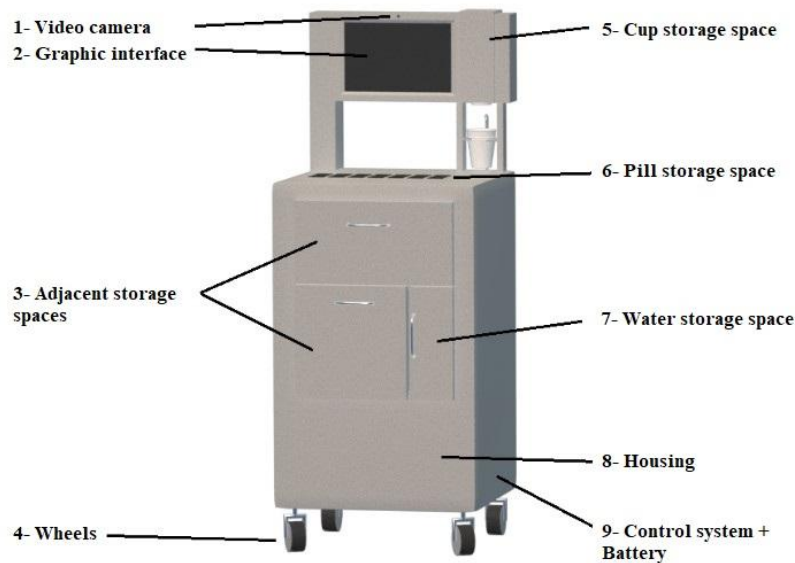


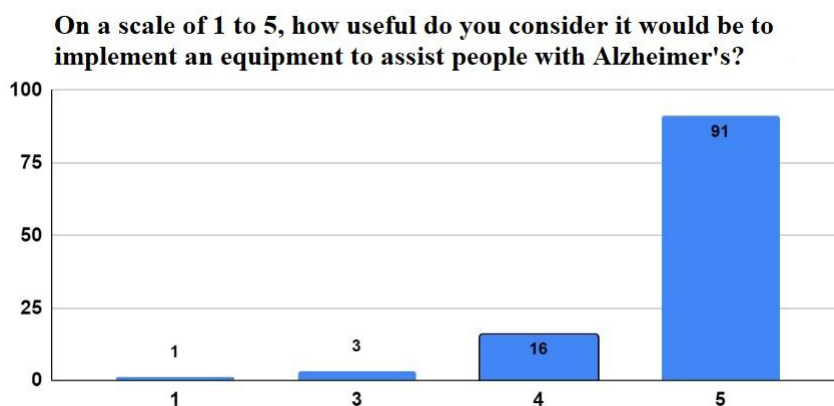
Fig. 2 Front view of mobile robot

3. Designing a questionnaire to evaluate the need for 3D modelling of a care and monitoring system for people diagnosed with Alzheimer's disease

The primary data collection method is a survey. The survey tool is the questionnaire. It was used on a random panel of 111 people. They were sent the questionnaire individually, digitally, in the form of a link. The questionnaire contains a short presentation, to explain to respondents the purpose of the questionnaire, and 11 questions, both open and closed (with multiple choice or scaled).

The research population is defined according to age and gender, resulting 60 male and 51 female respondents, ranging from 20 to 60 years.

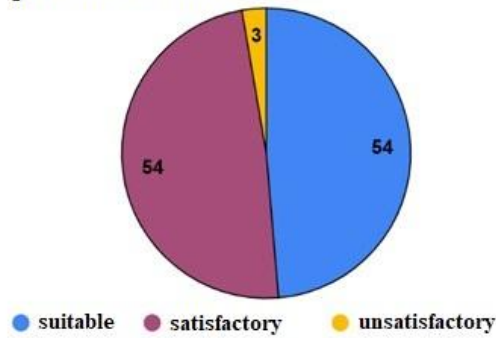
The main objective of the questionnaire was to find out the degree of respondents' interest in the assistive design of assistive equipment for people diagnosed with Alzheimer's disease. Following the question in the figure below, 82% of respondents considered it necessary to implement such equipment in their homes.



In the previous chapter, a concept that highlights the main functionalities of the desired system was designed and modelled in 3dsMax software. (see figure 1)

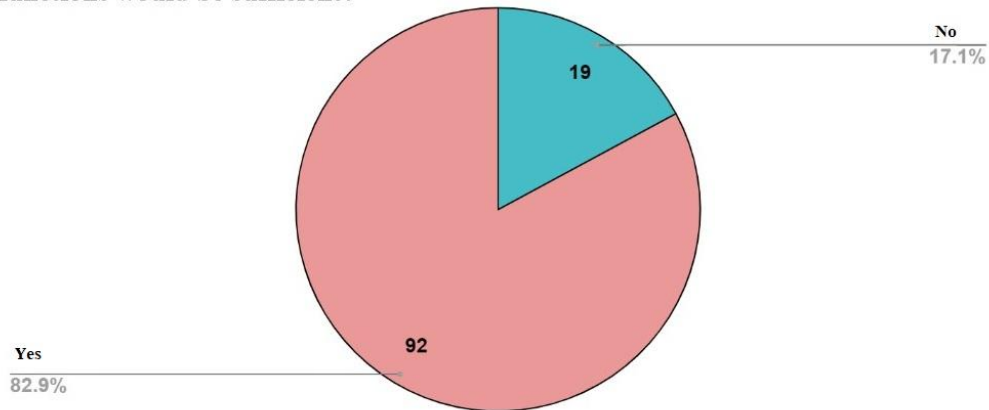
In the first diagram only 3 respondents considered the appearance of the modelled equipment to be unsatisfactory, while 108 considered that the equipment should not be modified.

How would you rate the ergonomics of the presented assistive device?



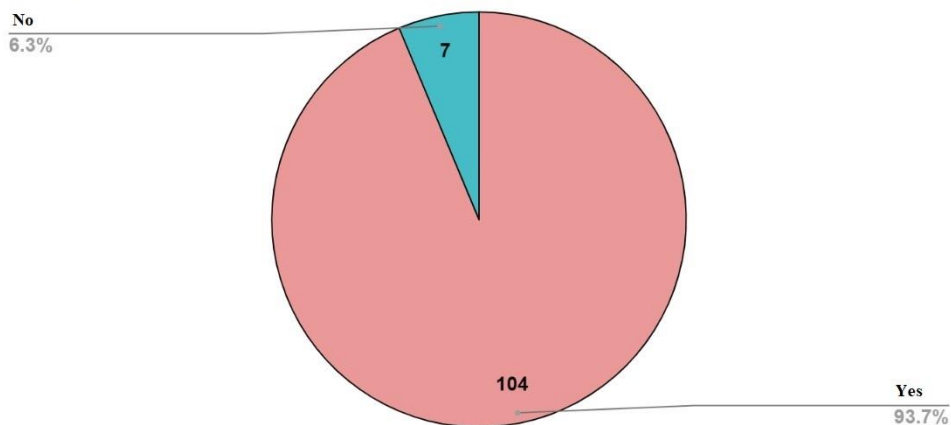
The following diagram shows that 92 of the respondents are satisfied with the functions performed by the robot.

The equipment presented ensures monitoring the patient, constant communication with the caregiver/family and efficient dosage of medication. Do you think these functions would be sufficient?



The study shows an increased awareness of the seriousness of this disease, so 93% of study participants would consider purchasing a device that assists Alzheimer's patients.

Would you consider purchasing this device to assist an elderly family member with Alzheimer's?



4. Design and 3D fabrication of assistive equipment

Computer-aided design (CAD) is using a software technology to design two-dimensional (2D) drawings and generate three-dimensional (3D) part models.

Computer Aided Manufacturing (CAM) is the process of making three-dimensional physical objects from a digital file by successively adding layers of material using a 3D printer.

3D printing technology differs from traditional methods of making objects because instead of removing excess material, it is deposited from the start in the desired shape, eliminating the need for further processing. 3D printing offers an excellent method for visualizing the geometry of the proposed model. Three-dimensional printable models can be created using dedicated 3D design software or by 3D scanning the actual model.

Aided design of the model (see figure 3) was achieved using the CATIA V5 framework, resulting in a geometric model that prefigures the final concept. The design of the assembly followed a technical approach, where the component parts were made to real scale and then assembled.

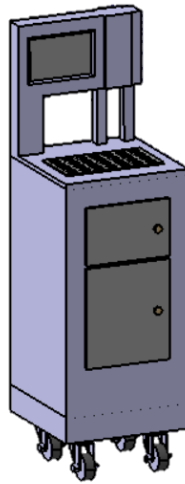


Fig. 3 Isometric view of the 3D model designed

The actual dimensional characteristics of the equipment are shown in Table 1:

Length	500 mm
Width	500 mm
Height of pill dispenser	1000 mm
Total height of equipment	1500 mm

The additive manufacturing technology used in the work is FDM (Fused Deposition Modeling), thermoplastic extrusion molding, which is the most commonly used manufacturing technique due to its simplicity and applicability. This manufacturing method has the great advantage of low cost, both in terms of materials used for printing and supplies. The main disadvantages of FDM technology, encountered in designs with complex geometry, are high printing time and inappropriate bonding of some layers.

A FDM 3D printer uses a continuous filament, which is fed through a gear mechanism into a heater that melts it. The molten filament is then ejected from the nozzle and deposited on the printing table in the desired geometry. After each layer, the printing table (or nozzle) is moved vertically and the next layer is added until the object is completely printed according to the CAD file.

The previously designed 3D model has been converted and saved in a .stl file because it must be processed in a slicer software application that divides the model into cross-sections called layers. The slicer software dedicated to the printer used generates a series of commands corresponding to the parameters of the printing process and the three-dimensional displacements (on the X, Y and Z axes).

The commands are transformed into G-code, the programming language used in computer-aided manufacturing to control 3D printers. To achieve the desired model shape, the 3D printer follows the commands in the G-code and successively deposits layers of material corresponding to the virtual cross-sections of the CAD model.

For additive manufacturing the dimensions of the equipment were scaled 1:100 and are shown in the figure below (see figure 4).

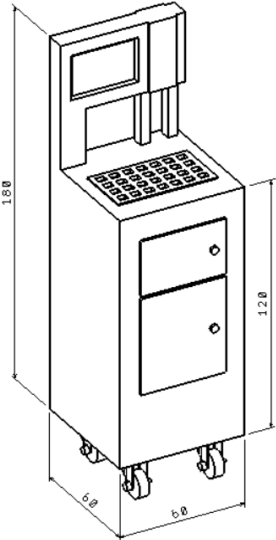


Fig. 4. Scaled equipment

The geometry of the 3D model, in .stl format, was reviewed using the Meshmixer program, then imported into the Cura slicer software. The model was conventionally oriented (see Figure 5), fixed on the printing table and the process parameters were chosen (material used, FDM printer, print type).

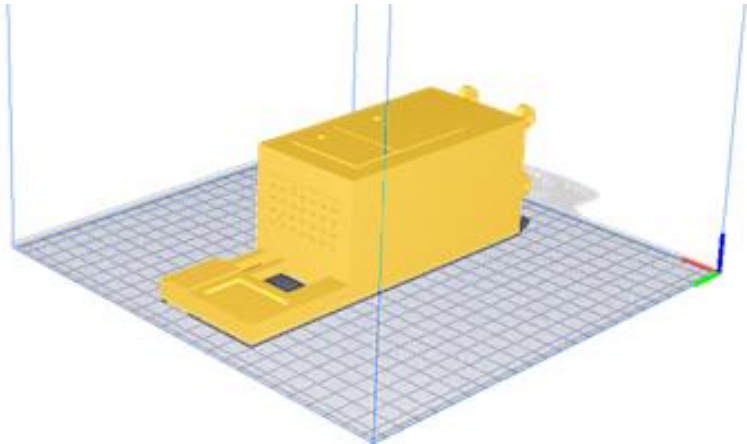


Fig. 5. Isometric view of the equipment before 3D printing

The process parameters set are shown in Table 2:

Tabel 2. 3D printing parameters

3D Printer	TwoTrees CoreXY SP-5
Material	PLA filament
Profile	Normal - 0,15 mm
Degree of filling inside the part	30%
Support	Yes

Assisted printing of the model was carried out using the TwoTrees desktop 3D printer model CoreXY SP-5 (see figure 6), ideal for prototyping and production of low-volume parts.



Fig. 6. 3D Printer used

The main technical features of the printer used are shown in the following table (see Table 3):

Tabel 3. Printer technical specifications

Number of nozzles	1
Nozzle diameter	0,4 mm
Print size	300*300*330 mm
Printing accuracy	±0,1-0,2 mm
Layer thickness	0,1 – 0,4 mm
Recommended speed	60 mm/s
Printing speed	max 200 mm/s

The material used for printing the prototype is polylactic acid (PLA), which is the most common material used in 3D printing with desktop printers due to its affordability and high mechanical properties (biodegradability, thermoplasticity, etc.). The specifications of the used material are shown below (see Table 4):

Tabel 4. PLA filament technical specifications

Material	Polylactic acid
Colour	Yellow
Transparency	Opaque
Tolerance	±0,05
Filament diameter	1,75 mm
Temperature of heated bed	50-60°
Temperature of the print head	200-235°

Figure 7 shows the model prepared for 3D printing and Table 5 shows the main specifications of the additive manufacturing process (see Table 5).

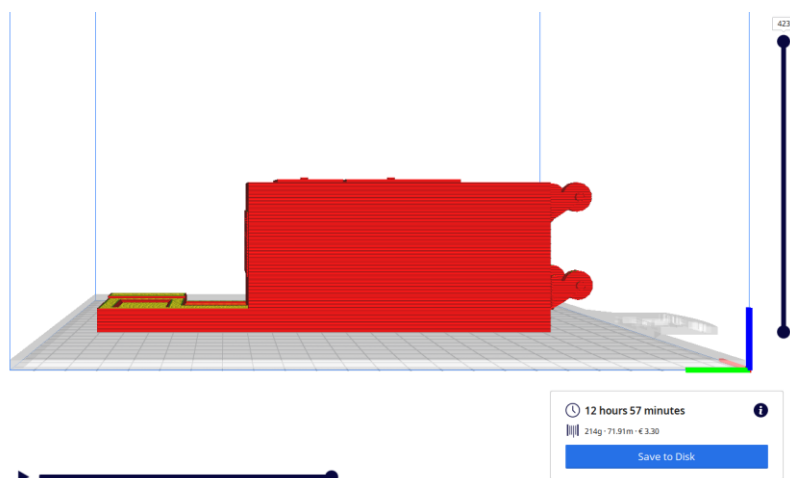


Fig. 7. Model prepared for 3D printing

Tabel 5. Main printing specifications

Manufacturing time	12h & 57min
Filament consumption	214 g / 72 m
Cost of filament consumption	3,3 €

Research conclusions

As people get older, they have to take daily medications, and cognitive decline can lead to undesirable events (failure to take the prescribed dose of medication). After a period of time following the outbreak of Alzheimer's disease, the patient becomes dependent on additional assistance, requiring hospitalisation in a dedicated care home. At the same time, a lack of qualified staff is noted, so in this work we have developed an assistive equipment dedicated to people with Alzheimer's, which ensures the independence of the beneficiary in his own home, his permanent monitoring, and the maintenance of a familiar environment.

In order to discover the need for the proposed equipment, as well as its possible improvements, I developed a questionnaire-type descriptive research on a sample of 111 people.

The proposed device was modelled using 3dsMax software, its technical concept was designed in Catia V5 software, and additive manufacturing was realized in Cura software application.

In the future, the design of the equipment is also pursued from a functional point of view, carrying out the simulation of the mechanisms incorporated in the equipment.

Bibliography

- [1].Shaheen E Lakhan, , MD, PhD, MEd, MS, FAAN (2022), Alzheimer Disease
- [2].Arshia Khan, Yumna Anwar, Paul Craig și Rana Imtiaz (2021), Robotic Assistive Technology Augmenting Dementia Care: Technology Design and Preliminary Acceptability
- [3].Kazi Shahrukh Omar, Afia Anjum și alții (2019), An Intelligent Assistive Tool for Alzheimer's Patient
- [4]. Mrityunjaya D H1, Kartik J Uttarkar2, Teja B3 și Kotresh Hiremath (2016), Automatic Pill Dispenser
- [5]. Diaa Salama Abdul Minaam și Mohamed Abd-Elfattah (2018), Smart drugs:Improving healthcare using Smart Pill Box for Medicine Reminder and Monitoring System
- [6].Anderson WL și Wiener JM (2015), The impact of assistive technologies on formal and informal home care

RESEARCH REGARDING SMART DEVICES FOR DIABETIC

PANAITE Andreea Lăcramioara

Faculty: Industrial Engineering and Robotics, Specialization: Equipments for Recovery Therapies,
Year of study:2021-2022, e-mail: andreeapanaite98@yahoo.com

Scientific supervisor: Prof.dr.ing. Cristina MOHORA, RSP Department

ABSTRACT: Diabetes, as it's commonly called, belongs in a group of metabolic disorders characterized by high blood sugar levels over a prolonged period of time. Symptoms often include frequent urination, increased thirst and appetite. In some cases, patients can even lose their limbs or fingers due to gangrene. In this scientific research I chose to speak about diabetes in general, it's socio-economic impact, showcase two smart devices dedicated for profilaxy treatment, a 3D model followed by a prototipe of one of the devices and a quiz regarding smart devices specifically tailored to gangrene prevention and monitorization of the illness.

Key words: Diabetes, socks, gangrene, Arduino, sensors

1. Introduction

This scientific study attempts to touch a few fine points, theoretical knowledge meant to better understand diabetes and Charcot's foot, discuss the different clinical approaches that apply to this particular complication and also talk about the associated risks involved. A short broaching of electrostimulation , normally used in muscular pathology and a preferred technique in Rehabilitation Medicine.

Based on the subjects listed above we strive to propose the implementation of new assistive devices, that monitors the plantar region of the patient, devices that should complement each-other for maximum efficacy.

Last but not least I have showed a series of statistics for better understanding and explaining the general population's perception of diabetes as a disease and the role of assistive devices in improving the patients quality of life.

2. The state of art.

2.1 Classical clinical approach of Charcot's Foot.

Charcot's diabetics foot represents one of the most important complication that can appear during the progression of diabetes, it is very destructive, through fractures, dislocations, and articular destruction in the affected limb. The active phase of the pathology is frequently erroneously diagnosed, a fact that inevitably leads to permanent deformation, ulcerations, and in the end, amputations. A proper therapeutical approach should manage to diagnose the disease in a time-efficient manner and avoid unwanted complications.

The patients that suffer from diabetic's foot have a shorter life-span of about 14 years mainly because of increased cardio-vascular risk in neuropathy. Clinically speaking, the patients go to the

hospital accusing redness, swelling, a burning sensation in the affected limb. Pain is present in approximately 50% of cases and can be joined by early permanent deformities.

Secondary to a positiv diagnosis, the foot is immobilised so that deformities are avoided (cast or orthosis), the evolution being monitored through specific investigations (MRI/CT) and interdisciplinary collaboration (orthopedics). After a period of three days the cast is removed and refitted (the affected limb returns to initial volume), the procedure is then repeated in 1-2 weeks.

In regards to post-therapeutical management, we must discuss the opposite limb “trap”, which, after the first limb is affected must sustain a heightened weight in the following weeks, a fact that can lead to a secondary diabetic’s foot, and as such, the patient must be informed about using assistive means for the healthy limb (Canadian crutch, appropriate footwear).

The most important step in post-therapeutical management is the rehabilitation of the patient, which, after prolonged immobilisation can sustain muscle loss, decreased bone density and can accuse articular rigidity. The normal course of action is a combination of physiotherapy and kinetotherapy.

2.2 Electro-stimulation: basic principles and applicability.

For a better understanding of how electrostimulation works, we have to talk about the mechanism on which neuropathy is based upon and the specific way it affects the nerves.

The main mechanism responsible for neuropathy is hypoxia, or better, a change in the physiological cellular metabolism that leads to a lack of oxygen intake, which in turn increases the neuronal gap and the distance a nervous impulse must travel, all this leads to a decrease of impulse capability and a lowered sensitivity in the affected area.

Initially, the felt sensation resembles a tickle in the affected territory because some impulses manage to reach said area, this phase is followed by more negative developments and as such, the sensation turns into one of pain, after which, in the end the entire segment is completely numb. Secondary to this process are muscle weakness, reduces blood flow (specific to diabetic angiopathy), deficiency in posture and mobility. .[5] [6]

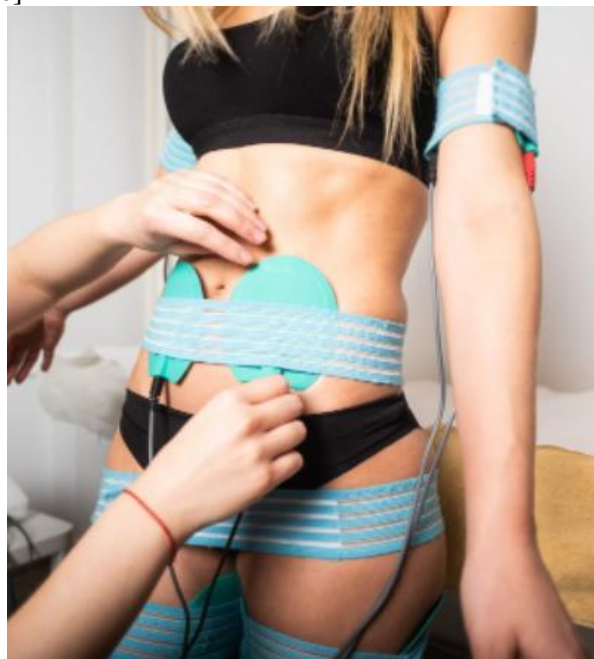


Fig. 1 Positioning the electrodes during an electrostimulation session

3. Case study.

3.1 A new approach in home-care management of neuropathy afflicted patients.

Following the discussion above, which helped us better understand some basic physiopathology, we can now focus our attention on the applicability of said knowledge in an efficient and beneficial way for the neuropathy patients.

This paper first described the possibility of using SMART socks for monitoring plantar temperature and detection of small variations that appear during Charcot's foot active phase. I propose to enhance the design and offer patients the possibility of both prophylaxis and rehabilitation in an autonomous and cost-efficient manner.

I propose a new idea, that of adding a stocking accessory so that it may perform a group of functions together with the sock, more specifically, to offer small electrotherapy sessions following pre-set guidelines established by the physician.

We will be using a structure made up from a normal stocking-like fabric on which we will apply a number of PMT electrodes that will stimulate the main nervous branches (Sciatic Nerve, Tibial Anterioris, Sural Nerve), this stimulation has a double purpose: it stimulates the patient's nerves (metabolic and neurotrophic role) in the latent period of the disease and it offers an analgesic effect for those patients that are in the active phase of the disease. [8]

There will be added a number of band-like electrodes for the main muscular groups (quadriceps femoris, biceps femoris, semimembranosus, semitendinosus, tibialis anterior). These bandlets will initialise the program using low-frequency currents (5-20V, Alternative Current) that are meant to relax the muscles and stimulate venous circulation in the lower extremities. Two specific electrodes will be appointed to each nervous fascicle, one that has rapid conductivity (for bridging the electrical neuronal gap) and one that has slow conductivity (for physiological-like stimulation). The electrodes described will begin their cycle after the bandlets end their activity [7].



Fig. 2. Visual representation of the positioning of the electrodes on the surface of the lower limb

At the end of the procedure we will introduce a combined stimulation of the two electrode types with a frequency of 7.83Hz, that should manage to generate a post-procedural secretion of endorphins that directly help with the patient's pain management.

In practical terms, the stocking works as a prophylactic type of therapy for diabetic patients at risk of developing Charcot's foot and as a pain management system for those that have the active disease. We use the supposition that one daily session should be enough for prophylactic purposes and two daily sessions for those suffering of Charcot's Foot, these sessions are adjusted according to the physician and the associated pathologies.

Bearing in mind the technical limitations of this paper, the project is still in early stages but has the potential of being an assistive device of reduced cost, easy to use and with a high safety profile. This

concept has the potential of enhancing the meaning of the term assistive device, managing to bring rehabilitation techniques in the homes of our patients, giving it a enormous value both socially and economically.

3.2 CAD Prototype and functionality testing.

Within this paper I have managed to construct a 3D simulation in CATIA V5 and a physical prototype meant to showcase the functionality of one pair of socks and it's ability to monitor plantar temperature. The CAD simulation and the physical prototype contain the same components as to facilitate the viewing of the whole process, from beginning to the end.

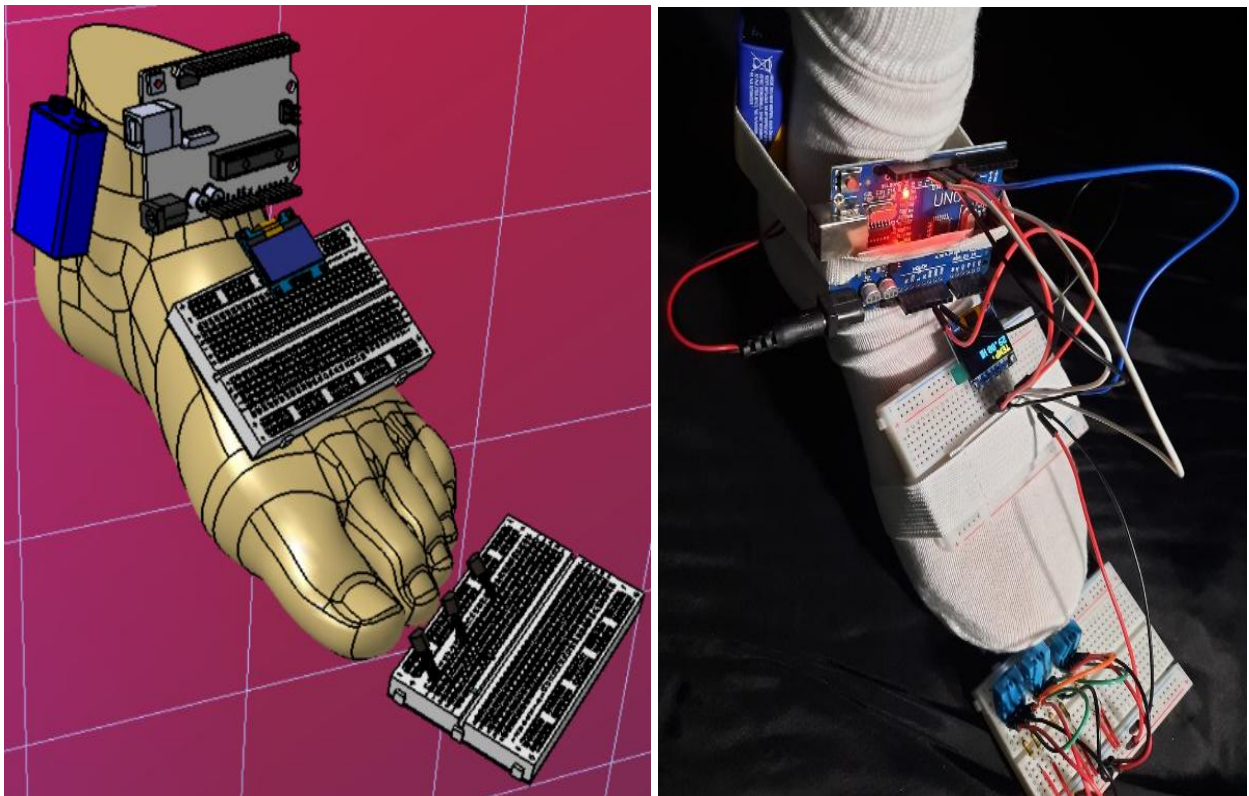


Fig 3. CATIA V5 Simulation (left) together with the physical prototype of the temperature monitoring assistive device

The ensemble is made up from one Arduino Nano R3 board, one OLED display and three temperature and moisture sensors (we will not be using the moisture function in our study), adjacent to these components there are also a number cables and connection devices (jumper cables).

The final result is an avarage of the three temperature measurements, avarage that should fluctuate to no more than 2 degrees in comparison to the healthy limb. If the device registers a fluctuation of more than 2 degrees than it alerts the users , such variation in temeprature is an important prognosis factor in Charco's foot diagnosis and stand to reason that it could prevent the onset of gangrene and eventual amputations. [2] [3] [4].

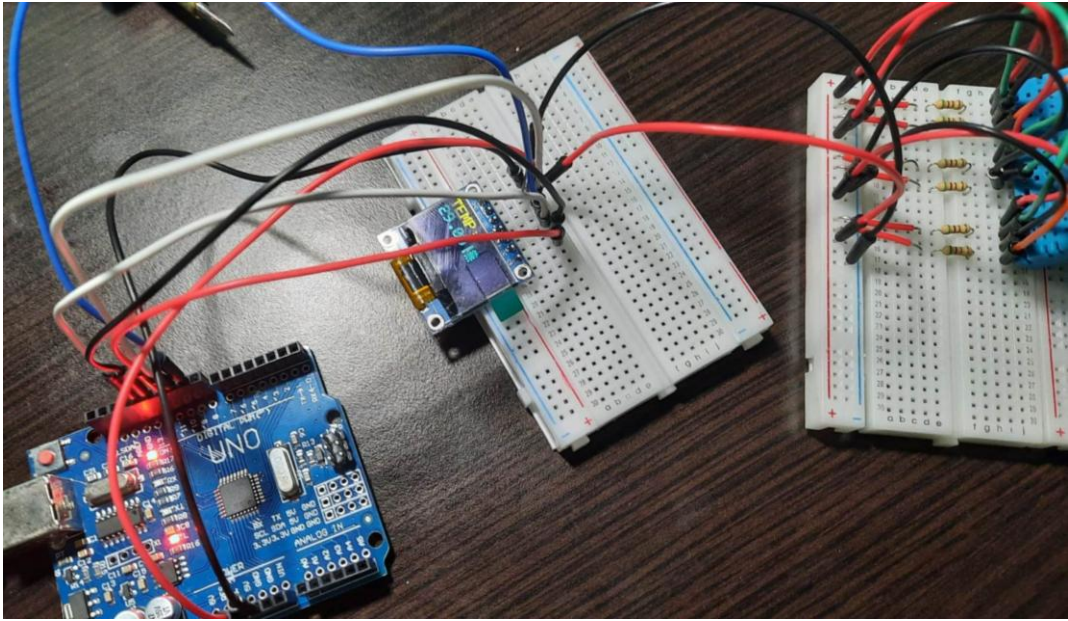


Fig. 4 The Arduino assembly that reads the temperature and displays it

3.3 Discussions regarding an opinion poll related to the population’s general knowledge of SMART devices for diabetes patients.

Using a statistical model which includes 123 people, we can observe that 87% of subjects have a acquaintance that suffers from diabetes. The participants believe that diabetes affects the quality of life for diabetic patients, 84.5% believe that the drop in quality of life is significant. 65% of subjects have stated that their acquaintances suffer from complications. 31.3% have mentioned diabetic retinopathy as the most common complication, soon followed by Charco’s foot and diabetic neuropathy with 21.3%.

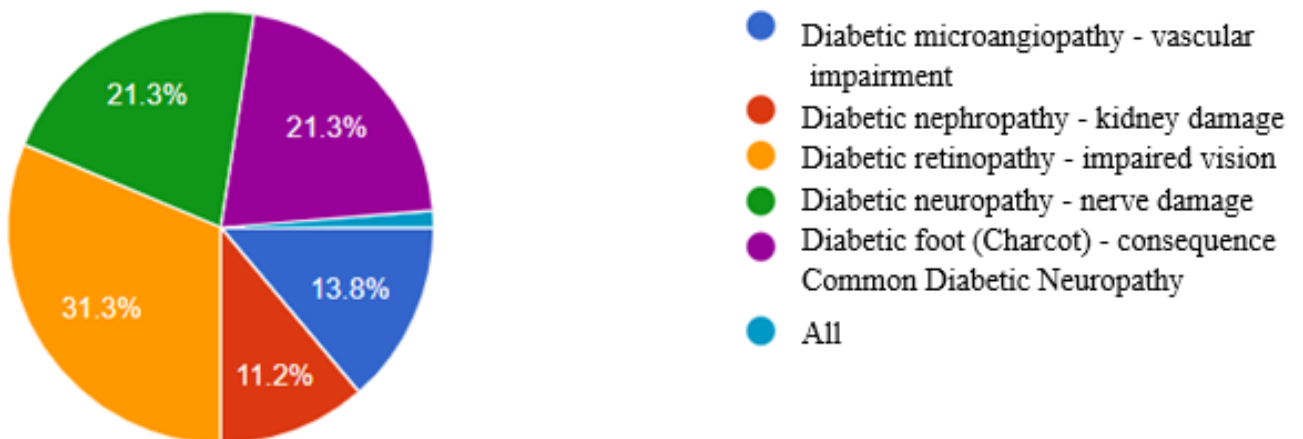


Fig. 5 Statistical representation of the most common complications in diabetes and their frequency

If we were to discuss the most important variable to our current paper, 38.2% of subjects have stated that they know at least one person that suffered amputation secondary to the progression of diabetes.

As for the the frequency of assistive devices in the households of our subjects, 83.7 have stated that they do not use or have relatives/acquaintances that use them. The most popular device chosen when asked if they would buy one such device is the physical assistance device.

Speaking specifically of assistive devices destined for diabetic patients, the most familiar device is the blood-sugar monitor device (45.5%) followed shortly by the insulin dosage monitoring device (19.5%).

Statistics speak for themselves, most patients in our country do not use assistive devices but 74.8% of subjects think they would benefit the diabetic patient and 97.6% of them would recommend one of the the devices mentioned in our query.

As for the plantar temperature monitoring socks, 70.7% of subjects would consider them useful and 82.1% would recommend them to an acquaintance.

Conclusions

This study can offer a broader view into a frequent and important pathology that has a high prevalence nationally and internationally. The purpose, is not informative, strictly speaking but also perspective as it can imagine the possibility of one device combining both prevention and long term conservatory treatment, we can then observe how a real public health issue can be easily monitored and approached, managing to increase both life span and life-quality in those affected by diabetes.

Bibliography

- [1] Plantar Temperature Response to Walking in Diabetes with and without Acute Charcot: The Charcot Activity Response Test - Bijan Najafi,1,2 James S. Wrobel,3 Gurtej Grewal,1 Robert A. Menzies,4 Talal K. Talal,4 Mahmoud Zirie,4 and David G. Armstrong- <https://www.hindawi.com/journals/jar/2012/140968/>
- [2] Protective socks for people with diabetes: a systematic review and narrative analysis- Simon J Otter, Keith Rome, Belinda Ihaka, Andrew South, Mandy Smith, Amit Gupta, Frances Joseph & Peter Heslop - <https://jfootankleres.biomedcentral.com/articles/10.1186/s13047-015-0068-7>
- [3] Study: Socks with sensors could help continuously monitor diabetic neuropathy- By Laura Lovett - <https://www.mobihealthnews.com/content/study-socks-sensors-could-help-continuously-monitor-diabetic-neuropathy>
- [4] Continuous Temperature-Monitoring Socks for Home Use in Patients With Diabetes: Observational Study- Monitoring Editor: Gunther Eysenbach; Reviewed by Monara Dini and Barbara Arnoldussen- <https://www.ncbi.nlm.nih.gov/pmc/articles/PMC6315272/>
- [5] Effects of electrotherapy in neuropathic pain management in patients with diabetic peripheral neuropathy: A narrative review by Maria Karypidou, Dimitrios Lytras, Anastasios Kottaras, Paris Iakovidis. Andreas Fotios Tsimerakis, Georgios Leptourgos- https://www.researchgate.net/publication/353104603_Effects_of_electrotherapy_in_neuropathic_pain_management_in_patients_with_diabetic_peripheral_neuropathy_A_narrative_review
- [6] The efficacy of physiotherapy interventions in mitigating the symptoms and complications of diabetic peripheral neuropathy: A systematic review- by Narges Jahantigh Akbari, Mohammad Hosseinifar, Sedigheh Sadat Naimi,corresponding Saeed Mikaili, and Soulmaz Rahbar- <https://www.ncbi.nlm.nih.gov/pmc/articles/PMC7843894/>
- [7] Effect of High-frequency (10-kHz) Spinal Cord Stimulation in Patients With Painful Diabetic Neuropathy by Erika A. Petersen, Thomas G. Stauss, James A. Scowcroft- <https://jamanetwork.com/journals/jamaneurology/fullarticle/2777806>
- [8] Spinal Cord Stimulation for Diabetic Peripheral Neuropathy by Arvind SommiMatthew GarzaArmaan Nallicheri- <https://diatribe.org/spinal-cord-stimulation-diabetic-peripheral-neuropathy>

ASSISTANCE EQUIPMENT USED IN SPINE DISEASES

SAVU Elena Andrada

Faculty of Industrial Engineering and Robotics, Specialization: Master Equipment for Recovery Therapies, Year of study: I, e-mail: savu.elenaandrada6@gmail.com

Scientific leader: Sl.dr.ing. **Dana TILINĂ**

ABSTRACT: Orthosis technology can help patients return to near-normal mobility and limb function after stroke or amputation. However, the method of developing specially designed devices requires time and effort. Research has shown that more than three-quarters of patients with dementia need to recover in the long term, many of whom have individual orthoses. Three-dimensional (3D) printing is a collection of practices for producing a model consisting of a physiological component or an installation in a short period of time, using 3D computer aided design (CAD) software. Usually, the creation of components or assemblies is done using 3D printing or "Additive Manufacturing" technology. 3D printing improves the performance of parts, speeds up the manufacturing process and progresses in reducing costs, which is a very significant factor for today's society.

KEY WORDS: spinal orthosis; adolescent idiopathic scoliosis; 3D printing.

1. Introduction

Spine orthosis is an effective non-surgical treatment, especially for children with adolescent idiopathic scoliosis. This treatment is prescribed for the patient with a moderate curvature (Cobb angle of 25-40 °), which presents a high risk of curve progression. Wearing the orthosis can range from a few hours only at night to full time, up to 23 hours a day. A spinal orthosis is made of rigid plastic, customized according to the shape of the patient's body, usually made of thermoplastic, such as polypropylene, with a thickness of 4 to 5 mm [2]. The orthosis has several pressure points to apply loads on the trunk to counteract the scoliotic curves. The mechanical load applied to the torso aims to stop the progression of the curve during the rapid period of growth of adolescence. The effectiveness of spinal orthosis treatment depends on the risk of progression of the curve, the correction in the orthosis, and the observance of its behavior.

However, compliance with a spinal orthosis is a problem, as current corsets are bulky, uncomfortable, and visible, which leads to decreased self-confidence that directly affects the outcome of treatment. A randomized control study with 116 patients recruited showed that the average percentage of patients wearing spinal orthoses is only 67% of the prescribed time [6]. Another study with 40 patients recruited showed an average of 55% of the wear time in the prescribed tightness interval, determined by the orthotist [3]. In addition, the conventional corset design process can be cumbersome, time-consuming, and costly for both the patient and the orthodontist. Currently, several steps are required to reach the final product. The manufacturing process may require packing a patient with plaster to obtain a negative body mold or the computer-aided design / computer-aided manufacturing (CAD / CAM) method that obtains a patient's body shape through a 3D scanner. The body shape file is then exported to a computer and goes through several manufacturing steps to create the orthosis [2].

With the rapid advancement of 3D printing technologies, clinical applications can create positive changes in the healthcare industry. A CAD / CAM system can create a 3D-printed orthosis

directly by capturing a shape and sending the stereolithographic output file (STL) to a 3D printer. Currently, some companies have started developing 3D printed corsets for the treatment of adolescent idiopathic scoliosis with this CAD / CAM approach. This new approach offers a new economical solution, reduces production steps, requires less labor, and also has the potential to reduce the time it takes to prescribe the orthosis to obtain it [2].

This research hypothesizes that a 3D printed spinal orthosis will be more comfortable, therefore, it increases compliance with wearing time, which leads to a more effective treatment. It can be lighter and does not cause profuse perspiration, being more breathable with the help of the design. Traditionally, 3D printing applications have been used primarily for rapid prototyping before the final design is completed. However, with the advancement of 3D printing technology, it has become a new method of additive manufacturing in the creation of functional parts.

Through this research, I propose to pursue the main objectives, such:

1. Investigate the proper method of 3D printing, the orientation, material, and thickness of a spinal orthosis;
2. Investigate the effectiveness and evaluate the manufacturing process of the 3D printed orthosis.

3D printing could reduce costs, increase the efficiency of orthoses and reinvent the innovative design industry, as 3D printing of custom orthoses has advantages over traditional orthosis manufacturing, which can produce custom shapes and geometries that are not possible with traditional orthopedic techniques. manufacturing, devices can be made faster and are easier to modify and reproduce. In addition, 3D printing can replace unsightly, itchy, itchy plasters. The 3D printed spinal orthosis is light, personalized, and comfortable and, for optimal hygiene, can be worn in the shower [4]. The advantage of 3D printing includes that it does not require specialized tools, such as molds. It is also very cost-effective to create custom parts compared to existing manufacturing methods. In the biomedical field, 3D printing applications include assisted bone healing with printed bone scaffolding for patients with fractured or diseased bone structures, hearing aids, anatomical models for surgical training, and orthoses for various anatomical segments [2].

On the other hand, for 3D printing to be used on a larger scale in orthoses, development and manufacturing times and the associated costs must be reduced. After examining the factors that influence the cost-effectiveness and feasibility associated with new 3D printing equipment, it is clear that there are still some technical limitations to printing custom orthoses. However, these limitations can be overcome and the associated costs can be reduced as technology evolves and as future innovations produce larger and faster 3D printers [4].

2. The current stage

A recent study [5] was based on the fact that the introduction of additive manufacturing, also known as three-dimensional printing (3DP), has shown great potential for medical solutions. This technique allows the creation of complex and customized devices based on digital models. 3D printing is an environmentally friendly process, producing limited waste and does not require molds. Each part can be customized and replicated at no extra cost. Less manual labor is needed, reducing the risk of human error and improving interoperability. Several 3DP methods have been applied in the healthcare field, such as poly jet modeling (PJM), selective laser sintering (SLS), stereolithography (SLA), and fused deposition modeling (FDM). The study considered the evaluation of variables such as durability, printability, toughness, hydrophobicity, flexibility, strength, chemical inertia, and even biocompatibility.

The study focused on testing a 3D printed orthosis on a patient diagnosed with scoliosis, a patient who had been wearing a classic corset for a year. The patient in the study had to be able to

orthosis for two weeks, with the clinical indication to wear it for at least 22 hours a day. At the end of the 2 weeks, the patient completed a short questionnaire about the acceptance, safety, and satisfaction of the 3D printed orthosis, compared to the traditional device produced by thermoforming. Overall, the study showed that the production of 3D printed corsets is feasible and was evaluated positively by the patient and the orthotist. The results provide encouraging preliminary findings and a clear direction for further improvement and the use of virtual modeling and 3D printing in the field of orthosis for the treatment of spinal diseases.

The cost analysis showed that about half of the cost was attributed to the cost of labor. This preliminary analysis also highlighted the significant influence of construction time on operating costs, highlighting the importance of high print speed [5].

Table 1. Detailed costs of 3D orthosis [5]

Layer height [mm]	Value		
	0.4	0.6	0.8
Machine cost – P [€]	1.08	0.69	0.56
Build time – T_b [h]	8.30	5.30	4.30
Purchase price – P_c [€]	7000	7000	7000
Expected life – Y_{life} [years]	7	7	7
Operative cost – O [€]	39.43	25.18	20.43
Operation rate – C_o [€/h]	4.75	4.75	4.75
Build time – T_b [h]	8.30	5.30	4.30
Material cost – M [€]	19.07	19.07	19.07
Support material factor – K_s	1.2	1.2	1.2
Number of parts – N	1	1	1
Part volume – v [cm ³]	417	417	417
Material rate per unit weight – C_m [€/kg]	30	30	30
Material density – ρ [g/cm ³]	1.27	1.27	1.27
Labor cost – L [€]	50.00	50.00	50.00
Labor time – T_l [h]	2	2	2
Labor rate – C_l [€/h]	25	25	25
Overall Cost – C [€]	109.57	94.93	90.05

Another study conducted in 2020 by Youyu Zhang [9] exposes an experiment based on the 3D printed spinal orthosis. The study was a prospective one, with two groups: the control group (named the TLSO group) and the experimental group (3D group). Participants enrolled in the TLSO group will be prescribed a conventional thoracic-lumbar-sacral orthosis (TLSO) after obtaining informed consent for the observational study, and participants in the 3D group will be allowed to choose between a TLSO and a 3D printed orthosis, after obtaining informed consent for the clinical trial. Parameters and radiographs for orthoses were obtained at hospitalization.

The orthoses were fitted with a temperature data logger. The latter was implanted in both 3D-printed orthoses and TLSO to record the date, time, and temperature every 15 minutes. The raw data has been downloaded for tracking and the battery will be replaced every 6 months. Participants were informed about the skin temperature monitoring logger so that the condition of the orthosis could be assessed; however, they were not informed about the time logger. The compliance result from the data logger will be statistically analyzed [9].

In most previous studies on the orthosis for adolescent idiopathic scoliosis, the result was evaluated on radiography, which cannot provide adequate information about the impact of the corset on patients. Adolescence is a period of transition that involves both physical growth and psychological instability. An externally visible device could further cause patients to comply with AIS. In this study, compliance (mean time to wear orthosis per day) and progression of the Cobb angle of the primary curve were measured. At the same time, the study did not include any non-interventional groups to increase the acceptability of randomization among participants. The progression of the curve above 5° as a primary outcome and the conversion rate to surgery (usually recommended for the main curve above 45°) as a secondary outcome was measured in this study. In addition, it should be noted that the team approach (physicians, kinesiologists, and licensed prosthetists / orthoses) may also play an important role in patient compliance [9].

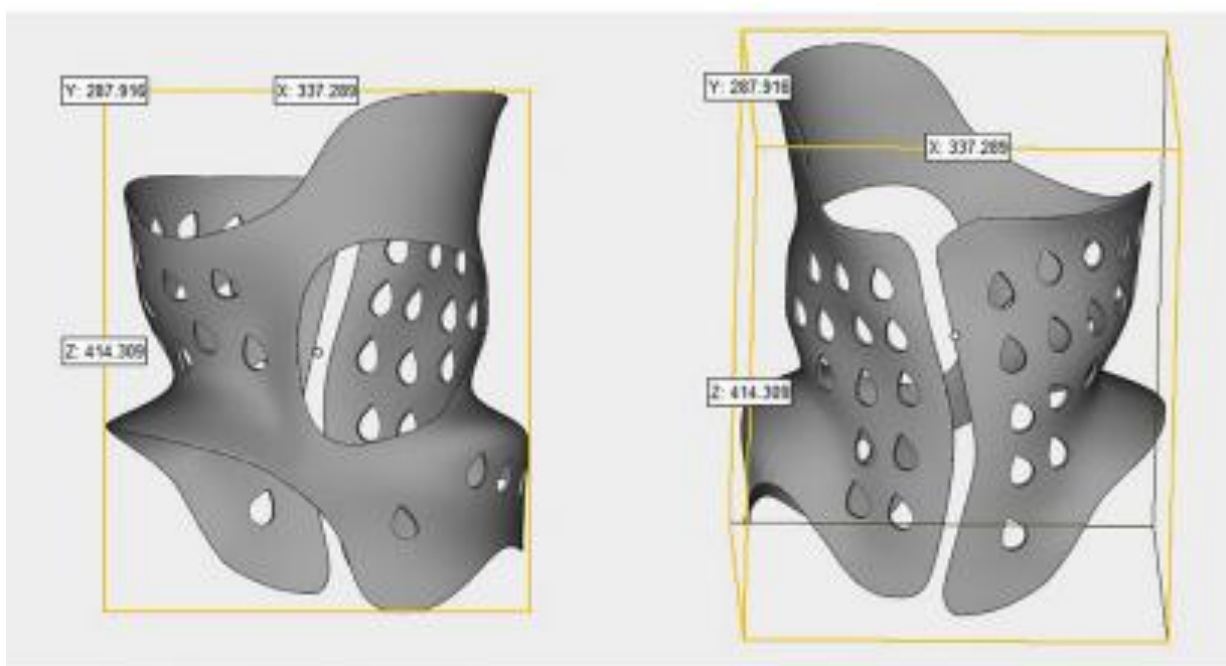


Fig. 1: 3D-printed orthosis design [9]

3D printing technology is computer-aided manufacturing and all are digitally controlled, it could avoid the accumulated error caused by various manual manufacturing procedures. Thus, it is assumed that the vertebral column orthosis manufactured by 3D printing deviates less from the original design of the 3D model, compared to the conventional orthosis manufactured by the conventional manual method. Most procedures can be performed on your computer, including positive casting has been replaced by 3D scanning; positive manual casting could be sculpted under a computer-controlled machine. Thus, the accumulated error could be mitigated by avoiding manual manufacturing, which is mainly based on experience [8].

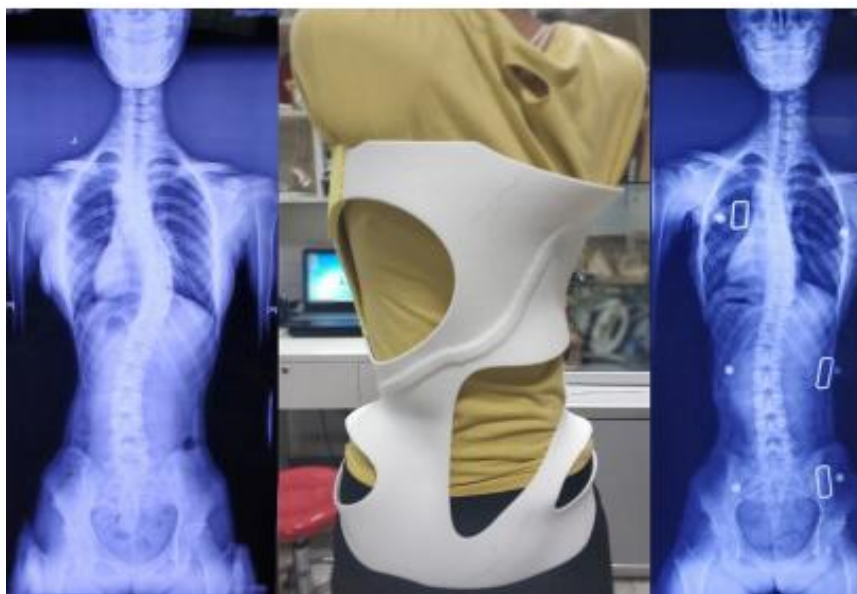


FIG. 2: Correction after treatment with 3D-printed orthosis [9]

Both the 3D printed orthosis and the conventional orthosis could offer similar durability without significant deformations. He indicated that the 3D printed orthosis was able to provide a durable orthotic treatment for clinical application. However, the level of deformation was more severe in the 3D printed orthosis compared to the conventional orthosis. One of the possible reasons was the significantly smaller thickness of the 3D printed orthosis (2.5 vs. 6 mm), which could influence the roughness [8].

Regarding the level of comfort when patients wear orthoses, the peak value and changes in temperature and humidity may show the difference in the level of ventilation of the orthoses. According to the results of the laboratory tests, the peak temperature value did not show any significant difference between the 3D printed orthosis and the conventional orthosis, due to the constant skin temperature and the ambient temperature. However, the heat dissipation speed was better on the 3D-printed orthosis. One of the possible reasons was the reduced thickness [8].

A fundamental part of the custom adjustment of a spinal orthosis is the individual shape of the patient. Three-dimensional scanners are devices used to capture and digitize objects and are used in a wide range of applications: they can be portable devices, or small or large fixed systems. Preparing a trunk model requires a scanner to act as a digital camera by capturing an image to be loaded into the CAD software for manipulation. The literature reports examples of 3D laser scanners used to capture body data for the creation of foam trunk models; Previous studies have shown positive results in reproducing the accuracy of matching with digital corrections. Digital scanning approaches for data acquisition can help with health outcomes, examples include computed tomography (CT), photogrammetry for facial prostheses, and laser scanning for the development of 3D printed wrist splints. The typical 3D laser scanner captures a "dot cloud" or voxels (3D volumetric pixels) of data (3D dots in space, referenced by XYZ coordinate values in sections). The distance between them, points refers to the resolution. "Point clouds" are transformed into 3D surfaces by a method called "polygonization". The point cloud is then used to generate a virtual network [1].

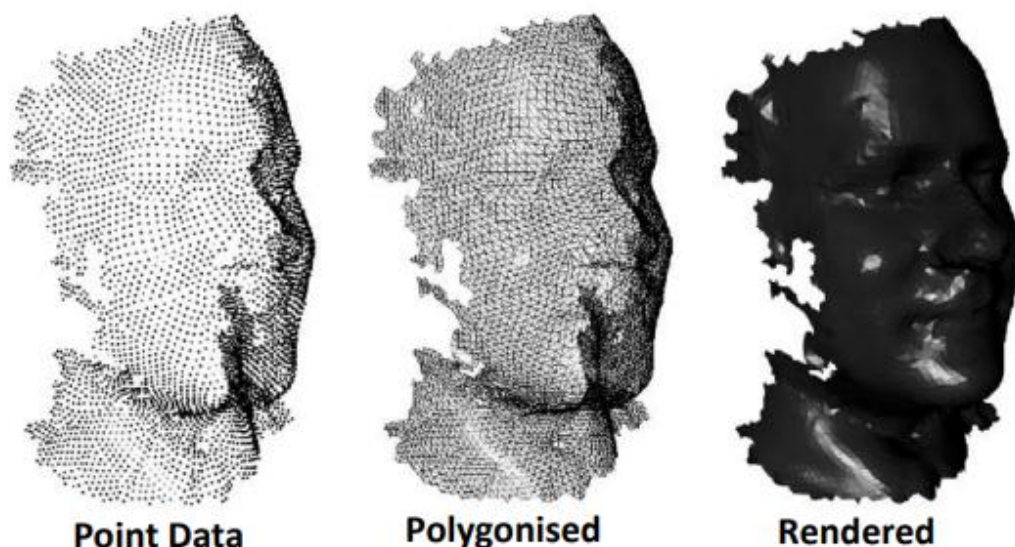


Fig. 3: A triangular polygon mesh created from a point cloud [1]

Wong summarized the benefits of 3D scanning compared to traditional techniques such as: *"Allows a larger number of patients to be scanned faster and easier; data can be analyzed and stored more easily; maximizes time and provides cost savings; reduces the waste of gypsum and foam materials."*[7]

Using the 3D scanner to perform anthropometric measurements may be necessary to consider repeatability of measurements, standardization of the capture position, orientation of scales, and calibration of instruments. Applying pressure to soft tissues can be a problem for replicability (a significant factor when considering adolescent idiopathic scoliosis), and patients may become tired and therefore may change their torso position if they are uncomfortable [1].

Some of the problems that might be encountered when scanning the trunk areas are [1]:

- The scanner beam may be divergent due to dust or high levels of ambient light;
- Postural balancing and breathing movements can affect the scan;
- Depending on the type of scanner, the methodology of building point clouds may affect some measurements;
- The resolution, color perception, luminance, and shading of body parts can influence the final data.

3. Conclusions

The application of 3D printing technology in the design and manufacture of spinal orthosis for AIS is feasible and some benefits can be obtained. As a spinal orthosis, the 3D printed orthosis can meet some of the requirements, such as the absence of toxic substances, it does not cause allergies easily, it is flexible enough, but also rigid, and it is durable for about 2 years. In addition, studies have shown that 3D printed orthoses can provide effective treatment results similar to conventional orthoses. The benefits of applying 3D printing technology can also be reaped. For example, spine orthosis is tailored for each patient with AIS, and usually, a patient may need to have 1-2 orthoses throughout the treatment period.

Another advantage is the flexibility of the design. Spine orthosis can be designed with models according to the patient's preference to improve acceptance and ventilation; this may be difficult to achieve by the conventional method. Moreover, the thinning can also be adjusted according to the

need to increase the thickness in the corresponding apical area and to reduce the thickness in the other area, such as the abdomen and the posterior area.

In addition, the workforce can be reduced by applying 3D printing technology, which for most of its manufacturing time has been automatically controlled by the computer. In terms of clinical efficacy, 3D printing technology can meet the need for current clinical services. Thus, there is a trend of applying 3D printing technology in the orthosis of the spine in the near future, expecting an increased manufacturing speed and a low cost.

4. Bibliography

- [1]Downey, K. C (2019), *Exploration of computer-aided design and additive manufacturing for the design and fabrication of custom-made spinal braces*, University of Manchester, Manchester.
- [2]Kenwick, J. L. N. (2019), *A Novel 3D Printed Brace Manufacturing Process for the Treatment of Adolescent Idiopathic Scoliosi*, University of Alberta, Edmonton.
- [3]Lou, E. H. M. și Hill, D. L. (2016), ” How quantity and quality of brace wear affect the brace treatment outcomes for AIS” in *European Spine Journal*, Springer, 495-499.
- [4]Perez, J. A. *3D printed orthosis design*.
- [5]Redaelli, D. F.; Abbate, V.; Storm, A.; Ronca, A. (2020), ”3D printing orthopedic scoliosis braces: a test comparing FDM with thermoforming”, in *The International Journal of Advanced Manufacturing Technology*, Springer, 1707-1720.
- [6]Weinstein, S. L.; Dolan, L. A.; Wright, J. G. și Dobbs, M. B. (2013), ” Effects of Bracing in Adolescents with Idiopathic Scoliosis”, in *The New England Journal of Medicine*, 1512-1521.
- [7]Wong, M și Cheng, C. Y (2006), ” A comparison of the clinical effectiveness of spinal orthoses manufactured using the conventional manual method and CAD/CAM method in the management of AIS”, in: *Studies in health technology and informatics*, IOS Press, Amsterdam, 123-225, ISSN 0926-9630
- [8]Yangmin, L (2020), *Could the effectiveness of orthotic management for patients with AIS be enhanced via 3D printing technology and pressure-adjustable system*, The Hong Kong Polytechnic University, Hong Kong.
- [9]Zhang, Y. (2020), ” 3D-printed brace in the treatment of adolescent idiopathic scoliosis: a study protocol of a prospective randsomised controlled trial”, in *BMJ Open*, BMJ.

USE OF STATIC CONVERTERS IN LOGISTICS SYSTEMS

ROMAȘCANU Dragoș-Mircea¹, POPESCU Constantin-Adrian²

¹Faculty of Industrial Engineering and Robotics, Study program: Industrial Logistics, Academic year: Master 1, e-mail: dragos.romascanu@yahoo.com

²Faculty of Industrial Engineering and Robotics, Robots and Production System Department, University POLITEHNICA of Bucharest

REZUMAT: This is a continuation of a previous project in which I talked about switch mode power supplies. For educational purposes this semester I will design a PCB and build my one power supply starting from a basic schematic proposed by the company that makes the integrated circuit SP6853. In the next semester I will test the functioning power supply and present datasheets for all the components that I used.

KEY WORDS: SMPS, PCB, SP6853

1. Introduction

A switching-mode power supply (SMPS or switcher) is an electronic power supply that includes a switching controller to convert electricity efficiently. Like other power supplies, an SMPS transfers current from a source, such as the mains, to a load, such as a personal computer, while converting voltage and current characteristics).

2. PCB design

2.1. General PCB design

A printed Circuit Board (PCB) is a staple in the electronics industry and is the physical backbone of electronic schematics and components. They consist of a substrate, usually made of glass cloth and a few microns thick copper foil.

Printed wiring is commercially available in the form of plates of various sizes, with one side plated with copper (single side) or with both sides plated with copper. In the industrial environment, they are used with several layers of copper, for example, the motherboards of the computers have up to 16 layers, but at the amateur level one or two states are enough, this is the reason why I chose to make the wiring on a ceramic plate that has only one layer of copper (top). The multi-layered ones are used for more complex schemes but in my case, it is not applicable. There are some very important steps that need to be followed in order to make good quality printed wiring:

- designing and drawing the wiring in specialized software, I used Eagle;
- printing the drawing on a medium suitable for the purpose;
- cutting a wiring board of the desired size;
- cleaning and degreasing the wiring;
- transfer the drawing on the wiring;
- wiring corrosion;
- cleaning, degreasing, and preparing the wiring;
- making holes for passing parts;
- soldering the parts and testing the wiring.

The design of the printed wiring consists of the allocation of the wiring of a space corresponding to each component of the electronic scheme and their interconnection through conductive paths arranged on one or more levels. Wiring design and drawing can be done with specialized software. Due to its ease and ease, it is possible to use, for example, the software for designing printed diagrams and wiring, Eagle Layout Editor. With this program it is possible to make wiring with a professional look, its possibilities

being innumerable. The Eagle program has three main modules called Control Panel, Schematic, and Board. In Control Panel mode you can find completed projects, component libraries, drawing rules, and more. In Schematic mode, the electrical diagram is drawn and checked for errors and in Board mode, the printed wiring itself is drawn.

As a first step in making a circuit, a principle scheme was chosen, the components were procured and checked on a test board, and then the entire circuit was tested on a test board. It was only when all this was verified that the actual design of the printed wiring was done. After establishing the connection holes of the components from which the design of the wiring design starts, the polarization components will be represented. The design can be done with a view from the components or with a view from the wiring, in which case the components are viewed from the pins (terminals). In order to avoid overturning the drawing in the mirror, the second option is recommended, which, although more complex, eliminates the intermediate stages, giving us the final version of the wiring.

In the second stage, the components from the bookstores were chosen and then placed in the workspace, following their interconnection and the association of a value to each component. The components can be connectors, integrated circuits, transistors, resistors, capacitors, diodes, etc. These components are available in bookstores with many capsule variants, which can be changed as needed when designing the printed wiring. Once the schematic has been made, the design of the printed wiring is based on the principle diagram (the design can be done on several layers). From the program, you can select to view only certain levels, for example, the well-known "top" and "bottom".

Once we have successfully completed the design of the computer and software / Once the design of the computer and software has been completed, we have proceeded to the actual execution of the wiring. I chose a textolite board, which is the best option for my project. Then, I saved the final PCB in the mirror in pdf format, after which I printed it on a photographic sheet, not very thick, the printing being done on a laser printer, so that the ink does not enter the sheet, to remain on the surface. sheets. Then I took the sheet on which the PCB was printed and reduced it to a certain size so that the sheet with the wiring was no bigger than the actual board. After doing this, I fixed the sheet very well on the board, and then by heat transfer with the help of the iron I printed the paths on the photo sheet on the textolite board. It should be noted that the sheet with the printed route must be facing down on the copper side.

The iron must be at a suitable temperature so that the sheet with the route does not burn either, but there must also be enough heat to make the heat transfer as good as possible. Once the tracks have been printed, the sheet will be attached to the plate, both taken and placed in hot water to peel off easily / and to carefully peel them off, the sheet, together with the plate, will be inserted in hot water. Once the routes have been discovered, check again that they have printed well, and if they have not printed well, they are wiped off the plate with acetone, and the last operation is repeated, the one with the iron. Repeat this operation until the route is printed correctly. There is also the possibility that a single line may be missing after printing the entire route. In this case, that line will be drawn with a permanent marker. After the routes have been done well, the holes are made in the plate, with a not very thick drill, I used a drill with a thickness of about 0.7 mm, the size of the hole must be large enough to have no problems at the time. in which pins must be inserted. After all these operations were done, the iron chloride was taken out and heated very little, which helped faster corrosion of the copper. Leave the chloride path plate for about 10 minutes, it should be placed in a plastic or glass bowl. It can be left longer, depending on the degree of wear of the chloride. After removal, check again if there are broken paths or if there are other faults, because if a path is interrupted then it is no longer justified to continue gluing the components to the board because that board will not do what we need anyway and that is not because of the components. If all is well, then it will be applied with acetone over the remaining routes, in order to remain only the copper, the welds being made much better on the bare copper.

2.2. Component identification

In order to make the static converter, I started looking for different components needed to make it. The first time I looked for the CR6853 integrated circuit datasheet that is responsible for the operation of the static converter. In the datasheet provided by the manufacturer, I found only generic information, which

did not recommend certain components, which led me to define my own technical specifications that must have the static converter, current, and voltage. Given that this project is for demonstration purposes, we decided that the source should have the following technical specifications: 12V, 2A output voltage as current, and most importantly, compact size of the equipment, in the industry this is very important. Most of the components are commercially available parts, resistors, capacitors, and diodes, the chopper transformer was more difficult to find because it must be of a certain type in order to operate in the parameters.

2.3.Principal scheme

This version is far too simplified, which led me to look for a schematic for a static converter with the same main component IC CR6853, produced by Chip-Rail but from another manufacturer. After searching, I found the SP6853 integrated circuit produced by Sync. Power Corporation, with identical specifications, but a much better scheme of principle and with much better explained technical specifications of the converter.

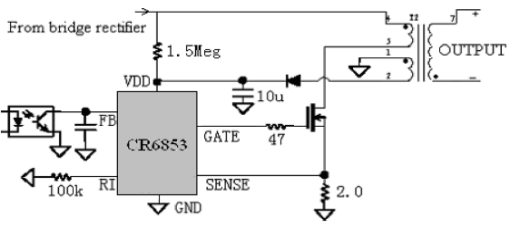


Fig. 1. Scheme proposed by the manufacturer

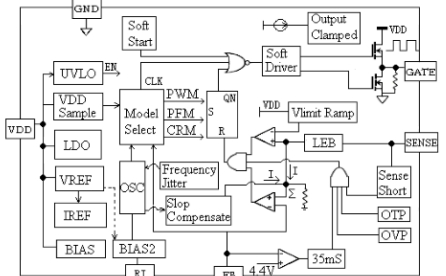


Fig. 2. Internal components of circuit CR6853

The wiring design was done using Eagle software using the schematic scheme proposed by the circuit manufacturer SP6853.

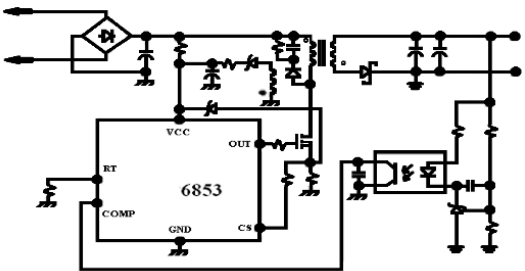


Fig. 3. Schematic diagram with integrated circuit SP6853

In the image below we have an image capture from the design software with some of the components that will later make up the static converter.

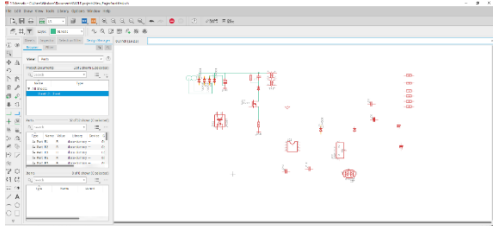


Fig. 4. Static converter electronic diagram

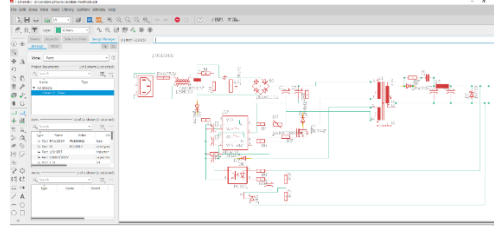


Fig. 5. Electronic scheme

In the image above we find the diagram in the final version of the static converter to be made. The following image shows the wiring to be printed on a photo sheet, the method of making the wiring will be by heat transfer.

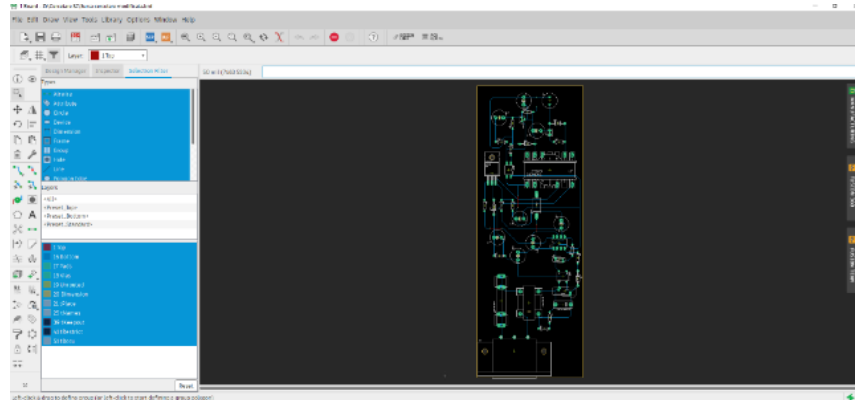


Fig. 6. Static converter wiring

3. Wiring

Below are all the steps we need to take to get the wiring done once it has been printed. Wiring preparation:

Wiring harness (figure 7).

Cleaning the wiring. After cutting, the wiring is first filed on the edges with a very fine file, fig. 8, after which a very fine layer of copper is cleaned with the help of sandpaper, and after that, it is cleaned of impurities and greases with the help of a dishwashing detergent fig. 9.



Fig. 7. Cut PCB to dimensions



Fig. 8. Filing PCB edges



Fig. 9. Clean PCB

After cleaning, the wiring is carefully handled to avoid contamination.

The toner on the photo paper is transferred to the wiring using the iron. The temperature of the iron should be around 200-230 ° C. We also need to press the iron hard enough to keep the toner from sticking to the wiring properly.

The next step is to put the wiring in a container of water to allow the paper to soften, fig. 10 and then we can detach it from the wiring very easily, leaving only the path printed on it, fig. 11.



Fig. 10. "Ironing" the PCB



Fig. 11. The photo paper before its soften in water

When the paper is soft enough it becomes slightly transparent and we can carefully peel it off. fig 12. In fig. 13 we can see what the wiring looks like after the photo paper has been removed. The next step is chemical reaction pickling with ferric chloride, (Fig. 14).



Fig. 12. The photo paper after its soften in water

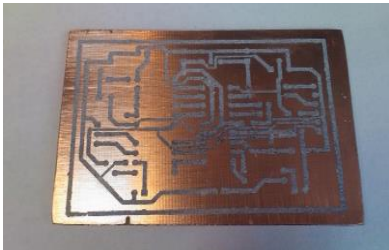


Fig. 13. PCB after the photo paper is removed

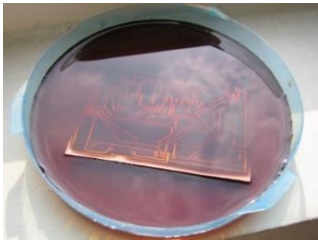


Fig. 14. PCB pickling

4. Planting the components

Once the copper layer is removed from the non-toner protected areas, the wiring is passed through a stream of water to remove traces of ferric chloride. The wiring is wiped with a cloth and then wiped with acetone to remove any toner from it. The wiring is then drilled and then we start planting the components that will later make up the static converter (fig. 15). The order of their planting is from the smallest to the largest dimensions (fig. 16, fig .17). In the picture in figure 18, we have the static converter completed.



Fig. 15. Perforated PCB

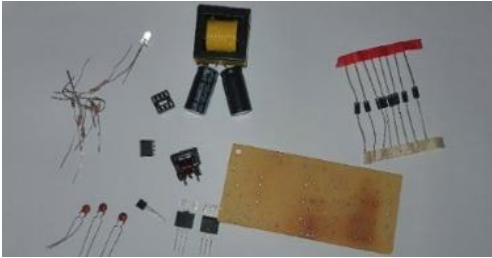


Fig. 16. The components that make up the static converter



Fig. 17. Placement of components on the wiring



Fig. 18. Static converter

5. Use of static converters in the industry

Today, ensuring uninterrupted supply is a predominant trend in all industries. As is well known, any power outage equates to huge losses in production and distribution, which not everyone can afford. Basic equipment, which now ensures the uninterrupted operation of any business, includes: UPS power supplies, industrial batteries and accumulators, power generators, and small industrial power supplies. The latter will be discussed in more detail below.

Modern industrial automation systems, as well as industrial tools and equipment, are made based on circuits with an increasing level of integration. Control structures are also becoming more complex, and printed circuits are being designed with increasing density. All this increases the sensitivity of the systems to any type of disturbance, including from the supply voltage. Therefore, power supplies with stabilized output voltage and free of defects characteristic of standard sources are most often used for power supply.

A good switching power supply must have the following characteristics:

- High efficiency;
- Wide range of input voltages;
- Dimensions and weight as small as possible;
- Stability of the output voltage, regardless of changes: input voltage, load current, and ambient temperature;
- The lowest possible index of the disturbances generated;
- Appropriate protection elements: overcurrent, short circuit, overvoltage;
- Galvanic separation of input and output.

In conventional power supplies (with transformer), the voltage change and galvanic separation were and are made on a steel core transformer operating at a frequency of 50 Hz, on a semiconductor rectifier, and a linear voltage stabilizer. The efficiency of such a system is very low and does not exceed 50%. This results from the fact that a significant part of the power is transformed into a transformer, rectifier, and stabilizer in heat. The recommended rated output power requires "oversizing" the transformer and a high heat output capacity. These unnecessary losses can be avoided by increasing the operating frequency even to a few hundred kHz and by replacing the voltage regulator with an electronic code with intelligent control.

There are currently many models of switching power supply manufacturers on the market. These include MeanWell, Omron, Siemens, Murr Elektronik, Taiwan's Cabur Enstick and many more. Several types of static converters are used in the industry, with different output voltages and powers.

Single-output built-in power supplies (single output voltage).

Models with powers of 15W, 25W, 35W, 50W, 70W, 100W, and 150W are now available on the market.

The second type is designed for DIN rail mounting, characterized by narrow housings (the smallest ones are only 22.5mm wide). Included are models with powers: 20W, 40W, 60W, 75W, 120W, and 240W and standard output voltages used in automatic: 5V, 12V, 24V, and 48VDC. The following range of power supplies is represented by multi-output power supplies:

- With two channels with 30W, 50W, and 120W powers and voltages: 5V, 12V, and 24V in different combinations;
- With three channels with the powers: 30W, 40W, 50W, 60W, and 100W and the voltages: 5V, 12V, 15V, 24V and -5V, -12V and -15V in different combinations;
- With four channels with the powers: 60W and 120W and the voltages: 5V, 12V, 15V, 24V and -5V, -12V and -15V in different combinations.

A novelty is the range of static converters of rain-proof type, in housings and with integrated fans, for forced external cooling. Models with powers: 100W, 150W, 250W and 350W and with voltages: 5V, 7.5V, 12V, 13.5V, 15V, 24V, 27V and 48VDC are available here. Each type of converter mentioned above is protected against overload, overheating, overvoltage, and short circuits. Receiving a stable working voltage at the output is possible after only about 150ms, of course at a full load at the output (or outputs).

6. Conclusions

In the future I will test and see how the power supply can perform in a day-by-day use. All the efficiency and reliability of a SMPS can come at a cost, down below there are some advantages and disadvantages of using a static convertor.

The most important advantages of switching power supplies compared to transformer power supplies are:

- Low weight and low volume at high power.
- Increased yield.
- Low capacity of high-frequency filter capacitors.
- No hearing impairment.
- Resistance to mains disturbances and short voltage drops.
- Short circuit protection integrated into the source circuit.
- Easy operation of different voltage outputs (sources with several outputs with different voltage values).

Major faults in switching power supplies include:

- Generation of broadband disturbances.
- Slow impulse response.
- Complicated input and output filters.
- A large number of subassemblies.

7. Bibliography

- [1]. https://en.wikipedia.org/wiki/Printed_circuit_board
- [2]. <https://www.alldatasheet.com/datasheet-pdf/pdf/1314382/ETC1/CR6853.html>.
- [3]. <https://www.alldatasheet.com/datasheet-pdf/pdf/301818/SYNC-POWER/SP6853.html>

EXPERIMENTAL RESEARCHES ABOUT DESIGNING AND REALIZATION OF AN EDUCATIONAL STAND WITH AUTOMATED GUIDED VEHICLE FOR TRANSPORT AND TRANSFER OF PALLETS

STAICU Mihai Laurențiu¹, POPESCU Constantin-Adrian²

¹Faculty of Industrial Engineering and Robotics, Study program: Industrial Logistics, Academic year: 4, email: staiculaur@gmail.com

²Faculty of Industrial Engineering and Robotics, Robots and Production System Department, University POLITEHNICA of Bucharest

SUMMARY: This project is a continuation of a previous project in which I realised a working prototype of an AGV with radio frequency identification, where I designed the main assembly components, chassis and case in Catia V5, then printing the parts in a 3D printer. The educational stand is represented by a PLS (pallet-lifting system) inspired from automotive-process flows powered by an actuator, drivers and scissors-type lifting system.

Regarding the robot, the sensors are as follows: one is a HC-SR04 ultrasonic obstacle-avoiding sensor, another is used in guidance/tracking the line, a kit with 3 infra-red QTR-8 sensors and a RFID sensor, compatible with industrial tags in order to make the reading and differentiation of the route to which the AGV is subjected; when the robot detects the tag, an informative message will be displayed on AGV by a 32bit-1602 display. Also, the body of the robot is composed by chassis, accessories, case and cover.

KEY WORDS: PLS, AGV, scissors-type, QTR-8, RFID.

1. Introduction

Automatization means to carry out/perform a procedure or a task (usually repetitive) using technology without any form of human assistance. As for the industrial field, in the last century, the autonomous mobile robots have evolved in terms of technology and complex processes so that people managed to focus on a more important work that the robots cannot perform at the moment.

The robots that have the guide technology called “follow the line” are one of the most common and easy to operate robots that are used in an industrial warehouse or production/distribution center due to the flexibility of the route and their reduced price.

2. Current stage

The current AGV prototypes are using similar infrared sensor modules to detect the line of intensity and variable reflectivity. What's new and innovative at this stage of making such prototypes is the RFID reader which is designed to generate a complex tracking route which is able to reprogramme and reconfigure the route of the AGV in real time. In addition, most of the automated guided vehicles are using elements/components of prefabricated camber made after the common prototype Arduino.

3. Virtual model projected in Catia V5

At the moment the prototype is fully functional, the AGV robots being the inspiration for its design. Each sensor is functioning properly and the tracking of the route and the reading of RFID cards is very precise if the sensor detects the line.

The pallet lifting system is being 3D modeled and it is made of 3 rods, linear actuator with 150mm maximum length and housing accessories.

The automated guided vehicle is equipped with electronics components and standardized components (chassis, cover etc), but it also contains 3D printed parts (the housing, RFID stand, IR sensors and h bridge stands).

The programming of the robot was done in the Arduino IDE (software dedicated to Arduino boards) in C++ programming language, using the tracking and line stabilization technology (PID = proportion-integral-derivative) algorithm adapted to the 3-channel QTR sensor mode.

PID it is a continuous loop mechanism, in which a controller who uses a generated signal by an entry element (IR sensor) it calculates continuously an error value noted $e(t)$ as a difference between a target_Point and a process measured value, by applying a correction based on 3 constants: K_p , K_i , K_d , defining for PID.

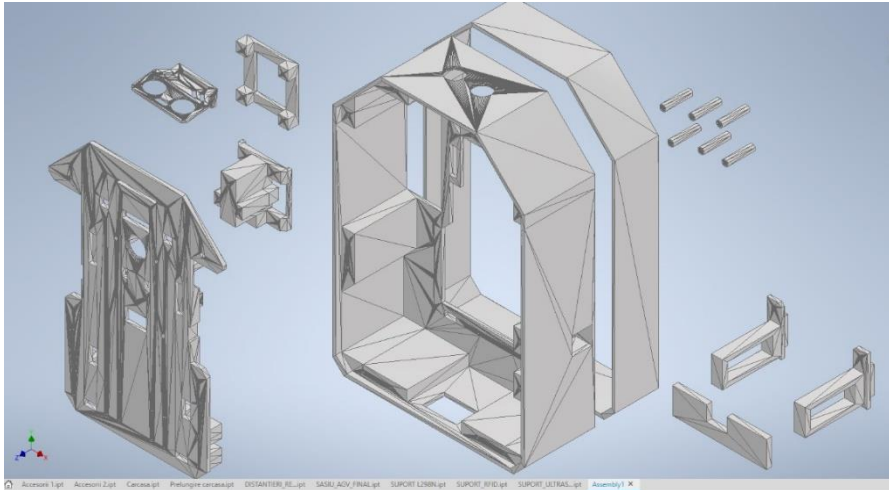


Fig. 1. Preparing mechanical components for 3D printing

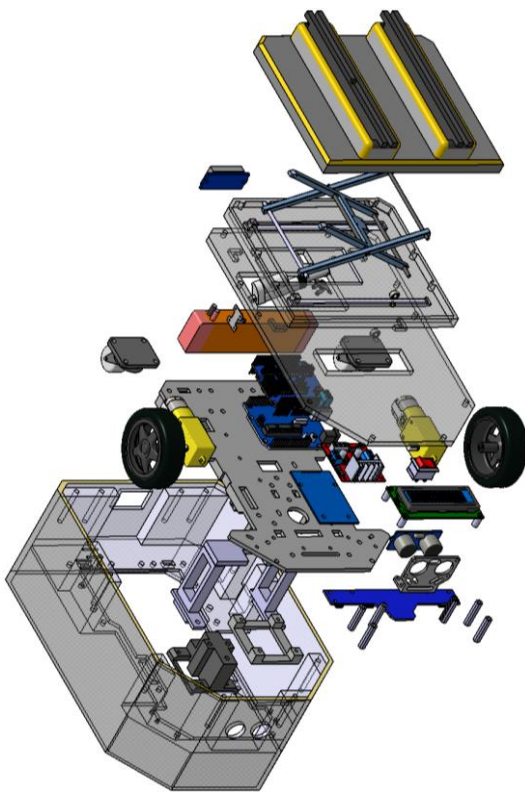


Fig. 3. Exploded AGV model

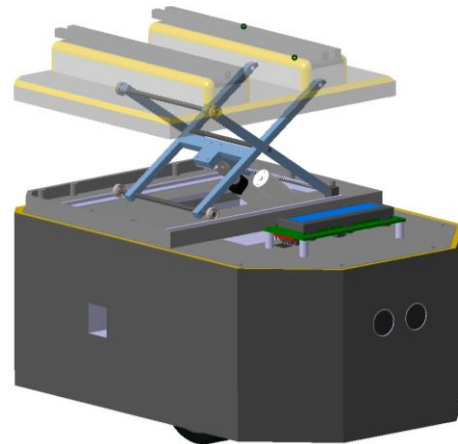


Fig. 2. 3D model made in CATIA V5

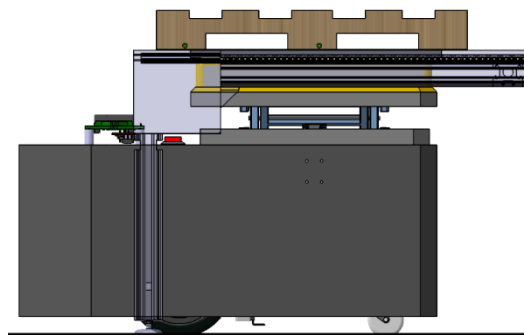


Fig. 4. 3D model during a pallet lifting task

In these two figures, the design of the virtual model was projected in CATIA V5 software, starting from the chassis, to the elements that support the electronic components and up to the housing. The lifting system (fig.4) allows a maximum stroke of 40mm, the total length being ideal for transferring pallets from the surface of the chain conveyor.

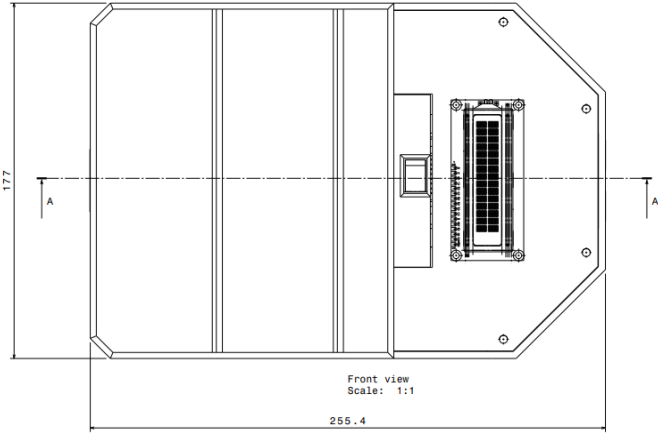


Fig. 5. Top view with dimension gauges made in Drafting

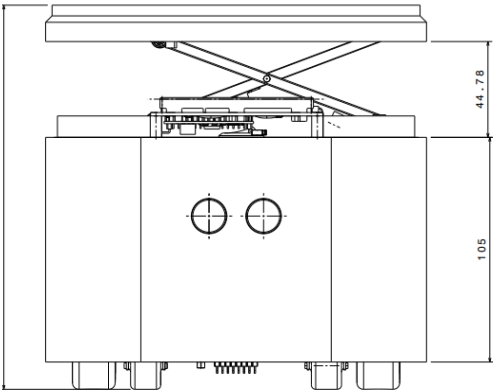


Fig. 6. Front view with gauge dimensions

4. Actual model

After virtual modeling, 3D printing of the parts and inspection of the final model, the next step is to assemble the mechanical components and connect the electronic connections between the motherboard, sensors, power supplies and motors, while testing the electronic connections with a digital voltmeter for potential short-circuit problems.

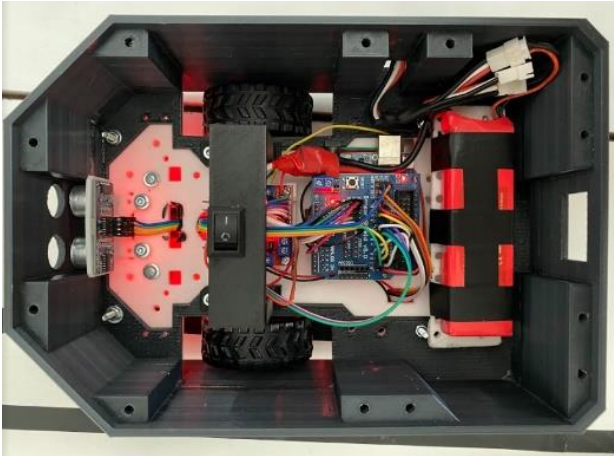


Fig. 7. Top view of the physical model



Fig. 8. Lower part of the physical model highlighting the sensors used

After assembly, the prototype can be simulated on a route to test line tracking, identify RFID cards, execute commands written in the source code via UID codes, and detect obstacles in the AGV's path on the guidance route. Therefore, the test track is provided with a white matte surface and black tape for IR sensor

accuracy, a STOP point, a path change point and a working point (PL_1) where the AGV will stop for a certain time (5 seconds).

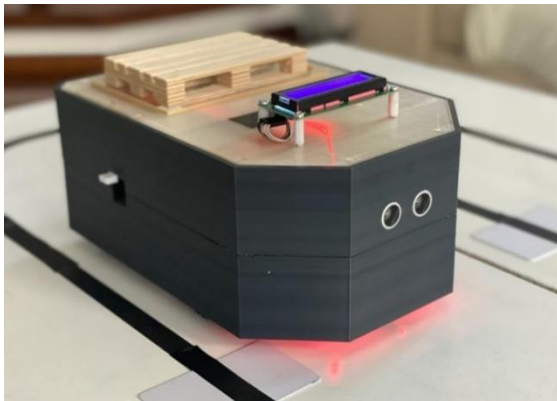


Fig. 9. Finished AGV prototype

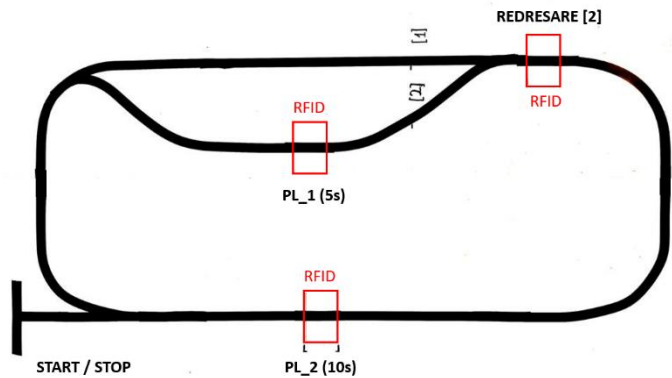


Fig.10. Experimental route of the AGV

The simulation of the AGV on the experimental route is performed using the C++ code in the AGV control algorithm, and when running the specific route change code, the AGV executes the left turn (route 2) and moves to the first working point. Also, if the RFID card is removed from the turn-around area, the AGV continues following the line on the route numbered with 1.

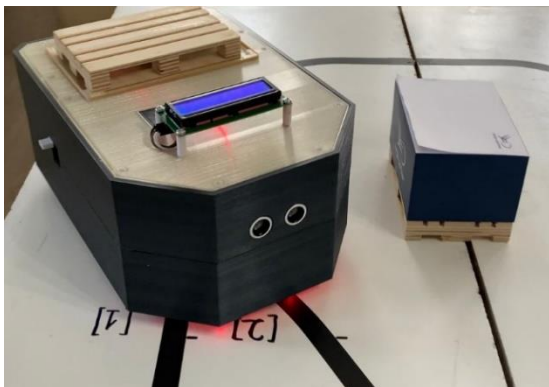


Fig. 11. Change of direction and continuation on route (2) due to RFID card identification

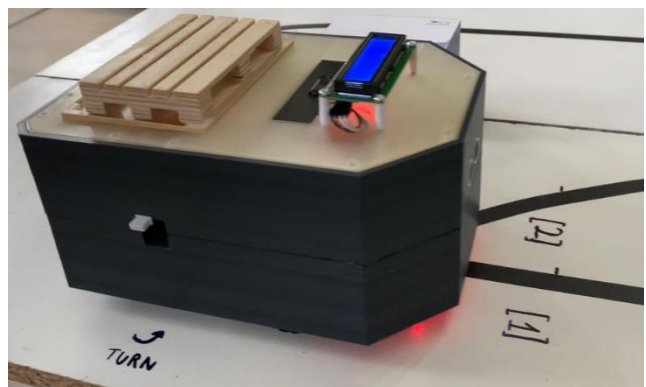


Fig. 12. Continuing direction of travel on route (1) without RFID card

5. Algorithm and PLS system

The AGV algorithm is made up of a series of loops, each sequence being integrated into the main algorithm, of which the following are part: code for line tracking with PID (linetrace), code for RFID card reading and execution (UID) and code for obstacle avoidance using the ultrasonic sensor (NewPing).

The loop() function in a programming language such as C++ is intended to create a continuously repeatable program, or a permanent loop (hence the name loop) in which the actual control program of the AGV is entered and what it is to do with the respective sensors based on the data provided by the sensors. For the PID, illustrated below in the algorithm, the reading and interpretation of the sensors against the colour band takes place. If one of the 3 sensors will detect the position relative to the line, the error will be automatically set according to the position in real time, the error being the difference between the AGV centre and the sensor position, memorizing the value of the constant (0 - 2000).

```

void linetrace() {
  //Reading Sensor Values
  int s1 = digitalRead(ir1); //Left Sensor
  int s2 = digitalRead(ir2); //Middle Sensor
  int s3 = digitalRead(ir3); //Right Sensor

  if (digitalRead(ir2) == 0){eroare = 0;}
  else if (digitalRead(ir1) == 0){eroare = -7;}
  else if (digitalRead(ir2) == 0){eroare = -1;}
  else if (digitalRead(ir2) == 0){eroare = 1;}
  else if (digitalRead(ir3) == 0){eroare = 7;}

  PID_error = eroare;
  PID_p = kp * PID_error;

  timePrev = Time;
  Time = millis();
  elapsedTime = (Time - timePrev);}

  //se calculeaza valoarea derivatei:
  PID_d = kd*((PID_error - previous_error)/elapsedTime);

```

Fig. 13. Code sequence used for line tracking using PID

```

Serial.print("UID tag :");
String content= "";
byte letter;
for (byte i = 0; i < mfrc522.uid.size; i++)
{
  Serial.print(mfrc522.uid.uidByte[i] < 0x10 ? " 0" : " ");
  Serial.print(mfrc522.uid.uidByte[i], HEX);
  content.concat(String(mfrc522.uid.uidByte[i] < 0x10 ? " 0" : " "));
  content.concat(String(mfrc522.uid.uidByte[i], HEX));
}

Serial.println();
Serial.print("Message : ");
content.toUpperCase();
if (content.substring(1) == "53 65 B9 38")
{
  Serial.println("Asteptare punct de lucru_1 (5 secunde)");
  Serial.println();
  lcd.print("Asteptare PL-1");
  lcd.setCursor(0, 1);
  lcd.print("pentru 5 secunde");
  linetrace ();
}

```

Fig. 14. Code sequence used to identify RFID cards

The sensor module consists of 3 pairs of phototransistors and photodiodes reflecting light through the difference in opacity of the strip from the working surface, placed in a module on a straight line with a wavelength of 1300nm.

This module connects directly to the SensorShield mounted on the Arduino board along with the rest of the sensors and electronics.

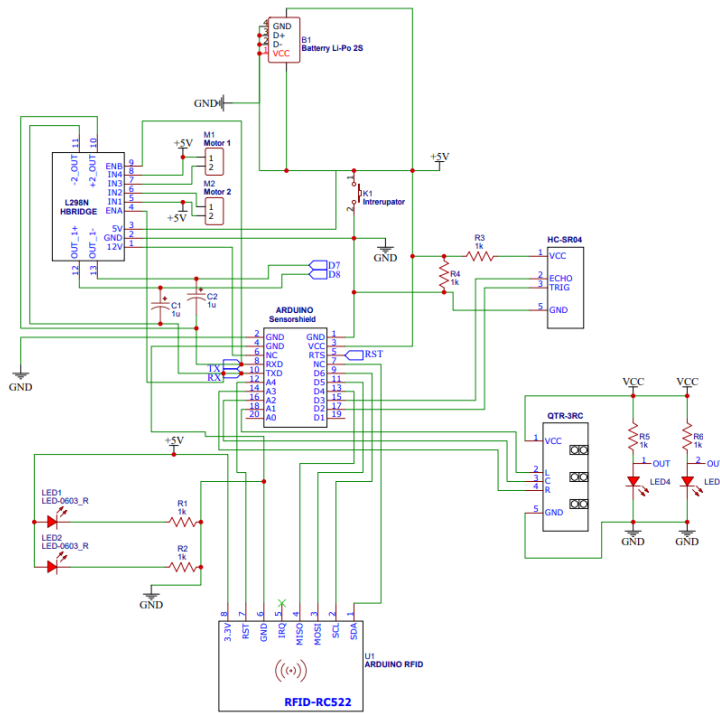


Fig. 16. Complete electrical block diagram of the AGV assembly

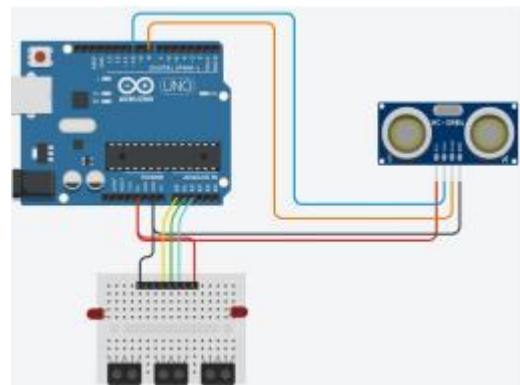


Fig. 15. Wiring diagram for IR and ultrasonic sensors

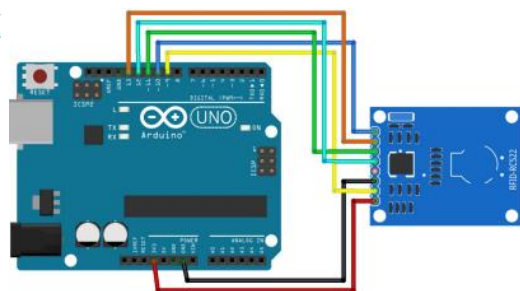


Fig. 17. RFID reader wiring diagram

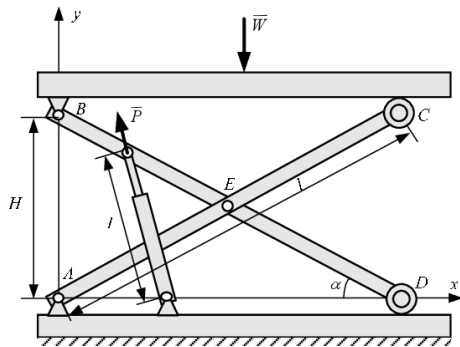


Fig. 18. Mechanical principle of operation of the PLS pneumatically operated double scissor fork system [4]

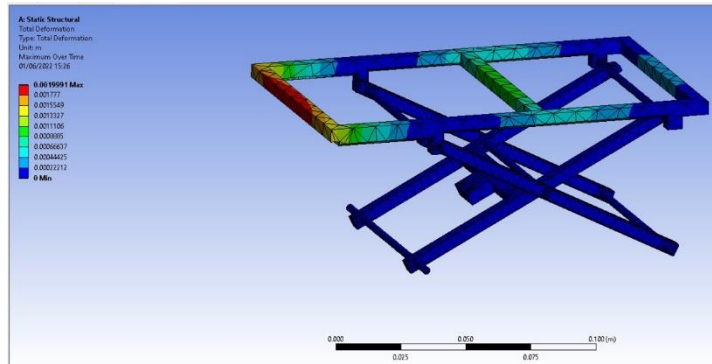


Fig. 19. Structural static analysis of the PLS lifting system with total deformations along the structure (maximum deformation = 1.9 mm)

6. Conclusions

For the future, I aim to change the current line tracking sensor to a better one and of course to make and add PLS system to the current prototype.

In conclusion, the project is a continuation of last year's research into the use of radio frequency identification technology in AGVs.

The multitude of industrial applications in which this type of prototype could be used (any industrial sector with a transfer/transport, handling, distribution role) together with the ease of adaptation of the route and user interface, lead to the organisation and systematisation of a company from an intra-logistics point of view, while reducing overall costs and increasing productivity.

7. References

- [1]. <https://www.hackster.io/anova9347/line-follower-robot-with-pid-controller-cdedbd>
- [2]. Bluett., "ThePIDController," 16.03.2015. Link: <https://wired.chillibasket.com/2015/03/pid-controller/>.
- [3] Link: <https://www.optimusdigital.ro/ro/senzori-senzori-optici/7241-senzor-infrarou-reflectiv-pololu-qtr-md-05rc.html>
- [4]. <https://www.semanticscholar.org/paper/Dynamic-Analysis-of-The-Hydraulic-Scissors-Lift-%C3%87irak/02c674e25d07a9adf678a9d415aff082606c68fc>
- [4]. <https://www.arduino.cc/>;
- [5]. <https://github.com/>;
- [6]. <https://ardushop.ro/ro/home>;
- [7]. <https://www.sigmanortec.ro/content/printare-3d>
- [8]. <https://lastminuteengineers.com/i2c-lcd-arduino-tutorial/>

8. Notations

The following symbols are used throughout the paper::

- PLS = Pallet lifting with "scissors"
- IDE = Integrated development environment;
- CAD = Computer aided design;
- RFID = Radio-Frequency Identification;
- AGV = Automated guided vehicle

STUDY ON THE USE OF SMART SENSORS TO MONITOR ENVIRONMENTAL FACTORS IN GREENHOUSES

SCARLAT Andrei Daniel¹, ȘTEFAN Theodora-Mihaela², POPESCU Adrian³

¹Faculty of Industrial Engineering and Robotics, Study program: Industrial Logistics, Academic year: 4, e-mail: nouageneza@gmail.com

²Faculty of Industrial Engineering and Robotics, Study program: Industrial Logistics, Academic year: Master 1

³Faculty of Industrial Engineering and Robotics, Robots and Production System Department, University POLITEHNICA of Bucharest

Summary: The purpose of this paper is designing a smart thermometer by using Arduino. This kind of thermometer would be used in greenhouses so the plants could thrive. The components of the circuit consist off: an Arduino board, a DHT 11 sensor and an LCD screen are used to display the temperature and humidity interpreted by receiving the signal. After the shell was designed in Catia, it was 3D printed and then the Arduino was placed carefully along the wires and the sensor.

KEY WORDS: Arduino, LCD screen, smart sensor, greenhouse, smart thermometer

1. Introduction

A greenhouse (or solarium) is a building special with glass or plastic roof and walls for housing and growing plants that do not stand the cold in the winter. Warming up the greenhouses is made in the differently ways : with hot water, water vapors, electrical energy etc. A classification of the obtained temperature depending of the plants' requirements is:

- -cold greenhouses with temperature in between 8 - 10 °;
- -temperate greenhouses with temperature in between 18 - 20 °;
- -warm greenhouses with temperature in between 25 - 30 °

So to see if temperature and the humidity falls in the normal parameters rule depending on the type of plants we want to grow, we made a smart thermometer that uses smart sensors which take in environmental and ambient data and processes them with the help of an Arduino board, and after processing it displays external data on an LCD screen so that it can be interpreted as well as changing temperature with the help of heating and humidification systems of the greenhouse.

2. The current stage

The current research was successfully completed, the thermometer prototype can to take over environmental information and display them. For the 3D model Catia V5 was used, where the virtual model of the thermometer was created. That's how the case was designed and it incorporated the LCD screen and smart sensor to take over environmental information. The case of the thermometer was made with the help of a 3D printer according to the virtual model.

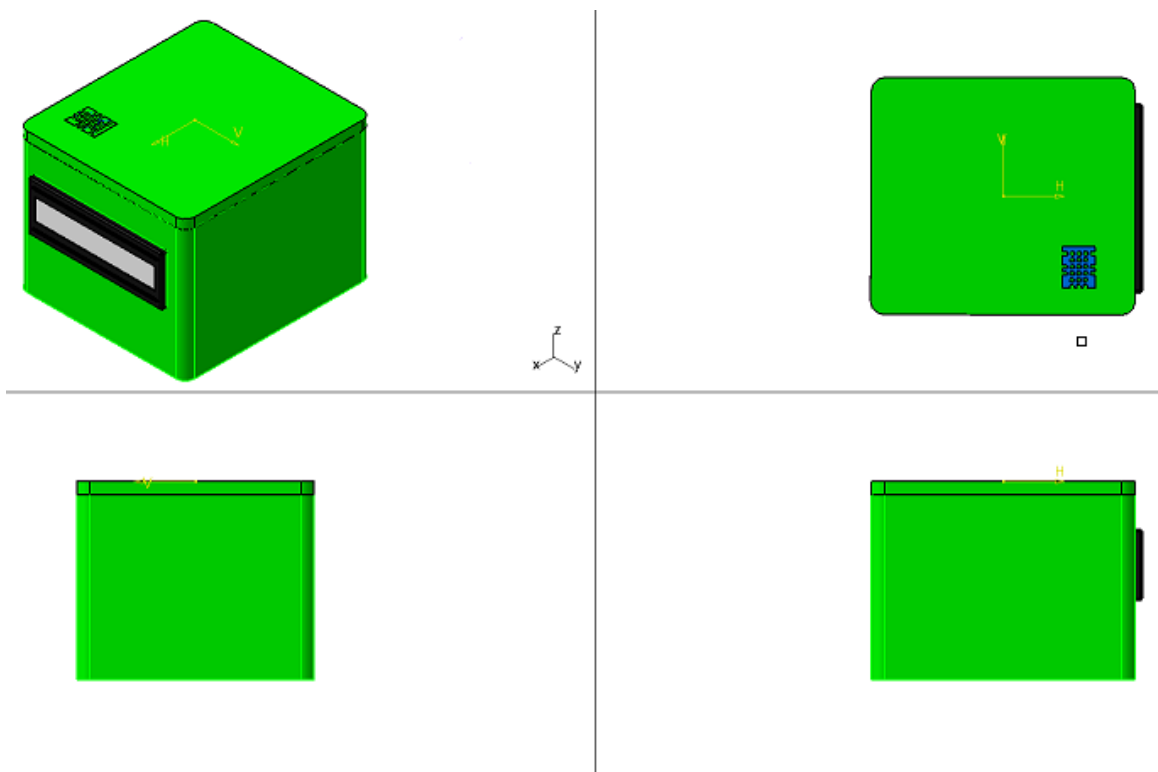


Fig. 1. Smart thermometer CAD model

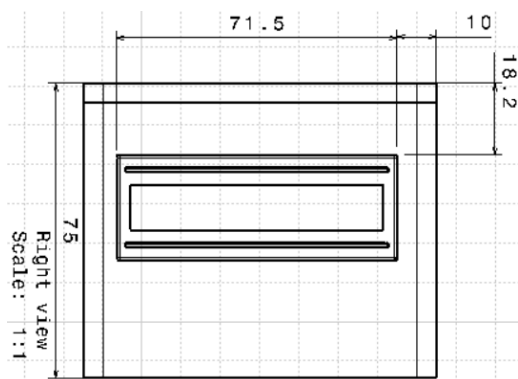


Fig. 2. Front view of the smart thermometer with overall dimensions

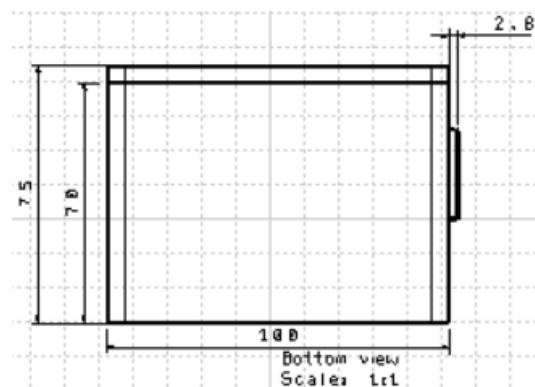


Fig. 3. The side of the smart thermometer with overall dimensions

The programming part was made with Arduino IDE software, where it was programmed to take over information provided by the humidity and temperature sensor DHT 11 and to display them on the LCD screen so that they can be interpreted. For making the scheme of the electrical components the Fritzing software was used, where connecting the smart sensor's Data pin to the MOSI pin of the Arduino board to provide data taken from the environment and to interpret it, was a crucial step. The connection of the LCD screen's SDA pin to A4 pin was intended for interpretation of the data received from the board and displaying them, and the connection of the SCL pin to the A5 pin of the board was intended for the transmission in real time of the data.

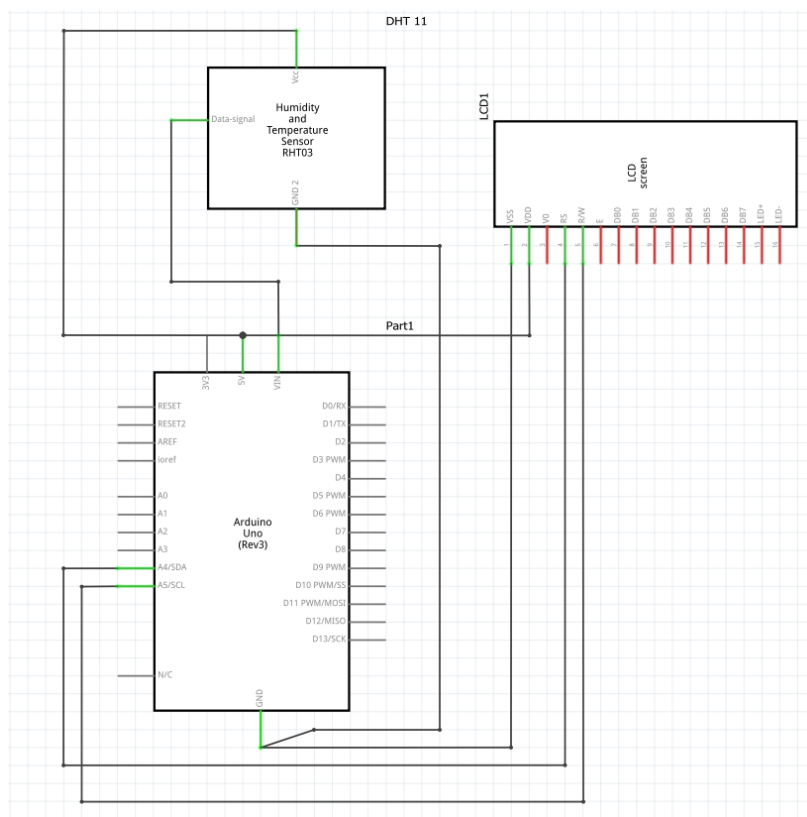


Fig. 4. Wiring diagram

After setting up every detail of the research, after connecting electrical components and uploading the code in the Arduino board, according to the virtual model created, the physical model was made as it follows:

The smart thermometer will be placed on different pillars of different heights to be able to monitor temperature from the ground level to the top floor of industrial greenhouses.



Fig. 5. The physical model

So the data can be shown on the display, the liquid crystal library will be used, and after the data will be received from the sensor it will be displayed as characters for temperature and humidity with the value interpretation of the DHT 11.

```

#include <LiquidCrystal_I2C.h>
LiquidCrystal_I2C lcd(0x27,16,2); // set the LCD address to 0x27 for a 16 chars and 2 line display
byte degree_symbol[8] =
{
    0b00111,
    0b00101,
    0b00111,
    0b00000,
    0b00000,
    0b00000,
    0b00000,
    0b00000
};

int gate=11;
volatile unsigned long duration=0;
unsigned char i[5];
unsigned int j[40];
unsigned char value=0;
unsigned answer=0;
int z=0;
int b=1;
void setup()
{
    lcd.init(); // initialize the lcd
    lcd.init();
    lcd.backlight();
    lcd.print("Temp = ");
    lcd.setCursor(0,1);
    lcd.print("Humidity = ");
    lcd.createChar(1, degree_symbol);
    lcd.setCursor(9,0);
    lcd.write(1);
    lcd.print("C");
    lcd.setCursor(13,1);
    lcd.print("%");
}

```

Fig. 6. Liquid crystal library

3. Conclusions

In conclusion, the smart thermometer is a innovative method to monitorize humidity and temperature in industrial greenhouses, offering accuracy for the data extracted from the environment and maintaining optimal parameters for the development and growing of the plants we want to cultivate. The product is a compact one, having a low size and being easy to place in the greenhouse. Our personal contribution was making the virtual model, programming it and making the component interconnection scheme of electronic parts. We want to continue this research through integration of the thermometer in an automated vertical greenhouse.

4. Bibliography

- [1]. <https://ro.wikipedia.org/wiki/Ser%C4%83>
- [2]. <https://ro.bio-green.net/6576353-all-about-greenhouses-characteristics-cultivation-techniques-and-which-plants-to-insert>
- [3]. <https://fritzing.org/download/>
- [4]. Traian Anghel (2020), Programming Arduino board, Editor Parallel 45, ISBN 978-973-47-3204-3
- [5]. O'Reilly (2012), Environmental Monitoring with Arduino, Maker Press Publishing, ISBN 978-1-449-31056-1

EXPERIMENTAL RESEARCH ON THE DESIGN AND CONSTRUCTION OF AN EDUCATIONAL STAND WITH AUTOMATIC GUIDED VEHICLE FOR THE TRANSPORT AND TRANSFER OF PALLETS

SCARLAT Andrei Daniel¹, ȘTEFAN Theodora-Mihaela², POPESCU Constantin-Adrian³

¹Faculty of Industrial Engineering and Robotics, Study program: Industrial Logistics, Academic year: 4, e-mail: nouageneza@gmail.com

²Faculty of Industrial Engineering and Robotics, Study program: Industrial Logistics, Academic year: Master 1

³Faculty of Industrial Engineering and Robotics, Robots and Production System Department, University POLITEHNICA of Bucharest

Summary: For this research the purpose was making an AGV which is used for carrying pallets. It was used: an Arduino board, a motor driver L293N2, 2 gear motors with 2 wheels, a distance sensor HC-SR 04 for avoiding obstacles that show up on the path, 2 modules of infrared sensor for following the guidance line, a holder for 2 LI-ion batteries and its batteries. A storage system located on the upper housing of the AGV is used to take over the pallets.

KEY WORDS: AGV, remote sensor, Arduino, 18650 Li-ion battery

1. Introduction

Such vehicles are used in the deposit to transport products or goods. AGVs look like small moving cars controlled in a warehouse. Moving control is provided by special software. With the help of this software AGVs know what they have to do is orient themselves in the deposit and avoid collision between them and other static objects.

There are many types of automatic vehicles produced by companies. Every one of them can be used to move pallets or even in picking operations. Some of the automated vehicles having the ability to move product shelves to be picked up.

The most common uses of these Automatic vehicles are in the production area at the supply working points with raw material. They are also used for picking finished products or semi-finished products and bringing them to the storage area.

Industrial pallets are like some storage buffers for different products that can be taken by different equipment and perform equipment picking operation.

2. The current stage

Traditionally, human operators have many disadvantages compared to automatic guided vehicles. In the warehouse storage system, this problem arises because humans work with emotions which means that their work depends on emotions. This causes problems, for example in warehouses operators usually take or leave objects to the nearest storage. While they may not take or leave the furthest storage and cause the furthest object to dust because it was never taken.

Another example, human operators might forget to record data storage. However, this problem can be solved by automated guided vehicles. AGV removes some of the potential for inaccurate workflows, reduces non-productive time and increases output, making operations more accurate and productive. When operators

have limited time, to increase production usually companies need 3 shift operators while AGV is able to operate 24 hours a day and 7 days a week. In addition, AGV is able to simplify warehouse management systems.

The research is successfully completed and operational. In the next page I will describe how to achieve it and how it works.

Let's start by presenting the scheme of principle and connection of the AGV created:

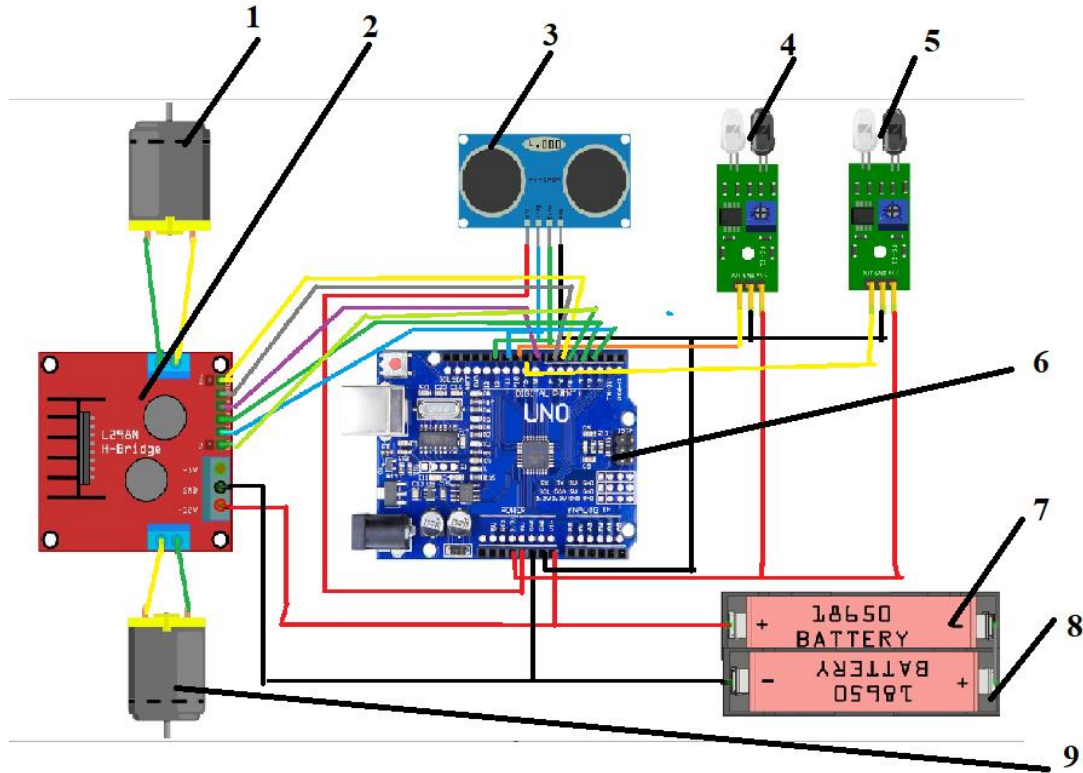


Fig. 1. Wiring diagram

Table 1. Component table

Nr.crt	
1.	Gear motor 1 (left)
2.	L298N driver
3.	sensors inside HC-SR04
4.	Left IR sensor module
5.	Right IR sensor module
6.	Pleasant ARDUINO
7.	Battery Li-ION 18650
8.	Support battery
9.	Gear motor 2 (right)

The AGV 3D virtual model was made in Catia V5R21, looking like this:

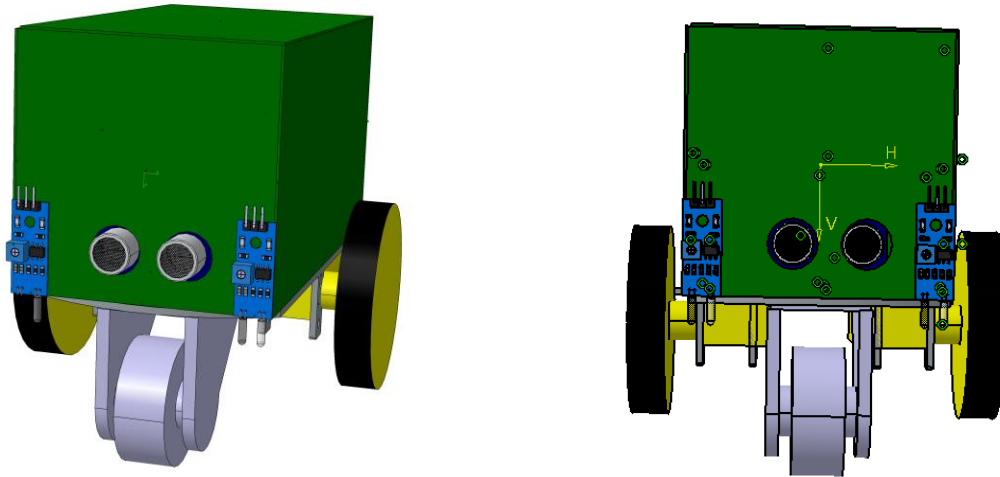


Fig. 2. The 3D model of the AGV

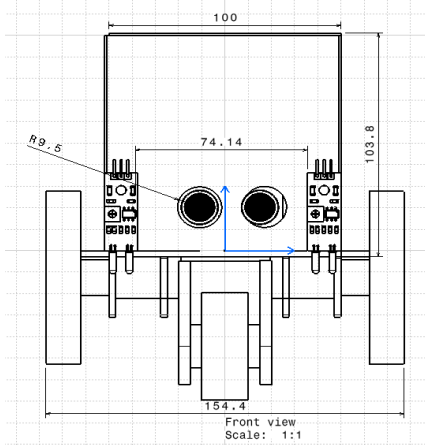


Fig. 3. The front of the AGV

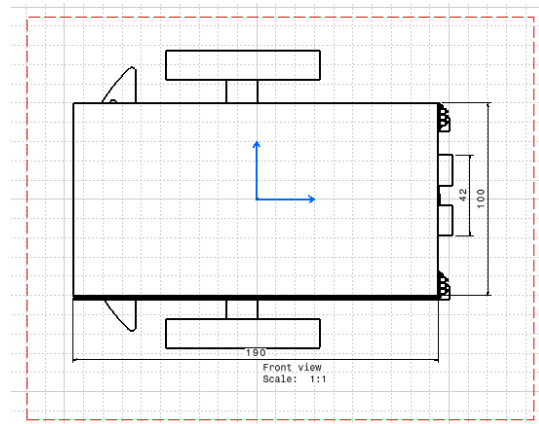


Fig. 4. Top view of the AGV

The pattern of the chassis is made of plexiglass, measuring 20x10, on the back of which the 2 gear motors with the 2 wheels was attached, and on the top surface the Arduino board was attached, an L293N motors driver, which was interconnected with Arduino board, the support for the batteries with batteries 2 Li-ION batteries.

The HC-SR04 distance sensor was also connected to the board to avoid obstacles and the 2 infrared IR sensor modules to follow the AGV guide line.

The links between the driver, board and sensors were done via jumper wires. The case was made of cardboard that later was painted to give it a more pleasant unique look, according to the virtual model.

First, the input variables need to be defined (ex.: pins of the distance sensor, pins of the motor and IIR's pins). Then the calculus algorithm for object detection is introduced.

```

void loop() {
  digitalWrite(trigPin, LOW);
  delayMicroseconds(2);
  digitalWrite(trigPin, HIGH);
  delayMicroseconds(10);
  digitalWrite(trigPin, LOW);
  duration = pulseIn(echoPin, HIGH);
  distance= duration*0.034/2;
  Serial.print("Distance: ");
  Serial.println(distance);
}

```

Fig. 5. Calculus algorithm

```

if(right_sensor_state == HIGH && left_sensor_state == LOW)
{
  Serial.println("turning right");

  digitalWrite (motorA1,LOW);
  digitalWrite (motorA2,HIGH);
  digitalWrite (motorB1,LOW);
  digitalWrite (motorB2,HIGH);

  analogWrite (motorASpeed, vSpeed);
  analogWrite (motorBspeed, turn_speed);
}

```

Fig. 6. The AGV' s movements

So the AGV knows when to continue the path and when it should stop, it calculates the distance of objects depending of the minimum distance set to avoid collision. If it's smaller, it stops and if it's bigger it will continue.

The principle of operation is:

L293N driver is working the 2 gear motors through the transmission and splitting the supply voltage received from the battery.

Arduino board orders AGV movement through the transmission of the commands from the board's microprocessor to the driver. The HC - Sr04 distance sensor detects objects that appear on the route and if it is at a distance of 10 cm, it redirects the AGV from the route for avoiding collision.

IR infrared sensor modules detect the base color of the floor and follow the black band, and when the band is perpendicular on the direction of moving it will give a command to the Arduino board to stop the moto-reducers because the AGV has reached its destination.



Fig. 7. AGV physical model

After completion of connecting items between them, uploading the code in the Arduino board I got a prototype as in the FIG. 9

3. Conclusions

In conclusion, the AGV is functional and easy to handle. It can carry easily the pallets from a processing point to a storage point, making life easier for the human operators. And due to the fact that it can detect obstacles which appear on the route it makes so they may avoid potential accidents at the work place and perform successfully its tasks.

4. Bibliography

- [1]. Traian Anghel (2020), Programming plaii Arduino, Editura Parallel 45, ISBN 978-973-47-3204-3
- [2]. O'Reilly (2012), Environmental Monitoring with Arduino, ISBN 978-1-449-31056-1
- [3]. <https://logistic-specialist.ro/logistica-automatizata-ce-sunt-agv-urile/>
- [4]. https://www.researchgate.net/publication/347805525_Development_of_Low_Cost_Pellet_Loadin_g_and_Unloading_AGV

STUDY ON THE IMPLEMENTATION OF WIRELESS CHARGING SOLUTIONS FOR AGVS

DRĂGAN Alin-Leonard¹, Popescu Adrian Constantin²

¹Faculty of Industrial Engineering and Robotics, Study program: Industrial Logistics, Academic year: Master 2, email: draganalin198@yahoo.com

²Faculty of Industrial Engineering and Robotics, Robots and Production System Department, University POLITEHNICA of Bucharest

In the industry but also for the area of logistics warehouses, the transit is made with vehicles with automatic guidance (AGV), which are used very often, they have evolved and are much more and the most important are the vehicles with wireless charging because energy transfer is much more efficient than electrical circuits, outlets and cables that degrade over time. Self-propelled vehicles that can be loaded during operation are a continuous flow to increase productivity and improve flexibility in the logistics warehouse or production flow.

1. Introduction

In order to implement a solution with automatic-guided vehicle-type transfer (AGV) equipment to be loaded wirelessly on the logistics flow within a warehouse, it is necessary to meet the following objectives:

- the use of 98% automated technology to allow wireless charging of transport-transfer equipment during working hours;
- the use of transport-transfer equipment which can be adapted to the level of demand in a number covering the entire flow; the use of a soft building systems management (BMS) for operators so that the flow is monitored 24 hours, 7 days a week;
- maintenance costs in the first 3 years must be a maximum of 5% .

2. The current stage

Automation in the production area or in logistics centers and storage areas involves the use of modern technology to increase productivity. Automation can be digital and refers for example to the automation of the inventory data collection process or it can be a more complex physical automation, involving mechanized and automated equipment and solutions [1].

Thus, in addition to using a warehouse management system that allows you to check where the goods are stored and what areas are available for storage of various items, the implementation of a flow that uses conveyors for transporting products or an automatic storage and recovery system will eliminate routes long and mixed cargo areas [2].

Physical automation of warehouses requires the use of automated equipment to eliminate manual movements and streamline logistics processes, this includes the use of automatic guided vehicles (AGV), automated palletizing systems, automated wrapping systems, robotic lifting systems, etc.

AGVs handle products in transport-transfer processes, which are connected to one or more loading and unloading points. When several AGVs are used (figure 1), they are connected to the network through an internal server that allows real-time management and monitoring of their activity. Route planning can also be changed in real time and the approval of sections on the route or intersections is done through GPS devices that communicate with each other. A very

complex system also needs a BMS that also monitors the loading of individual devices to maintain optimal availability [3].

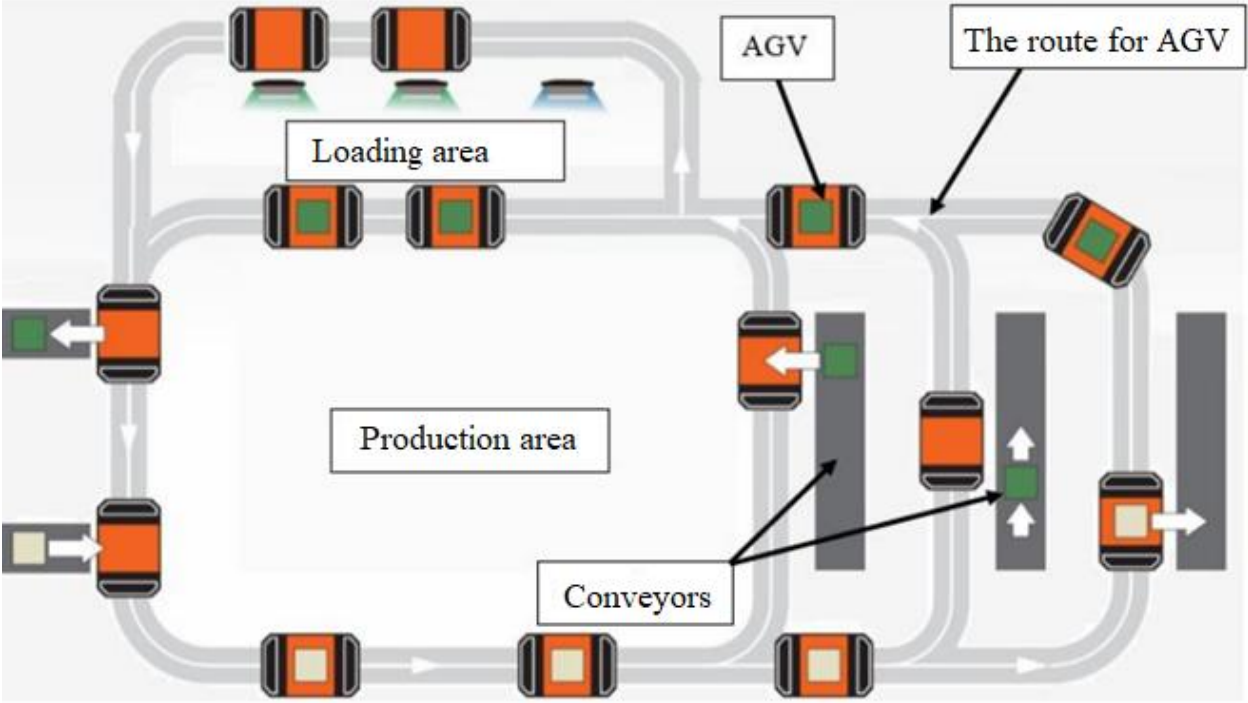


Fig. 1. Logistics flow for a production area with several AGVs

Automatic loading of self-guided vehicle transport-transfer equipment is very beneficial as it allows this equipment to work continuously without the need to park for long periods during loading. Also, the implementation of such a solution allows the required number of transport-transfer equipment to be smaller compared to the case where the classic load is used.

Wireless charging for AGV is the technology of the future when it comes to electric vehicles. In addition to the development of intelligent algorithms, sophisticated sensor technology and decentralized intelligence, which give AGVs intelligent behavior, the solution for inductive charging (wireless charging) transforms AGVs into fully autonomous equipment that can work independently of human operators. can be monitored remotely.

The charging system thus allows to increase the degree of automation of transport-transfer and storage operations without wasting additional time for charging the batteries [4].

Wireless or inductive charging is suitable for all types of batteries listed below:

- Acid-based lead batteries ;
- GEL / AGM batteries ;
- Pure lead batteries ;
- Lithium batteries.

2. Constructive solutions and implementation of wireless charging technologies for AGVs

Wireless charging of AGVs allows their functionality 24/7, this being a modern solution of "charging in the transit process without operator" that allows vehicles to be powered efficiently and completely automatically without operator intervention and without the need for AGV to interrupt the transport for very long loading breaks.

Wireless charging for automatically guided vehicles can be implemented both for AGVs used in industries and for those used in distribution centers or in any other type of activity that involves the handling of goods. The intermediate energy transfer allows the batteries in the AGVs the intermediate charge in order to keep the energy level of the transport-transfer systems at a constant level if it is a busier day in the flow.

The wireless charging process is as follows: when the AGV is positioned next to the charging station (figure 2) the control panel sends a signal to the active coil where an electromagnetic field is created that resonates with the charging unit where another coil is located and then the battery starts charging [5].

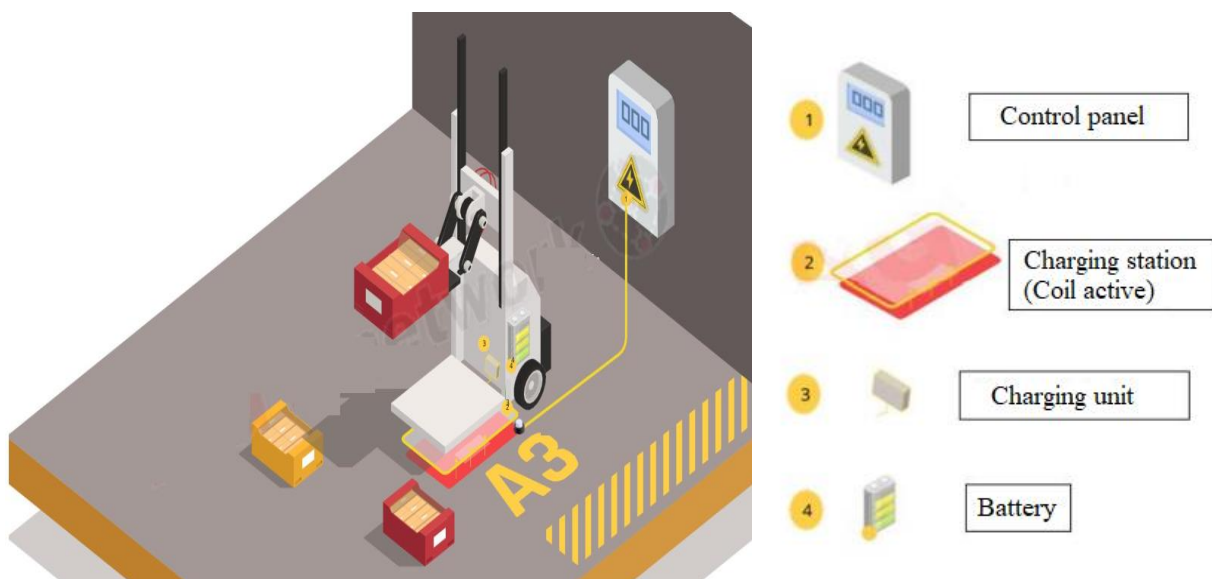


Fig. 2. Wireless charging station

Modernization in the logistics area means automation with wireless charging technologies, which do not require interventions in the infrastructure of the entire warehouse but only on a certain frequently traveled route or at the charging stations that can be placed on the walls or floor. Inductive coil charging systems are much easier to make mechanically because they do not require mechanical contacts, and their maintenance is much easier to achieve and is suitable for long-term continuous use.

The battery and the charging system (figure 3) together form a general solution for power supply and are connected via a CAN interface [6].

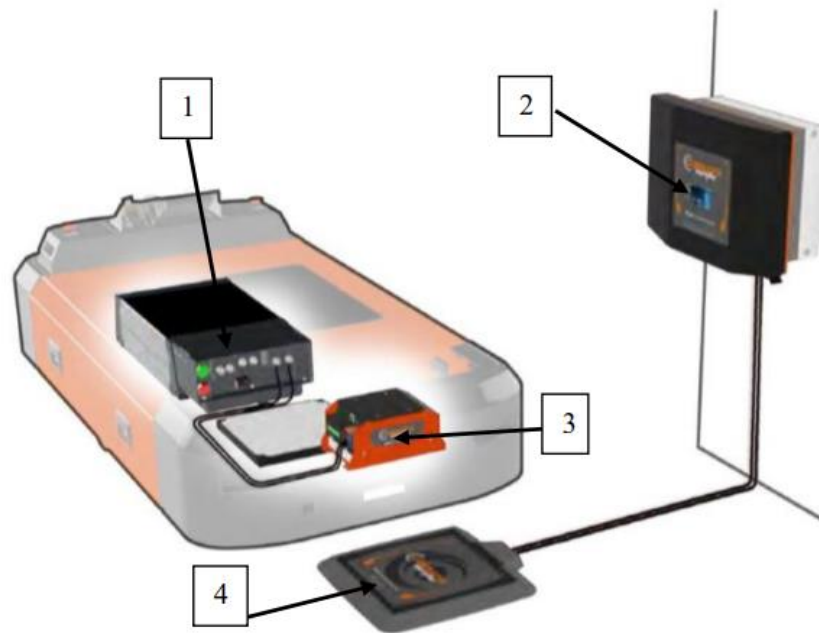


Fig. 3. The basic components of the AGV system and the charging station

The elements presented in figure 3 are: 1 - battery , 2 - HMI / IPS control unit (Inductive Power Supply), 3 - MPU controller (Mobile Power Unit) and 4 - ISP charging station (Inductive Stationary Pad).

The optimal location and distance between the two coils are shown in Fig. 4 where the two pads are highlighted: an inductive mobile pad mounted on the AGV and a stationary pad mounted on the charging station. The power supply converts the power of electricity to a frequency of several thousand hertz and uses the coil in the stationary charging plate to create an alternating field. This field, whose resistance is similar to that of a conventional induction resistor, induces a high frequency alternating current in the coil of the receiver board. The charger then uses this current to charge the batteries.



Fig. 4. Location and distance of the two coils

In the connection structure of the general elements, shown in figure 5, there is as a control unit an HMI interface (IPS) through which the main settings regarding the charging power in the range of 15-80 kw / h and the charging station can be made (ISP) where the active coil creates the electromagnetic field that is transmitted to the charger (IMP) positioned on the structure of the AGV . Within the wireless charging system there is a controller that has the role

of converting the energy required to charge the batteries of the AGV to specific parameters. (MPU) [7].

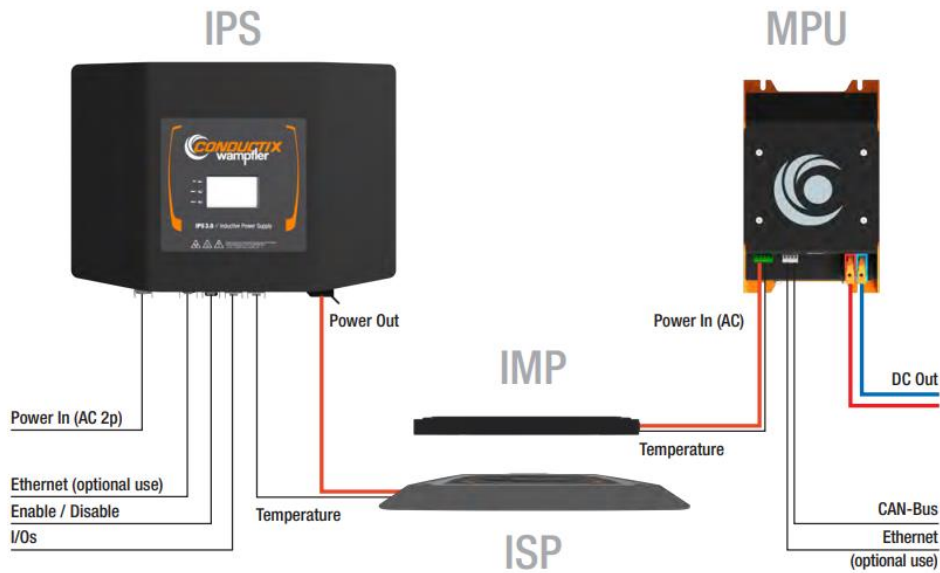


Fig. 5. Connection structure of the general elements

In fig.6. the PLC is connected to the AGV control system (CPU) for real-time monitoring of route changes, various work processes or if there are technical problems related to the operation of the AGV especially in the battery area, even if the batteries are provided with additional protection.

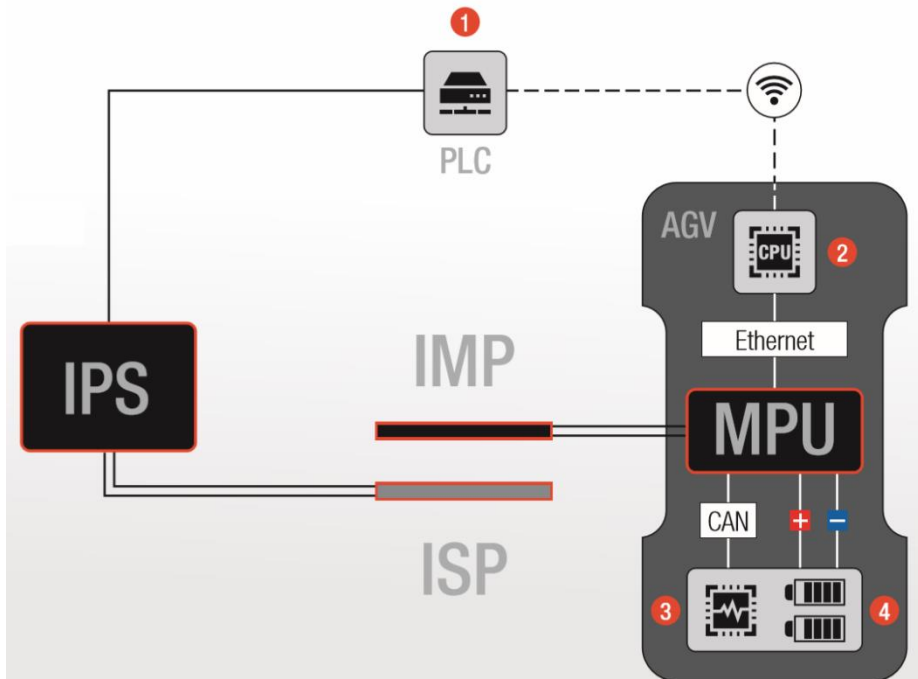


Fig. 6. General architecture of the elements

Electronic power units are required to convert the low-frequency mains current on the stationary side and to provide a stable direct current output to power an automatically guided vehicle [8].

3. Conclusions

The acquisition of AGV type transport-transfer equipment is a rather complex initial investment because it involves very high costs but the depreciation is done in a long time. A detailed analysis must also be performed to understand whether wireless charging can be a real advantage for the needs of the company.

In principle, the investment for automation in the transit area is a feature that is an advantage under certain conditions and depends on the total number of AGVs. For example, if for a logistics system that has 5 AGVs required to perform specific transfer-transport tasks, under the conditions of using wireless charging technology the number of AGVs can be reduced to 3 .

The wireless charging solution for automatically guided vehicles, regardless of the area in which they are used, is better than the traditional charging method, the charging time being considerably shorter and therefore the task fulfillment time is longer.

Although at the beginning the research in the development of the wireless charging solutions of the automatically guided vehicles used for the handling of goods in the production spaces and warehouses, one can notice sufficient advantages offered by the implementation of these new technologies.

4. Bibliography

- [1] <https://www.bollere-logistics.com/en/news/warehouse-automation/>
- [2] <https://www.dmmetalproducts.com/why-is-there-a-need-for-automated-guided-vehicles-agvs/>
- [3] <https://www.wiferion.com/en/products/energy-management-software-fleet-agv-etahub/>
- [4] <https://www.swisslog.com/en-us/products-systems-solutions/transport/agv-automated-guided-vehicles>
- [5] <https://www.agvnetwork.com/wireless-charging-for-agv-and-autonomous-mobile-robots>
- [6] <https://www.conductix.com/en/product-groups/inductive-power-transfer>
- [7]. https://www.google.com/search?q=Wireless+charging+for+AGV+%28Automated+guided+vehicle%29&tbm=isch&hl=en&chips=q:wireless+charging+for+agv+automated+guided+vehicle,online+chips:warehouse:0D47yW6tgWo%3D,online+chips:amr:tsH30eFJunA%3D&rlz=1C1GCEA_enRO873RO873&sa=X&ved=2ahUKEwiDpq2Pp9T3AhVf8LsIHV-AVYQ4lJo&wr
- [8]. https://www.google.com/search?q=AGV+charging+station&tbm=isch&hl=en&chips=q:agv+charging+station,online+chips:autonomous+mobile+robots:mdhuAMQ6Xps%3D&rlz=1C1GCEA_enRO873XAW&A63PsNT3AhVGkaQKHf5wA48Q4VYoAHoECAEQHQ&biw=1519&bih=754#imgrc=5WPArHIEOpNsWM

OPTIMIZING THE LOGISTIC FLOW OF MANUFACTURING KN95 MASKS BY USING MATHEMATICAL CALCULATION METHODS

SEILEANU Floarea-Loredana

Faculty of Industrial Engineering and Robotics, Specialization: Industrial Logistics,
Year of study: Master II, e-mail: seileanu.loredana@yahoo.com

Scientific leader: Conf.dr.ing. **Laurențiu POPA**

ABSTRACT: In this research paper, the optimization of the manufacturing flow of the KN95 protective masks was performed using the Simplex linear mathematical calculation method. The introduction describes the research topic and the proposed objectives to be achieved, after which the current state of research is presented. The next step was to perform the calculations to optimize the logistics flow. The calculations were then compared with the results obtained using a website that performs the calculation using the Simplex method. By performing these mathematical calculations by the Simplex method, the aim of this work was to achieve the goal of maximizing turnover and to diversify the KN95 protective mask models manufactured by the logistics flow.

KEY WORDS: optimization, logistic flow, Simplex.

1. Introduction

The paper main goal is to optimize the logistic manufacturing flow of KN95 masks with the help of the Simplex linear mathematical calculation method. The logistic manufacturing flow of KN95 masks was chosen after a comparison made between 3 different logistic flows.

The Simplex algorithm is a numerical method for solving linear programming problems. The aim of this mathematical calculation method is to achieve the proposed objectives, namely: to diversify the types of KN95 protective masks manufactured by the logistics flow and to maximize turnover.

2. The current stage

2.1. General presentation

Below is a brief presentation of the current state of the logistical flow of manufacturing of KN95 masks.

This automatic protective mask formation line uses ultrasound to automatically make foldable masks. The production line performs several processes, such as: wire feed to the nose, loop welding, folding, forming and cutting, and collected waste. Only one worker is needed to operate this process. [1]

The flow includes the following equipment:

- ✓ Wire supply system;
- ✓ System for stamping the shape of the mask and gluing the layers;
- ✓ Clamping system for gluing the clamps;
- ✓ Folding and mask forming system;
- ✓ Surplus material cutting system;

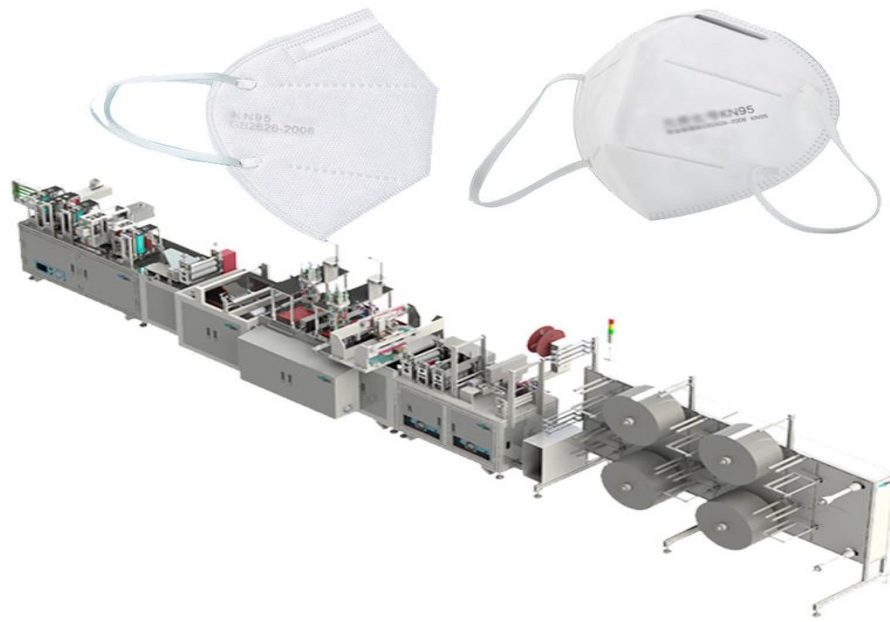


Fig. 2.1. KN95 protective mask manufacturing flow [1]

Flow specifications:

Table 2.1 Technical specifications [1]

Model number	KWKZN95
Equipment size	8539{L}x1318{M}x1985{H}MM
Voltage	200V 50/60 HZ
Capacity	30 – 50 pcs/min
Weight	1600 kg
Work table size	4965 {L}x670{M}x7985{H} MM
Air pressure	1 Pa
Power	8,5 KW
Automatic degree	Automatic
Frequency	50/60 Hz
Ear loop size	Width of 3 – 5 mm

2.2. Modelling, simulation and optimisation of the manufacturing flow

The modelling, simulation and optimisation of the manufacturing flow was made in Witness Horiozon (figure 2.2). After the preliminary simulation was achieved a productivity of 43149 masks in 24 hours.

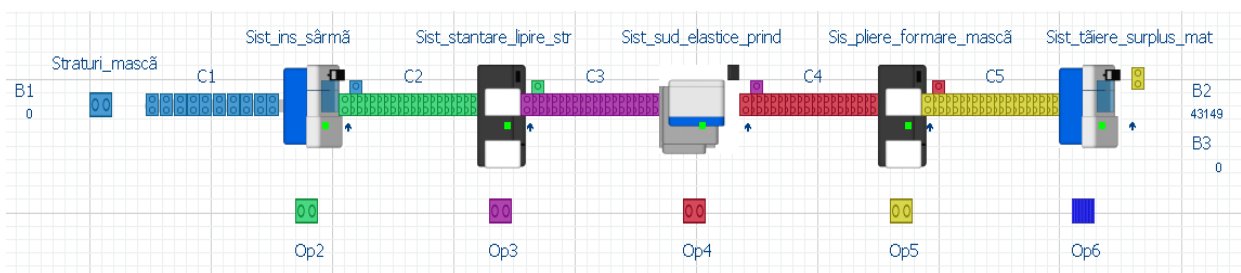


Fig. 2.2. The manufacturing flow before optimisation [2]

After the optimization was achieved a productivity of 71906 masks in 24 hours.

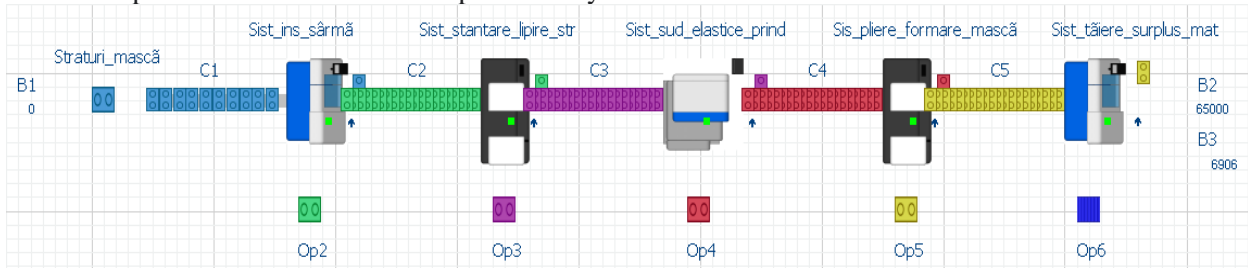


Fig. 2.3. Optimized manufacturing flow

2.3. Project management planning

In figure 2.4 are presented the project phases and activities including the following details: duration, start date, finish date, links between activities etc.

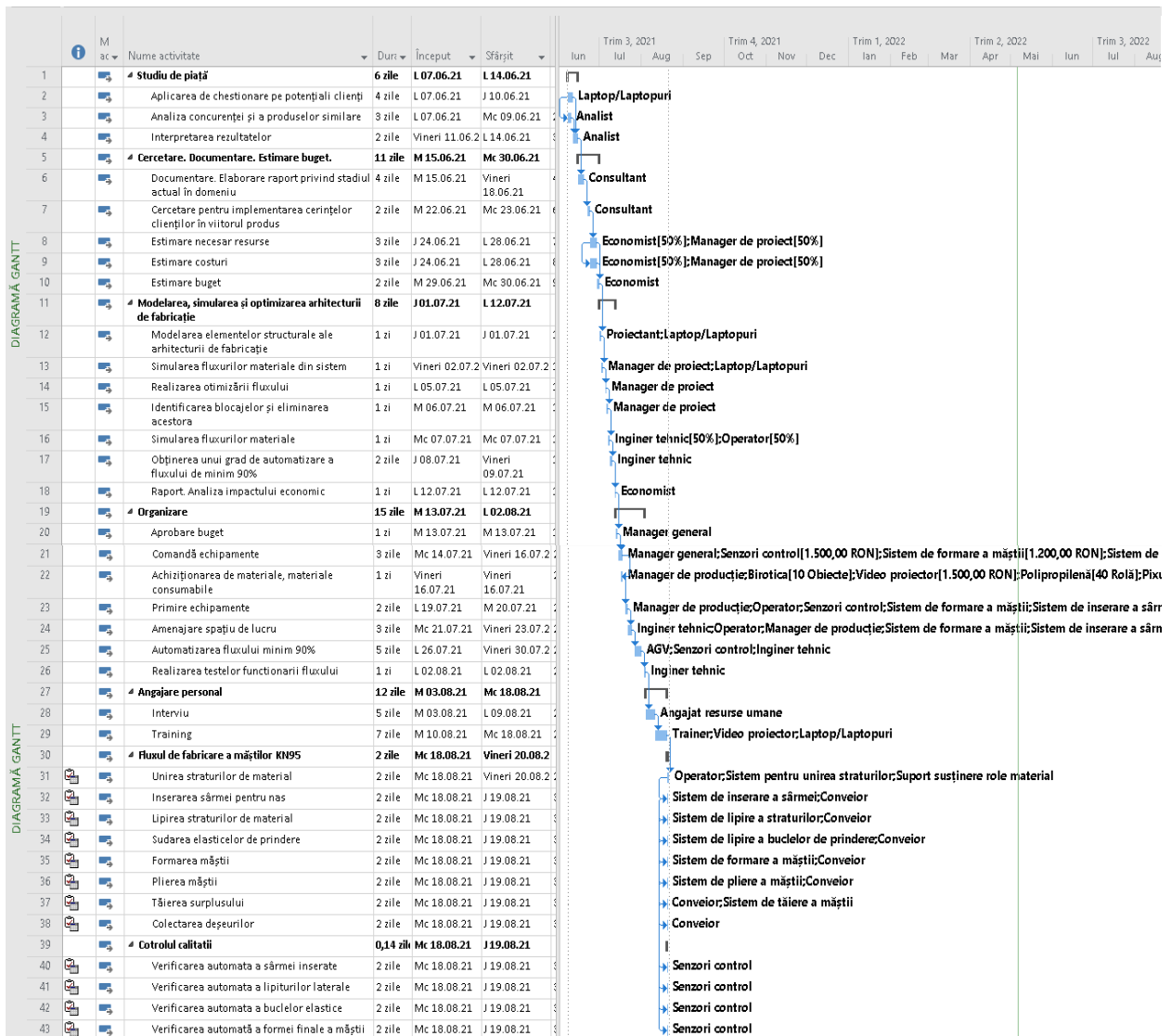


Fig. 2.4. Stages and activities of project management planning

2.4. Automatic quality control for surgical masks using the Vision sensor



Fig. 2.5. Standard image [3]

In figure 2.5 an image with a standard mask is shown after which the inspections for the other masks will be performed.

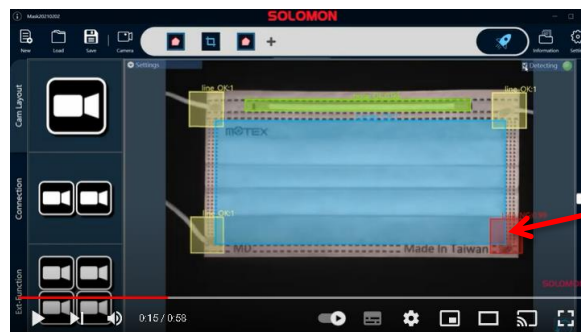


Fig. 2.6. Defective mask (improperly glued elastic) [3]

In figure 2.6. a mask that does not have the elastic band attached to the bottom right is shown.

3. Using the Simplex method to maximize turnover by optimizing the logistics flow

Three models of KN95 face masks are on sale: KN95 face mask (three-layer), KN95 face mask (five-layer) without valve and a KN95 face mask (five-layer) with valve. Given that these masks are mainly for medical use, but also for other people who want to protect themselves against viruses and bacteria, it is expected to sell all the masks manufactured. The price of the face masks is: KN95 protection mask (with three layers) - 4 lei, KN95 protection mask (with five layers) without valve - 7 lei and KN95 protection mask (with five layers) with valve - 12 lei. The only problem is the supply sector, which is limited by four raw materials: cotton filter, polypropylene, elastic band and valves. To make a three-layer KN95 protective mask requires two layers of polypropylene, one layer of filter and two elastic bands, the KN95 five-layer protective mask without valve requires four layers of polypropylene, one layer of filter and two elastics and the KN95 five-layer valve mask requires four layers of polypropylene, a layer of filter, two elastic bands and a valve. Knowing that the stock of polypropylene is 250,000 units, that of cotton filter is 72,000 units, that of elastic clamps is 144,000 units and that of valves is 18,000 units, how many masks must be made of each type, so that turnover is maximized?

Answer:

Note x_1 – the number of KN95 three layers masks, x_2 – the number of KN95 (five layers) masks without a valve and cu x_3 – the number of KN95 (five layers) masks with a valve, and z – turnover.

To maximize the objective function:

$$z = 4x_1 + 7x_2 + 12x_3 \quad (1)$$

With restrictions:

$$2x_1 + 4x_2 + 4x_3 \leq 250000 \quad (2)$$

$$x_1 + x_2 + x_3 \leq 72000 \quad (3)$$

$$2x_1 + 2x_2 + 2x_3 \leq 144000 \quad (4)$$

$$x_3 \leq 18000 \quad (5)$$

$$x_1, x_2, x_3 \geq 0 \quad (6)$$

We convert the model to the standard shape:

$$2x_1 + 4x_2 + 4x_3 + y_1 = 250000 \quad (7)$$

$$x_1 + x_2 + x_3 + y_2 = 72000 \quad (8)$$

$$2x_1 + 2x_2 + 2x_3 + y_3 = 144000 \quad (9)$$

$$x_3 + y_4 = 18000 \quad (10)$$

Turn:

$$x_1 = x_2 = x_3 = 0 \quad (11)$$

And it turns out:

$$y_1 = 250000 \quad (12)$$

$$y_2 = 72000 \quad (13)$$

$$y_3 = 144000 \quad (14)$$

$$y_4 = 18000 \quad (15)$$

Now all the variables are positive:

$$x_1, x_2, x_3, y_1, y_2, y_3, y_4 \geq 0 \quad (16)$$

Table 3.1. Initial table

	4	7	12	0	0	0	0		
	x_1	x_2	x_3	y_1	y_2	y_3	y_4		
y_1	2	4	4	1	0	0	0	250000	0
y_2	1	1	1	0	1	0	0	72000	0
y_3	2	2	2	0	0	1	0	144000	0
y_4	0	0	1	0	0	0	1	18000	0
	-4	-7	-12	0	0	0	0	0	z

In the column indicated by the number 1 arrow are the basic variables. The coefficients of the objective function are written on the highlighted lines, which are indicated by the arrow number 2. In the column highlighted by the arrow number 3 are written the free terms of the restrictions.

Table 3.2. Iteration no. 1 – Stage 1

	4	7	12	0	0	0	0		
	x_1	x_2	x_3	y_1	y_2	y_3	y_4		
y_1	2	4	4	1	0	0	0	250000	0
y_2	1	1	1	0	1	0	0	72000	0
y_3	2	2	2	0	0	1	0	144000	0
y_4	0	0	1	0	0	0	1	18000	0
	-4	-7	-12	0	0	0	0	0	z

The initial solution is not optimal because there is at least one negative value. We choose from the three negative solutions the highest in absolute value (that is, 12). The yellow column is divided by the pivot (green column), namely: 250000: 4 = 62500, 72000: 1 = 72000, 144000: 2 = 72000 and 18000: 1 = 18000.

Of these terms, the smallest is chosen (that is, 18000: 1 = 18000). The row (purple) that contains the smallest element will be the pivot row.

Table 3.3. Iteration no.1 – Stage 2

	4	7	12	0	0	0	0		
	x_1	x_2	x_3	y_1	y_2	y_3	y_4		
y_1	2	4	4	1	0	0	0	250000	0
y_2	1	1	1	0	1	0	0	72000	0
y_3	2	2	2	0	0	1	0	144000	0
y_4	0	0	1	0	0	0	1	18000	0
	-4	-7	-12	0	0	0	0	0	z



The initial pivot lives (y_4)

Tabelul 3.4. Iterația nr.1 – Etapa 3

	4	7	12	0	0	0	0		
	x_1	x_2	x_3	y_1	y_2	y_3	y_4		
y_1	2	4	4	1	0	0	0	250000	0
y_2	1	1	1	0	1	0	0	72000	0
y_3	2	2	2	0	0	1	0	144000	0
x_3	0	0	1	0	0	0	1	18000	12
	-4	-7	-12	0	0	0	0	0	z



y_4 left the table and entered x_3 . With the entry of x_3 instead of 0 in the objective function, the coefficient of x_3 will appear, ie 12.

Divide the line elements with purple at the pivot (ie divide the line elements with purple at 1).

In table 3.5. the results are shown after dividing the elements of the purple line by pivot 1.

Table 3.5. Iteration no. 1 – Stage 4

	4	7	12	0	0	0	0		
	x_1	x_2	x_3	y_1	y_2	y_3	y_4		
y_1	2	4	4	1	0	0	0	250000	0
y_2	1	1	1	0	1	0	0	72000	0
y_3	2	2	2	0	0	1	0	144000	0
x_3	0	0	1	0	0	0	1	18000	12
	-4	-7	-12	0	0	0	0	0	z

In the pivot column, ie the column of x_3 , apart from the element 1 which is the pivot, the rest of the column is completed with zeros.

Only cells in columns that are not colored will be counted.

Table 3.6. Iteration no. 1 – Stage 5

	4	7	12	0	0	0	0		
	x_1	x_2	x_3	y_1	y_2	y_3	y_4		
y_1	2	4	0	1	0	0	-4	178000	0
y_2	1	1	0	0	1	0	-1	54000	0
y_3	2	2	0	0	0	1	-2	108000	0
x_3	0	0	1	0	0	0	1	18000	12
	-4	-7	0	0	0	0	12	216000	z

The calculations in equations (17), (18), (19) and (20) are the results of the arrows in Table 3.5. and are listed in Table 3.6. with each color corresponding to the arrow.

The same calculation method is used for the other cells. (the number 1 below the fraction being the pivot).

$$\frac{2 \cdot 1 - 0 \cdot 4}{1} = 2 \quad (17)$$

$$\frac{4 \cdot 1 - 0 \cdot 4}{1} = 4 \quad (18)$$

$$\frac{0 \cdot 1 - 1 \cdot 4}{1} = -4 \quad (19)$$

$$\frac{250000 \cdot 1 - 18000 \cdot 4}{1} = 178000 \quad (20)$$

$$178000 \cdot 0 + 54000 \cdot 0 + 108000 \cdot 0 + 18000 \cdot 12 = 216000 \quad (21)$$

If there are only ≥ 0 numbers in the last line, the calculation stops. If not, the previous calculation steps are resumed until only positive results are obtained.

Table 3.7. Iteration no. 2 – Stage 1

	4	7	12	0	0	0	0		
	x_1	x_2	x_3	y_1	y_2	y_3	y_4		
y_1	2	4	0	1	0	0	-4	178000	0
y_2	1	1	0	0	1	0	-1	54000	0
y_3	2	2	0	0	0	1	-2	108000	0
x_3	0	0	1	0	0	0	1	18000	12
	-4	-7	0	0	0	0	12	216000	z

As there are still negative values, the procedure is continued. From the two negative values, choose the column with the highest absolute value, ie 7. Then divide the yellow column by the pivot column (green column) (178000: 4 = 44500, 54000: 1 = 54000, 108000: 2 = 54000 and 18000: 0 cannot be divided, the minimum positive is chosen). In this situation y_1 leaves the column (because it gives the positive minimum) and x_2 comes with the coefficient 7.

Table 3.8. Iteration no. 2 – Stage 2

	4	7	12	0	0	0	0		
	x_1	x_2	x_3	y_1	y_2	y_3	y_4		
x_2	0,5	1	0	0,25	0	0	-1	44500	7
y_2	0,5	0	0	-0,25	1	0	0	9500	0
y_3	1	0	0	-0,5	0	1	0	19000	0
x_3	0	0	1	0	0	0	1	18000	12
	-0,5	0	0	1,75	0	0	5	527500	z

The purple row is divided into pivots, ie 4, which is circled in Table 3.7. and enter the values in Table 3.8 .. Then make the calculations for the other cells in the columns that are not colored and also enter in Table 3.8. The calculations are performed as in Table 3.5. who has equations (17) \rightarrow (21), only now the pivot is 4 instead of 1. As there is still a negative value, continue the procedure.

Table 3.9. Iteration no. 3 – Stage 1

	4	7	12	0	0	0	0		
	x_1	x_2	x_3	y_1	y_2	y_3	y_4		
x_2	0,5	1	0	0,25	0	0	-1	44500	7
y_2	0,5	0	0	-0,25	1	0	0	9500	0
y_3	1	0	0	-0,5	0	1	0	19000	0
x_3	0	0	1	0	0	0	1	18000	12
	-0,5	0	0	1,75	0	0	5	527500	z

Being the only negative value left, the column of x_1 will be taken. Divide the yellow column by the green pivot column (44500: 0,5 = 89000, 9500: 0,5 = 19000, 19000: 1 = 19000, 18000: 0 - cannot be divided). The minimum positive is chosen, in this situation having two equal results, we take the first minimum positive result from the column. Thus y_2 leaves the column and x_1 comes with the coefficient 4.

Table 3.10. Iteration no. 3 - Stage 2

	4	7	12	0	0	0	0		
	x_1	x_2	x_3	y_1	y_2	y_3	y_4		
x_2	0	1	0	0,25	-1	0	-1	35000	7
x_1	1	0	0	-0,5	2	0	0	19000	4
y_3	0	0	0	0	-2	1	0	0	0
x_3	0	0	1	0	0	0	1	18000	12
	0	0	0	1,5	1	0	5	537000	z

The purple row is divided into pivots, ie 0.5, which is circled in Table 3.9. and the values will be entered in Table 3.10. After which the calculations are made for the other cells in the columns that are not colored and are also entered in Table 3.10. The calculations are performed as in Table 3.5. which has equations (17) → (21), only now the pivot is 0.5 instead of 1.

Because there are no more negative values on the last row of table 3.10. the calculation stops and this solution is the optimal one. From the calculation it results that, in order to have the maximum turnover, ie $z = 537,000$ lei, $x_1 = 19000$ (pieces), $x_2 = 35000$ (pieces) and $x_3 = 18000$ (pieces).

The calculations previously performed by the Simplex method can also be done with the help of a website called "pncalculators.com", which provides the calculation by the Simplex method.

Below will be presented images with the calculations resulting from this website, in order to compare and verify the correctness of the results obtained from the mathematical calculation.

Simplex Method Calculator - Free Version

Objective Function:
Maximize: $Z = 4x_1 + 7x_2 + 12x_3$

Subject to:

- $2x_1 + 4x_2 + 4x_3 \leq 250000$
- $1x_1 + 1x_2 + 1x_3 \leq 72000$
- $2x_1 + 2x_2 + 2x_3 \leq 144000$
- $0x_1 + 0x_2 + 1x_3 \leq 18000$
- $x_1, x_2, x_3 \geq 0$

Fig. 3.1. Objective function and restrictions [4]

Iteration 3

Table 4	C_j	4	7	12	0	0	0	0	
C_b	Base	x_1	x_2	x_3	s_1	s_2	s_3	s_4	R
7	x_2	0	1	0	1/2	-1	0	-1	35000
4	x_1	1	0	0	-1/2	2	0	0	19000
0	s_2	0	0	0	0	-2	1	0	0
12	x_3	0	0	1	0	0	0	1	18000
	Z	0	0	0	3/2	1	0	5	537000

The optimal solution is $Z = 537000$

$x_1 = 19000, x_2 = 35000, x_3 = 18000, s_1 = 0, s_2 = 0, s_3 = 0, s_4 = 0$

Fig 3.2. Iteration no. 3 [4]

4. Conclusions

The Simplex method has the advantage of being a versatile method, which can be used to solve any problem, the conditions of which are written in the form of a system of equations and inequalities.

In conclusion, with the help of the Simplex mathematical calculation method, it was possible to diversify the types of KN95 protective masks manufactured and to maximize the turnover at over 530,000 lei for 24 hours of work.

5. Bibliography

1. <https://www.kinwah-group.com/kn95-face-mask-machines.html>
2. Seileanu Floarea-Loredana – Scientific reserch project 2
3. <https://www.youtube.com/watch?v=2udYXIrQyKI>
4. <https://www.pncalculators.com/simplex-method-calculator/>

EXPERIMENTAL RESEARCH ON THE CONTROL OF A CNC AXIS ACTUATED THROUGH A STEP ENGINE

ROTARU Dragos¹, ENACHE George¹, COCIAȘU Cosmin²

¹Faculty of Industrial Engineering and Robotics, Specialization: Digital Production Systems, Year of study: III, e-mail: rotarudragos89@gmail.com

²Faculty of Industrial Engineering and Robotics, Specialization: Industrial Logistics, Year of study: III

During this research, the operation of the engine commanded with sequential strategies was studied. In this case MOV (021) commands are used which transfers a data word to the specific word and the ACC function (888) emits pulses to the specified output port at the specific frequency using the specified acceleration and deceleration speed. (The acceleration rate is the same as the deceleration rate.) It is possible to position independently or control the speed constantly. For positioning, ACC (888) is used in combination with PULS (886). ACC (888) can also be performed during pulse output to change the target frequency or acceleration / deceleration rate, allowing a smooth (sloping) change of speed

KEYWORDS: Stepper Motor, CNC Machine, PLC Programming, Microcontroller

1. Introduction

Recently, electric drive systems with stepper motors have developed more and more, due to the wide fields of use, but also due to technological advances in power electronics and microelectronics.

The most important areas of use are the peripheral and internal equipment of computers, such as printers, plotters, Floppy Disk, DVD RW, but also machine tools, robotics. Stepper motors (MPP) can be controlled by a numerical control in the open circuit due to increased accuracy and resolution.

The research focuses on the control of a numerically controlled axis driven by a stepper motor (MPP).

2. Current state of research

Technological developments in the field of electronics, especially mobile products, have led to the need for the emergence of machines for planting electronic parts on plates, those for automatic processing of metal parts, etc. Most of these machines are numerically controlled and contain high-precision moving parts. The operation of these machines is carried out with the help of DC motors, stepper motors, synchronous motors. Of these, stepper electric motors are the most common. DC motors have begun to be replaced by stepper electric motors (MPP) with the development of stepper motor control (MPP) techniques.

By sequentially supplying the motor phases with DC pulses, a discrete rotating magnetic field appears between the stator and the rotor. At the frequency guaranteed by the manufacturer, the rotor maintains its synchronism between the discrete movements and the discrete magnetic field in the air gap [2]. [3]. The electromagnetic torque of the stepper motor is triple [4], unlike that of the synchronous motor which is approximately constant. The rotational speed is given by the frequency of the voltage pulses applied to the phases in the case of the stepper motor. The electromotive voltage induced in the phases of the hybrid stepper motor, in the case of generator operation, is sinusoidal as in the case of synchronous motors. This is very important because the stepper motor with permanent magnets / hybrid can be modeled as a synchronous motor with permanent magnets with a number of pole pairs equal to the number of rotor teeth [5].

This research presents a classification of stepper motors, the components of a stepper motor and the open loop control of a CNC axis.

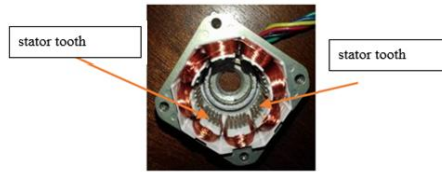


Fig. 1. Internal construction of a stepper motor (laboratory motor).



Fig. 2. Rotor of a hybrid stepper motor (laboratory motor).

3. Stepper motor classification

Because these engines have undergone a number of changes over time, a classification has been made according to the following criteria [1], [3]: by number of phases: Single phase MPP, Two-phase MPP, MPP with 3 or more phases, by rotor material and geometry: MPP with variable reluctance, MPP with permanent magnets, MPP hybrid, according to the shape of the rotor, MPP with disc rotor, MPP with cylindrical rotor by supply voltage type: MPP supplied with unipolar voltage, MPP powered by bipolar voltage.

4. Engine control system programming

Design and construction of an axle controlled by a stepper motor. In this research we will use a stepper motor that will be set in motion with the help of an OMRON CP1E controller, an MA860H driver and two inductive sensors to determine the **torque stroke**. Figure 3 shows the electrical connections.

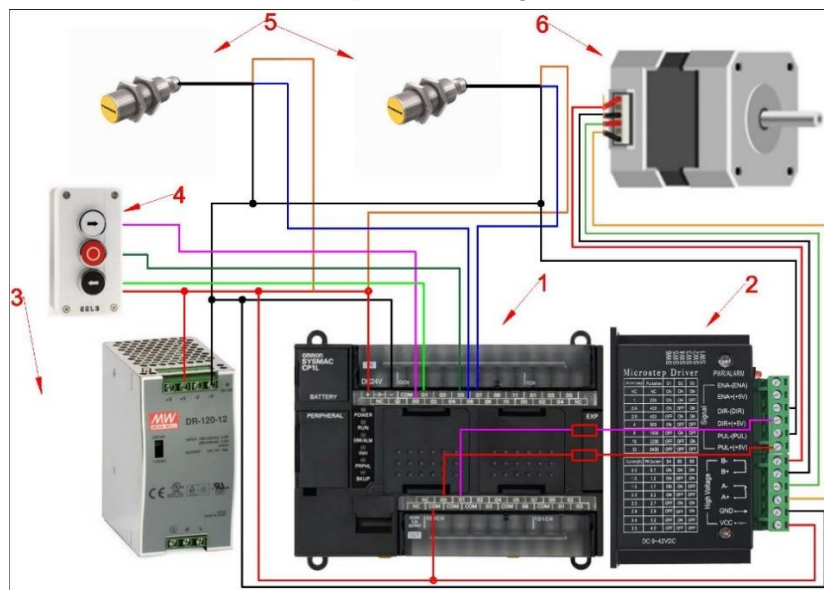


Fig. 3. Electrical connections

The components shown in figure 3 are: 1 - PLC, 2 - Stepper Motor Driver, 3 - Power Supply, 4 - Control Panel, 5 - Inductive Sensors, 6 - Stepper Motor.

As a first step, we use the CX ONE software from OMRON to develop the source code fig.4. After the source code is tested it will be transmitted to the PLC programmable controller.

The program used to operate the test platform highlights the cyclic movement of a mobile element operated by a stepper motor by means of a belt drive. The moving distance of the moving element is determined by two inductive sensors. The stepper motor operates after a well-defined cycle fig.5 with an acceleration and deceleration rate of 10 pulses at an interval of 10 ms until it reaches a target frequency of 4000 pulses. The program can be stopped at any time from the STOP button and resumed the cycle by pressing the left or right scroll button.

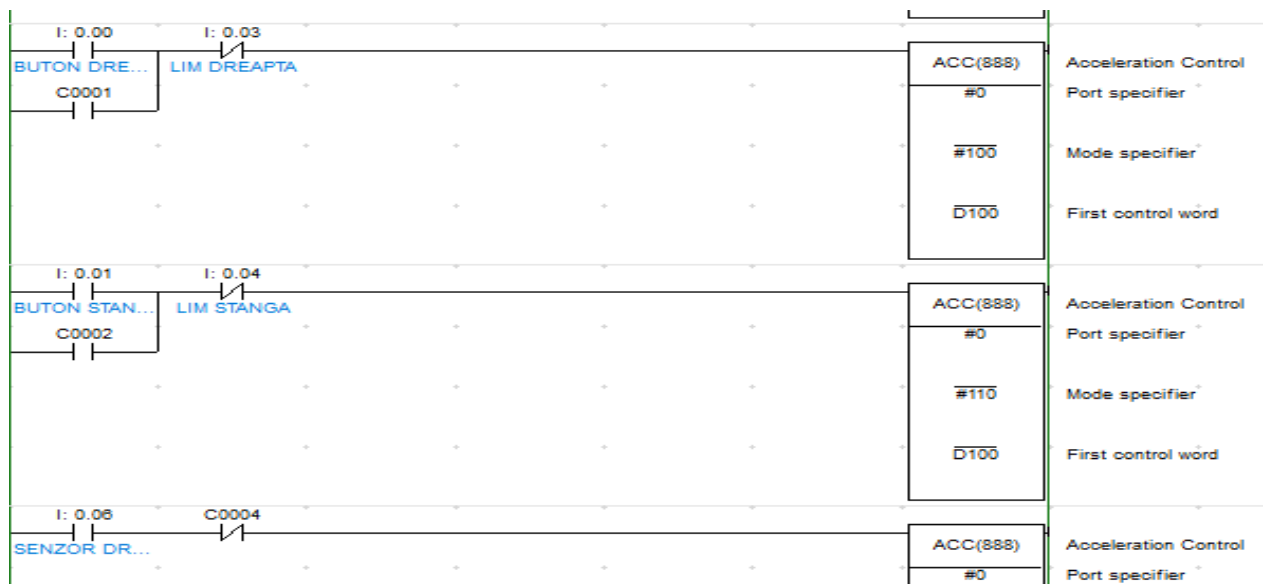


Fig. 4 Source code

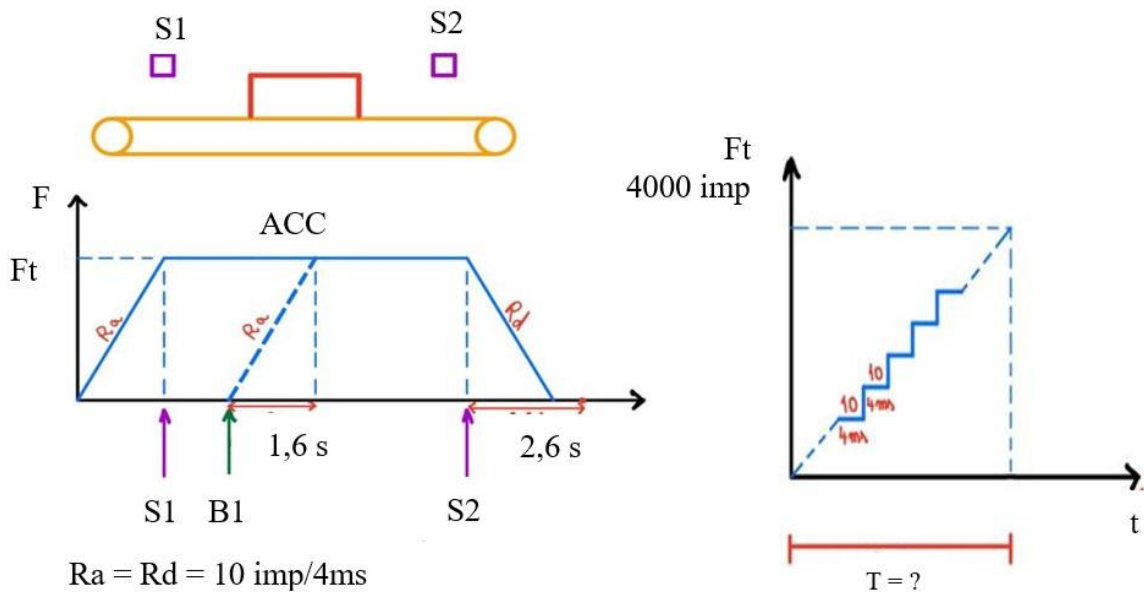


Fig. 5. Operation diagram

$$\frac{Ft}{Ra} = \frac{4000}{10} = 400 \text{ imp}$$

$$T = 400 \times 4 = 1600 \text{ ms} = 1,6 \text{ s}$$

When the B1 button is pressed, the ACC function starts to generate pulses with the acceleration rate Ra of 10 pulses every 4 milliseconds until the target frequency Ft is reached, this lasts 1.6 seconds, when the Ft frequency is reached, it continues its movement to the sensor S2 which triggers the deceleration with the same deceleration rate 10 imp / 4ms, after which it stops for a second and resumes the cycle in the opposite direction.

5. Starting and testing the platform

The start of the test platform can be achieved by means of three physical buttons B1 (start to the left), B2 (start to the right) and the STOP button that stops the platform regardless of its position (Figure 6).

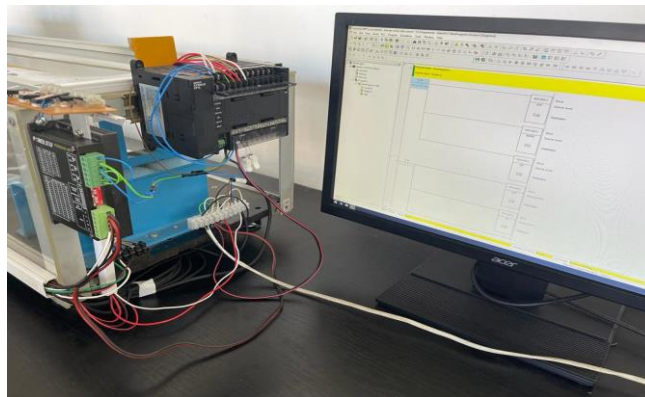


Fig. 6. Testing the platform

6. Conclusions

The construction of stepper motors has been described. A classification of these motors has been made according to several criteria such as: number of phases, geometric construction of the motor, rotor shape and polarity of the supply voltage. An open loop control study was performed. The electrical connections between the stepper motor, the driver and the OMRON controller were made.

Bibliography

- [1] A. Morar și Csaba Szasz, *Motorul pas cu pas în acționări electrice*, Târgu-Mureș: Editura Universității "Petru Maior", 2004.
- [2] A. Kelemen și M. Crivii, *Motoare pas cu pas*, București: Editura Tehnică, 1975.
- [3] B. Kuo, A. Kelemen, M. Crivii și V. Trifa, *Sisteme de comanda și reglare incrementală a poziției*, București: Editura Tehnică, 1981.
- [4] **G. Mihalache**, A. Zbanț (Adam) și G. Livint, „Open-Loop Control of Hybrid Stepper Motor with two phases using Voltage to Frequency Converter,” în *8 th International Symposium in Advanced Topics on Electrical Engineering (ATEE)*, Bucharest, 2013 (Indexată ISI Web of Science).
- [5] S. Ali și B. Mehdi, „Investigation of the micro-step,” *Mechatronics*, pp. 1175-1185, 2005

COLOR ANALYSIS AND PIGMENTS TECHNOLOGY IDENTIFIED FOR PRINTING ROMANIAN POSTAL STAMPS

PĂUNESCU Mihai

Facultatea: IIR, Specializarea: TSP, Anul de studii: II, e-mail: mhpaunescu@yahoo.com

Conducător științific: Conf. dr. ing. **Emilia BĂLAN**

ABSTRACT: The paper deals with the analysis of colors and pigment technology identified in the printing of Romanian postal stamps. A brief history of the pigments used to print postal stamps is provided. The presented methods are a novelty in the philatelic field, wanting to create a connection between the world of scientists and that of collectors (terminology, technique, PC). Most of the research done so far is based on the study of colors.

KEYWORDS: pigments, ink, color, color system, postal stamps.

1. Introduction

Ink is the classic material traditionally used for writing, that is, for recording graphic signs on media suitable for writing texts. Any type of ink is a mixture of ingredients in which two categories of main components are distinguished, namely, basic components and secondary components. The basic components are dye or pigment, liquid medium and binder. The dye or pigment is the fundamental writing element. It determines the characteristic color of the ink. Pigments are the colored materials in the composition of the ink. In this respect, a clarification is needed: there are dyes and pigments themselves.

A substance appears colored when the light it reflects or transmits lacks radiation of certain wavelengths and, as a result, the spectra show absorption bands. These are due to the presence in the molecule of groups of atoms called chromophores. Natural dyes dissolve in various liquids while the actual pigments of natural origin are colored materials insoluble in water or solvents. The liquid medium, also called solvent or, as the case may be, dispersion medium, is the substance in which the dye is dissolved or the insoluble pigment is dispersed. The amount of liquid in an ink is proportional to the writing instrument and the writing medium. The most common liquid media for the preparation of inks have, over time, been water and oils.

The binder is usually a substance or adhesive that ensures the stability of the pigment dispersion, improves the fluidity of the inks and ensures their fixation on the substrate during writing and after drying. The most used binders were vegetable glues (gum arabic, cherry glue, resin glue, starch, honey, sugar) and animal glues (gelatin, egg white, fish glue). Synthetic glues have been used in recent decades.

The paper deals with the analysis of colors and pigment technology identified in the printing of Romanian postal stamps. A brief history of the pigments used to print postal stamps is provided. The presented methods are a novelty in the philatelic field, wanting to create a connection between the world of scientists and that of collectors (terminology, technique, PC). Most of the research done so far is based on the study of colors.

2. State of the art

Inks are classified according to several criteria: durability, color, application procedure. Durability or stability over time divides the inks into stable inks that have a good behavior over time, good resistance to environmental factors and a neutral character in relation to the graphic support on which they are applied and unstable, water-sensitive inks, to light etc.

The color divides these preparations into black inks, colored inks, and invisible inks.

Carbon ink or soot ink is the oldest known type of ink in history.

Fig. 1 shows a study made by Professor Dr. Adrian Marian on pigments used in Romania (prehistory -1900). The area of interest of the study pigments is between 1858 and 1900.

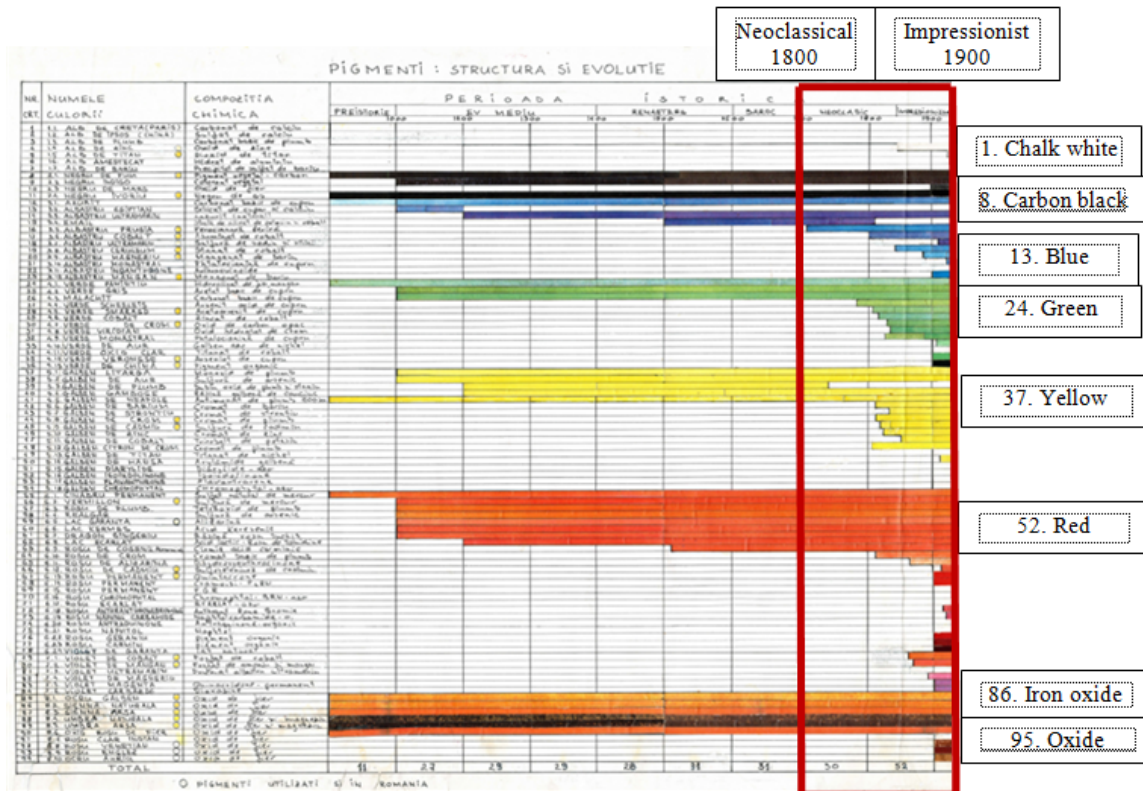


Fig. 1. Pigments - evolution from prehistory to 1900 [6]

For the traditional preparation of this type of ink, proceed as follows: collect and dry some spherical plant formations called scabies that usually grow on the back of oak leaves but also on the leaves of other plant species in Europe, Asia and North Africa.

The pigments used are of a very wide variability. Their main feature is that, unlike dyes, they are not soluble in water and had to be prepared in the form of dispersions. These pigments were originally obtained by processing colored earths: iron oxide (red), lead red or minium, cinnabar or chinovar called vermilion (red mercury sulfide), white zinc (zinc oxide), lapis lazuli blue), wax (white pigment, basic lead carbonate), chalk, azurite (azure blue, basic copper carbonate).

Other pigments were also used for the red color: minium (lead), alizarin (dihydroxy-anthraquinone), glitter (trihydroxy-anthraquinone), guar (extracted from Rubia tinctorum roots), carminic acid (a trihydroxymethyl-anthraquinone glucoside).

Fig. 2 shows the Colors Circle 54 - SCR 5959 which shows the main shades of colors according to the Romanian standard. The first printing inks were made of soot (carbon black) and were used to dye the wooden plates on which the printing text was engraved. There is a wide variety of printing inks depending on the pigment or dye used, the type of varnish and the purpose for which they were made. Black printing inks, generally based on carbon black, have good durability over time.

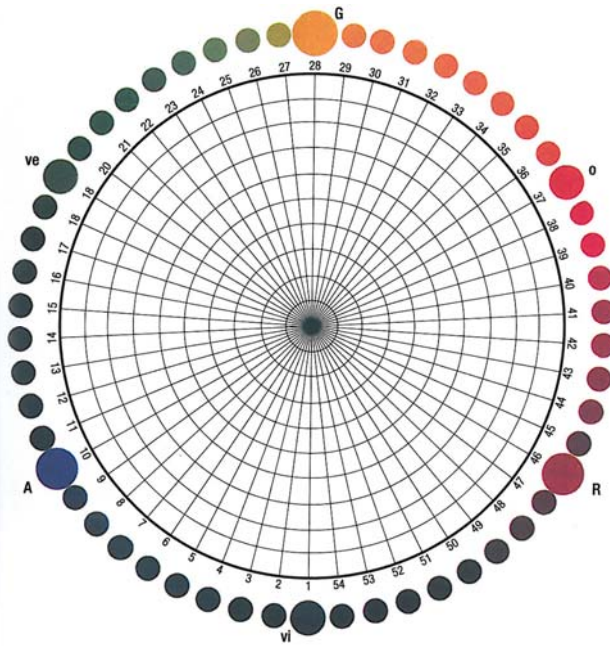


Fig. 2. Colors Circle 54- SCR 5969 [8]

The Michael Color Guide is used to identify the colors of stamps in Germany, using the pigments from that country [2] in accordance with the current standard. The color palette has a hole with a diameter of 5 cm where the stamp is placed (Fig. 3).

In Fig. 4 shows the color model used by X-Rite to calibrate the devices.

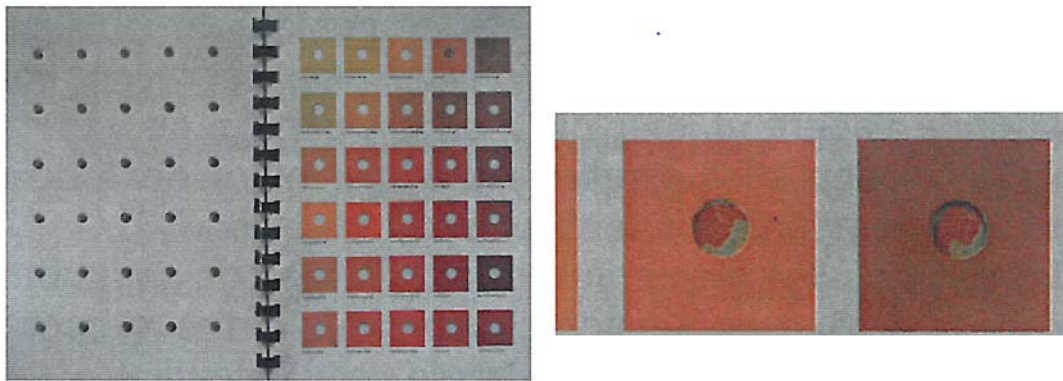


Fig. 3. Color card (left), stamp color identification (right) [1]

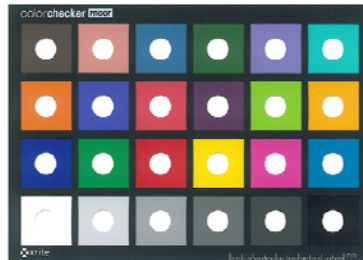


Fig. 4. X-Rite color palette

3. Case study

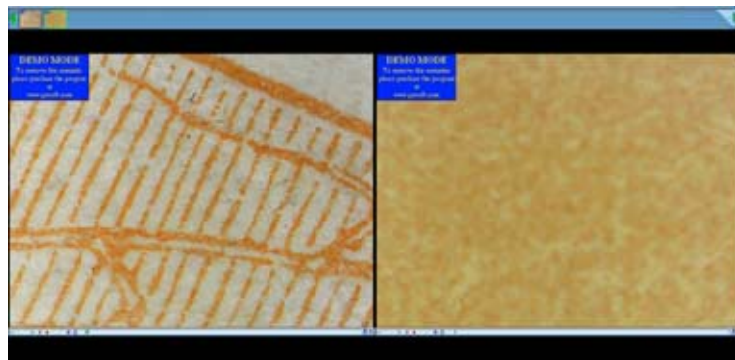
Papers of value such as banknotes, stamps, personal documents etc. are typographical products which are executed using special technologies which should ensure their protection against forgery. It is necessary to analyze the postal stamps as widely as possible, because in Romania no scientific studies have been carried out, no regulations have been established for color cataloging or for the detection of forgeries. It must establish the basis for stamping the stamp, the color and positioning in order to measure the stamps, their scientific cataloging.

This paper aims to analyze the pigments used in Romania until 1900. For this purpose I proposed two working methods.

Method I of color determination used a duplex microscope with calibrated devices for researchers and for people who have financial possibilities (microscope, laptop, high performance software) as it is shown in Fig. 5. The duplex microscope was designed and executed during the research by the author. This contains two digital microscopes mounted in parallel which can move simultaneously on the Oz axis and an adjustable and graded support for positioning the samples on the Ox and the Oy axes. The microscopes are calibrated from an optical and spectral standpoint at the beginning of the study based on the imposed tolerances. The visual field of the microscopes is illuminated in a controlled manner according to a standard light source, to properly ensure the correctness and consistency of the measurements [8].



a) the designed comparator device



b) Color stamp (4B) digital microscopes I and II

Fig. 5. Duplex microscope

Method II - I set out to create a Romanian Chromatic Circle, using the SCR 5969 model (its colors). This method is intended for philatelists who do not have modern technology.

The Chromatic Circle (Colors Star) is a creation of Johannes Itten [7] and consists of the following colors: primary colors + secondary colors + tertiary colors (Fig. 6). The primary colors are red, yellow and blue. The secondary colors are made by combining primary colors: red + yellow = orange; yellow + blue = green; blue + red = purple. The tertiary colors are created by combining a primary color and an adjacent secondary color: red + orange = orange-reddish; red + purple = purple-red; blue + purple = indigo; blue + green = turquoise; yellow + green = green-yellowish; yellow + orange = gold.

Based on the color samples printed with Romanian pigments, I made colorimetric measurements, I mounted gradations for each color, 12 segments, I managed to design a color palette, which is shown in Fig. 7 for primary colors and in Fig. 8 for secondary colors.

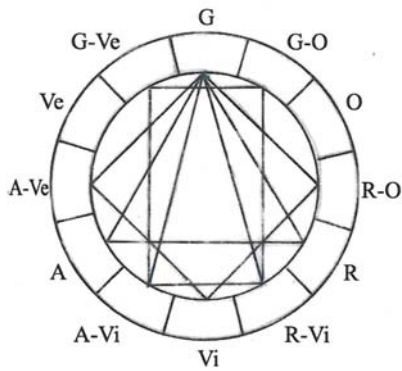


Fig. 6. Chromatic Circle (Colors Star)

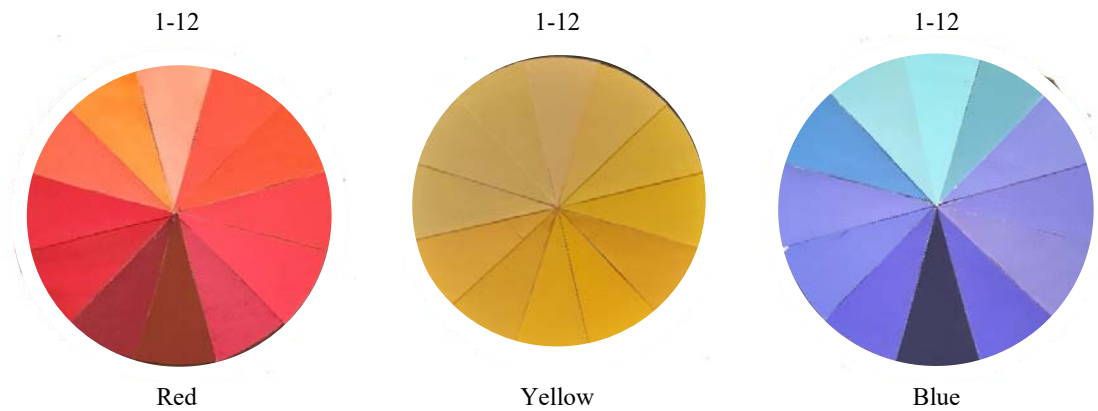


Fig. 7. Primary colors

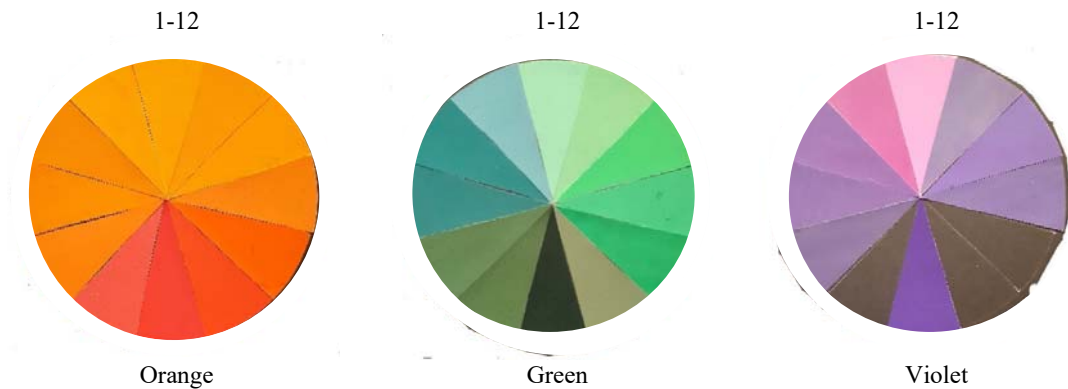


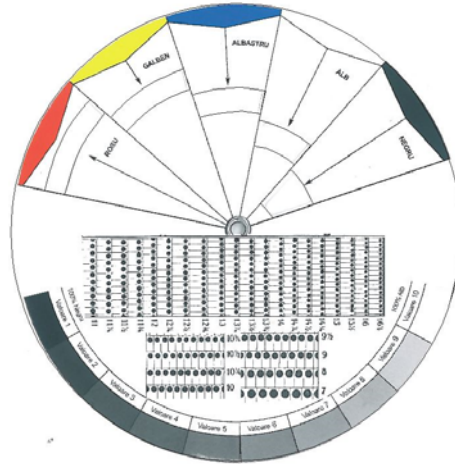
Fig. 8. Secondary colors

Fig. 9 shows the Romanian Chromatic Circle proposed by myself. By superimposing Face I and Face II, the Romanian Chromatic Circle is obtained. By rotating the two circles, the approximate color of the identified one is obtained.

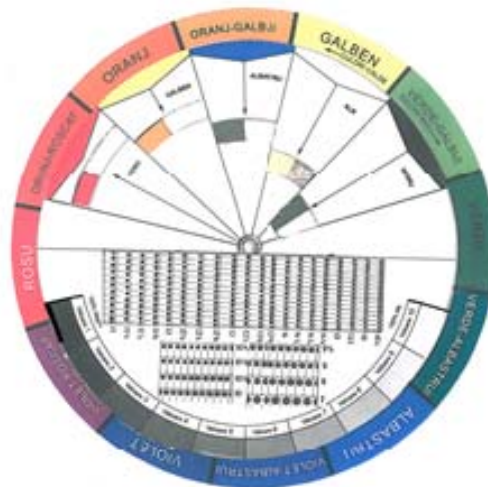
Fig. 10 presents the series “Wheat spike” published in 1893/1898: 1 Money - brown; 1 ½ Money - black; 3 Money - reddish brown; 5 Money - blue; 10 Money - green; 15 Money - red; 25 Money - purple; 40 Money - green-blue; 50 Money - orange; 1 Leo - light brown and pink; 2 lei - orange and brown.



a) Romanian Chromatic Circle 5969 (face I)



b) Romanian Chromatic Circle 5969 with ondotometer (face II)



c) Romanian Chromatic Circle 5969

Fig. 9. Romanian Chromatic Circle 5969 opened



Fig. 10. King Carol I - "Spic de grâu" with watermark PR -II, III, IV, V (1893)

Fig. 11 represents the Romanian Chromatic Circle in which I positioned the stamp from the "Wheat Ear" series published in 1893/1898 by 3 Money - reddish-brown which was compared to the color obtained from the circle. The resultant is correct.

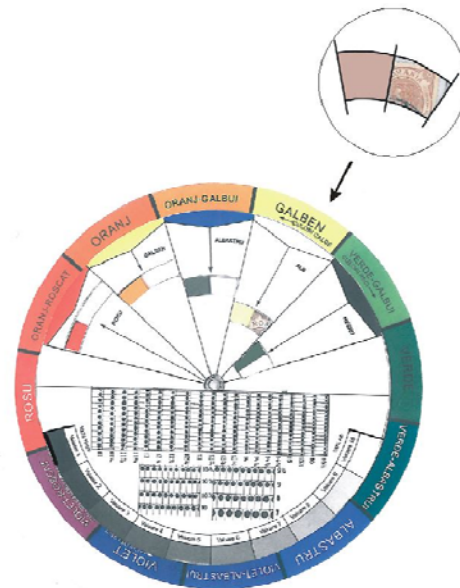


Fig. 11. Romanian Chromatic Circle 5969

4. Conclusions

Papers of value such as banknotes, stamps, personal documents etc. are typographical products which are executed using special technologies which should ensure their protection against forgery.

The work presents a characterization of the Romanian postal stamps "Wheat Spike" which come from the personal collection of the author in order to propose a method of identifying pigments to identify colors on stamps printed until 1900.

The use of color standards (SCR 5969) is necessary to establish the cataloging of the colors of the stamps, the colors assumed by the collector are now mentioned in stamp documentation.

It is necessary to analyze the postal stamps as widely as possible, because in Romania no scientific studies have been carried out, no regulations have been established for color cataloging, for the detection of forgeries and legislation to apply future regulations.

The subject must establish the basis for stamping the stamp, the color and positioning in order to measure the stamps, their scientific cataloging.

Scientific studies in Europe are carried out by highly qualified people, at a higher level than collectors, who cannot interpret the results of research (Method I).

The solution (Method II) is the use of the Romanian Chromatic Circle (SCR 5969) for philatelists who do not have the technology and method I.

Based on the color samples printed with Romanian pigments, I made colorimetric measurements, I mounted gradations for each color, 12 segments, I managed to design a color palette, named Romanian Chromatic Circle 5969. By rotating the two circles from face I and face II, the color of the postal stamp is obtained. The stage of making and measuring color samples printed with Romanian pigments is very important. High-performance printing and measuring equipment was used.

5. References

- [1]. I. Poiana, *Falsuri și contrafaceri în filatelie*, Editura Alma Mater, Sibiu, 2006, ISBN 978-973-632-276-1.
- [2]. Adrian M.M., *O istorie a ordonării culorilor*, Editura Artpress, 2011, Timișoara, ISBN 978-973-108-228-8.
- [3] Adrian M.M., *Culoare, număr, armonie*, Editura Artpress, 2007, Timișoara, ISBN 978-973-108-226-4.
- [4] Williams, L.N., *Fundamentals of Philately 1990*, Printed in USA, ISBN 0-933580-13-4.
- [5] Michel - Europa-Katalog 2007/2008, ISBN 978-3-87858-855-9.
- [6] <https://romanianstampnews.blogspot.com/2013/02/despre-culori-in-filatelie.html>
- [7] J. Itten, *Arta culorii*, ISBN 9786068977300.
- [8] M. Păunescu, M. Marusciac, E. Bălan, *Color analysis and technological errors identified in printing of Romanian postal stamps*, Annals of the Academy of Romanian Scientists, Series on Engineering Sciences, Vol. 13, Iss. 2, pp. 63 - 77, Ed. AOSR, ISSN 2066 – 8570, București, 2021.

AERODYNAMIC ANALYSIS OF THE FUSELAGE OF A FIXED WING AIRCRAFT TYPE UAV USING THE FINITE ELEMENT METHOD

Second lieutenant engineer Cătălin CUCU

Faculty of Industrial Engineering and Robotics, Master: Conception Intégrée de Systèmes Technologiques, 1st Year of study, e-mail: ionut.cucu@mta.ro

Scientific coordinator: Prof. PhD. Eng. Cristina PUPĂZĂ

ABSTRACT: Nowadays the unmanned aerial vehicles are employed on a large scale, from military to industry implementations, from battlefields to smaller units that people may be play outdoor. The military industry drones recorded an exponentially growth worldwide since '90s. They are used in missions that are dangerous for humans and can stay in the air for a large period of time. The UAVs have a complex cross-section shape of the fuselage. This paper explores the aerodynamic consequences of its shape, at the operational flight ceiling, in a comparative approach, using Computational Fluid Dynamics (CFD).

KEYWORDS: aerodynamic, CFD, UAV, fuselage, Spalart-Allmaras.

1. Introduction and state of art

The unmanned aerial vehicles (UAV) have touched a level of development without precedent and spread throughout the world massively. In the next twenty years they will take control on the battlefield. From a strategic point of view, from 1997 the United States of America published a long-term development plan, which was later modified so that one can talk today about a hierarchy of UAVs according to the destination, battlefield response capabilities and the conventional level of operation [1].

One of the first applications of an UAV was in the first Gulf War. In Iraq, eight years later, the allied forces employed three UAVs for surveillance and aerial research of the battlefield [1], [2]. Afghanistan was another battlefield where three UAVs RQ-1 Predator were used, but their mission was only combat and surveillance. The U.S. Army analysis showed that in 2006, 46% of the UAVs capacity requirement was not accomplished, especially with the correct location of the ground target acquisition and the precision of the attack.

The purpose of this study is to examine the status of the technological development in the domain and to make a comparison of the different types of designs. Drones are conceived and manufactured according to their mission and can perform some of the following tasks [1], [3], [4], [5]:

- Surveillance - representing the process of monitoring humans, objects, or processes behavior, to be compared to the expected or required norms (for example detecting chemical, biological or nuclear activities or phenomena).
- Reconnaissance - represents the scan or inspection of an area to obtain information.
- Insertion - is the activity for load delivery in specific areas for example weapons airdropping (not necessarily lethal), electronic war actions and target destruction actions. The electronic war actions can have two characteristics: the attack against the enemy, for the electronic jamming or by high energy weapon bombing of the convoys, and the protection of their own and allied communications, equipment, or objectives.
- Target - represented by an UAV that can be used to replicate a fighter aircraft or a missile in the following purposes:
 - a. Training for operators, in this case the UAV being considered as a practical target
 - b. Reproduce an aerial vehicle to take advantage of the surveillance devices of the enemy, in this case being used as a trap.

UAVs could be classified depending on the action range/altitude and as agreed within some industry events in [1]:

- handheld UAV – 600 m altitude and action range of about 5 km.
- close range UAV – 1500 m altitude and action range of about 10 km.
- NATO – 3000 m altitude and the action range of about 50 km.
- tactical (TUAV) – 5500 m altitude and action range of about 160 km.
- MALE (Medium Altitude, Long Endurance) – up to 9000 m altitude and action range of 200 km.
- HALE (High Altitude, Long Endurance) – above 9000 m altitude and unlimited action range.
- HYPERSONIC – high speed, supersonic (1 – 5 Mach) or hypersonic (above 5 Mach), flight altitude of more than 15200 m or sub-orbital altitude, having the action range of more than 200 km.

Under these circumstances, one of the most important advantages of the UAVs is their ability to remote control, which has made them popular in the aviation industry and especially in the military industry. The design of UAVs requires special attention due to the fact that the evolution in flight and its control is done remotely. Thus, great efforts are done on the structural design of these vehicles and in particular in their aerodynamic design. Simulating the air flow around the UAV is of great importance for studying the aerodynamic forces and stability of the aircraft during flight in order to determine optimal models to suit the missions they have to accomplish. The use of the Finite Element Simulation (FEM) software such as ANSYS Fluent can significantly reduce the costs of the design, construction and testing of these complex structures.

2. Presentation of models

Following a preliminary study conducted on a sample of twenty aircrafts, three reference aircrafts were chosen, the CAD models were generated in order to be analyzed in ANSYS Fluent software from the aerodynamic point of view.

Model one



Fig. 1. Model one



Fig. 2. Elbit Hermes 900 [6]

The Hermes 900 is a high-endurance UAV flying at medium altitude, designed by the Israeli company Elbit Systems to perform different types of tactical missions. They have been in service since 2012. The positioning of the wing is in the central part of the fuselage, the empennage is in the shape of a "V", and the propeller is driven by a Rotax 914 four-cylinder piston engine that develops a power of 86 kW (115 hp). The aircraft can be equipped with a radar system for tracking moving targets, intelligent electrical and communication system, electronic warfare system and hyperspectral sensors. [7].

Model two



Fig. 3 Model two



Fig. 4 Orion UAV [8]

The Orion UAV is a high-endurance unmanned aircraft operating at medium altitude. The position of the wing is intermediate, with an empennage in "V" and the propeller of the propulsion system positioned behind the empennage. Developed by the Russian company Kronshtadt Group as a reconnaissance system with equipment for mapping the terrain, identification, and transmission of the coordinates of the target, its design is similar to the MQ-1 Predator and MQ-9 Reaper aircraft.

The aircraft is equipped with a Rotax 914 piston engine with a power of 86 kW (115 hp), equipped with a turbocharger, a fixed angle of attack propeller of type AV-115 with a diameter of 1.9m. A complete Orion system consists of 6 UAVs, the control station, the communication network, and the launch system. [9]

Model three



Fig. 5. Model three



Fig. 6. MQ-4C Triton [10]

The Northrop Grumman MQ-4C Triton is a high-endurance aircraft operating at high altitudes in development for the U.S. Navy for surveillance purposes. The position of the wing is median, with empennage in "V" shape, and the propulsion system consists of a Rolls-Royce AE 3007 turbo-engine with a maximum traction of 40 kN. It can carry distinct types of sensors such as: thermal imaging camera (infrared) and aerial surveillance of ground targets. It employs an autonomous take-off and landing system, different types of radars and an automatic control system to return to the control center in case the radio connection is lost. [11]

The three CAD models presented above are similar, having the same wing, V empennage, surveillance devices, propellers, intake device and exhaust device, the difference being the shape and cross-sectional area of the fuselage so that the analysis is conducted under the same conditions and the results obtained can be compared strictly from this point of view.

Geometric features of the models

- The length of the fuselage is about 8.5 m for the three models.
- The wingspan is 17.3 m.
- The half-wingspan of the empennage V is 1.2 m.
- The diameter of the propeller is 3 m.
- The average diameter of the cross-sections of the fuselage is 0.84 m, 0.61 m, and 0.92 m.

3. Analytical approach to the phenomenon of fluid flow around an aerodynamic profile

Aerodynamic drag force is caused by the dynamic interaction between a body surface and the fluid which flows over it. Two major terms which govern the aerodynamic drag and lift coefficients are the normal stress and wall shear stress. Pressure distribution dominates the normal stresses acting on the body surface, while surface roughness contributes to the wall shear stress. The equations needed for calculating the lift and drag coefficients are remarkably similar. The lift force that an airfoil generates depends on the density of the air, the velocity of the airflow, the dynamic viscosity and the compressibility of the air, the surface area of the airfoil, the shape of the airfoil, and the airfoil's angle of attack. However, dependence on the airfoil's shape, the angle of attack, air viscosity and compressibility are very complex. Thus, they are characterized by a single variable in the lift equation, called the lift coefficient, so the lift equation is given by the equation (1). [12], [13]

Similar with to the lift coefficient, the drag coefficient of an airfoil depends on the air density, the velocity of the airflow, the viscosity and compressibility of the air, the surface area of the airfoil, the

shape of the airfoil, and the angle of attack [12], [13]. The drag coefficient is generally found through testing in a wind tunnel, where the drag can be measured, and the drag coefficient is calculated by rearranging the equation (2). [12], [13]

$$L = \frac{1}{2}\rho U^2 S c_L \quad (1)$$

$$D = \frac{1}{2}\rho U^2 S c_D \quad (2)$$

where

L is the lifting force [N]

D is the drag force [N]

ρ is the density of air [kg/m³]

U is the relative velocity of the airflow [m/s]

S is the reference area of the airfoil [m²]

c_L is the lift coefficient

c_D is the drag coefficient.

Lift coefficient

The lift coefficient for a wing at a specified angle of attack and for specific flow conditions can be determined using the following equation [12], [13]:

$$c_L = \frac{L}{\frac{1}{2}\rho U^2 S} \quad (3)$$

Drag coefficient

In fluid dynamics the drag coefficient commonly denoted as c_D is a dimensionless quantity that is used to quantify the drag or resistance of an object in a fluid environment such as air or water. It is used in the drag equation where a lower drag coefficient indicates the object will have less aerodynamic drag, it is always associated with a particular surface area. This parameter takes in consideration the effects of the body shape, air properties such as viscosity and compressibility. Drag coefficient can be determined using the following equation [12], [13]:

$$c_D = \frac{D}{\frac{1}{2}\rho U^2 S} \quad (4)$$

4. Description of the cross-section shape of the models

To achieve the cross-section shape of the models, a super-ellipse function was implemented in the MATLAB software:

$$Y = C * Z^{N_1} * (1 - Z)^{N_2}, \quad (5)$$

where

$Z = [0,1]$,

N_1 is a coefficient for the curvature of the lower part,

N_2 is a coefficient for the curvature of the upper part,

C is a scaling coefficient.

The CAD model was created in CATIA V5 software by importing four hundred points, which were calculated in MATLAB software, in the characteristic sections of the model aircrafts (Fig. 7, Fig. 8, Fig. 9).

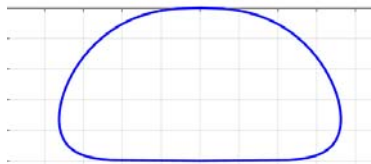


Fig. 7. Model one: Shape of the cross-section in MATLAB

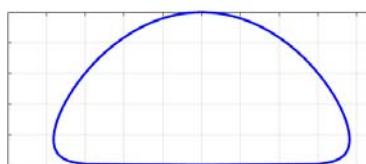


Fig. 8. Model two: Shape of the cross-section in MATLAB

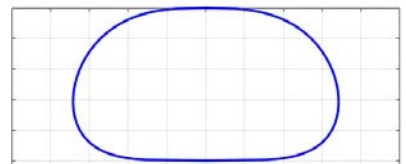


Fig. 9. Model three: Shape of the cross-section in MATLAB

5. Geometry and mesh of the fluid flow domain

The fluid flow domain was designed around a half of the models and has a structured poly-hexacore mesh which was generated in ANSYS Fluent 2021 R1. The eight inflation layers are uniform and for each major part of the aircrafts the first layer and the growth ratio were computed for accurate results of turbulence close to the walls. All three domains have approximately 3.5 million elements (Fig. 10 to Fig. 12).

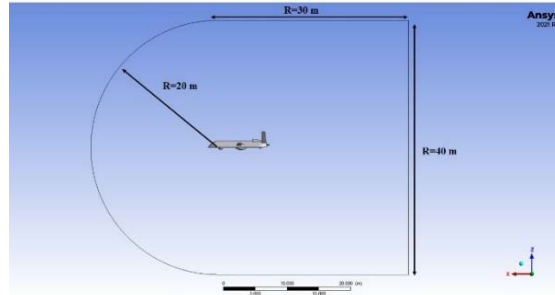


Fig. 10. Domain dimensions

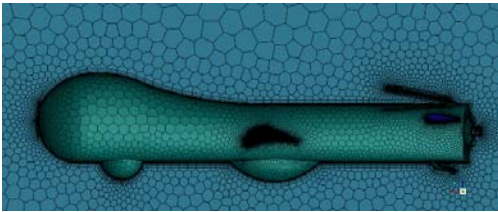


Fig. 11. Close view of domain mesh

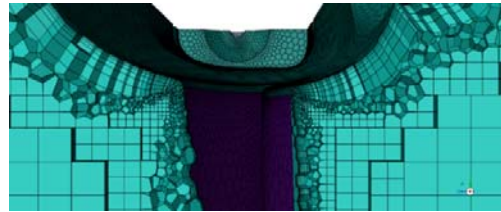


Fig. 12. Section view with inflation layers

6. Boundary conditions

For the CFD steady state analysis the Spalart-Allmaras turbulence model was employed, with a one equation Reynolds-Averaged Navier-Stokes (RANS) turbulence model. This model was chosen for the following reasons.

The $k-\epsilon$ model was proposed in the early 1970s, so this is the oldest of the turbulence models. It is used fairly widely in a variety of engineering disciplines but what was found when the $k-\epsilon$ was originally proposed and continues to be noticed today is that the $k-\epsilon$ model is not accurate at predicting boundary layer flows with adverse pressure gradients. So that it is particularly challenging for airfoils and wings at high angle of attack and for turbomachinery applications. The $k-\epsilon$ model tends to get even worse when shocks are present because it increases the strength of the adverse pressure gradient. Based on this observation it is desirable to have a better turbulence model, particularly for these applications and that is where the new model tends to come in.

The Spalart-Allmaras turbulence model was proposed in 1994 and it is fairly significant that this model is about the same as the $k-\omega$ model, which was proposed in 1988 and was essentially the same as the $k-\omega$ SST model. These models were simultaneously proposed, and they all aim to identify and help to improve the prediction of the same class of flows, which were the boundary layer flows subject to adverse pressure gradients.

Often the $k-\omega$ SST model is preferred to the Spalart-Allmaras for the majority of aerodynamic applications and this is mainly because both models were introduced at the same time, around 1994. However, since at that time a lot of comparative testing by a variety of groups was performed, generally the $k-\omega$ SST model has been found to give a better behavior. Therefore that is why for the majority of simulation attempts, the $k-\omega$ SST model tends to be employed and preferred. It is now recommended in most cases. But this model is much more computational expensive than the Spalart-Allmaras turbulence model which is a very straightforward and simple model to be implemented in the CFD aerodynamic applications. We expect to obtain satisfactory results using this model [14], [15], [16].

The test case analyzed in this research involved the atmospheric conditions of the flight ceiling of 10,000 m, the angle of attack of the air flow of 5° and the air flow velocity of 60 m/s.

The dynamic viscosity and density of the working fluid were considered constants, the Mach number is 0.2 and the Reynolds number is approximately the same for the three models, 1,344,000.

Table 1. Air proprieties at 10,000 m

Air proprieties at 10,000 m	
Density	0.412707 kg/m ³
Temperature	223,15 K
Pressure	26436,3 Pa
Viscosity	1,469 Pa*s
Sound speed	299,463 m/s

7. Comparison of the results achieved for the three models

The static pressure distribution

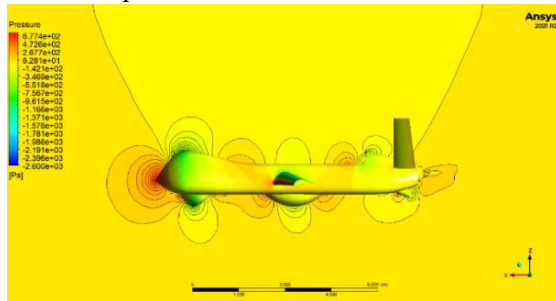


Fig. 13. Detailed close view of static pressure Model one

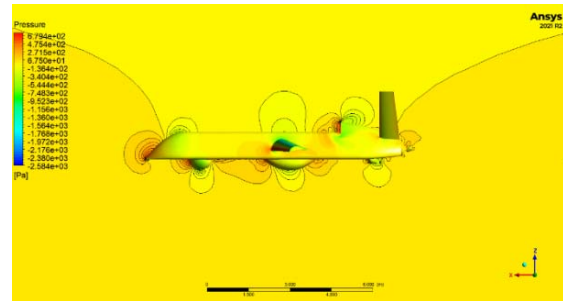


Fig. 14 Detailed close view of static pressure Model two

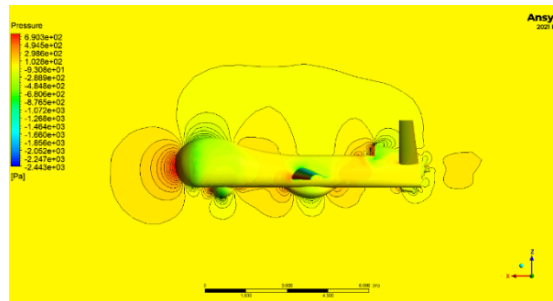


Fig. 15. Detailed close view of static pressure Model three

Velocity distribution

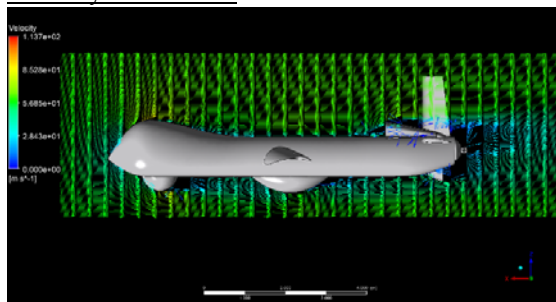


Fig. 16. Vertical velocity distribution Model one

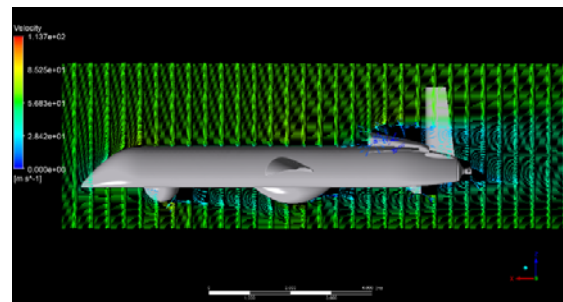


Fig. 17. Vertical velocity distribution Model two

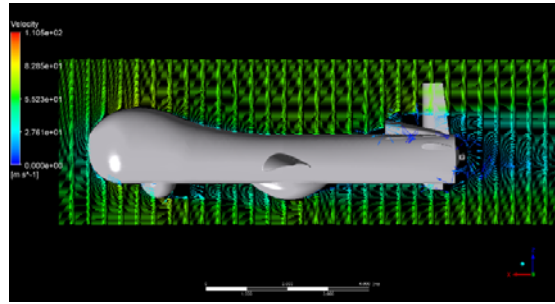


Fig. 18 Vertical velocity distribution Model three

Eddy viscosity distribution

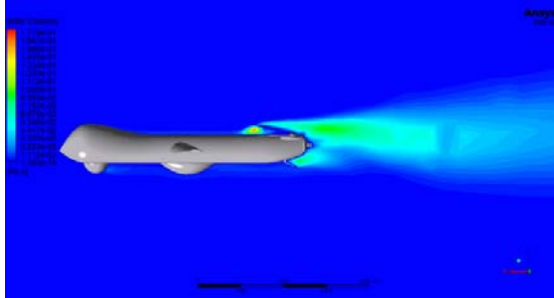


Fig. 19. Close view of eddy viscosity Model one

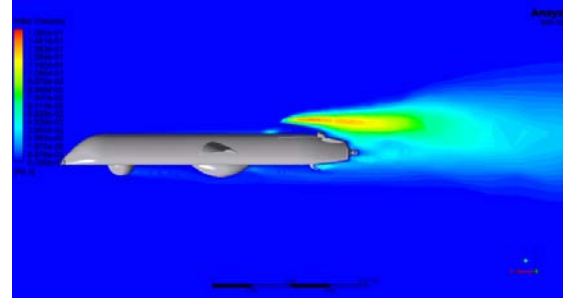


Fig. 20. Close view of eddy viscosity Model two

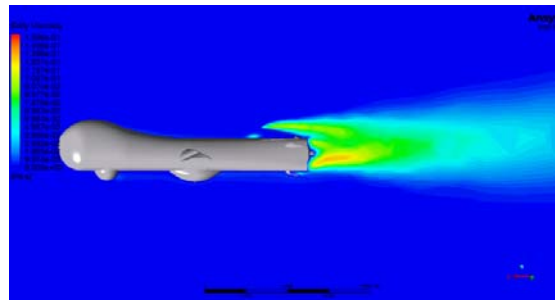


Fig. 21. Close view of eddy viscosity Model three

Comparison according to the distribution of static pressure:

- The first model has the lowest value of the static pressure which can be transposed in the lowest drag force, because the leading edge of the fuselage is sharp.
- The third model has the higher value of the static pressure because the leading edge of the fuselage is robust.
- The second model has an intermediate value of the static pressure because of the engine's inlet, but it has the lowest value of the static pressure at the leading edge of the fuselage compared to the other two models.
- All three models create a relatively good distribution of the lift force on the upper surface.

From this point of view model one is better in this configuration because the shape of it disperses rapidly the drag force.

Comparison according to the vertical velocity distribution:

- All three models have a uniform distribution of the velocity around the upper and lower surface.

Comparison according to the profile of eddy viscosity distribution:

- All three models have a relatively low turbulence on the upper surface of the fuselage which can be transposed in a good design of this area.
- On the lower surface of the fuselage turbulence occur, because of the surveillance equipment.
- The third model shows the largest turbulence zone on the lower part of the trailing edge of the fuselage.

- All three models show a large zone of turbulence after the engine's inlet which can't be avoid.
- The first model shows a greater value of turbulence on the engine's inlet compared to the other two models which can be translated in a bad fluid flow in the engine.

From this point of view model two is better in this configuration because it has the fewer zones which can create turbulences.

8. Conclusion

Based on the CFD steady state analysis of the flow over the three models of UAVs the following conclusions can be drawn:

1. The second model has the lowest drag force on the leading edge but also it has the lowest internal volume, which leads to poor equipment with surveillance devices.
2. For models one and three at the front of the fuselage, a low-pressure zone is created due to the acceleration of the air fillets on the upper surface of the fuselage, which lead to the appearance of a positive momentum on the pitch axis.
3. The third model has the largest turbulence zone at the trailing edge of the fuselage compared to the other two models, which can lead to a poor flow for the propeller and make it unstable.
4. The contours of the static pressure, eddy viscosity and velocity are discussed in detail.
5. In a future attempt, the CFD analysis should be performed for different angles of attack, for a better comparison of the models.
6. The mesh has to be refined, and the convergence criterion should be raised above 1e-3 to obtain more accurate results.
7. A more accurate turbulence model, like k- ω SST, is recommended to better capture the profile of the turbulence near the wall.
8. For a better comparison of the models a transient CFD analysis should be performed, with the rotation of the propeller taken into account.

Bibliography

- [1] Marin, N. and Spătaru, P. (2010), "The role and importance of UAV within the current theaters of operations", INCAS BULLETIN, Volume 2, Number 2/ 2010, pp. 66-72, DOI: 10.13111/2066-8201.2010.2.2.9;
- [2] Fulghum, A. D. and Sweetman, B. (2009), "Black UAV Performs in Afghanistan", Aviation Week.com;
- [3] Nehme, C. E., Cummings, M.I. and Crandall J. W. (2006), "A UAV Mission Hierarchy", Massachusetts Institute of Technology, HAL2006-09;
- [4] van Blyenburgh, P. (2008) "Unmanned Aircraft Systems - The Current Situation UAS", UAS ATM Integration Workshop EUROCONTROL, Brussels, May 8;
- [5] Story, A. and Gottlieb, A. (1995), "Beyond the Range of Military Operations", Military Operations, JFQ, pp. 99-104;
- [6] Porock, C. (2014), "Swiss Select Hermes 900 as New UAS", AINonline, June 11;
- [7] ** "Elbit Hermes 900", Wikipedia;
- [8] *(2018), "Photo of russia's orion uav armed with guided munitions appears online", South Front, July 21;
- [9] ** "Kronshtadt Orion", Wikipedia;
- [10] Trew, J. (2012), "Northrop Grumman Unveils US Navy's MQ-4C BAMS Triton unmanned aircraft", Engadget, June 16;
- [11] ** "Northrop Grumman MQ-4C Triton", Wikipedia;
- [12] Kandwal, S. and Singh, S. (2012), "Computational Fluid Dynamics Study of Fluid Flow and Aerodynamic Forces on An Airfoil", Volume 01, Issue 07, ISSN: 2278-0181;
- [13] Sharad, N. P. (2022), "CFD Modeling of Flow Over a Cylinder", CFD Flow Engineering;
- [14] Wimshurst, A. (2020), "[CFD] The Spalart-Allmaras Turbulence Model", Fluid Mechanics 101;
- [15] Kalitzin, G., Medic, G., Iaccarino, G. and Durbin, P. (2005), "Near-wall behaviour of RANS turbulence models and implications for wall functions", Journal of Computational Physics 204, 265-291;
- [16] Spalart, P. R. and Allmaras, S. R.. (1992), "A One-Equation Turbulence Model for Aerodynamic Flows", 30th Aerospace Sciences Meeting and Exhibit.,AIAA Paper, 92-0439.

RECHERCHE SUR LA FABRICATION DE LENTILLES ASSISTÉES PAR ORDINATEUR

Bendic Honoriu Eduard

Faculté d'Ingénierie et le Management des Systèmes Technologiques, Master: Conception Integree des Systemes Technologiques, Anul de studii:VI, e-mail: bendichonoriu@gmail.com

Coordonateur scientifique: Conf. Dorel Anania

RÉSUMÉ: Les programmes de simulation de lentilles sont d'une grande aide dans la création de nouveaux modèles de systèmes optiques par des concepteurs optiques. L'un de ces programmes est Zemax. Il utilise un catalogue de lentilles, où toutes les données relatives aux propriétés des lentilles telles que l'indice de réfraction, la transparence et la dureté des bouteilles optiques sont chargées. Le programme de conception optique est basé sur la trajectoire des rayons de lumière qui passent par le système optique, de sorte qu'après l'achèvement du système optique peut être effectué diverses simulations, par exemple des simulations d'images, diagramme ponctuel, etc.

MOTS CLÉS: lentilles, lentilles, rayons lumineux, simulation;

1. Introduction

Le concept de commande numérique a été utilisé pour la première fois au Massachusetts Institute of Technology (MIT) en 1951. Les applications sont utilisées par les programmeurs pour générer le code ISO nécessaire au traitement d'une pièce. Les chiffres sont entrés pour décrire la géométrie de la pièce et les données technologiques liées aux outils utilisés et aux vitesses de travail. Le logiciel CAM s'adresse en particulier aux machines-outils dans les machines à lacets et aux machines à moudre. Ces programmes utilisent la forme 3D de la pièce finie et la semi-fabrication de démarrage pour obtenir l'ajout de traitement qui sera ensuite enlevé par coupe.



Fig. 1.1. - Machine CNC

L'équipement CNC est généralement utilisé pour les catégories suivantes de machines-outils :

- Machines à moudre;
- Machines de forage;
- Cordes;
- Machines de rectification;
- Machines d'électroérosion filaire;
- Centres d'estampage avec contrôle numérique;

2. Notions générales sur l'utilisation des logiciels de CAO pour l'optimisation de la conception

Peu importe la mission à accomplir, les lentilles sont utilisées dans une multitude de systèmes optiques tels que les microscopes, les télescopes, les lentilles de caméra ou les lentilles de projection. Pour atteindre ces objectifs, les concepteurs ont besoin d'un programme qui simule la trajectoire des rayons de lumière selon les principes de la géométrie optique, où la diffraction et la propagation de la lumière à travers différents médias sont calculés en utilisant les lois de Newton de la physique.

Une limitation de ces logiciels est qu'ils ne peuvent pas être utilisés pour des éléments optiques de moins de 10 fois la longueur d'onde de la lumière ou pour certains lasers ou systèmes microélectroniques.

Le programme Zemax at focus Software (Tucson, AZ) est un programme de conception optique qui est utilisé pour un large spectre de systèmes optiques, des objectifs les plus simples à infrarouges (IR). Le logiciel a d'abord été publié sur les plates-formes Windows 3.0/95/NT et comprend l'utilisation de la simulation Monte Carlo, où un système optique est calculé de façon répétitive comme un système dont les variables sont définies dans des combinaisons aléatoires en fonction des limites de ses tolérances. Le résultat est une estimation statistique que le nombre doit avoir.

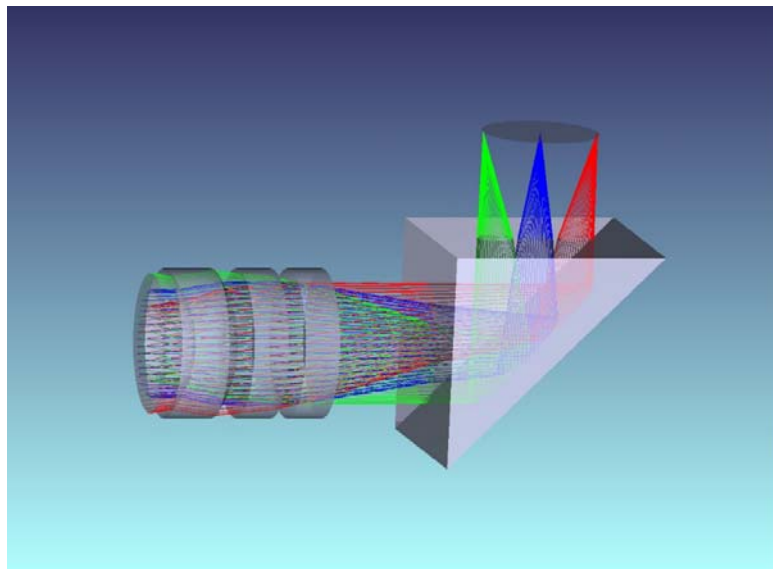


Fig. 2.1. – Système optique développé dans le programme Zemax

Source : <https://fc.institutoptique.fr/training/optical-design-with-zemax-opticstudio-advanced-476>

Des programmes tels que Zemax, qui suivent les rayons lumineux séquentiellement, sont limités à la suite sans opposition des rayons de lumière, la réflexion, la réfraction, la diffusion et l'éclairage. Cependant, des programmes de suivi non séquentiels ont été créés pour résoudre ces problèmes. Avec leur aide, chaque segment du faisceau lumineux peut être défini indépendamment, ce qui donne la possibilité de développer des systèmes optiques plus complexes. Le logiciel OptiCAD d'Opticad Corp. (Santa Fe, NM) peut modéliser des systèmes optiques simulant des sources lumineuses multiples ou étendues, des réfractances multiples ou des surfaces dures qui peuvent réduire l'intensité lumineuse. Avec ces avantages à l'esprit, OptiCAD est une excellente solution pour optimiser la conception des systèmes d'éclairage tels que les lampes, les réflecteurs ou les tubes de lumière. L'éclairage complexe des bordures de véhicules est une application où les concepteurs veulent étudier l'éclairage de différentes surfaces à partir d'une seule source.

Les lentilles de haute qualité devraient être recouvertes d'un revêtement antireflet pour réduire les reflets causés par la modification de l'indice de référence de la surface de la lentille. Pour les applications visibles, la protection antireflet la plus utilisée est le fluorure de magnésium, qui réduit l'indice de réfraction de quelques pour cent à 1 pour cent. Certains revêtements anti-éblouissement contiennent plusieurs couches de matériaux qui réduisent les reflets de 0,05 % à 0,5 %. Certaines applications nécessitent des surfaces très réfléchissantes, auquel cas les surfaces transparentes sont recouvertes de métaux tels que l'argent ou l'aluminium. Les filtres Dicroic peuvent être créés en stockant plusieurs couches de revêtements sur des substrats transparents, de sorte que seuls certains rayons traversent ces couches.

La plupart des concepteurs optiques ne produisent pas de couches de revêtement, en general, ils ne donnent que des spécifications de couverture qui seront respectées par un fabricant spécialisé. Cependant, lorsqu'un système laser de haute puissance est fabriqué, les effets de polarisation sont très importants, et les revêtements seront fabriqués par le même homme qui a réalisé le design.

Pour résoudre le problème d'optimisation et de conception de l'objectif, la première phase consistera à changer les rayons incidents à travers le diaphragme, la longueur d'onde et le champ de vision.

Pour la construction de l'objectif, il est tenu compte:

-il y aura 5 objectifs regroupés, 2 doubles et un objectif.

-l'ouverture relative sera de 2,5;

-l'angle du champ d'exploration sera égal à 5°;

-l'objet observé sera à une distance relativement grande.

-afin de pouvoir monter sur une caméra relativement nouvelle, le diamètre utile du plan d'image sera de 20 mm;

La pupille d'entrée sera calculée selon l'ouverture relative choisie, ainsi, pour 2,5, il en résultera un diaphragme de 34 mm. Compte tenu des exigences de montage et de résistance mécanique, le diamètre maximum des lentilles sera de 36 mm.

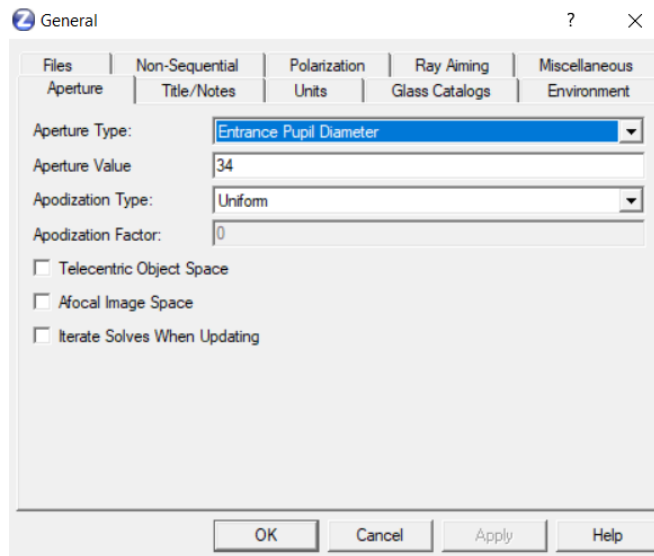


Fig 2.2.- Entrer le diamètre d'ouverture

Dans l'onglet des données du champ, saisissez la valeur du demi-point du champ, qui vaut $10^\circ / 2$, sur la colonne de $y = 5^\circ$.

Un système de 5 lentilles sera introduit. Insérez les épaisseurs de départ des lentilles de 5 mm pour chacun d'eux. Les distances entre les lentilles non fixées seront de 5 mm. Et les flacons optiques à partir desquels ils seront fabriqués seront choisis dans le catalogue offert par le programme.

La dernière zone de l'objectif doit être définie à partir de l'onglet rayon pour être calculée en tenant compte de l'ouverture relative, 2,5.

Surf	Type	Comment	Radius	Thickness	Glass	Semi-Diameter	Conic
OBJ	Standard		Infinity	Infinity		Infinity	0.000
STO	Standard		Infinity	0.000		25.000	0.000
2	Standard		Infinity V	5.000 V	SF6	25.000	0.000
3	Standard		Infinity V	5.000 V	F4	25.244	0.000
4	Standard		Infinity V	5.000 V		25.515	0.000
5	Standard		Infinity V	5.000 V	BK7	25.952	0.000
6	Standard		Infinity V	5.000 V	SF11	26.241	0.000
7	Standard		Infinity V	5.000 V		26.487	0.000
8	Standard		Infinity V	5.000 V	F4	26.924	0.000
9	Standard		-81.035 F	5.000 V		26.945	0.000
IMA	Standard		Infinity	-		25.687	0.000

Fig 2.3.- Tableau de l'éditeur de données d'objectif

La fonction de mérite sera activée à partir de l'onglet MFE, conception, fonction de mérite séquentielle. Comme je vais concevoir un système focal, le RMS, le rayon du spot, les options Centroid seront définis, le nombre d'anneaux du spot graphique sera de 4 et le nombre de bras 6. L'optimisation de la lentille commencera lorsque le bouton d'optimisation locale sera enfoncé, le principe de fonctionnement de ce programme sera de tester toutes les combinaisons de valeurs qui peuvent être assignées aux variables pour diminuer la valeur de la fonction de mérite. Ça va aller à 0. Modifiez les valeurs dans l'option Valeurs limites d'épaisseur, ce menu exigera que les épaisseurs de bord de lentille soient entre 2 et 30 mm et que les surfaces d'espacement d'air soient entre 0,5 et 25 mm, cela empêchera l'intercalation des lentilles ou l'apparition de très longues distances entre elles.

Après avoir terminé cette étape, la commande Optimisation du marteau sera utilisée.

Selon les valeurs que nous voulons atteindre pour la fonction de mérite, cette option peut fonctionner même pendant quelques semaines, pour une très bonne exactitude.

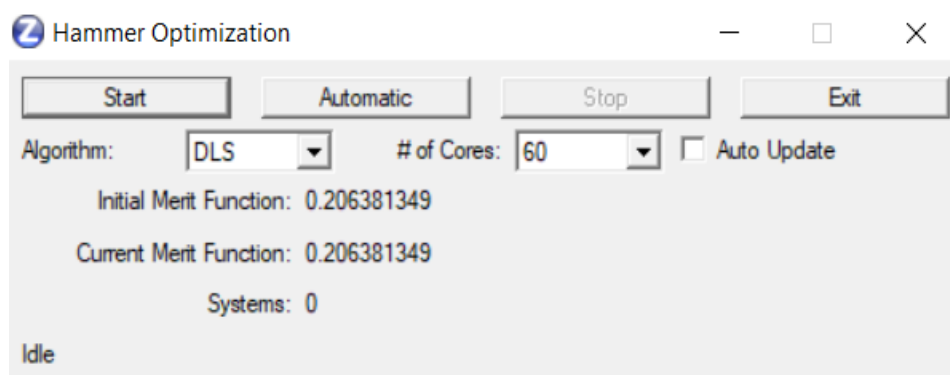


Fig 2.4.– Fenêtre d'optimisation du marteau

Les résultats de cette optimisation finale seront les suivants :

Surf	Type	Comment	Radius	Thickness	Glass	Semi-Diameter	Conic
OBJ	Standard		Infinity	Infinity		Infinity	0.000
STO	Standard		Infinity	0.000		17.000	0.000
2	Standard		41.278 V	2.456 V	LAF9 S	17.334	0.000
3	Standard		19.495 V	25.728 V	SFL56 S	16.222	0.000
4	Standard		21.228 V	0.500 V		13.101	0.000
5	Standard		20.892 V	21.935 V	LAKN7 S	13.514	0.000
6	Standard		-22.601 V	28.160 V	SF57HT S	11.796	0.000
7	Standard		-23.821 V	0.925 V		10.436	0.000
8	Standard		-19.710 V	29.999 V	KZFS1 S	10.005	0.000
9	Standard		70.685 F	8.114 V		7.629	0.000
IMA	Standard		Infinity	-		10.000	0.000

Fig 2.5.– Tableau avec les valeurs finales du système optique



Fig 2.6.– Simulation d'une image observée avec l'objectif

Avec ces simulations à portée de main, nous pouvons analyser la performance du système optique pour voir s'ils répondent à tous les critères qu'il doit remplir.

3. Défauts d'image et méthodes de correction

Aucun autre facteur ne détermine plus la qualité de l'image que les lentilles utilisées pour créer le système optique. Il existe une grande variété de conditions qui peuvent déterminer la performance de l'objectif. La précision et la qualité des systèmes de fixation, la précision de l'exécution des lentilles, les propriétés des bouteilles et des revêtements ont un grand effet sur les images du système optique. La lumière passe et est réfléchi sur la surface du verre et a de multiples effets. Le défi est d'utiliser la lumière entrant dans le système optique et de la focaliser pour obtenir l'image avec une perte minimale pour obtenir une image claire et lumineuse.

Les différentes ondes du spectre utilisé passent à travers la lentille et peuvent se plier à des angles différents, semblables à un prisme. Certains objectifs ou différents types de verre sont nécessaires pour capturer chaque couleur de base pour former l'image correctement.

Il existe deux autres types de déformation, le type pad(1) et le type barrel(2). Ceux-ci sont causés par le fait que le centre et les bords de l'image ont des agrandissements différents. La variation du grossissement provoque une distorsion du centre vers les bords de l'image, et ces formes n'ont pas de perspective réelle. La distorsion de type barillet augmente l'image centrale

plus que l'image marginale, provoquant un « gonflage » de l'image. La distorsion de Pertone augmente l'image centrale moins que les coins provoquant la diminution de la partie centrale.

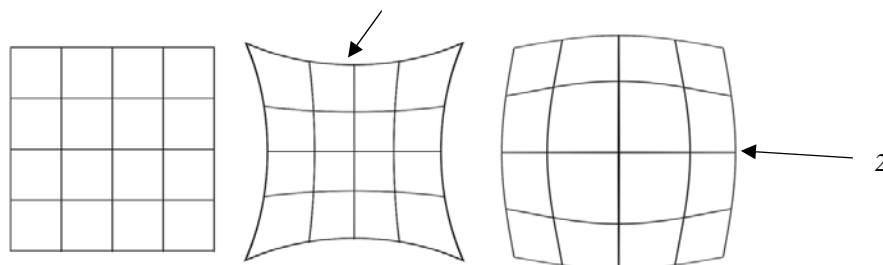


Fig. 5.1. – Types de distorsion

Les éléments qui ne sont pas corrigés produisent des images douces qui montrent la distorsion et les couleurs fanées. Les types de verre spéciaux sont connus pour empêcher la distorsion et d'autres problèmes associés au passage de la lumière à travers la lentille. Les fabricants de dispositifs optiques commencent peu à peu à utiliser des bouteilles et des minéraux de plus en plus exotiques et denses comme la fluorite en combinaison avec des conceptions sophistiquées pour résoudre ces problèmes.

4. Conclusions

Étant donné que le verre optique a été utilisé et étudié depuis l'antiquité, il illustre que ce matériau était impératif pour le développement de notre technologie et la connaissance du monde environnant. Cependant, ce n'est qu'à la fin du 17^e siècle que le véritable art de la fabrication de lentilles a été découvert avec l'avènement des télescopes et des microscopes.

Au début, la fabrication des lentilles était assez compliquée, mais avec l'avancée technologique, de nouvelles façons de contrôler et de perfectionner le verre optique sont apparues. Le logiciel de simulation CAO pour les systèmes optiques tels que Zemax a grandement simplifié le processus de fabrication des lentilles. Ils peuvent simuler le trajet des rayons lumineux à travers un système optique conçu par l'utilisateur. Le programme peut simuler un très large spectre de longueurs d'onde, de sorte que vous pouvez même faire des systèmes optiques qui fonctionnent dans le domaine infrarouge. Ce dernier peut être utilisé pour les systèmes de vision thermique.

Un autre avantage des programmes de simulation est qu'ils peuvent simuler différents graphiques pour déterminer la qualité du système optique conçu, ainsi que simuler une image qui peut illustrer les défauts du système, tels que les aberrations géométriques ou la vignettation d'image.

La dernière phase du système optique est la fabrication effective du système optique, compte tenu des distances, des épaisseurs, des formes et du type de verre optique générés par le programme de conception à la fin du processus.

5. Bibliographie

- [1] <https://fc.institutoptique.fr/training/optical-design-with-zemax-opticstudio-advanced-476>
- [2] <https://www.cameralabs.com/nikon-z-58mm-f0-95-noct-review/>
- [3] <https://imagebank.asrs.org/file/7258/retinal-pigment-epithelial-detachment-with-no-subretinal-fluid>
- [4] <https://www.masterclass.com/articles/basic-photography-101-understanding-camera-lenses>
- [5] <https://www.labmanager.com/product-focus/advancements-in-lens-manufacturing-768>
- [6] <https://petapixel.com/2021/12/22/researchers-develop-cheaper-and-faster-way-to-manufacture-lenses/>
- [7] <https://www.youtube.com/watch?v=ww1NCzLSI7A&t=36s>
- [8] https://en.wikipedia.org/wiki/Eyepiece#/media/File:Orthoscopic_1880.png
- [9] <https://www.edmundoptics.com/knowledge-center/application-notes/imaging/what-is-swir/>
- [10] <https://www.militarysystems-tech.com/taxonomy/term/563>
- [11] <http://atozresearch.com/technology-media/thermal-imaging-market-growth-segment-trends-2021/>
- [12] https://dic.academic.ru/pictures/wiki/files/68/Distorton_barrel_and_pincushion.png
- [13] <ro/support/documentation/supplemental/18/calculating-camera-sensor-resolution-and-lens-focal-length.html>
- [14] wikimedia.org%2fwikipedia%2fcommons%2f6%2f6%2fChromatic_aberration_%2528comparison%2529.jpg
- [15] <https://www.lonelyspeck.com/a-practical-guide-to-lens-aberrations-and-the-lonely-speck-aberration-test/>

ACCESS METRO SOLUTION ET INGENIERIE WDM

(SERIE OSN 1800)

Joulia Garbaya

Faculté d'Ingénierie et le Management des Systèmes Technologiques, Master: Conception Integree des Systemes

Technologiques, Année d'étude : 2021/2022, e-mail : garbayajoulia@gmail.com

Coordinateur scientifique : Prof.dr.ing. **Miron ZAPCIU**

Coordinateur de Huawei : Ingénieur Support de transmission optique. **Hamza KHarchoufi**

RÉSUMÉ : *Le NCE est la première plate-forme d'automatisation et d'intelligence réseau de l'industrie qui intègre des capacités de gestion, de contrôle, d'analyse et d'intelligence artificielle chez Huawei. Il applique efficacement les intentions opérationnelles sur les réseaux physiques et assure la gestion, le contrôle et l'analyse centralisés des réseaux mondiaux. Principalement utilisé dans les centres de données, les campus corporatifs, les lignes privées corporatives et les scénarios de réseaux d'exploitants. IMaster NCE permet la cloudification des ressources, l'automatisation du cycle de vie complet et la gestion intelligente en boucle fermée basée sur l'analyse en fonction des intentions commerciales et de service. IMaster NCE fournit des API de réseau ouvert pour l'intégration rapide avec les systèmes informatiques et accélère la transformation des services et l'innovation. Vers les opérateurs et les entreprises en améliorant la simplicité, l'intelligence, l'ouverture et la sécurité des réseaux.*

MOTS CLÉS : NCE, Intelligence artificielle, Huawei.

1. Introduction

Afin de gérer un réseau optique et faire des opérations et des configurations à distance il est nécessaire d'avoir un gestionnaire tel que NCE (Huawei Network Cloud Engine).

NCE est un moteur cloud réseau innovant développé par Huawei. Positionné comme le cerveau des futurs réseaux basés sur le cloud. NCE intègre des fonctions telles que la gestion du réseau, le contrôle des services et l'analyse du réseau. Il s'agit du système d'activation de base pour la mise en commun des ressources réseau, l'automatisation et l'auto-optimisations des connexions réseau et l'automatisation O&M.

2. Gestion de réseau NCE

Architecture logique logicielle :

Basé sur la plate-forme cloud, NCE implémente trois modules logiques de l'administration, de contrôle de réseau et d'analyse de réseau et diverses applications orientées scénarios en tant que services et composants. Les clients peuvent ainsi déployer les NCE de façon souple et modulaire pour répondre à leurs besoins particuliers.

Gestion de réseau NCE

L'équipement WDM peut être géré via le port ETH (port Ethernet de gestion) à l'aide du network Cloud Engine (NCE), et il prend également en charge le protocole de gestion de réseau simple (SNMP).

L'équipement WDM adopte la modélisation de l'information de gestion standard et la technologie de gestion axée sur les objets. Le NCE peut échanger les informations directement avec le logiciel NE via le module de communication, qui réalise la gestion des alarmes et des performances, et implémente la configuration de bout en bout sur le plan de gestion.

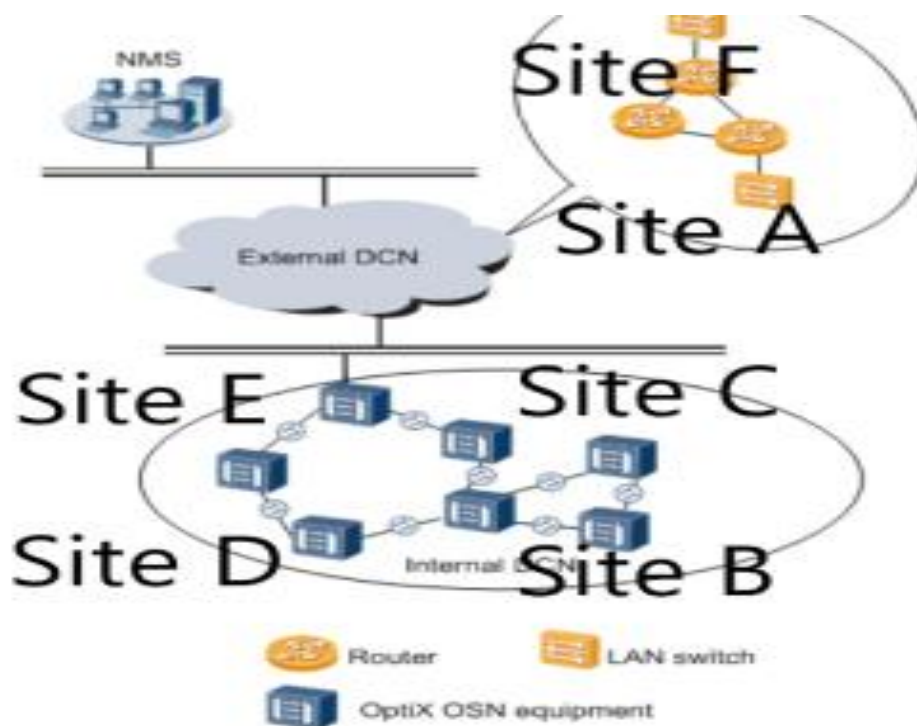


Fig.1.Gestion de réseau NCE

3. Moteur Cloud réseau

Le NCE intègre les fonctions du NMS, du contrôleur SDN et du système d'analyse de réseau. Il ne fournit pas uniquement les fonctions traditionnelles de défaillance, de configuration, de comptabilisation, de performance et de sécurité (FCAPS). Mais aussi des fonctionnalités avancées du réseau pilote prévu, telles que la visualisation du réseau, l'automatisation des services et le fonctionnement et l'entretien intelligents.

4. Application sur NCE

Exemple de création/Extension pendant l'opération :

- **Page de garde** : qui définit le but et l'endroit et autres informations de l'opération demandé par notre client (ORANGE France)

Dans cette opération on est demandé de swapper des cartes des contrôles (SCC) par des cartes d'une version plus récente et ajouter des cartes de synchronisations (DSFIU et AST2) et des cartes transpondeurs (LDCA).

1. IDENTIFICATION ET SUIVI DU PROJET

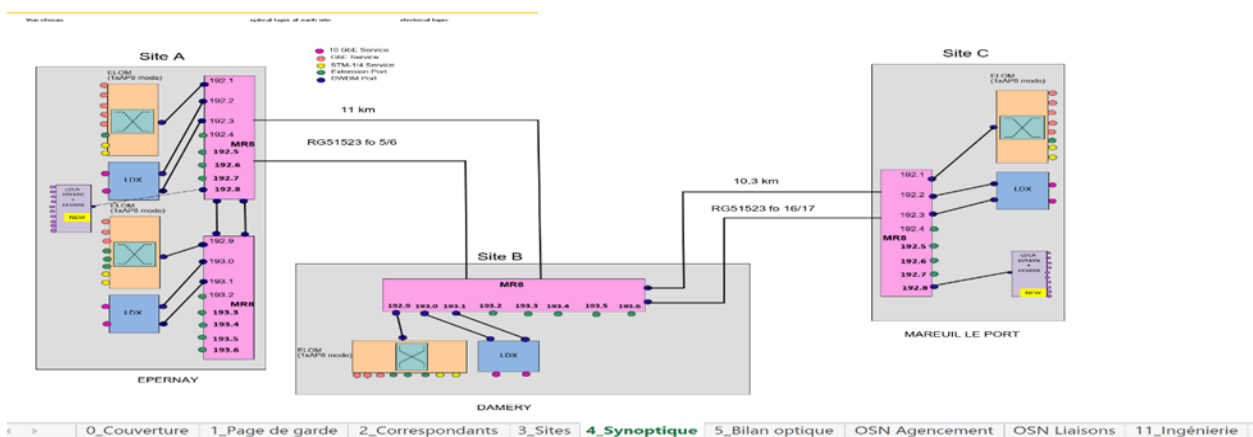
Nom du système	EPERNAY - DAMERY - MAREUIL LE PORT
N° de gamme OPUS	
UPR	Nord Est
UI	Champagne Ardenne
Type d'opération	Création
Type d'extension (carte(s) sur châssis existant / châssis) si opération d'extension	HNO - EXT LDCA EPERNAY - MAREUIL + Insertion DSFIU/AST2 + SWAP F1SCC par F3SCC + EXT CABLAGE EPERNAY et MAREUIL + EXT CHASSIS EPERNAT
Date de MAD souhaitée	8/1/2022
Nom de l'artère	Epernay Grandpierre - Damery - Mareuil le Port
Codification, nom Ironman	EPERNAYMPRE.WDB.01
Appellation dans le GLM (si différent de la codification Ironman)	

Date Rédaction version v1	1/14/2022
Date d'Envoi au fournisseur version v1	1/14/2022

Nom du Responsable de Projet	Baptiste Morin
Signature	

N° Version Modifiée	Objet	Date
---------------------	-------	------

- **Synoptique : le design de la topologie en objet**

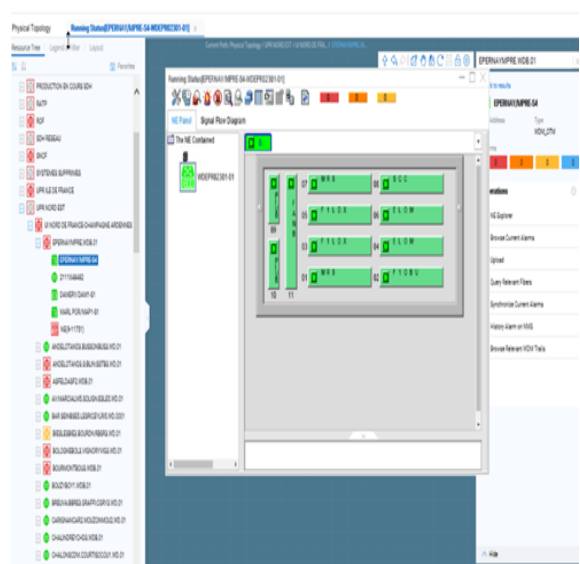
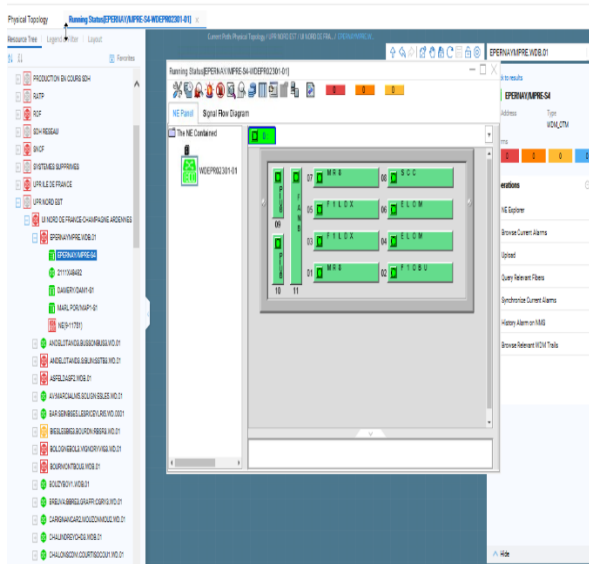


- **Agencement des cartes : qui indique l'emplacement des cartes dans un châssis OSN1800**

AGENCEMENT DES CARTES SUR LE CHÂSSIS											
OSN8001 - Add					OSN800V Pro - Add					Add	
Delete					Delete					Delete	
Site A / Chassis 1					Site A / Chassis 2						
EPERNAY 5120EPK					EPERNAY 5120EPK						
slot 10 PIU	slot 9	SLOT 7	MFIB-192.98.93.6TH2	SLOT 8	F3SCC	SLOT 10		SLOT 11		FAN Slot 9	
slot 11 PIU	FAN	SLOT 8	LDK	SLOT 9	ELEM	SLOT 11		SLOT 12			
		SLOT 9	LDK	SLOT 10	ELEM	SLOT 12		SLOT 13			
		SLOT 10	MFIB-192.98.93.6TH2	SLOT 11	CEU	SLOT 13		SLOT 14			
Power		159.4W		Version Actuelle		Version Cible					
					Recolement Energie						
					Power					736.5W	
					Version Actuelle					Version Cible	
OSN8001 - Add					OSN8001 - MA (Metro Access)					Add	
Delete					Delete					Delete	
Site B / Chassis 1					Site B / Chassis 1						
DAMEFV 5120DAM					DAMEFV 5120DAM						
slot 10 PIU	slot 9	SLOT 7	MFIB-192.98.93.6TH2	SLOT 8	F3SCC	SLOT 10		SLOT 11		FAN Slot 9	
slot 11 PIU	FAN	SLOT 8	LDK	SLOT 9	ELEM	SLOT 11		SLOT 12			
		SLOT 9	LDK	SLOT 10	ELEM	SLOT 12		SLOT 13			
		SLOT 10	MFIB-192.98.93.6TH2	SLOT 11	CEU	SLOT 13		SLOT 14			
Power		159.8W		Version Actuelle		Version Cible					
OSN8001 - Add					OSN8001 - MA (Metro Access)					Add	
Delete					Delete					Delete	
Site C / Chassis 1					Site C / Chassis 1						
MAREUIL LE PORT 5146MAP					MAREUIL LE PORT 5146MAP						
slot 10 PIU	slot 9	SLOT 7	MFIB-192.98.93.6TH2	SLOT 8	F3SCC	SLOT 10		SLOT 11		FAN Slot 9	
slot 11 PIU	FAN	SLOT 8	LDK	SLOT 9	ELEM	SLOT 11		SLOT 12			
		SLOT 9	LDK	SLOT 10	ELEM	SLOT 12		SLOT 13			
		SLOT 10	MFIB-192.98.93.6TH2	SLOT 11	CEU	SLOT 13		SLOT 14			
Power		285.2W		Version Actuelle		Version Cible					

Après avoir regardé le fichier fourni par le client qui décrit la tâche à faire ainsi le design de la topologie. On passe maintenant sur le gestionnaire NCE pour le déploiement

- L'emplacement des cartes comme indiqué sur " agencement des cartes "
- Aperçu sur le châssis déjà existant.



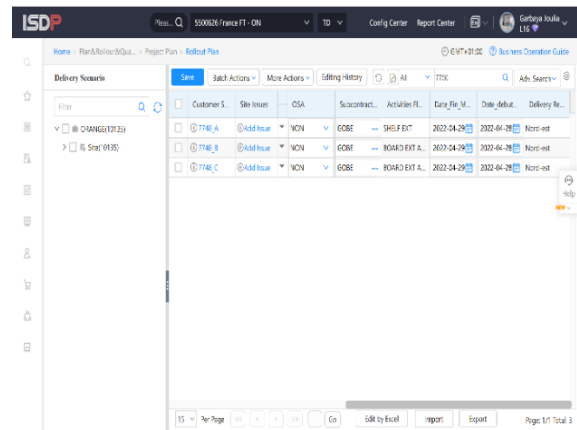
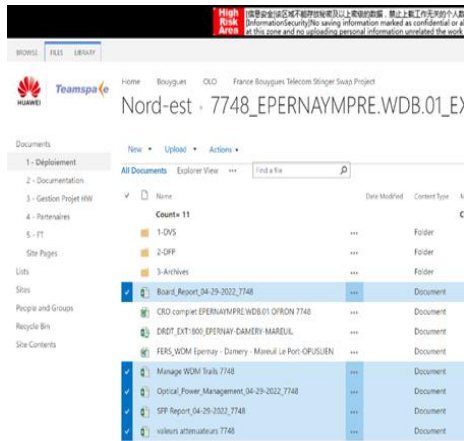
Channel	Optical Interface Name	Channel Use Status	Optical Interface Loopback	Laser Status	DGC Threshold	DGC Monitoring Times	Deg
NOEPF0201-02-She(WiLabook)-5-BI45T2-01NOZ(TX)-1	FXG(TX)	Unused	Non-Loopback	On	200	7	1E-4
NOEPF0201-02-She(WiLabook)-5-BI45T2-01NOZ(SAMEY-NOZ(TX))	FXS(SAMEY-NOZ(TX))	Used	Non-Loopback	On	200	7	1E-4

NE Name	Slot ID	Board No.	Port	Input	Refr.	Input Power Refr.	Input	Refr.	Refr.
NOEPF0201-02	She(WiLabook)-1	BI45T2	19M1(TX)	/	/	/	/	/	/
NOEPF0201-02	She(WiLabook)-1	BI45T2	21F5(SAMEY-NOZ(TX))	17.6	17.8	2022-04-29 01:33:50 DST	Normal	20.0	-12.0
NOEPF0201-02	She(WiLabook)-1	BI45T2	37M1	40.0	/	/	/	/	/
NOEPF0201-02	She(WiLabook)-1	BI45T2	57M2	1.8	1.9	2022-04-29 01:33:50 DST	Normal	1.1	0.9

- Création des fibres (intra et inter)

NE Name	Slot ID	Board No.	Port	Input	Refr.	Input Power Refr.	Input	Refr.	Refr.
NOEPF0201-02	She(WiLabook)-9	BI.LOCA	14R12(TX)	40.0	0.4	2022-04-29 01:35:30 DST	Critical Alert	5.8	13.4
NOEPF0201-02	She(WiLabook)-1	BI.LOCA	14R13(TX)	40.0	7.4	2022-04-29 01:36:20 DST	Critical Alert	4.4	12.4
NOEPF0201-02	She(WiLabook)-1	BI45T2	57M2	1.8	1.9	2022-04-29 01:33:50 DST	Normal	1.1	0.9
NOEPF0201-02	She(WiLabook)-4	BI45T2	37M1	1.8	1.8	2022-04-29 01:35:51 DST	Normal	1.4	0.9
NOEPF0201-02	She(WiLabook)-1	BI45T2	57M2	1.3	1.5	2022-04-29 01:36:41 DST	Normal	1.5	0.5
NOEPF0201-02	She(WiLabook)-1	BI45T2	37M1	1.3	1.4	2022-04-29 01:36:41 DST	Normal	1.6	0.4
NOEPF0201-01	She(WiLabook)-3	FX.LX	61M41-P01-MAP1-EPEVNA1-MPFE-100E101-ROZ(TX)	/	0.4	2022-04-29 01:50:50 DST	/	0.4	0.4
NOEPF0201-01	She(WiLabook)-3	FX.LX	61M41-P01-MAP1-EPEVNA1-MPFE-100E101(TX)	/	0.4	2022-04-29 01:50:50 DST	/	0.4	0.4
NOEPF0201-01	She(WiLabook)-3	BI.LOCA	12R10(TX)	40.0	0.5	2022-04-29 01:49:54 DST	Critical Alert	0.5	-0.5
NOEPF0201-01	She(WiLabook)-3	BI.LOCA	14R10(TX)	40.0	0.5	2022-04-29 01:44:55 DST	Critical Alert	0.5	-0.5
NOEPF0201-01	She(WiLabook)-3	BI.LOCA	60R0(TX)	40.0	0.2	2022-04-29 01:36:32 DST	Critical Alert	0.2	-0.2
NOEPF0201-01	She(WiLabook)-3	BI.LOCA	10R10(TX)	40.0	0.4	2022-04-29 01:47:00 DST	Critical Alert	0.4	-0.4
NOEPF0201-01	She(WiLabook)-5	FX.LX	50M41-01M1-EPEVNA1-MPFE-100E101(TX)	/	0.4	2022-04-29 01:51:50 DST	/	0.4	-0.4
NOEPF0201-02	She(WiLabook)-9	BI.LOCA	60R0(TX)	40.0	4.9	2022-04-29 01:47:47 DST	Critical Alert	0.6	-0.6
NOEPF0201-02	She(WiLabook)-9	BI.LOCA	70R0(TX)	40.0	0.7	2022-04-29 01:47:47 DST	Critical Alert	0.7	-0.7
NOEPF0201-02	She(WiLabook)-3	BI.LOCA	30R1(TX)	40.0	0.7	2022-04-29 01:36:32 DST	Critical Alert	0.7	-0.7
NOEPF0201-02	She(WiLabook)-9	BI.LOCA	80R0(TX)	40.0	0.8	2022-04-29 01:47:47 DST	Critical Alert	0.8	-0.8
NOEPF0201-01	She(WiLabook)-5	FX.LX	61M41-P01-MAP1-EPEVNA1-MPFE-100E101-ROZ(TX)	7.5	0.8	2022-04-29 01:48:31 DST	Normal	0.8	-0.8
NOEPF0201-01	She(WiLabook)-5	FX.LX	61M41-P01-MAP1-EPEVNA1-MPFE-100E101(TX)	4.9	4.9	2022-04-29 01:36:32 DST	Normal	0.9	-0.9
NOEPF0201-01	She(WiLabook)-3	BI.LOCA	40R0(TX)	40.0	7.0	2022-04-29 01:36:32 DST	Critical Alert	0.0	-2.0
NOEPF0201-02	She(WiLabook)-9	BI.LOCA	50R0(TX)	40.0	7.1	2022-04-29 01:47:47 DST	Critical Alert	0.1	-2.1
NOEPF0201-02	She(WiLabook)-9	BI.LOCA	110R0(TX)	40.0	7.2	2022-04-29 01:47:47 DST	Critical Alert	0.2	-2.2

- Téléchargement des rapports de l'opération dans l'interface intermédiaire Huawei-Orange (Share Point et ISDP)



- Les rapports finaux à envoyer au client à la fin de l'opération

TP Notification --- Succès	
RFC NO.	NC20220420100016
TP NO.	T203217014
TP Description	HNO - EXT LDCA EPERNAY - MAREUIL + Insertion DSFIU/AST2 + SWAP F1SCC par F3SCC + EXT CABLAGE EPERNAY et MAREUIL + EXT CHASSIS EPERNAT
Date	TP HNO planifié en S17: Dans la nuit du jeudi 28 au vendredi 29 Avril 2022. De 23h15 à 05h15
Subnet Name	7748 // EPERNAYMPRE.WDB.01_EXT1_100G_HNO_2022
NMS Engineer	Joulia Garbaya 07.78.09.69.41
Field Engineer	Amine EL AZRAK [REDACTED] Emmanuel CAMPAN [REDACTED] Grégory LEUX [REDACTED]
GSC On-Call	Hebin
Cross check	
Traffic Cut duration	23:25-01:40
Open issue and Action	
Operation Procedure	22 : 15 Appel le technicien 23 : 15 Appel au GSR au début du TP – OK. 23 : 25 – 01 : 40 HNO - EXT LDCA EPERNAY - MAREUIL + Insertion DSFIU/AST2 + SWAP F1SCC par F3SCC + EXT CABLAGE EPERNAY et MAREUIL + EXT CHASSIS EPERNAT 01 : 40 – 01 : 50 équilibrage IN 01 : 50 – 03 : 00 Comptages 100GE/10GE LAN 03 : 10 Appel au GSR au fin du TP – OK 03 : 30 Fin de l'opération MAC MAPPING OK

Joulia Garbaya
NIS Remote Delivery Dept, GSC Romania



Mobile : 0040.728.108.051 / 0033.778.096.941

Email: garbaya.joulia@huawei.com

HUAWEI TECHNOLOGIES ROMANIA
301-311 Barbu Vacarescu Blvd.
The Lake View Building, 4th Floor, 2nd District

6. Conclusions

Les projets d'innovation de Huawei avec les principaux opérateurs ont rendu possibles les fonctions clés d'iMaster NCE. Intégration complète dans des scénarios d'affaires novateurs en collaboration avec les clients. Cela accélère l'automatisation et l'innovation en intelligence dans une variété de scénarios de réseau. Huawei est résolue à construire un réseau autonome qui « laisse la complexité à lui-même et apporte la simplicité aux clients ». NCE accélère ce processus et permet à l'industrie des réseaux de se développer en particulier dans le domaine de la transmission optique WDM.

7. Bibliographie

- [1]. GEROME. F ; 2005 - « Conception et caractérisation de fibres compensatrices de dispersion chromatique pour application aux liaisons optiques WDM » Thèse de doctorat de l'Université de LIMOGES.
- [2]. Cédric Cochrane, Serge R. Mordon, Jean Claude Lesage et Vladan Koncar, « New design of textile light diffusers for photodynamic therapy », Materials Science and Engineering: C, vol. 33, 1er avril 2013, p. 1170–1175 (DOI 10.1016/j.msec.2012.12.007, lire en ligne [archive], consulté le 8 juillet 2016)

- [3]. « Mesure de déformation par fibre optique » [archive] [PDF], sur www.ifsttar.fr, octobre 2015 (consulté le 31 août 2018).
- [4]. MERZOUK. K ; 2018 - « Etude d'un système bas cout de transmission optique par multiplexage temporel ». Thèse de doctorat Optique, Optoélectronique et Microondes. Institut Polytechnique de Grenoble.
- [5]. MEUNIER. J - P ; 2013 – « Télécoms Optique » : Composants à fibres systèmes de transmission. Ed. Hermes. Paris.
- [6]. "Indicateurs mondiaux de la propriété intellectuelle 2021" (PDF). OMPI. Récupéré le 30 novembre 2021.
- [7]. Huawei Technologies Co.2022.
- [8]. <https://datasheets.globalspec.com/ds/4783/HuaweiTechnologies/7ECA7ABC-3CF3-4DA8-9C9F-354E6A3C6205fr>.
- [9]. OSN 1800 Product Documentation.
- [10]. Documentation de Huawei.

8. Notes

Les symboles suivants sont utilisés dans le document :

NCE = Network Cloud Engine
API = Application Programming Interface
WDM = Wavelength Division Multiplexing
O&M = Operation and Maintenance
OSN = Optical Switch Node
SDN = Software-Define Networking
OSS = Optical Supervisory Channel
BSS = Base Station Sub-system
IDN = Internet Driven Network
GUI = Interface Utilisation Graphique
SNMP = Simple Network Management Protocol
NMS = Network Management System
ESC = Canaux de Supervision Electrique
OSC = Canaux de Supervision Optique
DCC = Data Communications Channel
GNE = Gateway Network Element
DCN = Data Communication Network
TCP/IP = Transmission Control Protocol/Internet Protocol
NTP = Network Time Protocol
OA = Optical Amplifier
FIU = Fiber Interface

EXPLICIT DYNAMIC ANALYSIS OF DISPOSABLE PLASTIC TRAYS CONSIDERING AN EFFECTOR PROGRAMMING ERROR

MARCU Rareș-Ionuț

Faculty of Industrial Engineering and Robotics, Robotics Bachelor's programme, 4th year
e-mail: marcu.rares.ionut@gmail.com

Scientific coordinator: Prof. dr. eng. **Cristina PUPĂZĂ**

ABSTRACT: *The aim of the study is an explicit dynamic analysis of the elastic-plastic behavior of a plastic tray package to a faulty handling of the industrial robot. The robot is equipped with a multi-purpose effector for handling and palletizing operations in an industrial automated cell. The research is focused on the elastic-plastic behavior of the package due to an accidental impact of the robot frame effector with the clamping paddles, when the travel is incorrectly configured by the operator.*

KEYWORDS: *Explicit dynamics, plastic trays, experiments, verification*

1. Introduction and related work

Robotic cell units are widely used in industry for rapidly handling trays packages. In the studied case a single tray package handling operation is performed. The containers are arranged in columns of 20 samples, which are placed by the industrial robot IRB 4600 in cardboard boxes, for further operations carried out by the robot and the palletizing system (Fig. 1). The columns enter the robotic cell through a tape conveyor and are then taken by the robot for storage purposes. Figure 2 illustrates the clamping system of the plastic tray.

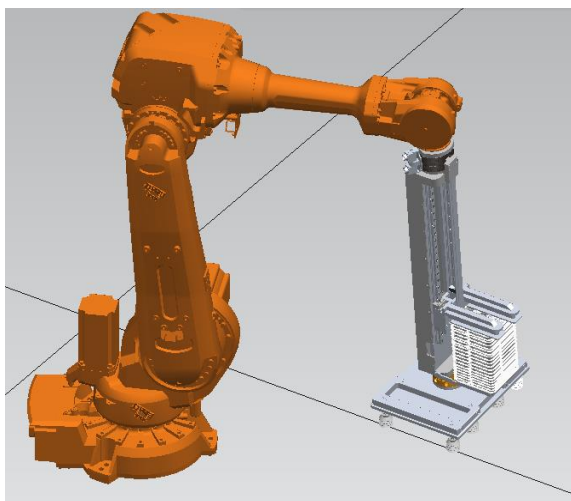


Fig. 1. Robotic unit and handled tray package in a Tecnomatix interface simulated sequence

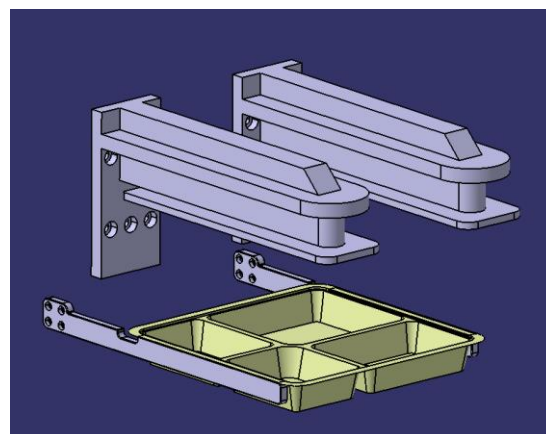


Fig. 2. Assembly of the anchoring and clamping elements of the plastic trays in the Catia V5R21

In order to efficiently perform the analysis in terms of computation time, the number of the trays in the manipulated column was reduced. Therefore, the simulation focused on the container material behavior, in order to accurately capture the plastic deformation of the trays.

Recent studies regarding computational modeling supported by experimental validation of sheet trays [1] demonstrate the topicality and importance of the research domain, but most of the assessments were related to aluminum containers and the research was devoted to the manufacturing

processes. Lindberg [2] also published a case study on the forming operations of initially plane paperboards, but the reported advances searched to increase the precision of the results coming from a simulation model of the tray forming and computation was performed with an implicit procedure. As such the proposed procedure is a novel approach in the field.

The present work is divided in the following sections: chapter two describes the main preprocessing stages, chapter three is an assessment of the main results, section four presents the experimental verification of the results and the last section summarizes the main achievements and conclusions.

2. Preparation of the computation model

All the anchoring and clamping elements of the plastic trays were imported in the preprocessing module from the CAD system in a neutral step format. The geometry was then simplified and defeatured in order to allow a fine controlled mesh and to significantly reduce the computation resources (Fig. 3). The areas where the boundary conditions will be further applied are marked with a red line.

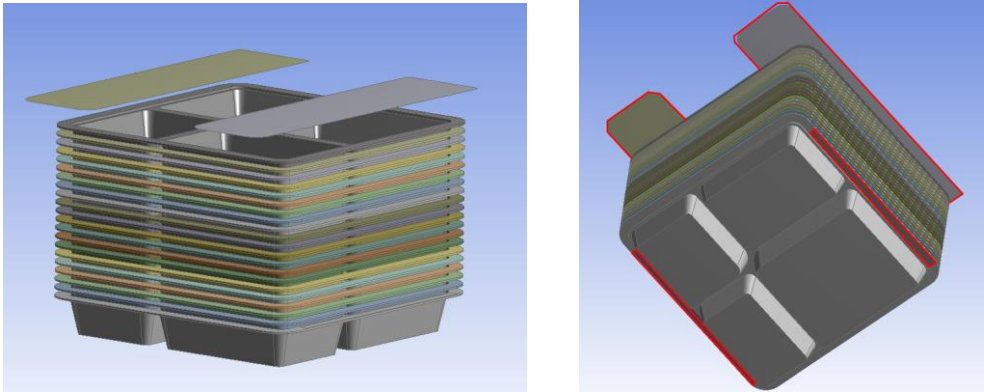


Fig. 3. Simplified geometry of the assembly

CAD details were removed and the assembly topology was cleaned (Fig. 4). The base of the trays was also simplified and the connecting rays were erased. When the primary model was ready the package pattern was generated and the column assembly was generated. Multiple checks were carried out to assure an appropriate connectivity between parts.

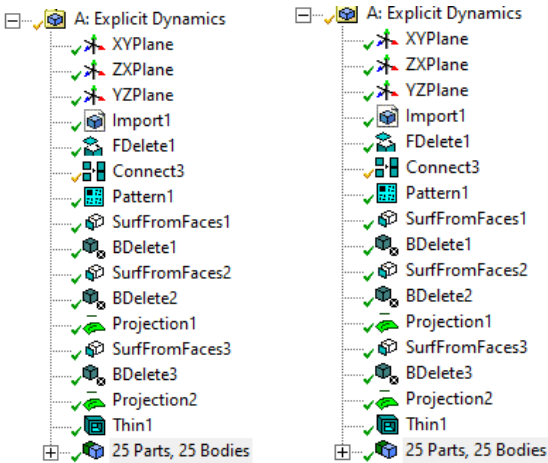


Fig. 4. Modeling and topology cleaning commands

The 3D model was then reduced to a 2D one, by extracting midsurfaces. Another important stage of the study was the assignment of appropriate materials and material laws on each component employing the Engineering database available in ANSYS and also defining new materials. A research on the web was completed to find the most appropriate material properties and material models for the components. All the data related to material definition are summarized in Table 1.

Table 1. Material properties

Material	Density [kg/m ³]	Young's Modulus [Pa]	Poisson's ratio	Specific Heat [J/kg ·C]
Aluminum Alloy	60	$7.1 \cdot 10^{10}$	0.33	875
Polyethylene	950	$1.1 \cdot 10^9$	0.42	2300
Stainless Steel	7750	$1.93 \cdot 10^{11}$	0.31	480

A high quality controlled mesh was performed and an average of 0.99 global element quality was achieved (Fig. 5). Fig. 6 illustrates the tray column mesh configuration.

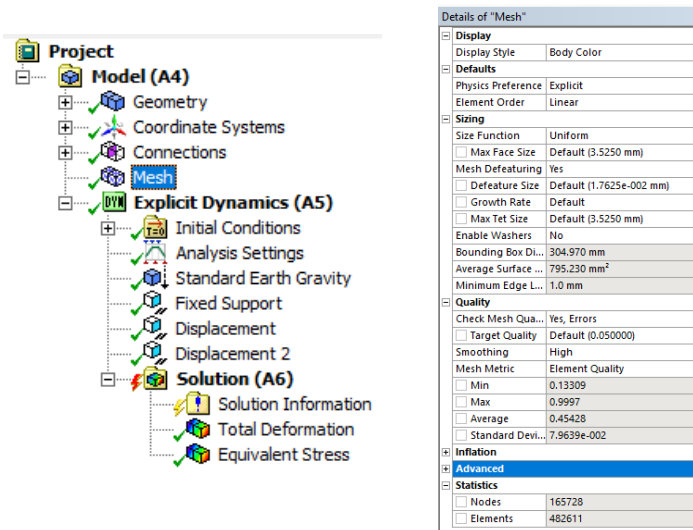


Fig. 5. Simulation work tree and mesh settings

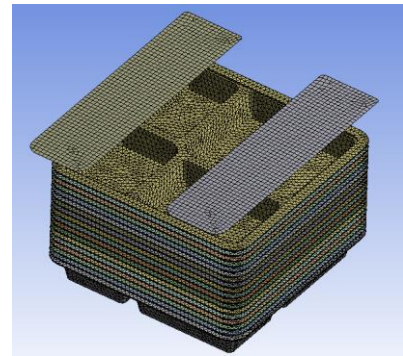


Fig. 6. Mesh details

3. Explicit dynamics analysis of the column tray

The explicit analysis algorithm works relatively easily with non-linear contacts and materials. During the computation the conservation of mass, momentum, and energy in Lagrange coordinates has to be fulfilled. These, together with a specific model of material and a set of initial data (eg. initial speeds, etc.) and boundary conditions fully define the dynamic phenomenon to be solved.

The computation algorithm calculates the accelerations at time n , the velocities at time $n + \frac{1}{2}$ and the displacements at time $n + 1$. Based on the displacements $\{x\}$, the strains are determined. Then the stresses are calculated and the cycle repeats for the next time step.

For the Lagrange formulations, the mesh distorts with the material, so that mass conservation is automatically satisfied. During the solution the conservation of mass, momentum and energy must be conserved. That is why energy conservation is constantly monitored on the graph that also expresses the quality of the results.

Initial data:

- The clamping system moves on the Z-axis 120mm.
- The simulation time is 0.005s.

It is worth mentioning that despite successive simplifications done on the geometry and the efficient choice of the resolution settings the computation time remain high and the solution was achieved after 60 000 computation cycles performed by the explicit solver. This is why several successive treys were completed each lasting about 17-20 hours. Figures 7 to 10 plot the main simulation results.

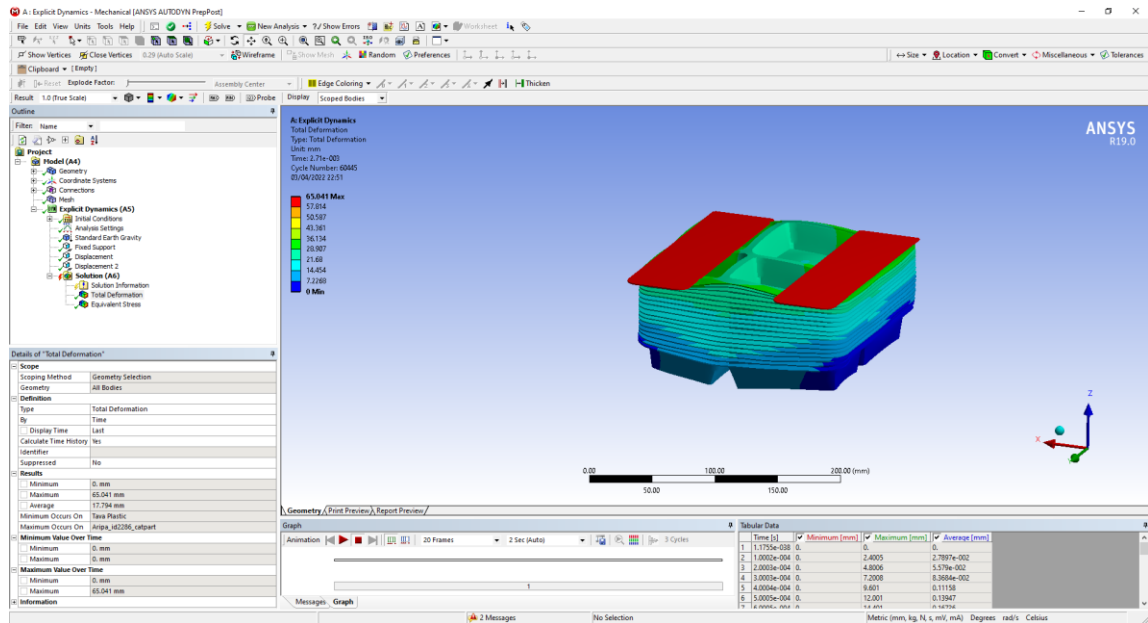


Fig. 7. Total deformation of the column tray

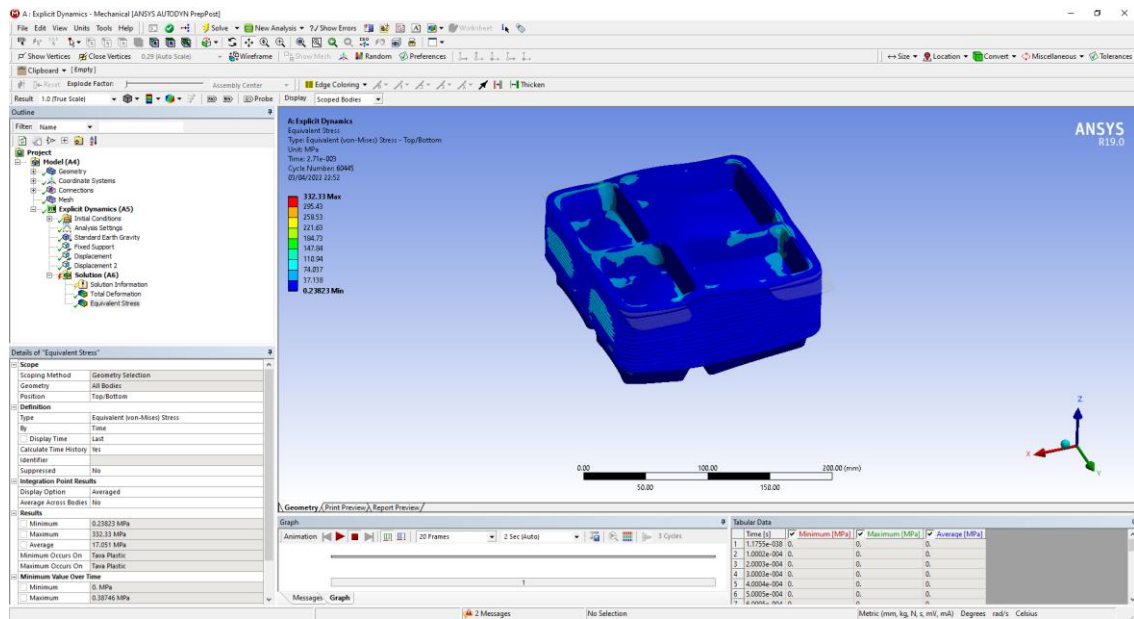


Fig. 8. The maximum equivalent von Mises stress of the column tray

The final computation took about 60 hours due to the plastic behavior of the tray pack and the fine mesh required capturing the phenomenon.

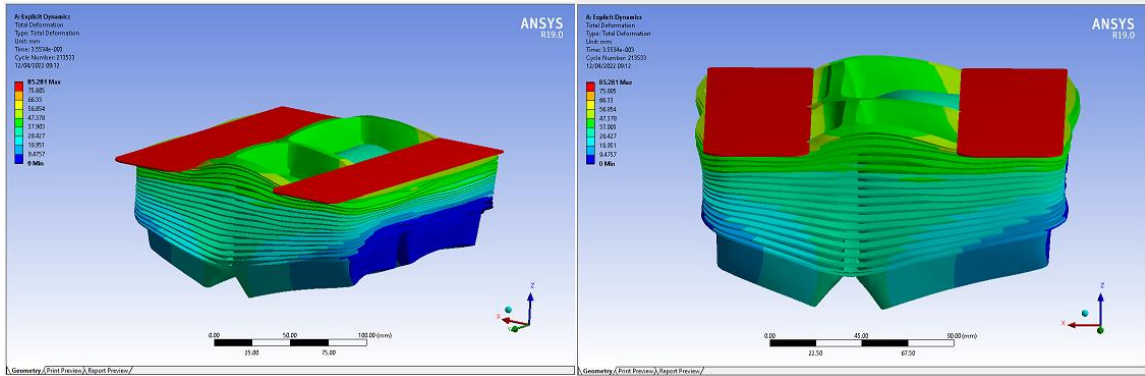


Fig. 5 Total deformation of the package in different perspectives

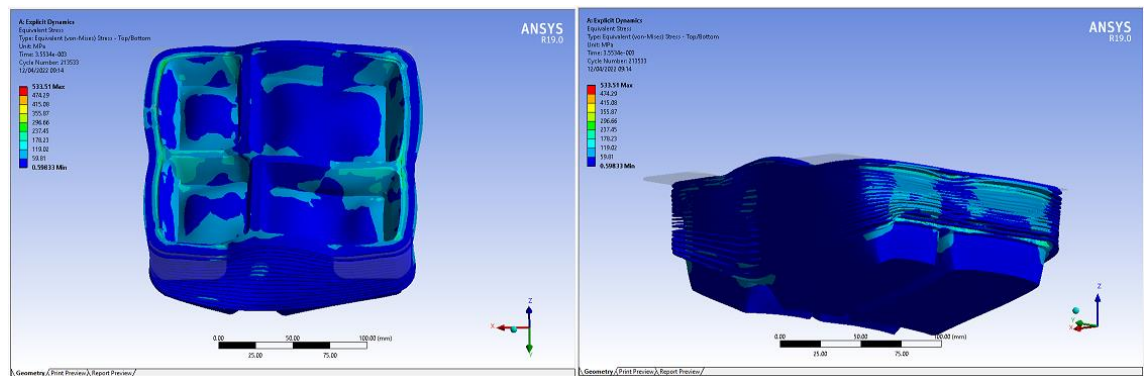


Fig. 10. Final results on the Top/Bottom part of the shell elements

4. Experimental verification of the results

Experimental investigation of the package behavior at impact with the clamping system was accomplished on an INSTRON 8872 - System for static and dynamic axial tests. The two-column system ensures increased rigidity. The drive cylinder and force cell are positioned at the top on the movable cross member. The experimental results confirmed the correctness of the calculation model and validated the simulation results. The measured exfoliation of the column reached 65 mm. The experimental results confirmed the correctness of the calculation model and validated the simulation results.

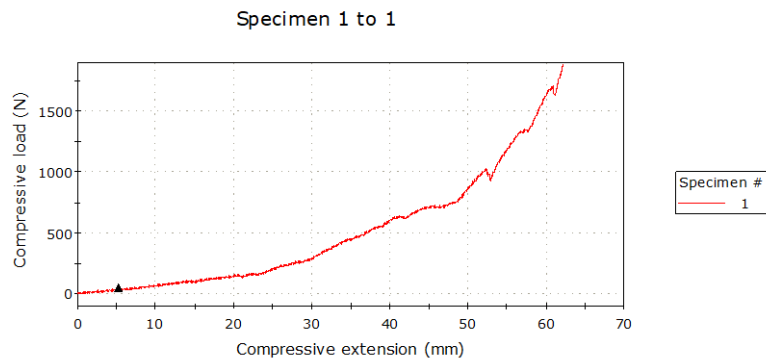
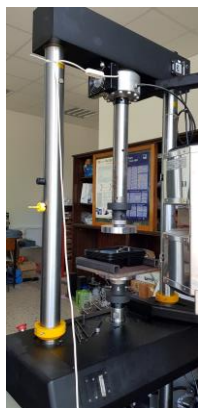


Fig. 11. Experimental setup and compressive load

5. Conclusion

The effect of the plastic deformation of the tray package has been studied by means of an explicit dynamic analysis. The results obtained on the 2D model were successful in terms of graphs and number of calculation cycles performed by the program, but the real phenomenon could not be visually captured on reduced models.

Successive material tests with composite plastics improved the results of the 2D simulations, but the final results are not realistic, because plastic containers behave as if they were manufactured of aluminum, which was not the case.

The transition from a 2D model to a 3D one brings spectacular results both from a graphical point of view but also in regard to the accuracy. The advantage of a 2D analysis is that the computation time is considerably shorter than on a 3D model. As such, the 2D analysis required 7500 calculation cycles with total time duration of 3 hours and the 3D analysis required 214 000 calculation cycles with total time duration of 60 hours.

The simplification of the geometric model was necessary at the beginning of the research as the multitude of unnecessary details would have made the analysis even more challenging. It is obvious that in an explicit dynamic analysis the accuracy of the results relies on the mesh, more than on the simulation settings. In this case a high-performance computer is required to perform the explicit dynamic analysis on a 3D model.

6. Acknowledgements

The authors of the work would like to express special thanks to prof. dr. ing. Florin BACIU, from the Materials Strength Department who gave us the opportunity to undertake laboratory verification of the simulation results.

7. Bibliography

- [1]. Mahmoodi, P., et al. „Towards a wickless smooth-Wall aluminum food packaging tray mold tool digital twin” - Advanced computational modeling supported by experimental validation. *Applied Mathematical Modeling* 105 (2022): 375-386.
- [2] Lindberg, Gustav, and Artem Kulachenko. „Tray forming operation of paperboard: A case study using implicit finite element analysis”, *Packaging Technology and Science* 35.2 (2022): 183-198.
- [3] Pupăză, C. *Modelare CAD-FEM*. Politehnica Press, Bucharest, 2013.
- [4]. *** ANSYS User’s Guide V19.0
- [5]. Chavarria, F. and Paul, D.R. 2006, “Morphology and properties of thermoplastic polyurethane nanocomposites: Effect of organoclay structure”, în: *Polymer nr. 47*, Elsevier;

EXPLICIT DYNAMIC SYMULATION OF THE FLUID BEHAVIOR IN MANIPULATED BOTTLES CONSIDERING AN ACCIDENTAL STOP OF THE COVEIOR

GIURCAN Andreea-Loredana

Faculty: Industrial Engineering and Robotics, Batchelor's programe: Robotics, 4th Study year
e-mail: andreeagiurcan@outlook.com

Scientific coordinator: Prof. dr. eng. **Cristina PUPĂZĂ**

The study consists in modeling and simulation techniques of the sloshing phaenomenon when semi-filled bottles are manipulated in an industrial robotic cell environment. The preparation of the 3D model of the plastic bottle by simplifying the complex surfaces, in order to obtain simulation results as close as possible to reality, as well as the stopper design from a simple rectangular sketch, and the liquid definition inside the bottle were the first steps of the study. The proper choice of the material properties, model parametrization and mesh generation followed the attempt. A brief description of the analysis, the formulae used as theory background and the explicit dynamic simulation where the main targets of the research. The results were validated by experiments and personal conclusions were drawn.

1. Introduction

The studied robotic cell (Fig. 1.1) integrates an articulated arm type robot with 6 numerically controlled axes. This cell is a virtual copy of an industrial application found in [1]. The red border highlights the area considered in the research.

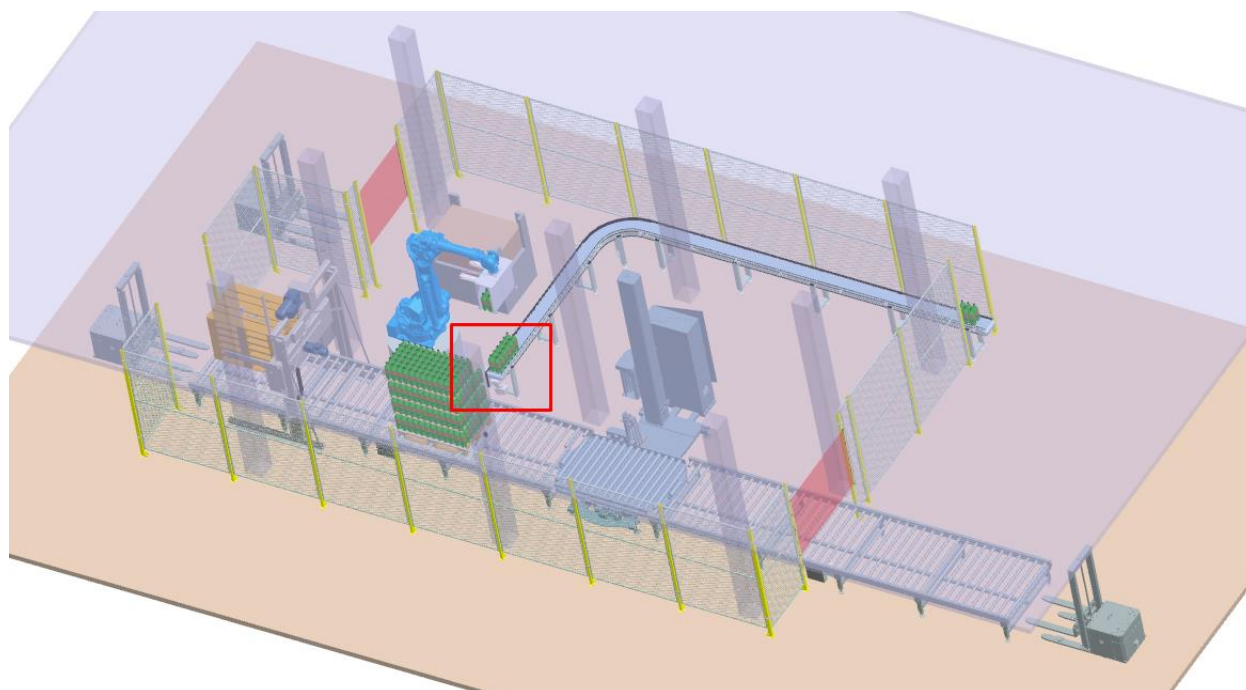


Fig. 1.1 The studied robotic cell in the NX interface

The paper consists in explicit dynamics simulation studies of the fluid behavior of the manipulated bottles (Fig. 1.2), considering an accidental sudden stop of the conveyor in ANSYS Workbench 19.0 environment.

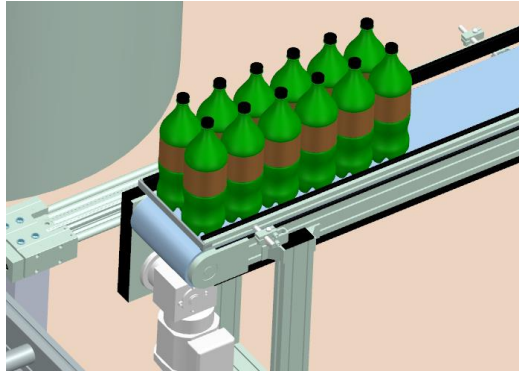


Fig. 1.2 The bottle package assembly in the NX interface: belt conveyor → plastic bottle boxes → stopper

The objective was to emphasize the fluid behaviour and the sloshing phenomenon, which are advanced simulation targets. The liquid energy, the total velocity, as well as main structural response results regarding the bottle behavior were processed and conclusion were summarized. The simulation results were verified experimentally, in the Faculty laboratory employing a color liquid and a transparent bottle. In order to obtain accurate and fast analysis results the computational model was simplified, and only a single plastic bottle and the stopper were considered.

2. State of art regarding the sloshing phenomenon

Many published papers investigate the finite element formulation of the liquid sloshing in partially filled rigid tanks of different shapes [2], [3], [4]. For exemplification purposes one of the research articles [4] was chosen to describe the mathematical model of the phenomenon, where the liquid domain is divided into two-dimensional four-node rectangular elements with the liquid velocity potential representing the nodal degrees of freedom. The sloshing effects induced were studied in terms of the slosh frequencies, liquid velocity field, free surface displacement and hydrodynamic forces acting on the tank walls. In this regard, the model is employed to study the effects of inserting a bottom-mounted vertical rigid baffle, as well as side-mounted horizontal baffles that are wholly immersed in the liquid region, in an attempt to investigate their viability in acting as slosh suppression devices.

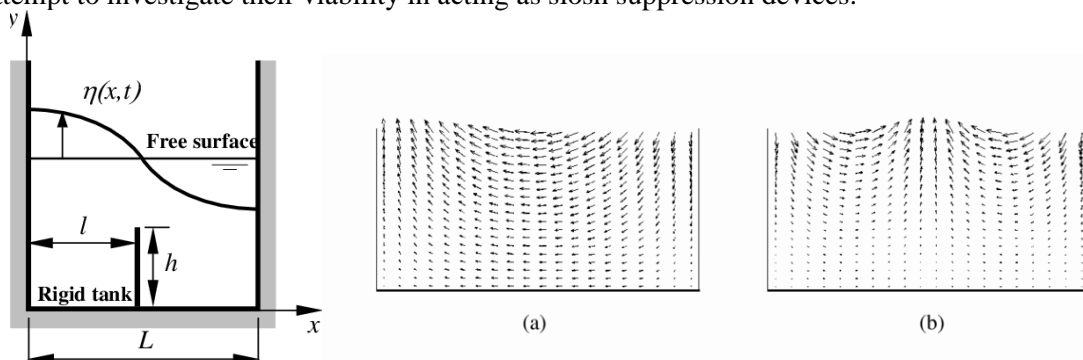


Fig. 2.2 Rigid rectangular tank. Liquid velocity field at the (a) first and (b) second slosh mode [4]

Although most of the research describe the mathematical model and experimental investigation of the liquid sloshing few papers assess the dynamics from a computational dynamics perspective, due to the numerical and modeling issues. On the other hand, recent advances in the FEM solvers surpass the numerical problems. That is why a combination Lagrange-Euler approach was chosen and the

investigation of the liquid sloshing phenomenon was carried out employing explicit dynamics functionalities.

3. Preparation of the computational model

The plastic bottle model was imported from NX in a neutral STEP format. Therefore a “cleaning” attempt for geometry was needed, and defeaturing commands were performed. The stopper was created in ANSYS Workbench because a simplified geometry was required. This stage of "cleaning" the model is done because we want to get the most realistic results.

The steps of "cleaning" the geometry represent the simplification of the model, All the details that are not relevant for the explicit dynamics simulation were deleted and a high quality mesh was prepared by merging or face splits, as well as projections and slice commands. All the model preparation stages are illustrated in Fig.3.1 and 3.2.

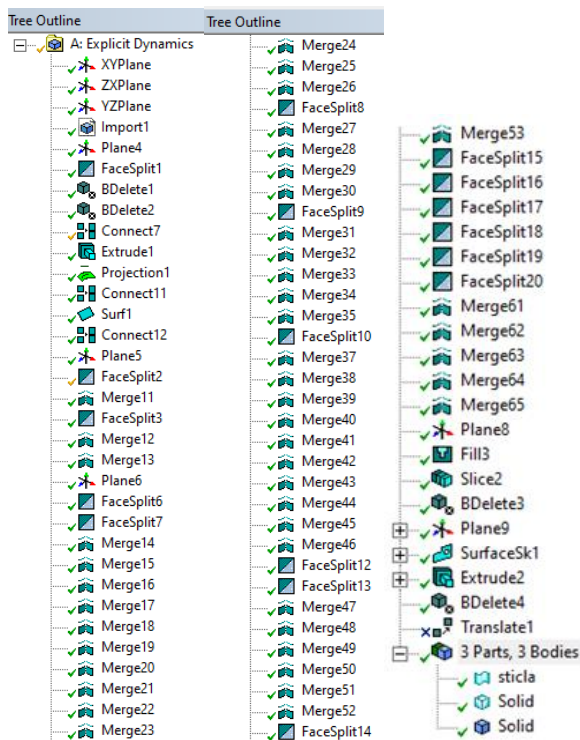


Fig. 3.1 Model preparation stages in DesignModeler

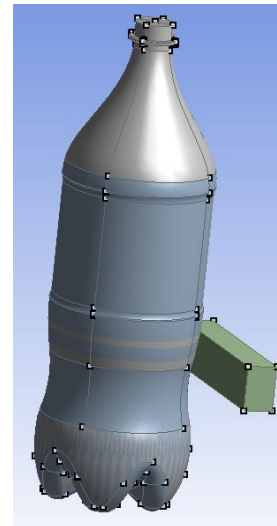


Fig. 3.2 Final geometry

Material description was done in the Engineering Data interface (Fig. 3.3). In addition to the default material used for the stopper – structural steel, plastic and a water-like material were included for the bottle and the bottle content.

Properties of Outline Row 4: Polyethylene				Properties of Outline Row 5: WATER				Properties of Outline Row 5: Structural Steel			
A	B	C	D E	A	B	C	D E	A	B	C	D E
1	Property	Value	Unit	1	Property	Value	Unit	1	Property	Value	Unit
2	Material Field Variables	Table		2	Material Field Variables	Table		2	Material Field Variables	Table	
3	Density	950	kg m ⁻³	3	Density	998	kg m ⁻³	3	Density	7850	kg m ⁻³
4	Isotropic Elasticity			4	Isotropic Elasticity			4	Isotropic Elasticity		
5	Derive from	Young's Modu...		5	Derive from	Young's Modu...		5	Derive from	Young's Modu...	
6	Young's Modulus	1,1E+09	Pa	6	Young's Modulus	2E+11	Pa	6	Young's Modulus	2E+11	Pa
7	Poisson's Ratio	0,42		7	Poisson's Ratio	0,3		7	Poisson's Ratio	0,3	
8	Bulk Modulus	2,2917E+09	Pa	8	Bulk Modulus	1,6667E+11	Pa	8	Bulk Modulus	1,6667E+11	Pa
9	Shear Modulus	3,8732E+08	Pa	9	Shear Modulus	7,6923E+10	Pa	9	Shear Modulus	7,6923E+10	Pa
10	Specific Heat, C _p	2300	J kg ⁻¹ C ⁻¹	9	Parameter S1	1,921	s m ⁻¹	10	Specific Heat, C _p	434	J kg ⁻¹ C ⁻¹

Fig. 3.3 Material properties defined in Engineering database

A controlled mesh was generated (Fig. 3.4) and multiple quality criteria checks were completed

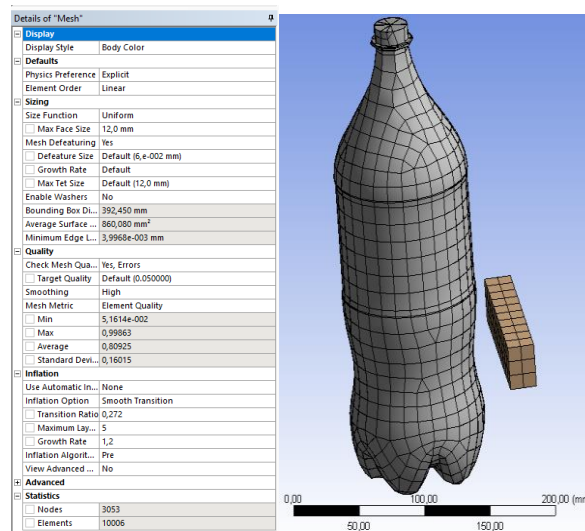


Fig. 3.4 The mesh settings and mesh quality checks

4. Explicit dynamics simulation

Explicit dynamic is employed for transient phenomena with short time duration and extreme nonlinearities [2]. This includes: extremely large deformations, rupture, destruction of the materials and structures, very nonlinear material behavior. The result is a permanent deformation of the assemblies, loose of structural stability or severe fluid flow phenomena. Some of the peculiarities of the explicit dynamics analysis are:

- ❖ Time is sampled in very small time steps and the solution is directly solved for each time increment.
- ❖ During the simulation the solution depends only on the results from the previous time step;
- ❖ It involves a very short end-time (microseconds) - so the duration of the simulated phenomenon is very short;
- ❖ The time step size depends on the mesh;
- ❖ Can solve problems with severe nonlinearities.

The explicit algorithm has the advantage that it does not calculate the stiffness matrix. This significantly reduces the computation time for transient dynamic regimes. Nowadays the explicit algorithm allows the control of calculation errors. The main differences between implicit and explicit solvers are, in fact, how the equilibrium equations are solved. Some other peculiarities of the algorithm are:

- ✚ Just like the default implicit solver it considers mass/inertia and damping, but uses a different solver;
- ✚ Iterations are not required. Results are calculated directly (or explicitly) for each time step;
- ✚ During coputation it does not matrix inversion;
- ✚ There is no inherent limit to the size of the time step;
- ✚ The time step must be less than the Courrant time step.

A brief description of the computation algorithms is: → accelerations are calculated $\{\ddot{x}\}$ at time n , velocities $\{\dot{x}\}$ at time $n + \frac{1}{2}$ and deformations $\{x\}$ at time $n+1$. Based on displacements $\{x\}$, the strains $\{\epsilon\}$ are assessed. Then the stress vector is determined $\{\sigma\}$. And the cycle is repeated for the next time step.

The Explicit Dynamics solver uses a differential time integration scheme called the Leapfrog method [5]. After calculating the forces in the nodes (resulting from internal stresses, contact or boundary conditions), the nodal accelerations are obtained by dividing the force to the mass:

$$\ddot{x}_i = b_i + \frac{F_i}{m} \quad (1)$$

where \ddot{x}_i are the components of nodal acceleration ($i = 1,2,3$), F_i are the forces acting in the nodes, b_i are the components of the acceleration of the body and m is the nodal mass.

With the accelerations at the time $n - 1/2$ the speeds are calculated at the time $n + 1/2$:

$$\dot{x}_i^{n+1/2} = \dot{x}_i^{n-1/2} + \ddot{x}_i^n \Delta t^n \quad (2)$$

Finally, the node positions are updated at time $n + 1$ by integrating the speeds:

$$x_i^{n+1} = x_i^n + \dot{x}_i^{n+1/2} \Delta t^{n+1/2} \quad (3)$$

For each time step these equations are explicitly solved for each element in the model, based on the input values at the end of the previous step. In the first the solution is computed based on the initial conditions. When solving the equations only the conservation of mass and momentum is applied. However, in explicit simulations, mass, momentum and energy should be conserved. That is why energy conservation is constantly monitored during computation on the graph, which also illustrates the quality of the results.

Solution settings were configured as illustrated in Fig. 4.1. The stopper was considered rigid. The simulation regime was considered: the conveyor velocity: 500 mm/s; total duration of the analysis 0.2s, the duration until the impact: 0.06 s

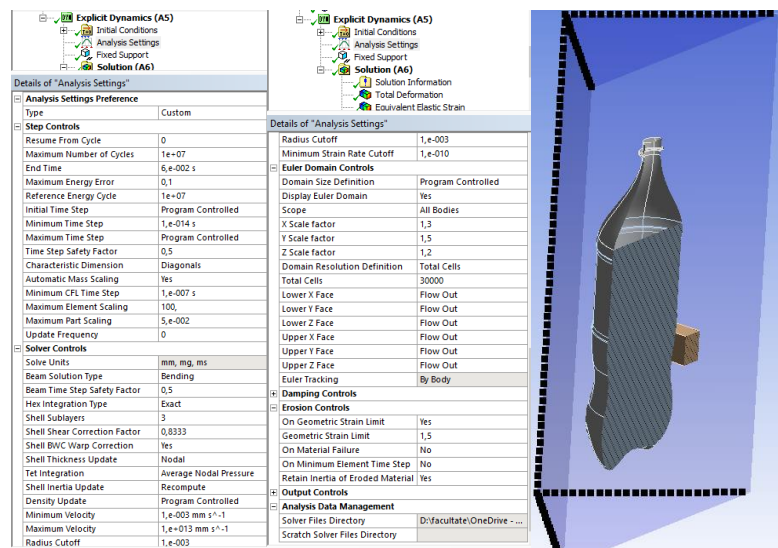


Fig. 4.1 Analysis settings

5. Results discussion

In an explicit dynamics analysis the model encompasses not only the equations of motion but also the propagation of shock waves phenomenon throughout the material. Un example of shock waves modeling is the Equation of state for the Hugoniot shock (Fig. 5.1), that allows the sloshing waves to occur on the results. This model was chosen for the liquid behavior.



a. Hugoniot and Rayleigh shock line in p-v plane for weak shock b. Hugoniot elastic limit in the p-v plane for shock in the elasto-plastic field

Fig. 5.1 The Hugoniot shock description [6]

The Hugoniot shock describes the location of all possible thermodynamic states in which there may be a material behind a shock, projected on a two-dimensional state plane [6]. Therefore, it is a set of equilibrium states and does not specifically represent the way in which a material undergoes transformations. Weak shocks are isentropic (the entropy is constant) - the material is charged from the initial state to the final state by a compression wave with converging characteristics (Fig. 5.1.a). When a severe shock occurs these simplifications can no longer be assumed. However, for engineering calculations, the isentropic is considered to be close enough to Hugoniot that it can be considered a linear approximation (Fig. 5.1.b). If between the initial state and the final state the charge is given by Hugoniot's law for an "equivalent" compression wave, then the shock conditions can be modeled by a straight line between the initial and final state. This line is called the Rayleigh-Hugoniot line and has the following equation:

$$p_2 - p_1 = u_s^2 \left(\rho_1 - \frac{\rho_1^2}{\rho_2} \right) \quad (4)$$

The solution was monitored employing the kinetic and internal and contact energy and the hourglass energy which gives a measure of the mesh quality and model behaviour (Fig. 5.2).

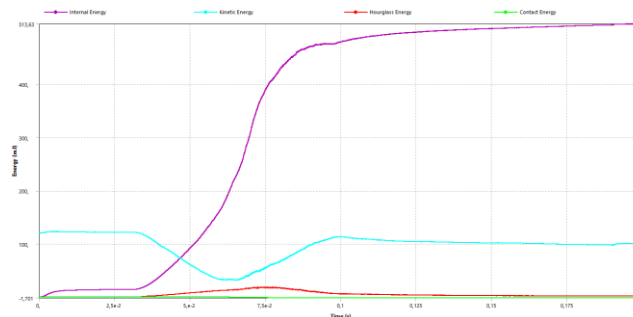


Fig. 5.2 Energy summary during computation.

During the simulation the kinetic energy (light blue) decreases when the impact occurs, the internal energy (purple) increases being influenced by the model displacement and strain in the model and the hourglass energy (red) helps to identify mesh errors, if the values reach a maximum allowable limit, which did not happen in our case.

Figures 5.3 to 5.6 summarize the main simulation results.

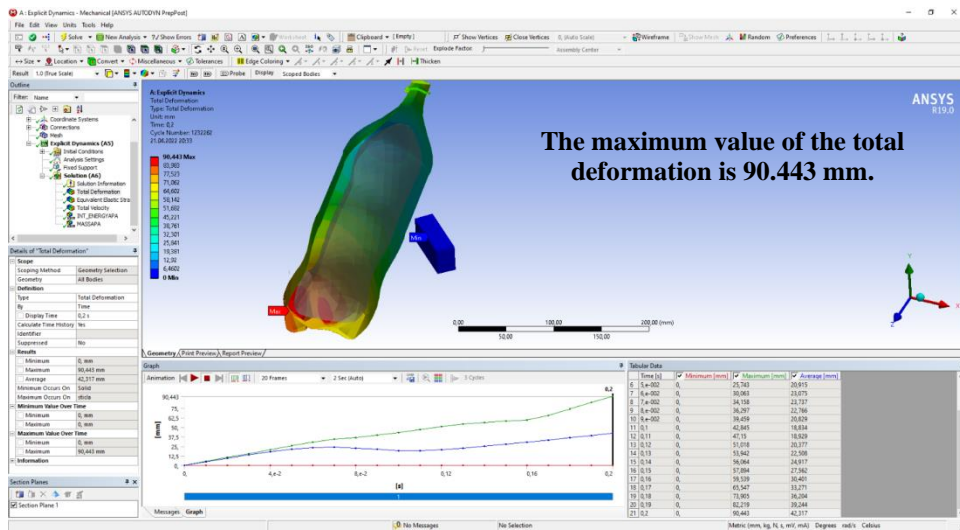


Fig. 5.3 Total deformation of the model

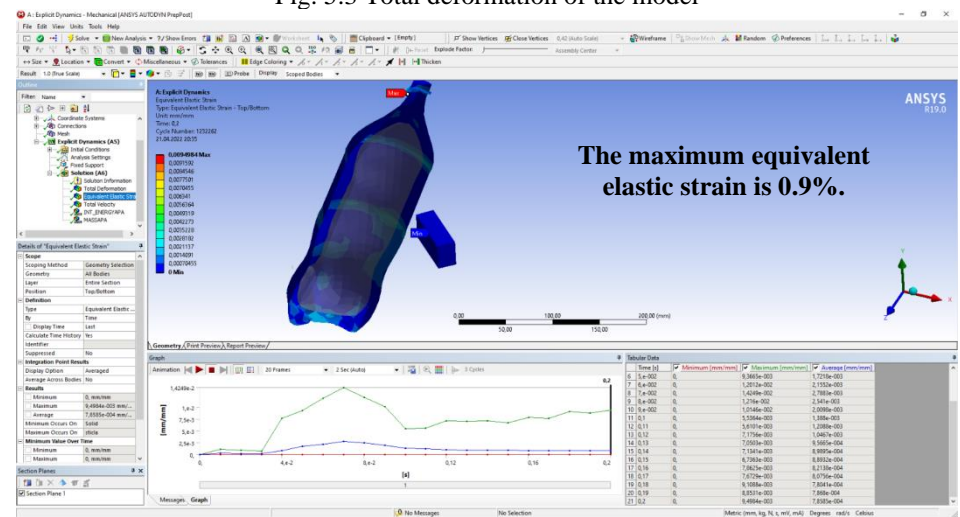


Fig. 5.4 The equivalent elastic strain

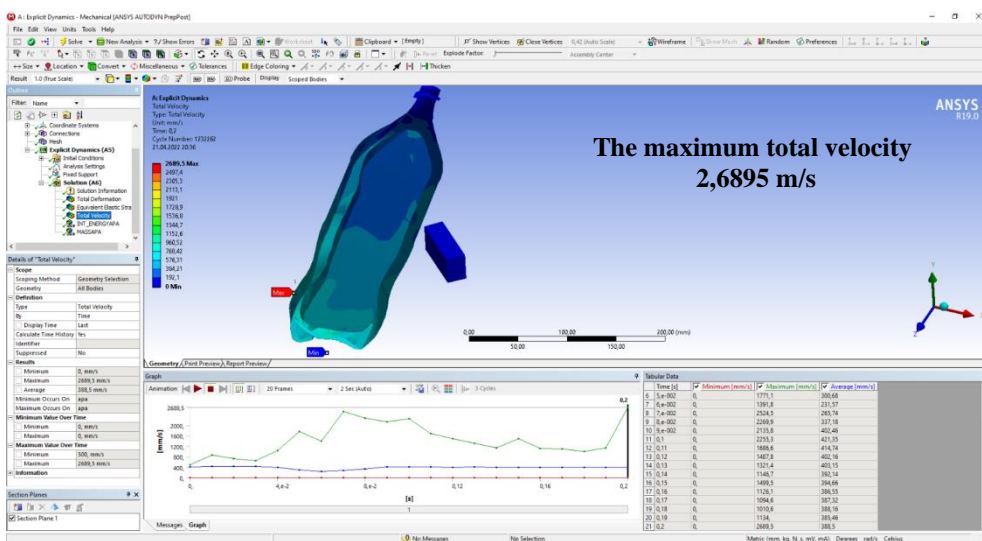


Fig. 5.5 Total velocity

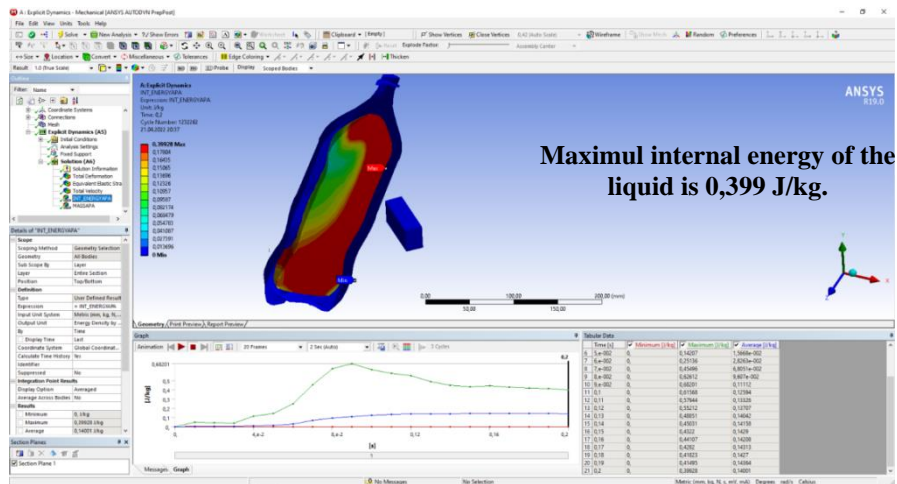


Fig. 5.6 The results obtained from the processing of water energy

The simulation results were validated by experimental tests in the faculty Logistics laboratory (Fig. 5.7). The same behaviour of the liquid was observed.



Fig. 5.7 Laboratory experiments

6. Conclusion

The simulation was successfully completed in 19.5 hours on a laptop. The model was initially generated by many complex surfaces, A detailed and manual simplification of the polyethylene bottle model was needed in order to obtain accurate results. The solution was attained using two solvers: Lagrange solver for the structural components and the Euler solver was activated for the liquid behaviour, which allowed the visualization of the sloshing phenomenon. The visual effect was diminished by the fact that the bottle was considered almost fully filled. Future work may focus on a liquid mixture and bubbles effect.

7. Bibliography

- [1] *** Robotic cell: <https://www.youtube.com/watch?v=cyLx9ogbAnM>
- [2] Brietman, N., Pinhas Z., Bar-Yoseph, and Suponitsky, V. - Nonlinear liquid sloshing dynamics: Post-processing of conventional finite element solutions by digital filters. *Ocean Engineering* 249 (2022): 110837.
- [3] Xue, Mi-An, et al., Sloshing dynamics in cylindrical tank with porous layer under harmonic and seismic excitations, *Ocean Engineering* 235 (2021): 109373.
- [4] Mustafa, A., Finite element analysis of sloshing in liquid-filled containers, *Production Engineering and Design for Development (PEDD'07)*, (2006): 793-803.
- [5] Pupăză, C.. *Modelare CAD-FEM*. Politehnica Press, Bucharest, 2013.
- [6] Gregg, F., Grady, D. and Vogler, T.G - "Modeling thermodynamic compression states in distended materials and mixtures" *Procedia Engineering* 58 (2013): 724-731.

SIMULATION OF A TACTILE TESTING SYSTEM OPERATION BASED ON THE TRANSIENT STRUCTURAL DYNAMIC ANALYSIS

GEAMĂNU I. Mihai-Bogdan

Faculty of Industrial Engineering and Robotics, Robotics specialization, 4th academic year,
email: bogdan.asx14@gmail.com

Scientific coordinator: Professor **Tiberiu DOBRESCU** PhD. Eng.

Scientific coordinator: Professor **Cristina PUPĂZĂ** PhD. Eng.

SUMMARY: The research consists in the simulation of a tactile testing system employed in the computer industry, comprising the end-effectors of the industrial robot, based on a Finite Element Analysis in a transient regime. Considering the detailed physical design of the end-effectors and intelligent computing devices, the components of the automated testing system are modeled in the CAD environment. By transferring the CAD database to the CAE preprocessing system, assigning the appropriate materials, and defining kinematic joints and constraints, simulation results can be extracted, and the behavior of the end-effectors and the components of the tested device can be assessed. The results can be further employed for the design optimization of the computing devices by replacing the materials from which some components are made, optimizing the shape of the keys and of the touch panel, but also optimizing the physical testing methods.

KEYWORDS: laptop, materials, tactile end-effector, dynamic behavior, optimization.

1. Introduction

Testing of the touch screens, keyboards, and touch panels of smart devices, such as mobile phones, tablets, and laptops, involves performing pre-set routines according to international standards, for instance: punctual precision testing, testing the input resolution, testing the replication of the trajectory established by the program, etc. These test procedures can be performed manually by humans, but the execution times of the tests is long, and the productivity is poor. Therefore, the tests are performed automatically with the help of industrial robots, which have end-effectors devoted to this task.

The overall size of the smart device test cell (Fig. 1) relies on the size of the device to be tested. The robot is then chosen in relationship with the workspace required to reach any point that is a target to be reached and tested. Generally, the robotic cell consists of the industrial robot, the tested device, the tactile end-effectors, end-effector storage system (if the robot is equipped with an automatic coupling-decoupling system), and the modular clamping system of the tested device, the computer through which the data acquisition is done, and the results of the tests are monitored.

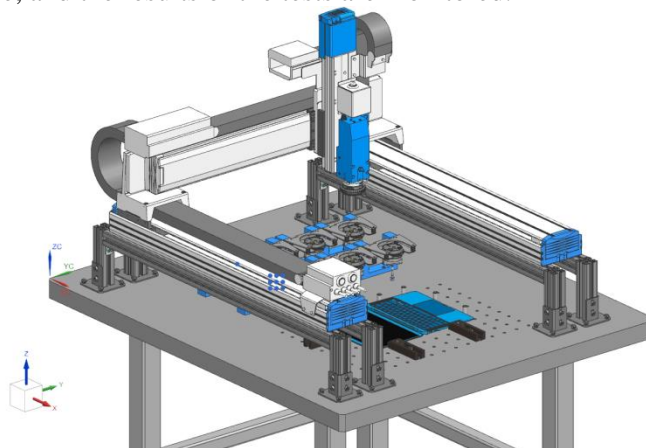


Fig. 1. Isometric view of the robotic cell virtual model

The robotic cell works in the following steps:

- The robot equips an end-effector corresponding to the test to be performed from the end-effector storage system;
- The robot moves to the point where it can start the testing procedure;
- The scheduled test is performed by pressing the tactile end-effector on the tested item (key, touch panel, touch screen);
- The robot moves to the safe position of the scheduled test;
- The robot moves to the point where it can store the tactile end-effector in the storage system;
- The end-effector is stored in the storage system, and the robot passes to the next programmed point.

This research is focused on the operation of the tactile testing system, respectively the tactile end-effectors employed by the industrial robot, based on a dynamic Finite Element Method (FEM) analysis in the transient regime.

The original design of the end-effector (Fig. 2) is the first objective to create the computational model.

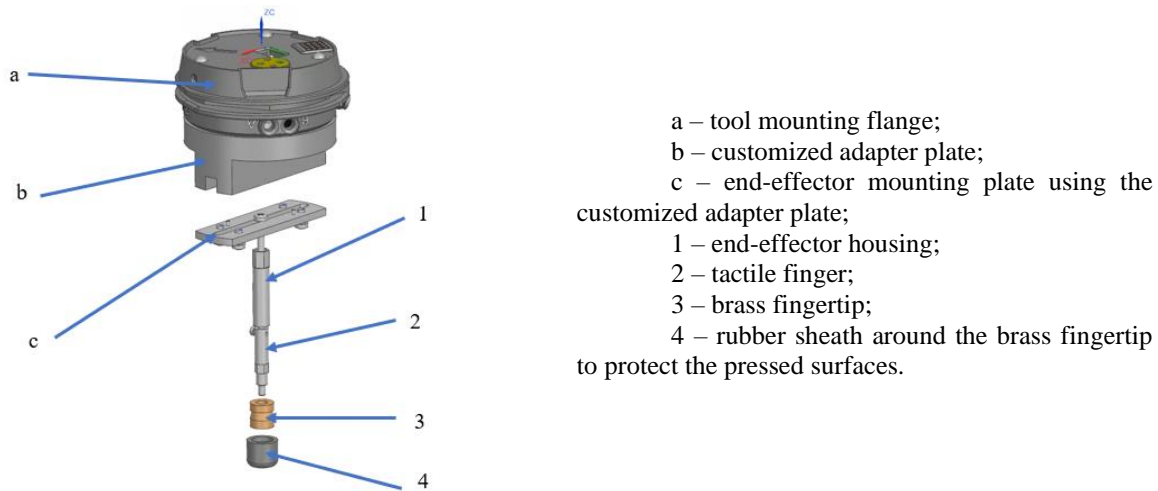


Fig. 2. CAD model of the end-effector employed in the computer testing system

Additionally, the connection between the upper housing and the tactile finger of the end-effector is made by means of a helical spring.

The objective of the simulation employing FEM is to analyze the behavior of the tactile system during the interaction with the tested device. The most important elements of the tactile end-effector design are *the helical spring* and *the rubber sheath* around the brass fingertip. The rest of the paper is divided in: a brief assessment of published studies on the topic in Chapter 2, a description of the computational model preparation stages included in Chapter 3, discussion of the simulation results in Chapter 4 - conclusion regarding the industrial use of the tactile testing system and future work.

2. Related work

While the technology of using industrial robots with tactile end-effectors to test the functionality of touchpads, keyboards and touchscreens is still at the beginning, the research done regarding this new technology is still developing [1], [2], [3]. The studies on tactile end-effectors are focused on the end-effectors design, stiffness, and the manufacturing technology. None of the published works treats the dynamic response created by pressing the tactile end-effector employing an industrial robot on the tactile surfaces. The only available information about tactile surface testing automation and optimizing the test methods by analyzing mechanical information are the videos shared by some companies on YouTube, which can not be considered scientific published works.

3. Preparation of the computational model

The major difference between the CAD model of the robotic cell and the computational model in a CAE environment is that the FEM model encompasses fewer components - only those relevant to the simulation - and these parts have undergone geometrical simplifications. The reason for geometric defeaturing is that the discretization can much more correctly approximate simple geometries rather than detailed ones and we can avoid small distorted finite elements generation.

Figure 3 illustrates the simplified geometry of the computational model. It is evident that the housing of the computing device has been replaced with a simplified geometry that approximates the exact shape of the original housing, the keyboard keys that are not used in the simulation have been removed from the geometry, and for each tested item (touch panel, key, touch screen) a corresponding effector has been placed to perform the specific test during the simulation, as happens on the real robotic cell. The operation of each effector will be defined on different time steps in the transient analysis settings, to simulate the successive and individual compressions performed by the robot. Regarding the simplification of the end-effector geometry (Fig. 3-b), the fillet diameter of the lower finger was replaced by a simple cylinder with the same outer diameter, the key radius was deleted from the housing geometry, and the brass tip geometry was simplified and transformed into a cylinder

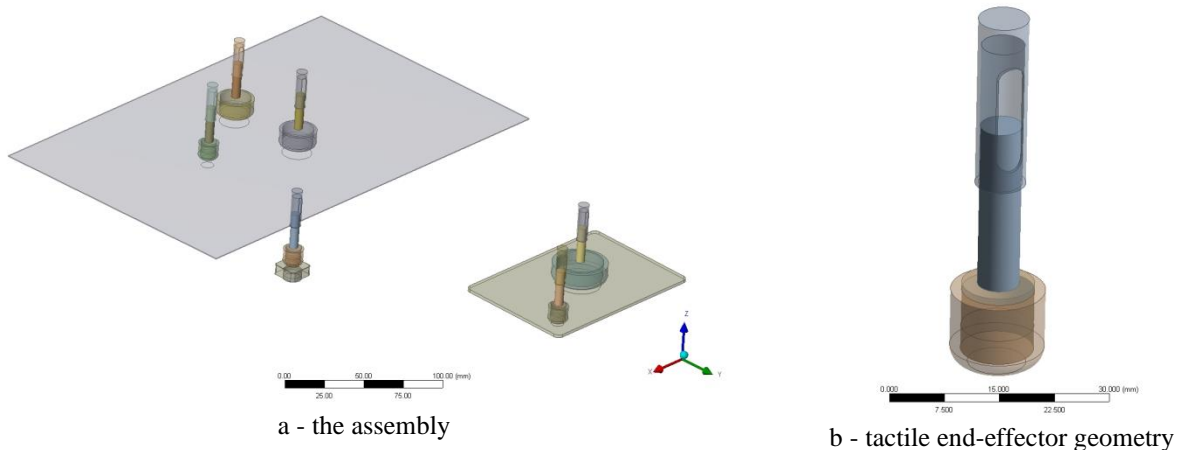
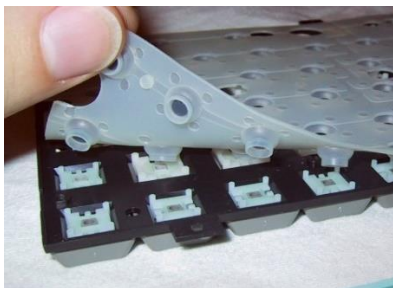
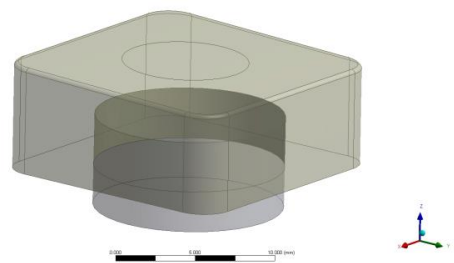


Fig. 3. Simplified geometry of the computational model

A detail of the model is illustrated in Figure 4-b where a simple model of the membrane under the keyboard is required. The membrane makes the connection between the compressed key and the contact corresponding to the key on the motherboard. Since the scope is to press a single key, it is sufficient to model a cylinder similar in size to the membrane under a key and to create a cavity inside in the imported CAD model.



a - the membrane beneath the keyboard that transmits the impulse force of the key to the electric board



b - cavity model in the pressed key and the simplified membrane insert

In order to perform a reliable simulation, it is essential to properly define the materials of the components. As such, the materials employed will be the followings (Fig. 5): • aluminum alloy -

imported from the ANSYS Workbench materials library; • brass - defined; • glass - imported from the ANSYS Workbench materials library; • polycarbonate - defined; • rubber - defined.

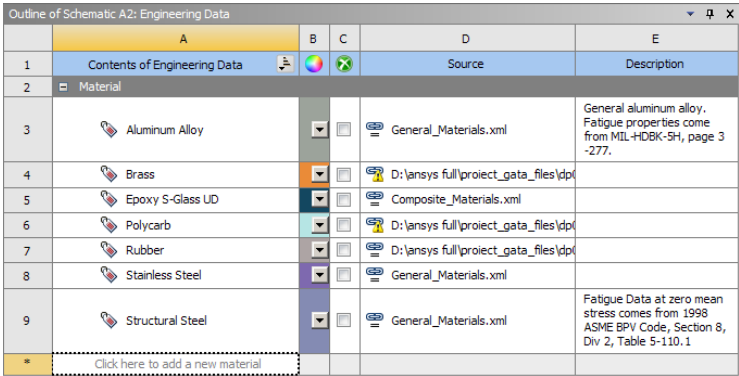


Fig. 5. Employed materials

For the newly defined materials the relevant properties are [4]: • density; • modulus of elasticity (Young's modulus); • Poisson's ratio; • transversal modulus of elasticity & the incompressibility parameter for rubber. The material properties defined for brass and polycarbonate are summarized in Table 1.

Table 1. Material properties for brass and polycarbonate

Material	Density g/cm ³	Isotropic elasticity	
		Young modulus MPa	Poisson's ratio
Brass	8.39	1.17 · 10 ⁵	0.34
Polycarbonate	1.2	2400	0.37

The rubber material properties are as follows: isotropic elasticity (Young's modulus = 60 MPa and Poisson's ratio = 0.475); tensile yield strength: 250 MPa; compressive yield strength: 250 MPa; tensile ultimate strength: 460 MPa;

For the rest of the materials employed in the project all the properties were imported from the ANSYS Workbench materials library. The transient structural analysis determines the dynamic response of the structure to the time-varying forces based on an implicit calculation scheme of the equations of motion [5]. [6]. The main results obtained from the transient analysis are: displacements, equivalent strains, equivalent stresses, force reactions, contact forces, etc. This analysis type can also be used to monitor the operation of the assembly throughout the kinematic cycle for a limited time, for which the functional simulation is performed.

The most important issues when running a transient analysis are: the appropriate choice of the material properties and material behavior laws, the accurate definition of the contact types between the components, and the right definition of the kinematic joints between the components. The kinematic joint motion between components can be programmed according to time duration of the simulation.

Because in the transient structural analysis the time response of the structure is nonlinear and the analysis involves large displacements of the parts in the computational model, the parameter of large deformations is considered as active.

In addition, nonlinearities occur during the simulation due to the interaction conditions and contact between parts by taking into account friction and contact stiffness, as well as the system damping. Therefore, the time step controls are established in the following way:

- duration of the time step: $t = 1$ s;
- initial time step: $\Delta t = 0,05$ s;
- minimum time step: $\Delta t = 0,05$ s;
- maximum time step: $\Delta t = 0,1$ s.

These values may vary depending on the studied phenomena, being higher in the case of smaller nonlinearities of the model and a very good mesh, or lower otherwise. In addition, during the simulation the contact between the components can be activated or deactivated using the “Contact step control” advanced functionality. The simulation starts with preliminary checks of the geometry integrity (the model topology) and mesh quality criteria.

The components for which the mesh is intended to be disregarded during simulation, such as laptop case, keyboard, etc., their behavior has been set to “Rigid”. The second step in performing the simulation is to define the interaction between the components, either contacts or kinematic joints. The links between the parts that have been defined are:

- Fixed joint between the tested device and the worktable;
- Fixed joint between the touch panel, screen, and keyboard membrane and the tested device;
- Bonded contact - securing the lower finger of the effector with the brass fingertip;
- Translational joint between the upper housing and the lower finger of the end-effector;
- Bonded contact between the brass fingertip and the rubber sheath;
- Frictional contact between the end-effectors and the tested device;
- Spring joint - the elastic connection between the upper housing and the lower finger using a helical spring.

Regarding the boundary conditions of the structural elements the following assumptions were done (Fig. 6):

- the touch panel has been realistically attached to the case, leaving the buttons free;
- the membrane of the key was fixed on the entire circumference of its base;
- the screen was fixed by recessing it using its side faces.

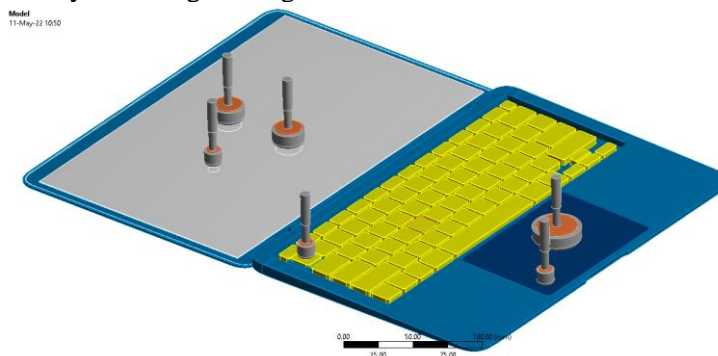


Fig. 6. Assembly in ANSYS Mechanical

To improve the default generated mesh to obtain accurate simulation results, the following mesh settings have been considered:

- the size of the mesh is different for each element, depending on its size and importance in the simulation;
- the mesh is mapped to the surfaces that allows this technique;
- the mesh for the upper housings, the lower fingers of the end-effectors, the brass fingertips, the rubber sheaths, the membrane of the pressed key and the housing of the pressed key is created with dominant hexahedral elements;
- the mesh in the contact area complies compatible mesh requirements between parts, such as: the mesh on the outer surface of the rubber sheath is projected to the touched surfaces.

Finally, using the global mesh quality criterion (Fig. 7) the mesh has reached an average value of 75.44%.

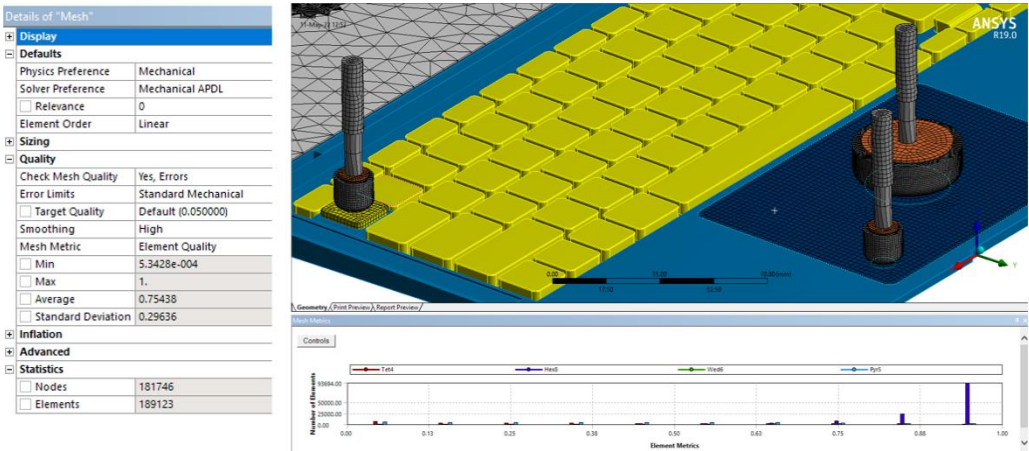


Fig. 7. Mesh and mesh quality and its graphical representation

Loads and constraints. In order to define each load pair and contact action as a function of time, it is compulsory to measure the initial distance between the parts that will come in contact and the movement of the mobile element (end-effector) with the added pressured distance. This distance was measured using the “Distance finder” command in the ANSYS Workbench Design Modeler. Remote displacements were defined to simulate the negative Z-axis movement of the robot and control the contact activity between each end-effector and the laptop.

The simulation solution was performed on a computer with the following specifications: CPU: Intel Core i5-3570K @4.0-4.4 GHz; RAM: 32 GB DDR3; SSD: 981 GB. The total elapsed time was 8 hours and 30 minutes. The results were obtained after 474 iterations (Fig. 8), after 10-time steps and a single bisection occurred during the simulation. Each time step was calculated from 0.05 to 0.05 seconds, according to the initial settings of the analysis. The bisection occurred when the 30 mm end-effector is separated from the touch panel and can be neglected due to the good overall global response of the assembly.

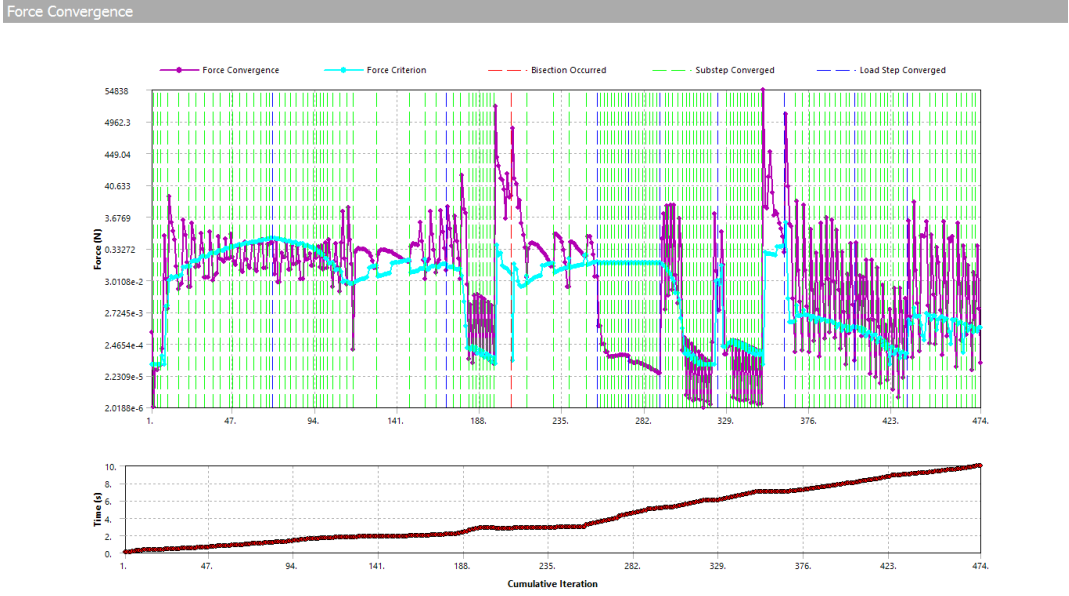


Fig. 8. Graph representing the evolution of the forces over time (force convergence)

The results were customized as follows: for the rubber sheaths of the end-effectors and the membrane of the key the equivalent elastic strains was processed (Fig. 9 and Fig. 12); - for the touch panel and the touch screen both the equivalent stress and the directional displacements on the Z-axis (Fig. 10, Fig. 11, and Fig. 13 to Fig. 16).

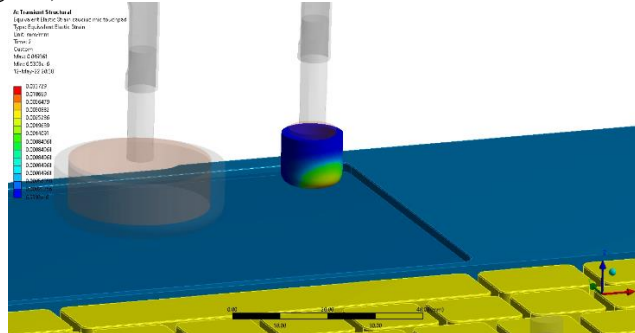


Fig. 9. The maximum elastic strain of the 10 mm rubber sheath when pressing the touch panel is 3.7%

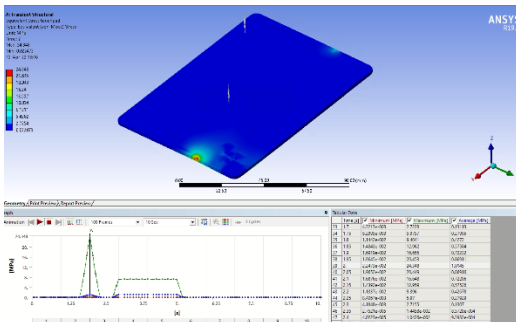


Fig. 10. The maximum equivalent von Mises stresses of the touch panel is 24.348 MPa

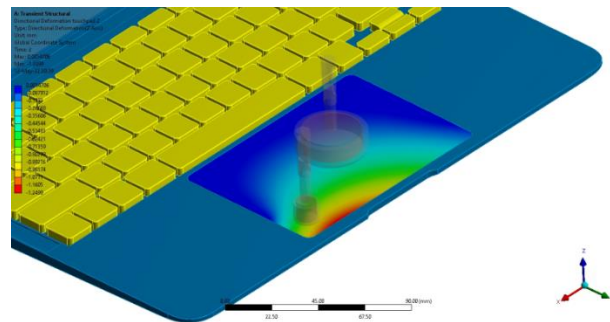


Fig. 11. The maximum deformation on the Z-axis of the touch panel is -1.2499 mm

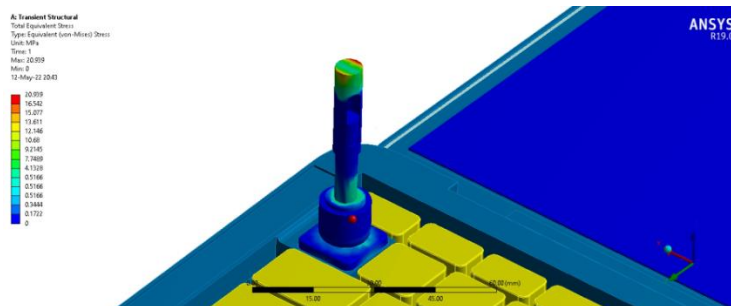


Fig. 12. The maximum equivalent stresses in the pressed key appear in the fixing area of the end-effector and are equal to 20,939 MPa

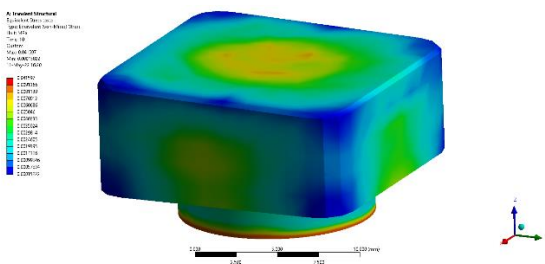


Fig. 13. Equivalent stresses occur in both the pressed key and the membrane; the maximum stress is equal to 0.04 MPa

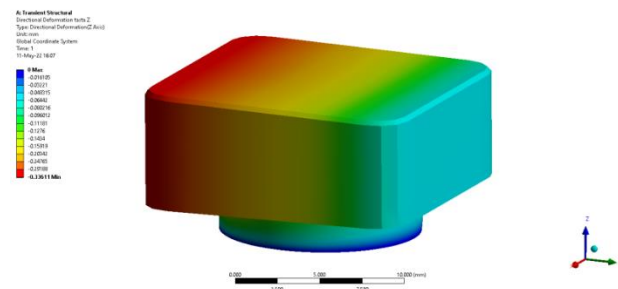


Fig. 14. Maximum directional deformation on the Z-axis of the pressed key occurs when it's pressed, and the deformation is equal to -0.33 mm

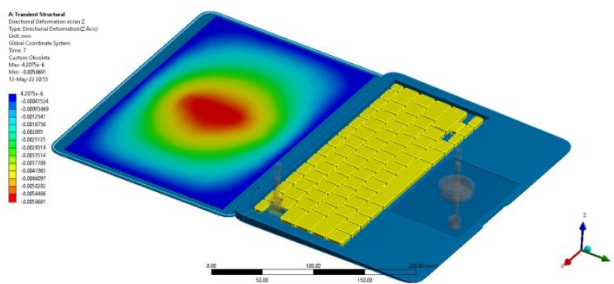


Fig. 15. Maximum deformation on the Z-axis of the screen occurs when it's pressed, and the deformation is equal to -0.006 mm

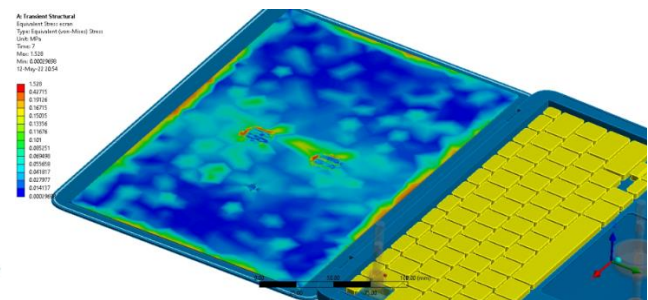


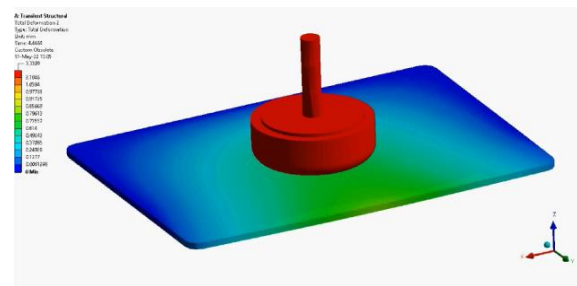
Fig. 16. Maximum stresses occur in the screen when pressed and are equal to 1.53 MPa

4. Conclusions

The transient structural analysis shows that the behavior of the elastic elements can be accurately analyzed and investigated over time and the simulated response of the system can be synchronized with the forces monitored on the real test bench.



a- real life touch panel confidence test [7]



b- simulated touch panel confidence test along with its results

Fig. 17. The touch panel confidence test – detecting involuntary human touches

The purpose of this research is to verify the laptop design when operating at extreme conditions. The possibility of material replacement for different components can be taken into account, but the results proved that for the analyzed system this was not needed.

FEM demonstrated its capabilities for creating virtual conditions for testing a laptop's components in order to check if it meets the hardware manufacturers, and the customer's requirements.

5. Bibliography

- [1]. Țîmpea Ș., Cosma C., Șoșdean D. (2019), "Touch Screen Tester Device End-Effector", volume 56 (issue 2), pages 444-448, Materiale Plastice magazine.
- [2]. *** Tactile Automation Official Youtube Channel, updated on May 12nd 2022
- [3]. *** Tactile Automation – Spring Finger Datasheet & Fingertip Datasheet, updated on May 12nd 2022
- [4]. *** AZO Materials – datasheets for rubber, brass, and polycarbonate, article numbers 6380, 920, 1934, updated on May 12nd 2022
- [5]. *** Wikipedia – Augmented Lagrange Method
- [6]. *** ANSYS Theory Manual, V19.0
- [7]. *** www.upload.wikimedia.org/wikipedia/commons/6/6e/Membrane_keyboard.jpg

ROBOTIC CELL FOR VIDEO INSPECTION, WITH FOUR WORKSTATIONS, INTEGRATING AN INDUSTRIAL ARTICULATED ARM ROBOT ON TRACK MOTION PLATFORM AND FOUR PERIPHERAL ROBOTIC SYSTEMS

CHISCOCIU Violeta-Georgiana

Faculty: Industrial Engineering and Robotics, Specialty: Robotics, Year of study: 4;
e-mail: violeta.chiscociu7@outlook.com;

Scientific leader: Prof.dr.ing. **Florin Adrian NICOLESCU**

The 3D vision offline quality and metrology cell is the ABB standard cell for off-line quality inspection. It offers a faster, more dynamic technology than traditional CMM (Coordinated Measuring Machine) based methods. The measurement is performed without contact, using only structured light for the object geometry, by projecting light patterns onto the measured part, with the resulting data being used to create a digitalised high-density 3D point cloud representation of that part.

The procedure for calibrating the working volume consists in taking images of the space of interest from different positions and with different camera angles. Each shot locates an independent number of simple targets, coded targets and the scaling bar. Once the whole capture process has been completed, the data are processed and the user is provided with a file with the XYZ position of all the measured simple targets. These XYZ references will be used to combine all the digitalization made while the parts are measured.

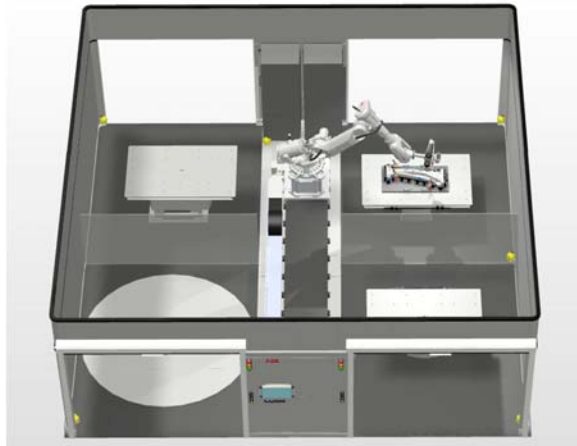
1. Introduction

The study aims to present a revolutionary robotic inspection cell, integrating an industrial articulated arm robot from ABB, equipped with ABB SIDIO AIRUS optical scanner.

The robotic cell contains four workstations, an industrial robot on track motion platform, four peripheral robotic systems, safety system, storage systems, transfer systems, monitors and controllers, all in a thermostatic enclosure.

The industrial articulated arm robot from ABB corresponds to IRB 6700 series, 3.20mm reach and 150kg model.

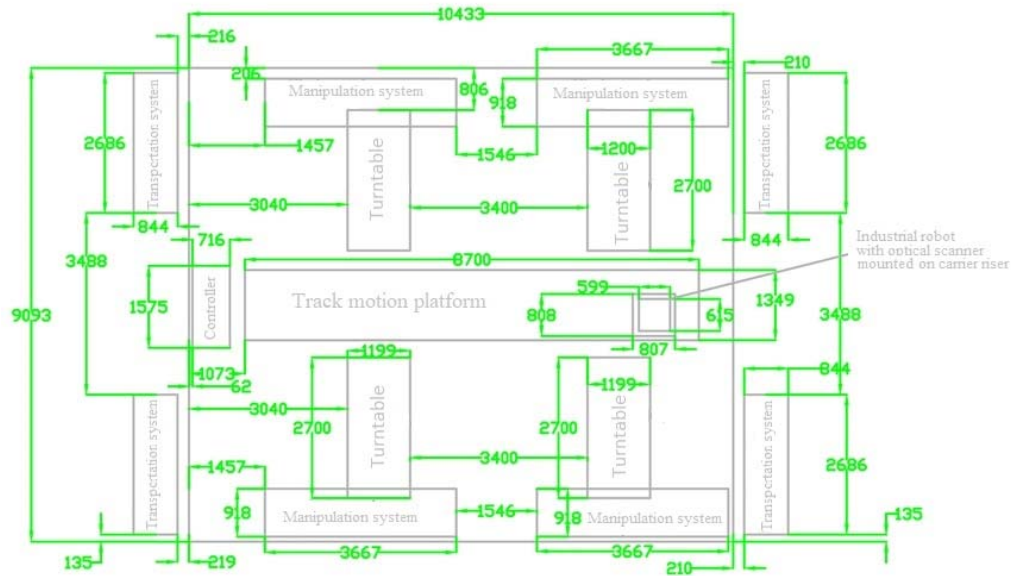
The project was based on a virtual prototype suggested by ABB, as a top developer of robotic solutions for inspection applications. The reference model is shown in the image below.



Img.1. ABB 3DQI virtual prototype

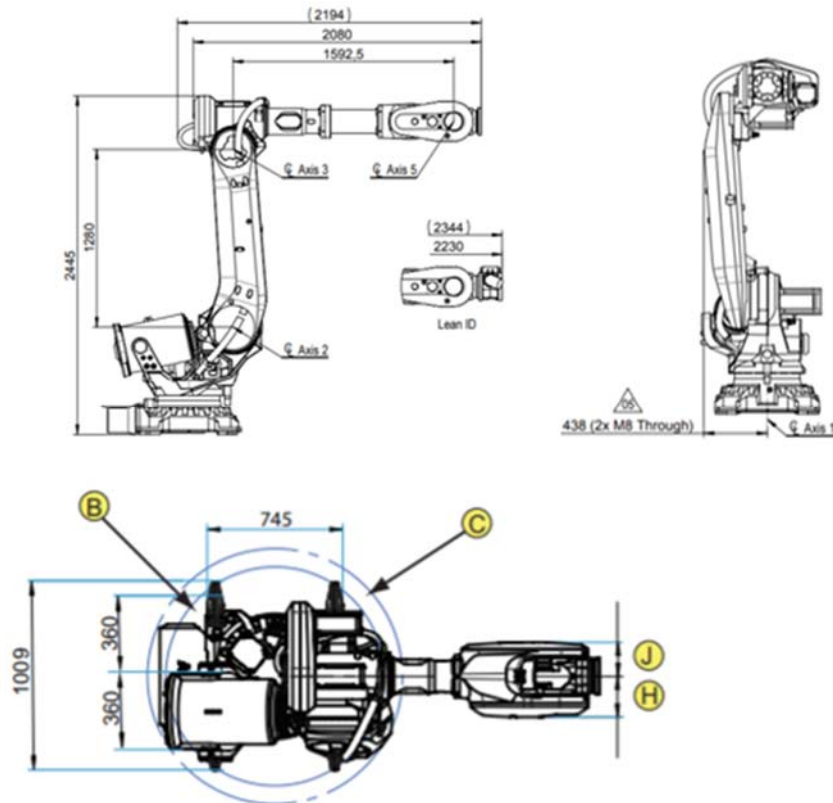
2. Current phase

An important chapter of the project is the modeling of the cell and its simulation, in specific working environments from the Siemens company, NX design software, respectively Process Simulate simulation software.



Img.2. Block diagram of the robotic application with overall dimensions

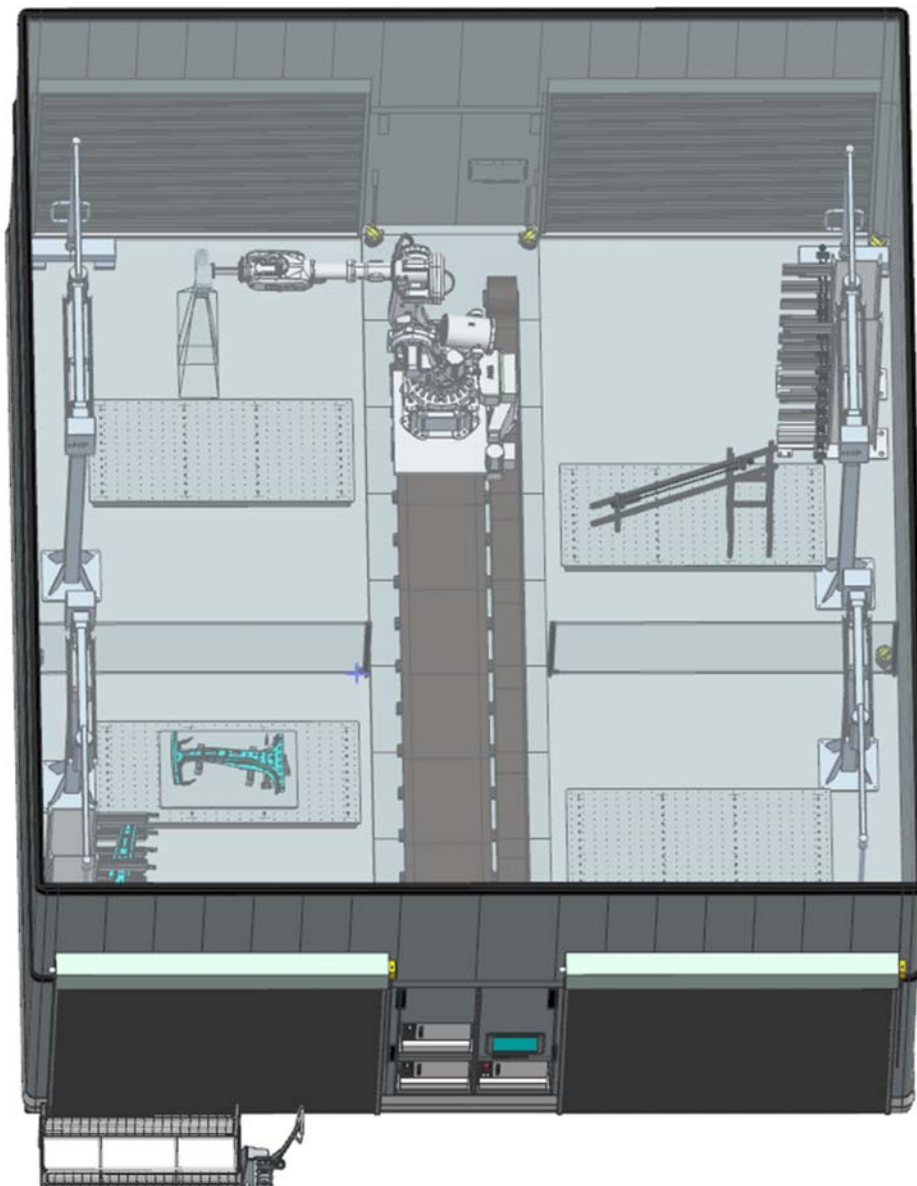
The industrial robot: ABB IRB 6700-150/3.2



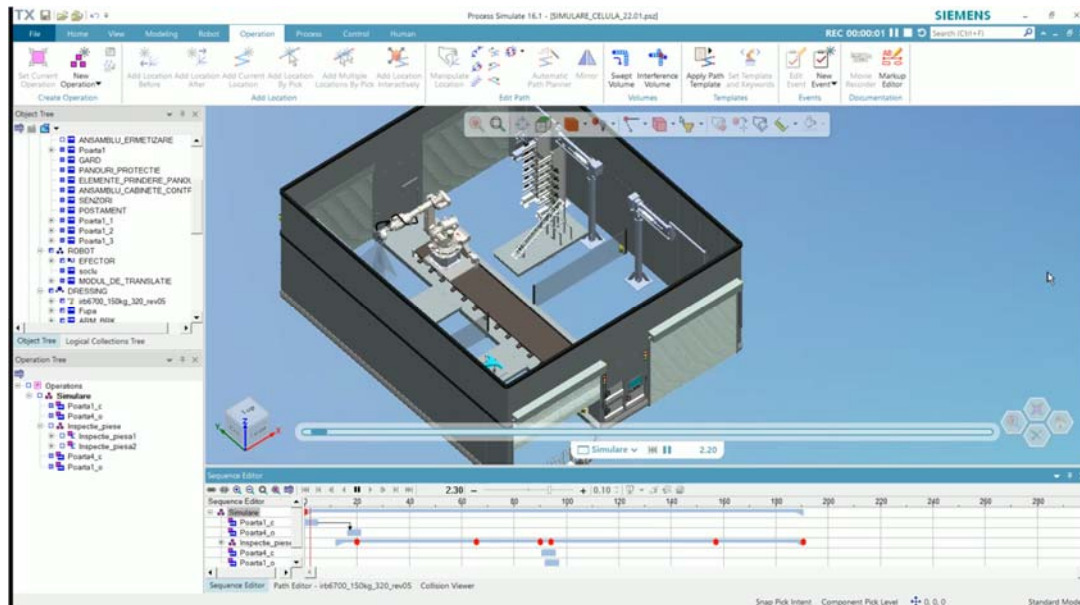
Img.3. Orthogonal views of ABB IRB 6700-150/3.2 robot

Table 1. Product specification ABB IRB 6700-150/3.2

Reach without LeanID	3.20 [m]
Handling capacity without LeanID	150 [kg]
Centrul gravitatii without LeanID	300 [kg]
Momentul incheieturii without LeanID	1135 [Nm]
Distanta maxima pe care o poate atinge with LeanID	3.20[m]
Capacitatea de manevrare with LeanID	145[kg]
Center of gravity with LeanID	300 [kg]
Wrist Torque with LeanID	1135 [Nm]
Supply voltage	200-600 [V], 50/60 [Hz]
Energy consumption	2.8 [kW]
Robot weight	1280 [kg]
Position repeatability	0.10 [mm]
Path repeatability	0.15 [mm]



Img.4. Virtual prototype of the robotic application, modeled in NX design software



Img.5. Simulation of the robotic cell

3. Bibliography

1. Anania D. – Fabricatie asistata, note de curs UPB, 2020
2. Bucuresteanu A. – Actionarea Pneumatica a Robotilor Industriali, note de curs UPB, 2019
3. Bucuresteanu A. – Elemente si sisteme pneumatice pentru actionarea robotilor industriali, Editura Printech, ISBN 978-606-23-0081-4, Bucuresti 2013.
4. Cristoiu C. – Proiectare asistat de calculator 3 - NX CAD, note de curs si suport aplicatii, UPB, 2018
5. Cristoiu C. – Automate programabile, note de curs si suport aplicatii, UPB, 2018
6. Dobrescu T. – Bazele Cinematicii Robotilor Industriali, Ed. Bren, ISBN-973-9427-02-2, București, 1998
7. Dorin A., Dobrescu T., Pascu N., Ivan I., – Cinematica Roboților Industriali, Editura Bren, ISBN-978-973-648-970-9, București, 2011
8. Dobrescu T., Dorin Al. – Încercarea Roboților Industriali, Editura Bren, ISBN-973-648-115-8, București, 2003
9. Dobrescu T., Pascu N. – Roboti Industriali. Încercare si Receptie, Editura Bren, București, 2013,
10. Dorin Al., Dobrescu T. – Actionarea Pneumatica a Robotilor, Ed. Bren, ISBN-973-648-060-7, 2002
11. Dorin Al., Dobrescu T., Bucuresteanu A., – Actionarea Hidraulica a Robotilor Industriali, Ed. Bren, 2007
12. Enciu G., Popescu A. – Senzori Industriali, note de curs, UPB, 2019
13. Ivan M. – Proiectare asistata de calculator pentru sisteme de prindere modulare, note de curs si suport laborator, UPB 2019
14. Ghinea M. – Masini si Sisteme de Productie, note de curs, UPB, 2019
15. Gheorghita M. – Tehnologia Fabricarii Componentelor Robotilor Industriali, note de curs, UPB, 2020
16. Nicolescu A., Coman C. - Robotica 2, note de curs si aplicatii, UPB, 2017
17. Nicolescu A., Coman C. - Robotica 3, note de curs si aplicatii, UPB, 2018
18. Nicolescu A., Coman C.– Actionari electrice pentru mecatronica si robotica, note de curs si metodologii de proiectare, UPB, 2018,
19. Nicolescu, A., Cristoiu C. – NX CAD Basic – Proiectare asistat de calculator, Editura Politehnica Press, ISBN 978-606-515-914-3, 2020, Bucuresti
20. Nicolescu A., – Componente mecanice tipizate, note de curs si metodologii de proiectare, UPB, 2018
21. Nicolescu A. – Proiectarea Robotilor Industriali. Partea I. Conceptul sistemic unitar de robot

- integrat în mediul tehnologic. Subsistemul mecanic al RI. Motoare de actionare utilizate la RI, UPB, 1997
22. Nicolescu, A. – Conceptia si Exploatarea Robotilor Industriali 1, note de curs si aplicatii UPB, 2018
 23. Nicolescu, A. – Conceptia si Exploatarea Robotilor Industriali 2, note de curs si metodologii de proiectare, UPB, 2019
 24. Nicolescu, A., Stanciu, M.D., Popescu D. – Conceptia si Exploatarea Robotilor Industriali - Vol.1 Tendinte actuale in conceptia si exploatarea RI. Precizia de lucru si precizia volumetrica. Componente organologice specifice. Tehnici si metode de studiu al comportarii elastice si performantelor robotilor industriali. ISBN 973-718-007-0, Ed. Printech, 2004, Bucuresti
 25. Nicolescu, A., Roboti Industriali – Vol.1 Sub sisteme si ansambluri componente. Structura axelor comandate numeric ale RI, ISBN 973 – 30 – 1244 – 0, Editura Didactica si Pedagogica RA, 2005, Bucuresti
 26. Nicolescu A., Dobrescu T., Ivan M., Avram C., Brad S., Doroftei I., Grigorescu S. – Roboti Industriali, Tehnologii si Sisteme de Productie Robotizate, Ed Academiei Oamenilor de Stiinta din Romania, 2011, ISBN 978 – 606 – 8371 – 48 – 1
 27. Nicolescu A., Conceptia si Exploatarea Robotilor Industriali, Editura Politehnica Press, 473 pag., ISBN 978-606-515-916-7, 2020, Bucuresti
 28. Nicolescu, A. – Implementarea Robotilor Industriali in Sistemele de Productie, note de curs si metodologii de proiectare, UPB, 2019
 29. Nicolescu, A., Cristoiu C. – Implementarea Robotilor Industriali in Sistemele de Productie, indrumar de laborator si proiect, Editura Politehnica Press, ISBN 978-606-515-915-0, 2020, Bucuresti, 2020
 30. Nicolescu, A. – Conceptia si Exploatarea Sistemelor de Productie Robotizate, note de curs si metodologii de proiectare, UPB, 2020
 31. Nicolescu, A., Marinescu D., Ivan M., Avram C., Conceptia si Exploatarea Sistemelor de Productie Robotizate – Vol. I, Ed. Politehnica Press, 2011, ISBN 978 – 606 – 515 – 339 – 4, ISBN 978 – 606 – 515 – 340 – 0, Bucuresti, 2011
 32. Olaru A. – Dinamica Robotilor Industriali, Ed. Bren, 2005
 33. Olaru A. – Aplicatii Labview, note de curs, UPB, 2019
 34. Pascu N.– Proiectare Asistata de Calculator 1, note de curs, UPB, 2017
 35. Pascu Nicoleta, Dobrescu Tiberiu Gabriel, Grafica Pentru Ingineri, Editura Bren, ISBN-978-606-648-034-5, București, 2012, 562
 36. Popescu D. – CADSFF, Note de curs, UPB, 2020
 37. Popescu D. – Proiectare 3D CATIA, note de curs si suport aplicatii, UPB, 2019
 38. Popescu D. – Indrumar CAD CATIA V5R8, ISBN 973-700-011-0, Editura Aius, 2004
 39. Pupaza C. – Inginerie Asistata de Calculator 1,2, note de curs, UPB, 2020
 40. Silvestru C. – Bazele Programarii Off-line a Robotilor Industriali, note de curs si suport aplicatii, UPB 2020
 41. Stanciu M. – Programarea Calculatoarelor 1,2, note de curs, UPB, 2016
 42. *** – Cataloage / carti tehnice / prospecte de roboti industriali, componente perirobotice, subsisteme de transport, componente organologice, etc. recomandate de titularii de curs si conducatorii de proiect de diploma
 43. *** – Web – site –urile recomandate de titularii de curs si conducatorii de proiect de diploma pentru studiul programei de fabricatie a firmelor producatoare de roboti, componente perirobotice, subsisteme de transport, componente organologice, etc.
 44. *** – Baze de date nationale / internationale cu brevete de inventie.

THE DESIGN AND FABRICATION OF AN INDUSTRIAL ROBOT SCALE MODEL, WITH POSITION CONTROL VIA A WEB INTERFACE

DATCU Tudor-Răzvan

Faculty: FIIR, Specialization: Robotics, Year of studies: III, e-mail: datcutudor@gmail.com

Scientific coordinator: D. Eng. Andrei Mario IVAN

In this project I designed a scale model replica of an industrial robot, with 6 degrees of freedom and direct driven axes. The robot can be controlled via a web interface either by individually addressing the axes, or through inverse kinematics by specifying a specific effector position.

CUVINTE CHEIE: Arduino, Web control, Kinematics

1. Introduction

In the following paper I will present a functional scale replica of the IRB 6700-175 / 3.05 industrial robot printed in 3D, controlled via a NodeMCU ESP-12E development board with Wi-Fi, programmed via Arduino. The 6 axes of the robot are replicated by means of servomotors directly coupled to the driven element. With the help of an Arduino library, the microprocessor can perform calculations for direct and reverse kinematics.

Thus, the replica model of the robot can be used for educational purposes, as a demo presentation model, or it can be integrated in a miniature structure similar to that of a flexible manufacturing cell, in order to be able to replicate it on a more convenient scale with similar movements.

2. Current status

I. Robot design



Fig. 1. The robot model that the project is based on

IRB 6700 is a series of large industrial robots produced by the Swedish-Swiss company ABB since 2013, as a successor to the 6640 series. Intended predominantly for spot welding, handling, and

machine tending applications, with a load-bearing capacity between 150 and 300 kg, and a maximum length between 2.7 and 3.2 m

The 3D model for IRB 6700-175 / 3.05 was taken from the company's website and inserted into Autodesk's Fusion360 design software. Then it was scaled to 15:100 to fit the maximum size of the 3D printer, while keeping the possibility to add motors to drive each axis.

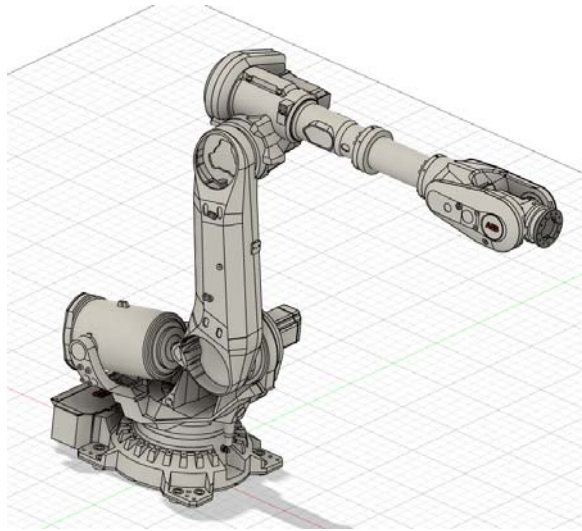


Fig. 2. 3D model of the robot in the CAD workspace

Thus, the first step was to clean the model by removing the edges that were too thin to be 3D printed and strengthening the base to provide the possibility of screw mounting. The next problem was finding the space in the robot's body for the 6 motors, without influencing the kinematics of the robot or its external appearance.

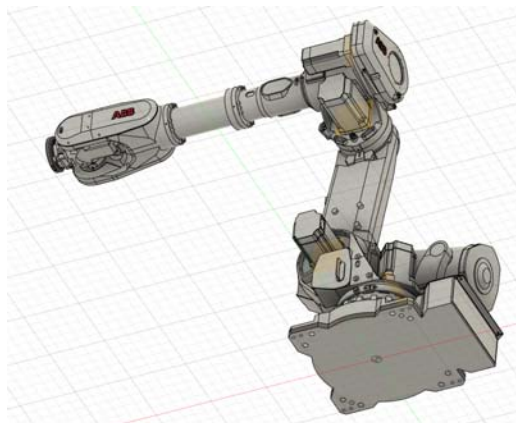


Fig. 2. 3D model of the robot with highlighted motor positions

For axes 1, 2 and 6, the same location of the motors was used as in the real robot. For the others this was not feasible, so they were placed in the most convenient place for operation.

The motors used are 180° digital hobby servos. For the first 4 axes, the model used is TowerPro MG995, and for the pitch and roll axes of the orientation system, it was the TowerPro MG90S. The

overall dimensions and the arrangement of the mounting holes were measured, and the slots for them were cut into the CAD model.

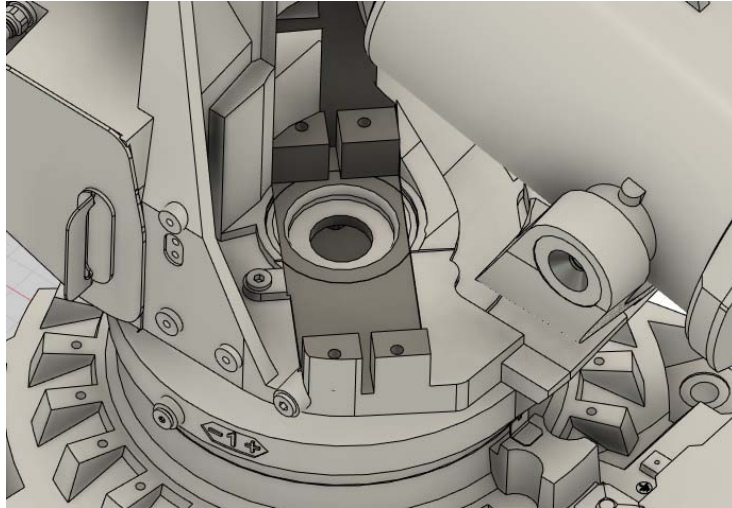


Fig. 3. The space for the Axis 1 motor, cut from the robot's turntable

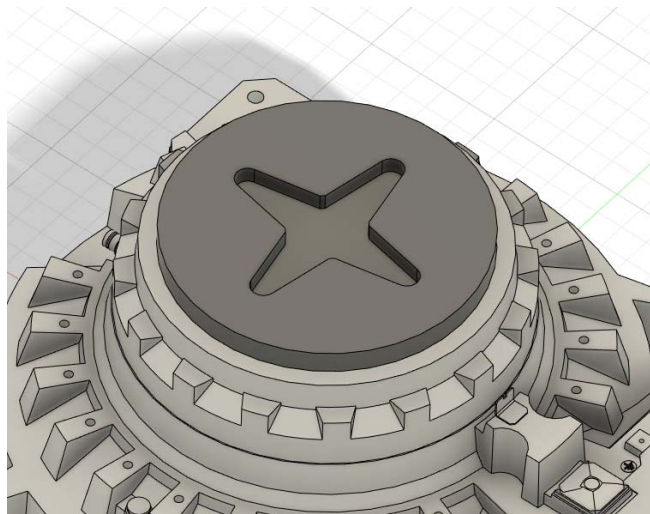


Fig. 4. The slot for the servo flange, cut out of the robot's base

A similar process followed for the other robot couplings, using the different shaft-mounted flange shapes to allow each component to be driven. This was followed by the separation of the box containing the electronic part of the robot to be hollowed out, and the addition of slots for the power plug and switch.

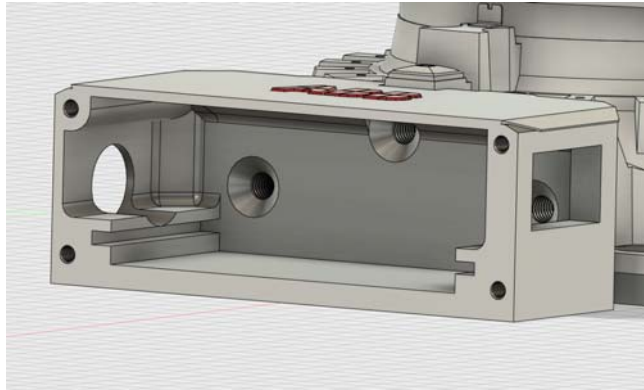


Fig. 5. The box for the robot's electronics

The static balancing device of the robot has been implemented here as well, to counterbalance the weight of segments 1 and 2 when the robot bends forward. Thus, an elastic band was fastened to the end of the inner cylinder with a screw, passed through the hole at the base of the outer cylinder, tensioned and fastened with another screw. Thus, an effect similar to that of the real model is obtained, on a much smaller scale.

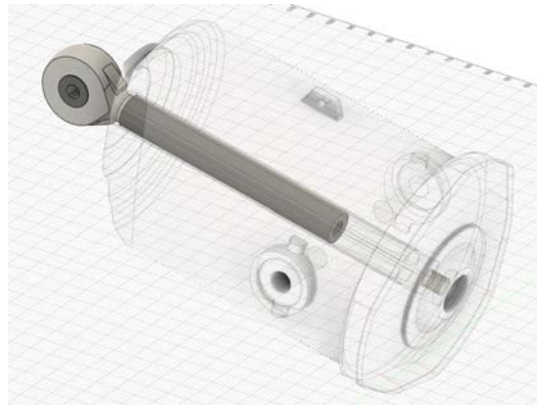


Fig. 7. The robot's balancing device

The final step was to prepare the routing for the cables, so that they would not limit the movement of the robot. A passageway was made through segment 1, similar to the actual robot, and segment 2 was partly hollowed out and split I half, to allow the passage of cables for motors 5 and 6, as well as the correct assembly of motor flange 4.

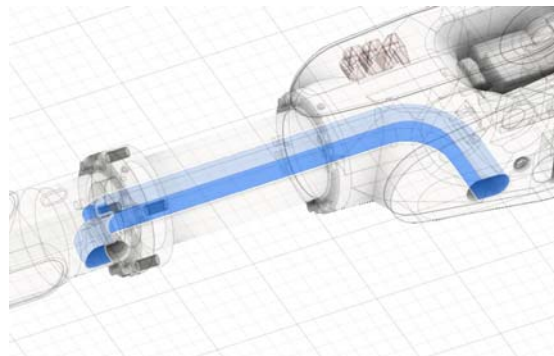


Fig. 6. The wire path through the robot's second segment

II. Fabrication and implementation of the robot

The robot model was fabricated on a Tiertime Cetus Mk.III 3D printer. The parts are made of white PLA and assembled with various screws and self-locking nuts.



Fig. 7. Actual physical model of the robot

The electronics were designed with an emphasis on simplicity, in order to highlight the web interface control. Thus, the NodeMCU ESP-12E board has 6 PWM digital pins connected to the 6 servo motors. Communication with the computer can be done either via USB serial interface or through Wi-Fi.

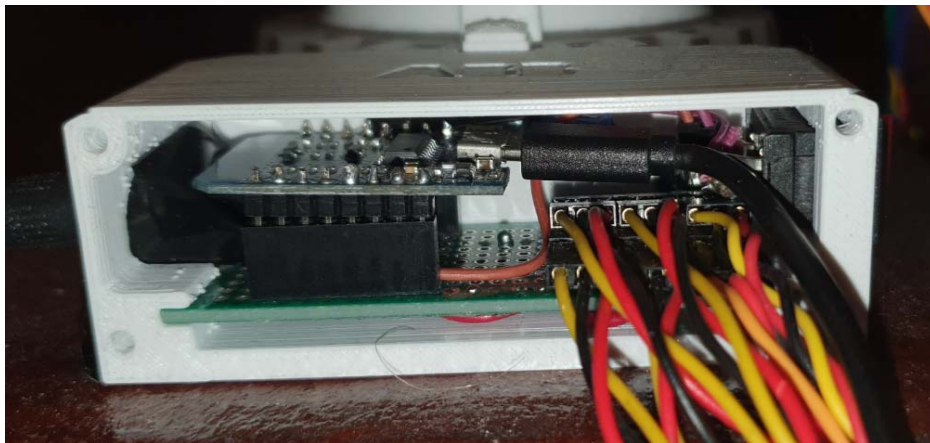


Fig. 8. The robot's electronics

The programming was done through the Arduino IDE, using the Kinematics library, which can solve the direct and inverse kinematics of the robot. However, it has some limitations, as it is not possible to define the maximum angles for each axis, which leads to many positions that are impossible to achieve in this configuration. Also, the NodeMCU board processor is relatively weak, and cannot perform many iterations of the Newton-Raphson method in a short time. This leads to rather rudimentary position control.

The web interface was created using the RemoteMe website, a cloud platform for Internet of Things projects, which integrates easily into the Arduino workspace. On this platform, the control panel and the robot itself are defined, and they can communicate via the Internet. Thus, because the computer does not connect directly to the development board, the two do not have to be in close proximity to function, as long as they both have access to the network.



Fig. 9. The robot and the control panel on the RemoteMe platform

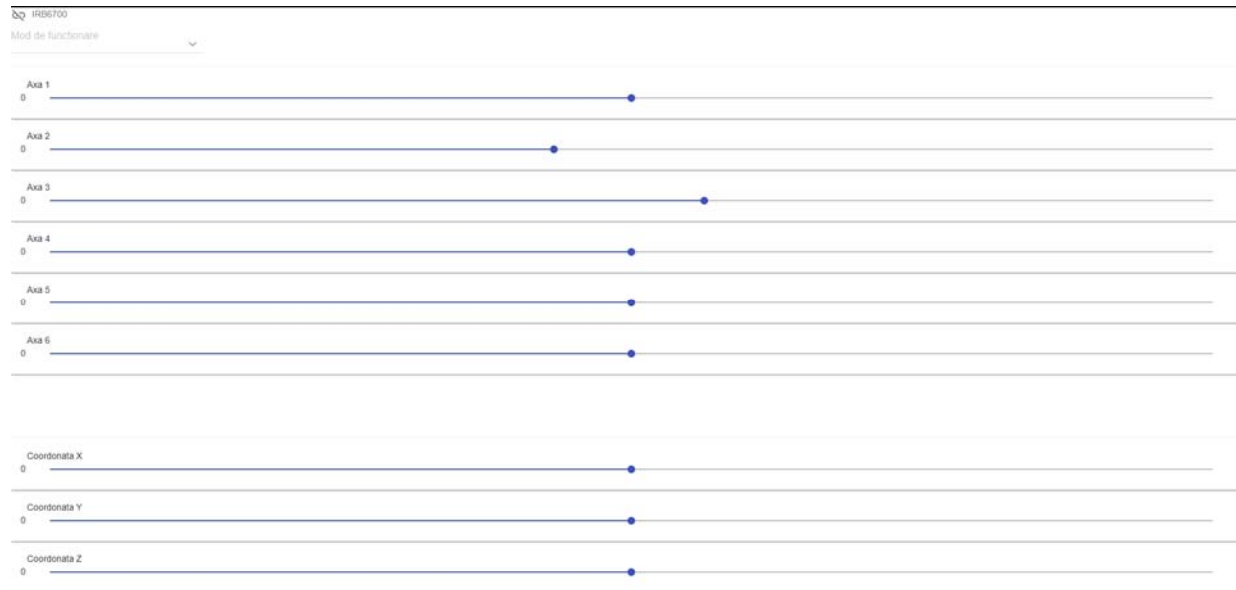


Fig. 10. The command screen interface

Through the control panel it is possible to switch between the 2 operating modes of the robot: Individual axis control and Tool centre point. Using the sliders on screen, the angle of the robot's axes or the coordinates of the effector can be controlled.

3. Conclusion

To sum up, the robot model is functional and can be used for scale simulation of a robotic application. For the future, this could be improved by using a different way of calculating reverse kinematics, such as using the RoboDK platform with a driver for Arduino, which would solve the problems with position control.

4. Bibliography

- [1]. Kevin M. Lynch (2017), *Modern Robotics: Mechanics, Planning, and Control*, Cambridge University Press, Cambridge, 1107156300.
- [2]. <https://github.com/kousheekc/Kinematics>
- [3]. <https://www.youtube.com/c/NorthwesternRobotics>
- [4]. <https://new.abb.com/products/robotics/industrial-robots/irb-6700>
- [5]. <https://www.remoteme.org/>

ROBOTIZED PALLETIZATION CELL WITH TWO INPUTS AND TWO OUTPUTS, FOR CARDBOARD BOXES, INTEGRATING AN INDUSTRIAL ARTICULATED ARM ROBOT

STOICA Raluca-Georgiana

Faculty: Industrial Engineering and Robotics, Specialization: Robotics, Year of study: IV, e-mail: ralucastoica123@gmail.com

Scientific leader: s.l.dr.ing.Andrei Mario IVAN

The paper includes the stages of modeling and 3D design of a robotic palletizing cell with 2 inputs and 2 outputs of cardboard boxes integrating an ABB IRB 460 robot. technological for the parts to be manufactured separately and to verify the operating parameters following all stages of the CAE process.

1. Presentation of the robotic cell

The robotized cell for palletizing cardboard boxes with two inputs and two outputs comprises a FANUC M-410iC / 110 palletizing robot, a pallet dispenser and a system for arranging cardboard separators outside the cell.

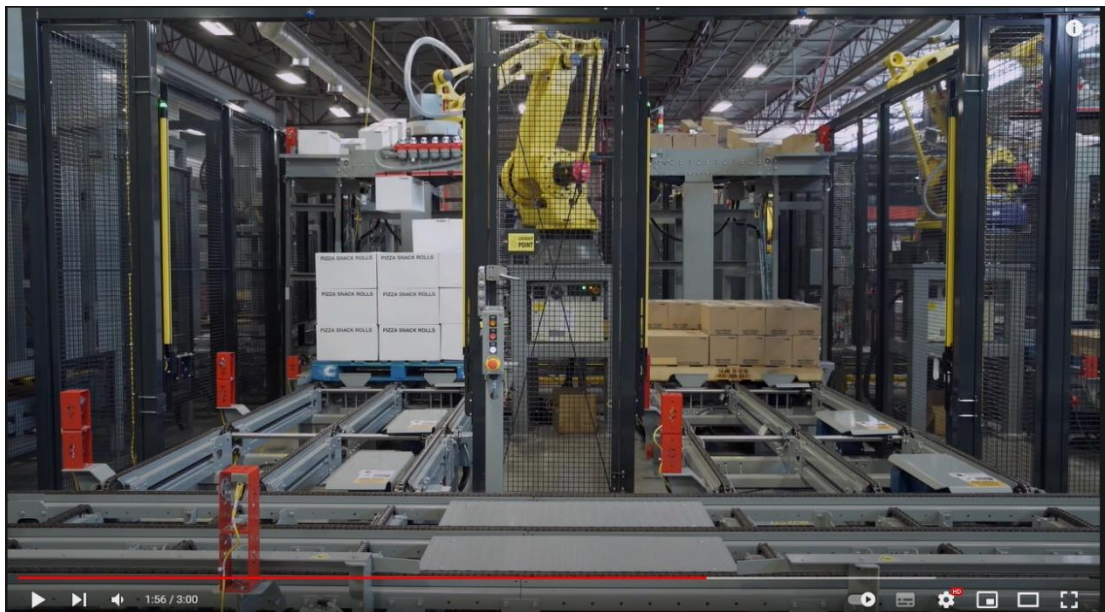


Fig. 1 Front image of the cell

The inlet conveyors in the cell are represented by the long, inclined conveyors, where in extension there is a roller conveyor.



Fig. 2 Image with tilted input conveyor

The boxes, when stopped in the stop, will be pushed by the piston located on the side of the conveyor. Finally, the boxes are transported on the central belt conveyor, also provided with a stop and a piston, which have the role of centering and fixing the boxes, so that they can be picked up by the robot.

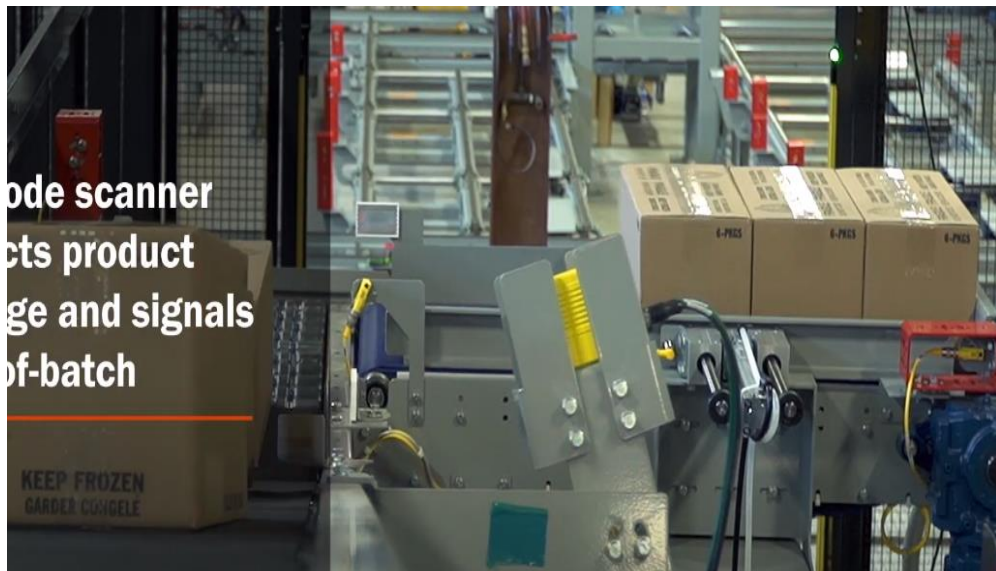


Fig. 3 Picture with the box pickup area

The pallets on which the boxes will be placed will first leave the pallet storage, outside the cell. Parallel to the conveyor on which these pallets are transported is another conveyor, which will have the

role of feeding the pallet storage. Subsequently, a portal robot will have a separator on each pallet.



Fig. 4 The pallet distributor outside the cell

From here, the pallet can continue on two routes: the first would be if the lifter remains high and then the pallet will reach the conveyors with 3 chains in extension, or, the second case, in which the lifter goes down, the pallet is driven on the transverse conveyor with 2 chains, it will reach the second lifter, which will lift the pallet and will continue its route on the conveyors with 3 chains in extension. Once in front of the robot, the stopped pallets are ready to be loaded with 2 types of boxes. This palletizing operation is performed by the central robot, FANUC M-410iC / 110, placed on an overhead support and equipped with a vacuum effector. The effector is custom-made, because it has several groups of suction cups that allow you to take over a different number of boxes.



Fig. 5 Cell overview

The stack includes 4 rows of boxes of 10 boxes per row, respectively 14 boxes per row. The complete stacks will be transported outside the cell, where there are two other elevators, which when they go down, allow the stacks to continue the route on the conveyor with 3 output chains.

2. Kinematic diagram of the robot

Although the video for the foundation of the diploma project includes the Fanuc robot variant, due to the absence of internal documentation, I chose to equate it with the ABB IRB 460 robot, having the same load-bearing masses and radii of action.



Fig. 6 ABB IRB 460 robot overview

From the captures in the datasheet, the following defining parameters of the robot can be noticed:

- Maximum distance: 2.4 m;
- Load carrying capacity of the arm: 110 kg
- Number of ACN: 4;
- Mounting method: ground location;
- Repeatability in position: 0.02 mm;
- Dimensions of the robot base (1007 x 720 mm);
- Robot weight (925 kg).

Axis number	Workspace	Maximum speed/axis
Axis 1: Arm rotation	+165° to -165°	145°/s
Axis 2:	+85° to -40°	110°/s

Axis 3	+120° to -20°	120°/s
Axis 4	+300° to -300°	400°/s

Spațiu de lucru robot IRB 460-110/2.4

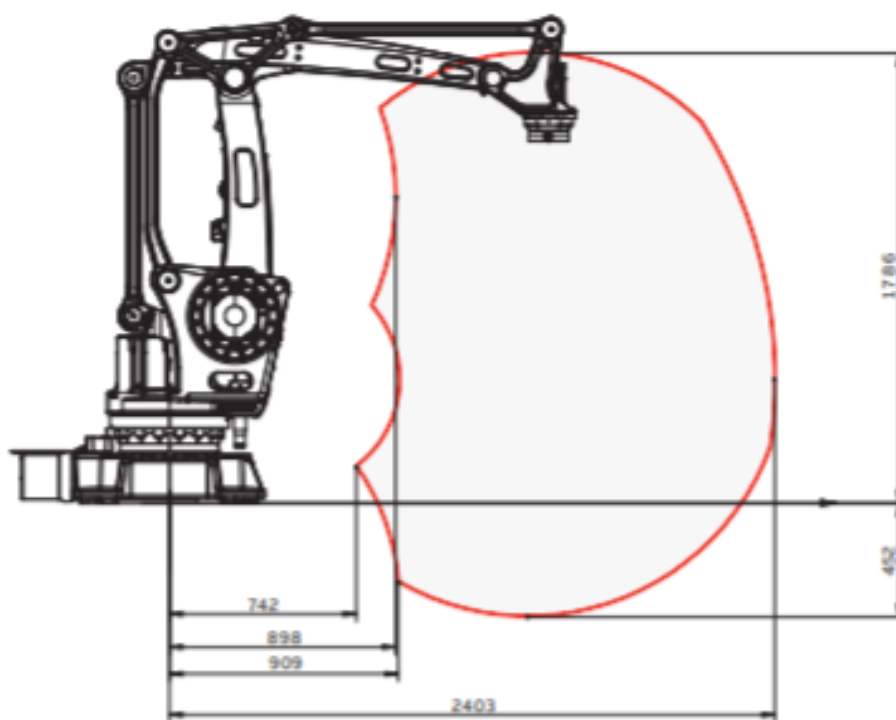


Fig. 7 Robot workspace

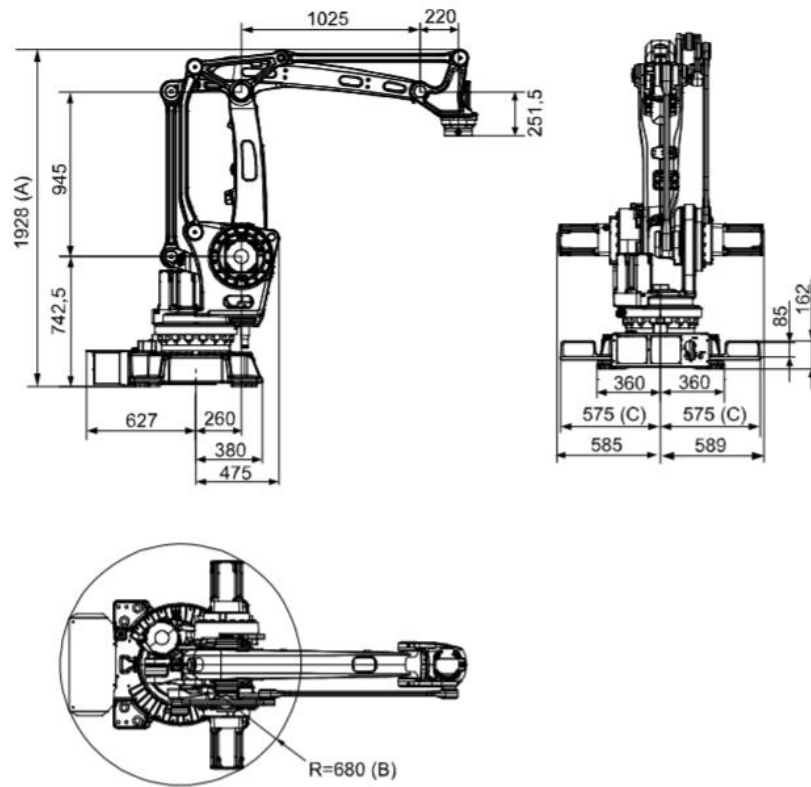


Fig. 8 The dimensions of the robot

The structural kinematic diagram shows the main axes of rotation and the passive torques of the robot, which form the triad and the dyad of the robot specific to the palletizing robots.

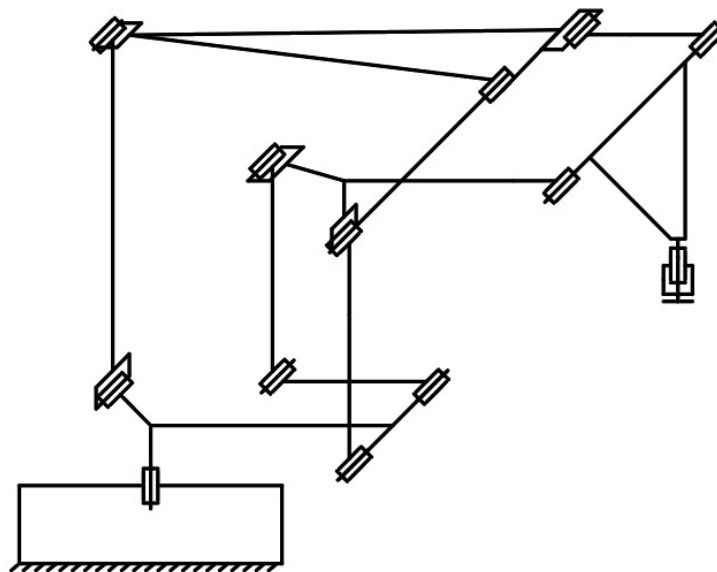


Fig. 10 Structural kinematic diagram of the robot

3. The technological film of the piston guide

To make the guide model in the figure below, we started from the execution drawing below. The overall dimensions of the piece are 200x40x80 mm.

To make the technological film, it is necessary to mark all the surfaces to be processed.

The material from which the piece is made is A356 aluminum alloy, which allows the piece to be made by cutting from a bar with a square section measuring 80x80x500 mm.

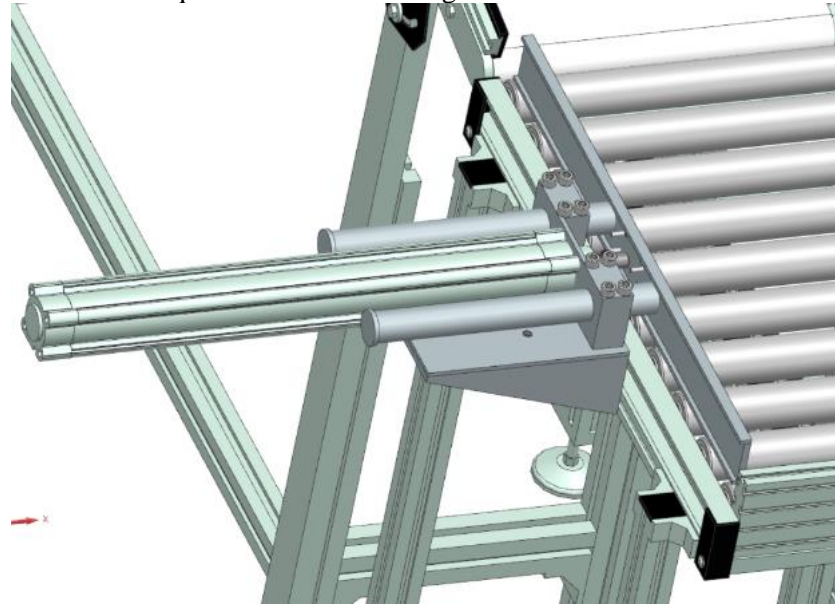


Fig. 13 3D model of the piece

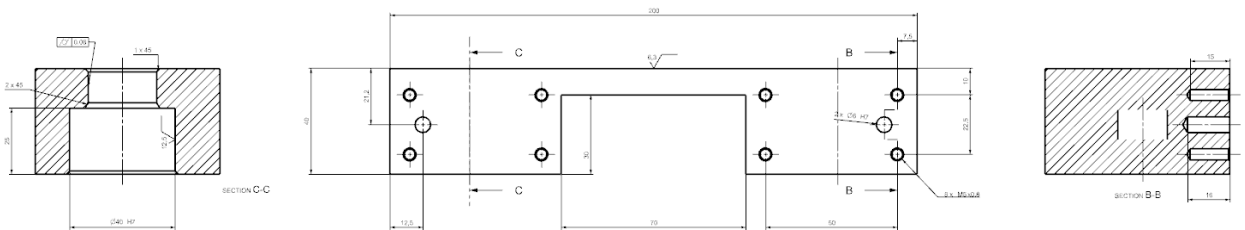


Fig. 14 Execution drawing of the piece

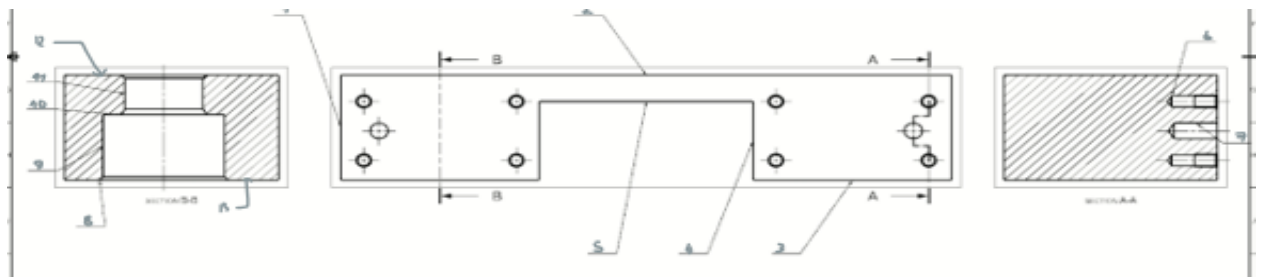


Fig. 15 Drawing with numbered surfaces

4. Scheme of surface operations

After grading the surfaces, it is necessary to establish the roughness, the main size and the shape and position tolerances.

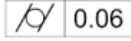
<u>S_i</u>	<u>Forma suprafetei</u>	<u>Dimensiuni principale[mm]</u>	<u>Rugozitatea R_a [μm]</u>	<u>Treapta(clasa)</u>	<u>Toleranta de forma[mm]</u>	<u>Pozitia reciproca</u>	<u>Alte conditii</u>
S1	Plan	200	6.3	IT13			
S2	Plan	40	6.3	IT13			
S3	Plan	65	6.3	IT13			
S4	Plan	30	6.3	IT12			
S5	Plan	70	6.3	IT12			
S6	<u>Cilindrica interioara</u>	M5x15	3.2				
S7	<u>Cilindrica interioara</u>	∅6	1.6	IT7			
S8	<u>Conica(tesitura)</u>	1x45	6.3	IT13			
S9	<u>Cilindrica interioara</u>	∅40	12.5	IT13		Baza de referinta	
S10	<u>Conica(tesitura)</u>	2x45	6.3	IT13			
S11	<u>Cilindrica interioara</u>	∅26	12.5	IT7			
S12	Plana						
S13	Plana						

Fig. 16 Establishing roughness and tolerances

Once these dimensions have been established with the tolerated dimensions, it is necessary to identify the role of the surface.

<u>Categoria de suprafata</u>	<u>Codul suprafetei</u>	<u>Rolul suprafetei</u>
<u>Principală (funcțională)</u>	S11	<u>Bază de referință a piesei, asigură ghidarea unei piese de tip arbore (tija pistonului)</u>
	S6	<u>Asigură centrarea în corpul ansamblului</u>
	S7	<u>Asigură fixarea piesei prin suruburi</u>
	S9	<u>Suprafața pe care se va monta lagăr</u>
<u>Tehnologică</u>	S1, S2, S3, S4, S5	

Fig. 17 Determining the role of the surface.

Finally, the workpiece processing stage can begin. Depending on each surface, the tool to be used for machining that surface will be calculated, as well as the necessary machines that will be used for

cutting operations.

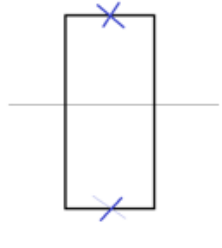
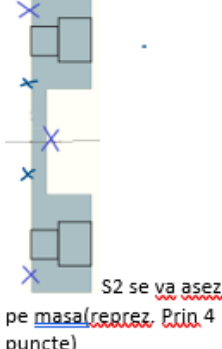
Operatie		Utilaje si sdv-uri			
Nr si denumire	Schita simplificata a operatiei	Fazele operatiei	Utilaj si scula aschietoare	Dispozitiv de prindere si verificare	
10. Operatie complexa		Nr.	denumire	Centru de prelucrare: EMCOMILL 350 2. CoroMill 245 3. CoroMill 390 4. CoroMill 390 5. CoroDrill 880	Prinderea se realizeaza cu menghina Verificarea se realizeaza cu subler
		1	Orientarea si fixarea sf		
		2	Degrosare si finisare S2		
		3	Frezare S4, S5		
		4	Degrosare si finisare S3		
5	Gaurire S9, S11				
20. Operatie complexa		1	Orientarea si fixarea sf	Centru de prelucrare: EMCOMILL 350 2. CoroMill 245 3. CoroDrill 860 4. CoroMill Plura 5. CoroMill Plura	Prinderea se realizeaza cu menghina Verificarea se realizeaza cu subler
		2	Degrosare si finisare S12, S13		
		3	Gaurire S7		
		4	Gaurire cu tarod S6		
		5	Frezare S10, S8		

Fig. 18 Phases of the operation

5. The CAE process of the box alignment system

An interesting element of the cell is the box alignment system, which consists of a piston mounted on the side of the conveyor and a stop located at the end of travel of the transport system.

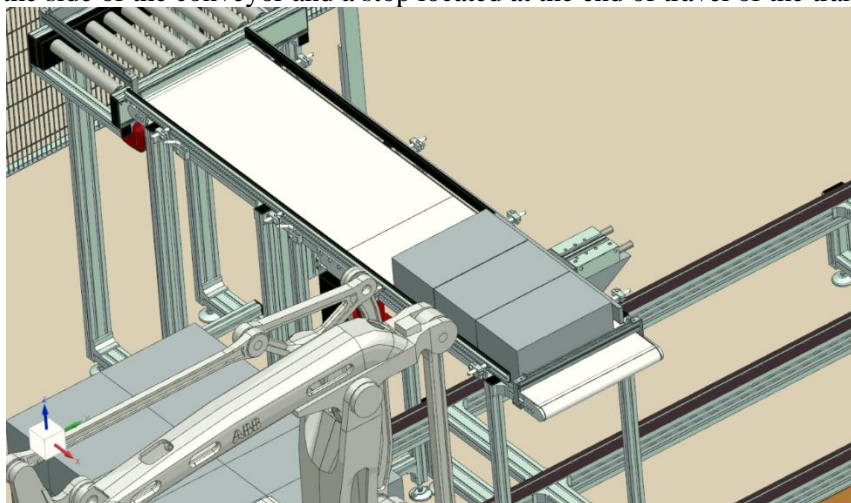


Fig. 19 3D model of the alignment system

In the first stage we exported as STEP file from NX all the components of the assembly to be analyzed: the belt conveyor, the 3 boxes to be taken by the robot, the piston that will push the boxes and the end-stopper mounted at the end of the conveyor.

After importing the file into Ansys, I started the operation of "cleaning" the model, which aims to simplify the geometric model, eliminate insignificant details in terms of simulation and thus reduce computation time, but also to use as much as possible few types of material.

"Cleaning" a model refers to the elimination of all elements that will not be included in the analysis and therefore will not affect the simulation.

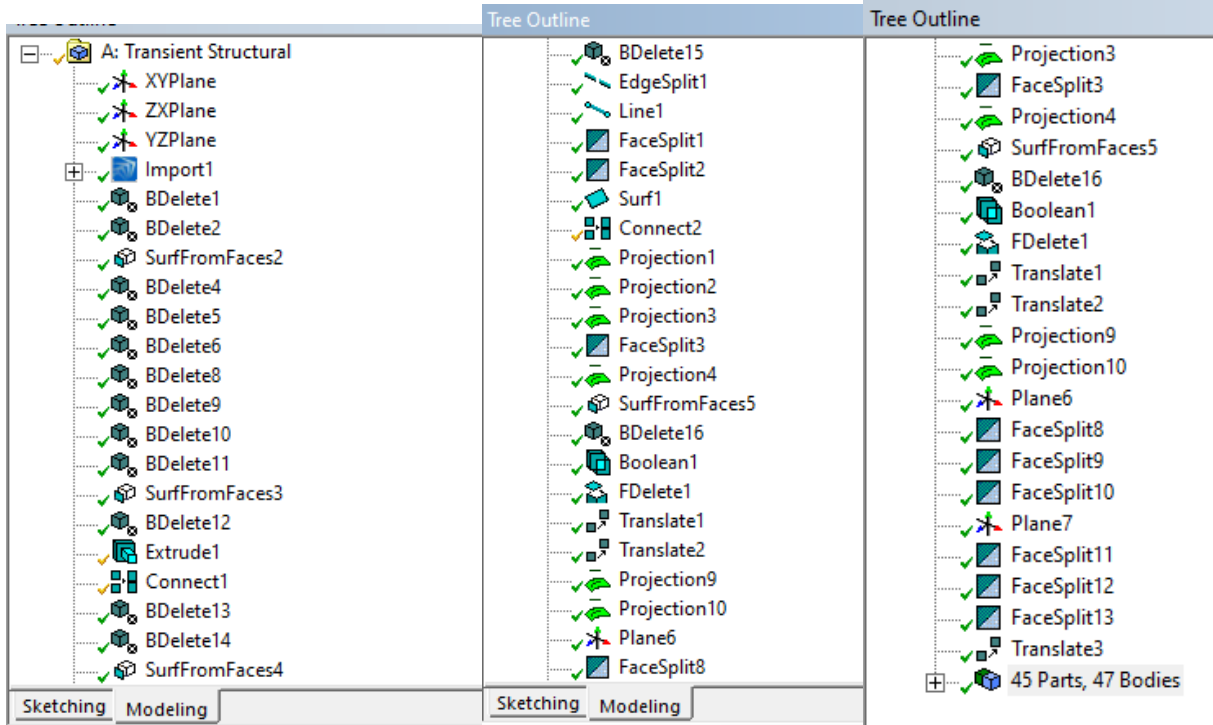


Fig.20: List of orders used for cleaning

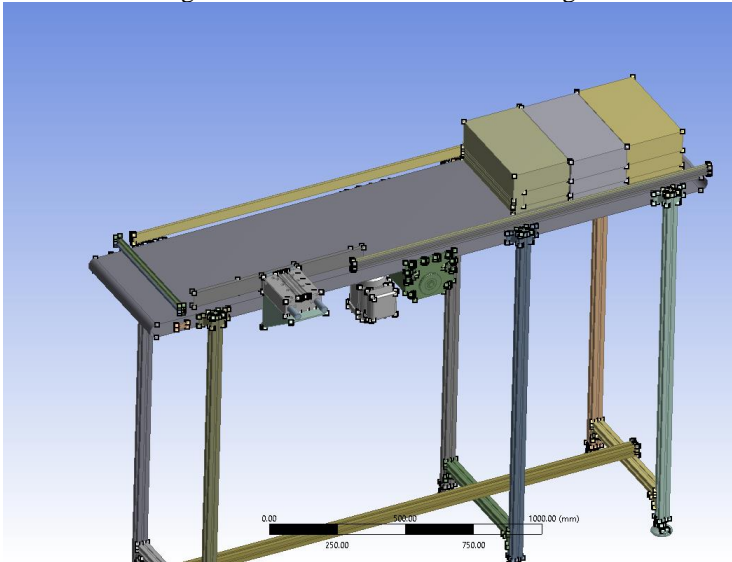


Fig.21 Geometric pattern after cleaning

Transient analysis (Structural Transient) determines the dynamic response of the structure to a time-varying force (response in time) through an implicit calculation of the equations of motion. The results

are: displacements, specific deformations, stresses, reactions, contact forces, etc. - all results illustrating the variation over time of these response quantities.

The initial data that we entered as parameters of the transient regime were calculated following the simulation performed in the Process Simulate program, which were centralized in an excel file (Fig. 3.2):

Pozitia	Cursa	Timp	Comentariu
1	1400	5	cutii vin pe pozitia din capat
2	56.6198		cursa piston pana la cutii
3	10.307		cutia 1 din marginea conv
4	15.315		cutia 2 mijloc
5	5.3303		cutia 3 spre opritor
6	1408.7	1.66667	cursa cutia 3 inspre opritor
7	1411.7	1.66667	cursa cutie 2 spre capat
8	1411.7	1.66667	cursa cutie 3 spre capat

Fig.21 : Centralized data in excel

Also, the solution settings influence the convergence of the results and because it is a transient analysis, the number of steps in which the simulation is performed must be set:

Step Controls	
Number Of Steps	2.
Current Step Number	1.
Step End Time	5. s
Auto Time Stepping	Off
Define By	Substeps
Number Of Substeps	20.
Time Integration	On
Solver Controls	
Solver Type	Program Controlled
Weak Springs	Off
Large Deflection	On
Restart Controls	

Fig.22: Number of simulation steps

In the dynamic analysis, contact types and kinematic torques must also be defined.

Therefore, we defined several types of contacts as follows: 3 “Frictional” contacts with a coefficient of friction $\mu = 0.4$, 3 “Frictionless” contacts and other “Frictional” contacts with $\mu = 0.42$.

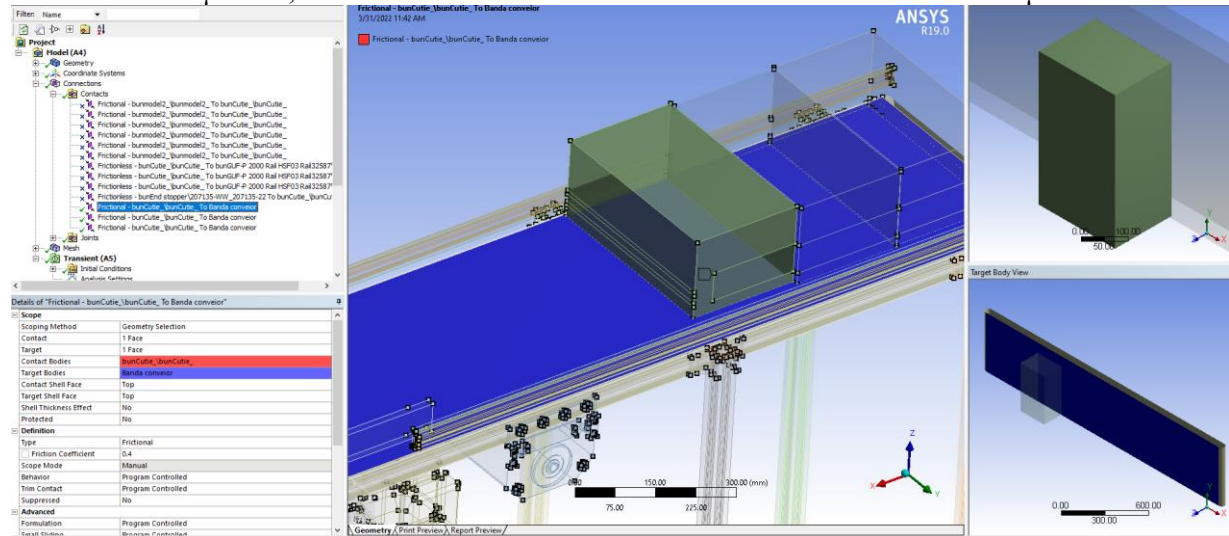


Fig.23 : Contact cu frecare de tip “face to face”, între banda conveiorului și fața cutiei.

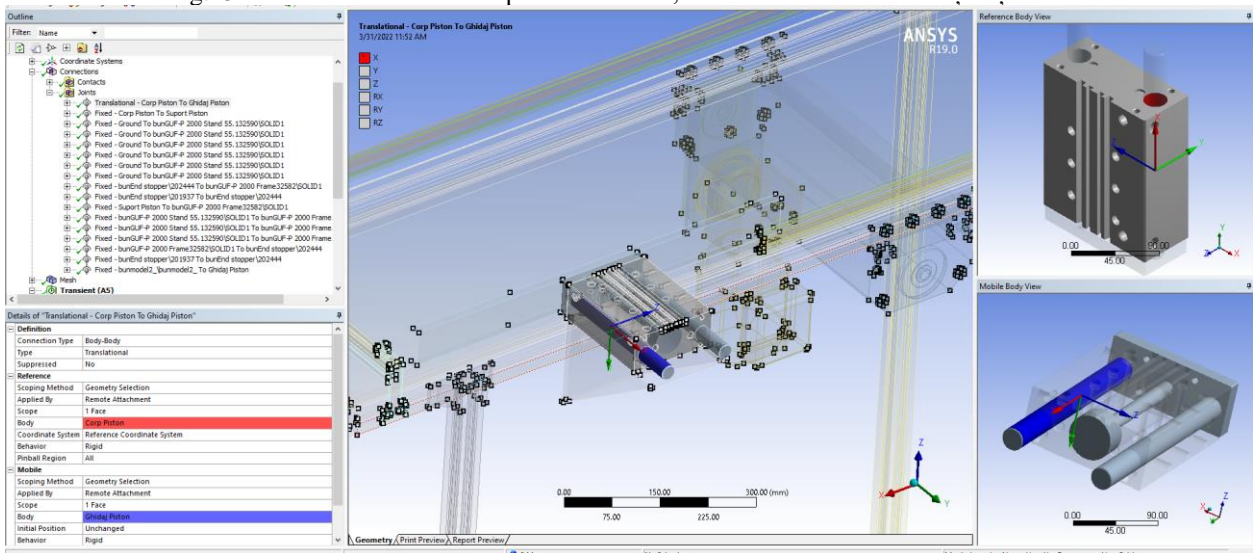


Fig.24 “Translational” kinematic coupling, “body to body”, between the piston body and the rod body to which the piston “blade” is connected.

The next step is to discretize the geometric pattern.

Discretization is the approximation of the geometric model through a network with a large but finite number of elements with a simple geometric configuration.

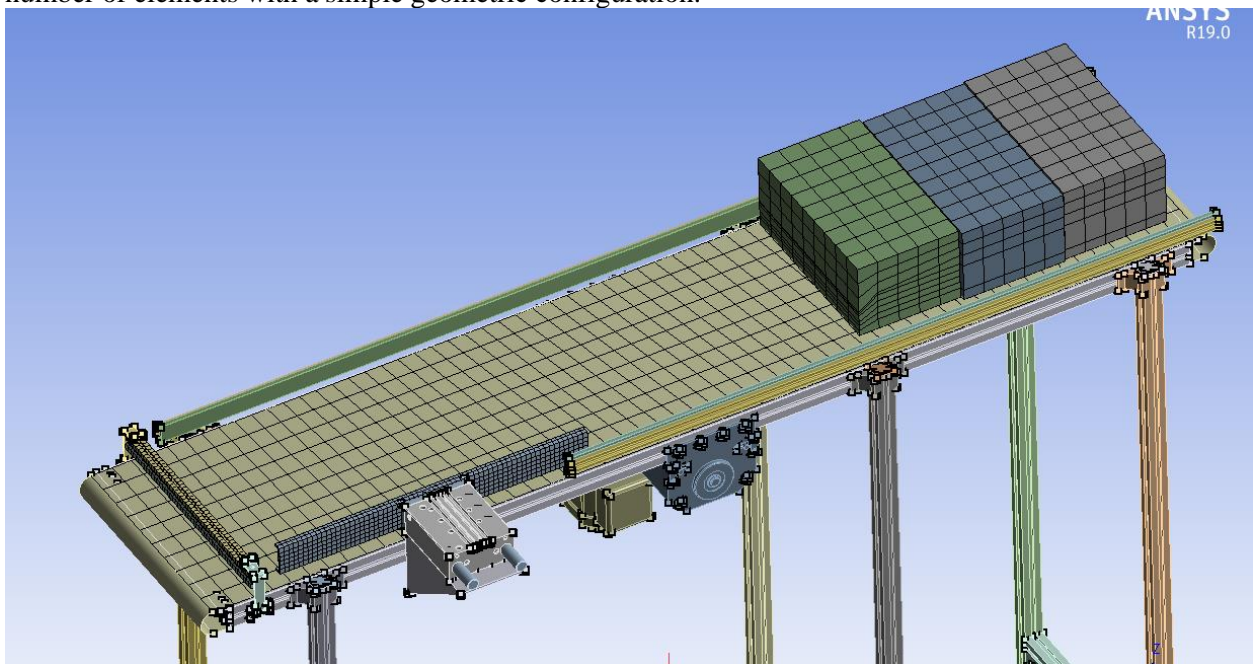


Fig.25. Discretized components of the assembly

Once the discretization is completed, we can start the dynamic analysis in transient mode.

Each box will have its own stroke, because their alignment will be done when the electric piston is actuated.

Only three types of materials were used: Structural steel (general purpose steel) for piston and stopper, Carton - separately defined material for boxes and rubber - separately defined material for the conveyor belt.

At that point the piston will start operating, so the boxes must move along the Y axis at the distance corresponding to each at that time:

- Box 1 moves 5.33 mm at the time of 7.8 seconds;
- Box 2 moves 15,315 mm at the time of the second 7.3;
- Box 3 moves 10,307 mm at a time of 7.5 seconds;

After performing the dynamic analysis in transient mode and obtaining some results, in the graphical interface of Workbench we could process the displacements, specific deformations, but also the stresses that appear on the chosen components in the form of a color gradient where: blue areas are the least required areas. and the red ones represent the areas with the most demands.

Following this analysis, the following results were obtained:

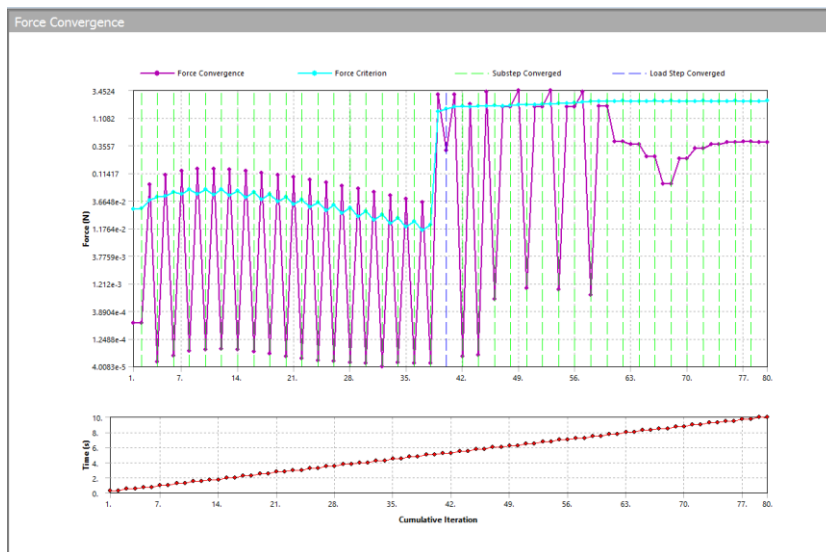


Fig.26: Monitoring the solution according to the criterion of convergence of forces

The bisections represent strong discontinuities in the model during the simulation that the program tries to solve forcibly. They often occur due to poor discretization. The fact that the number of iterations is low and the result of the simulation does not show bisections, is an indicator that the analysis performed is correct: it means that the discretization is correct and the geometric model is good, valid.

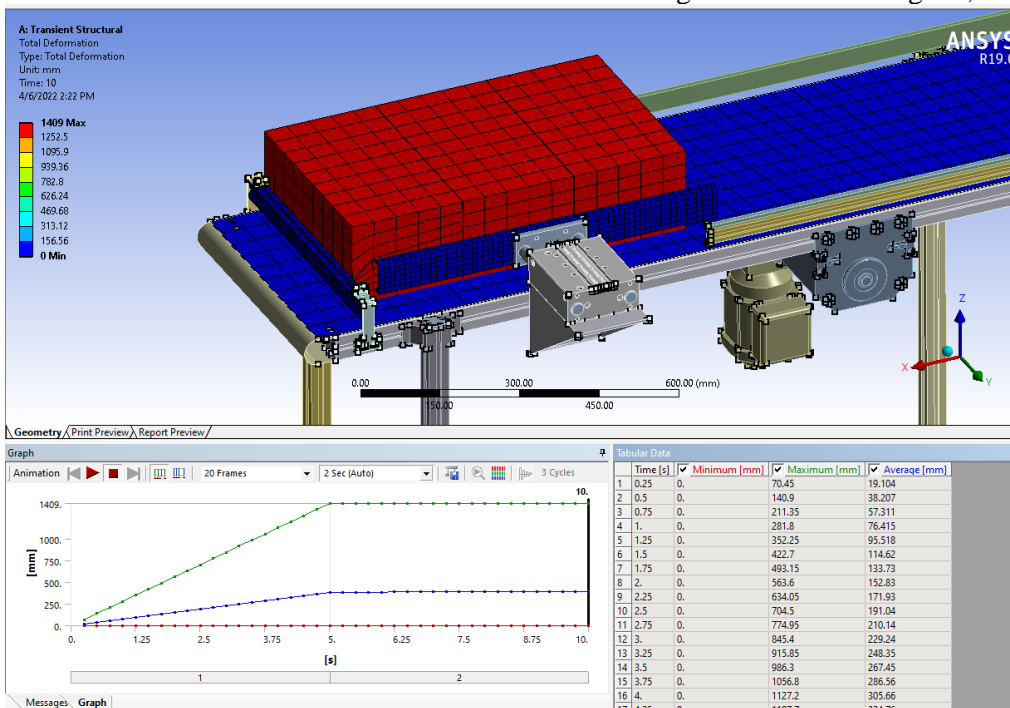


Fig.27: Total displacements for all objects

The total displacement reaches a value of 1409 mm in an interval of 10 seconds, the average being 397.4 mm.

6. 3D modeling of the robotic cell

3D modeling of the cell was performed in the Siemens NX software, where various components were imported as native STEP files, and other components were modeled in this software.

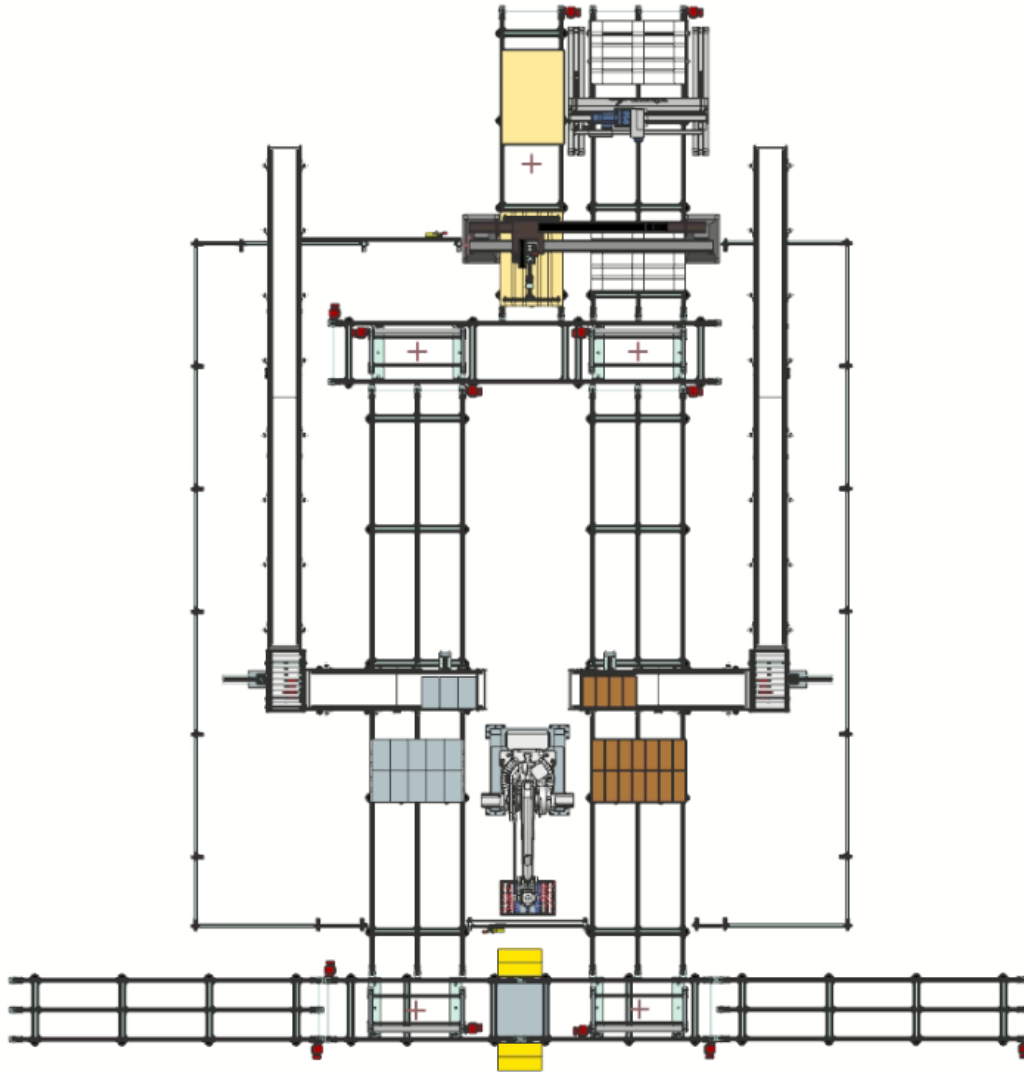


Fig. 28 Top view of 3D modeled cell in NX

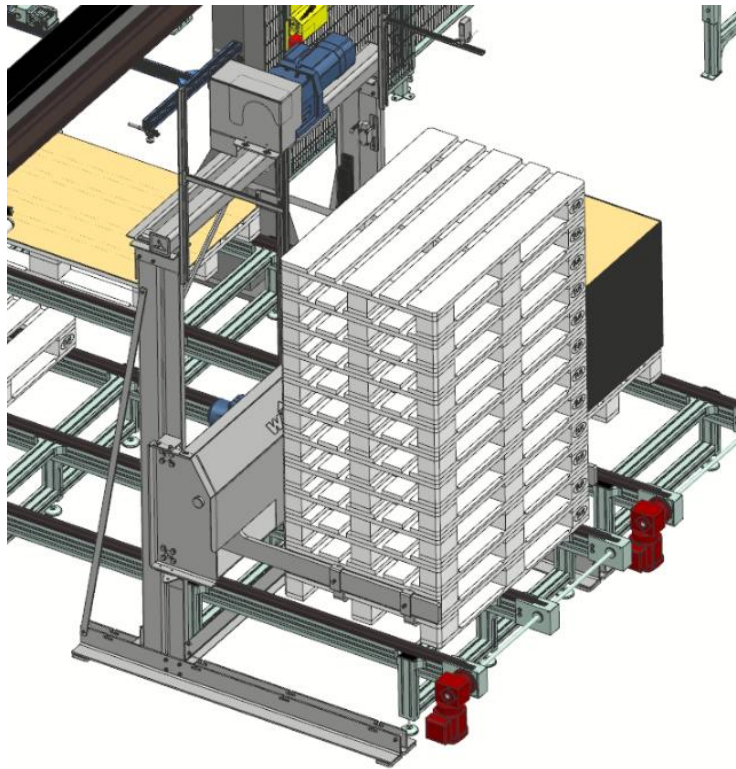


Fig. 29 Isometric view of pallet dispenser

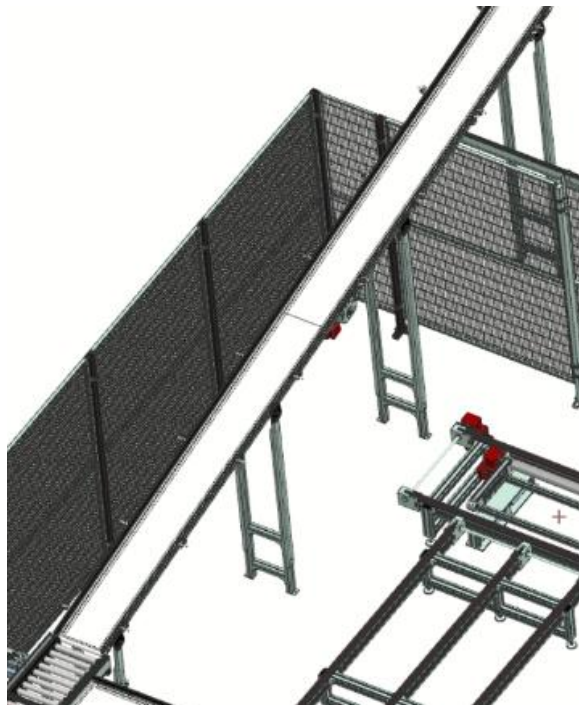


Fig. 30 Isometric view of the input conveyor

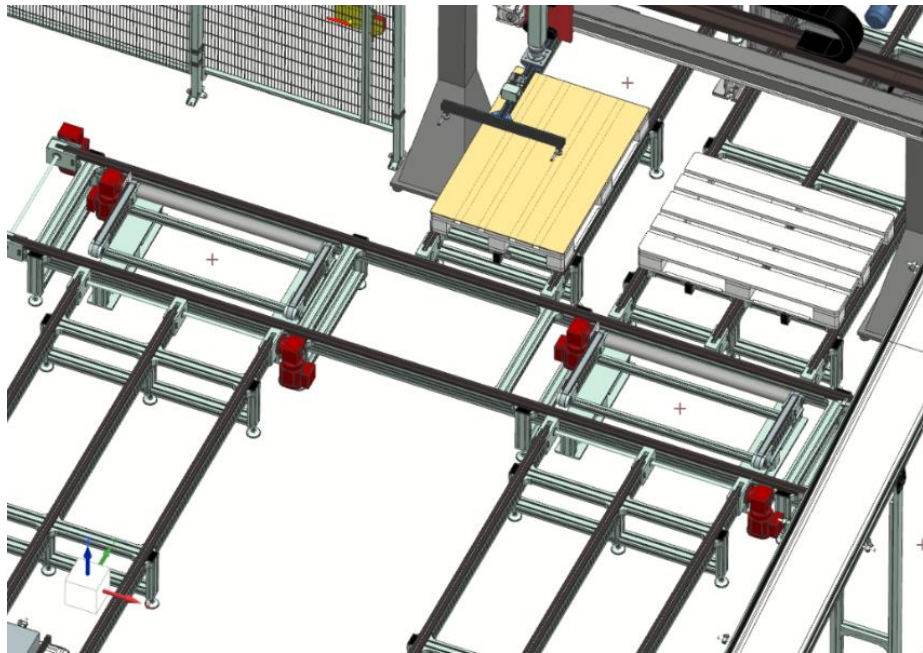


Fig.31 Isometric view of the distribution area of separators and pallets

6. 3D modeling of the effector

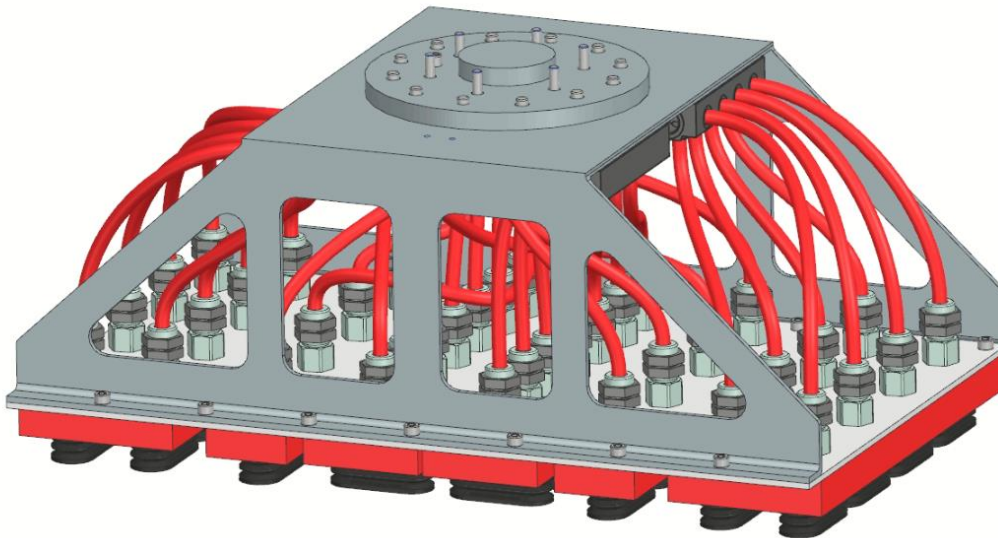


Fig. 32 Isometric view of the pneumatic effector

The body of the effector is made of Aluminum A356, weighing about 9 kg. The effector has 6 housings with a number between 10 and 15 suction cups, each group of suction cups being operated separately to be able to handle one box individually, depending on the type of box.



Fig.33. Picture with the arrangement of the suction cups

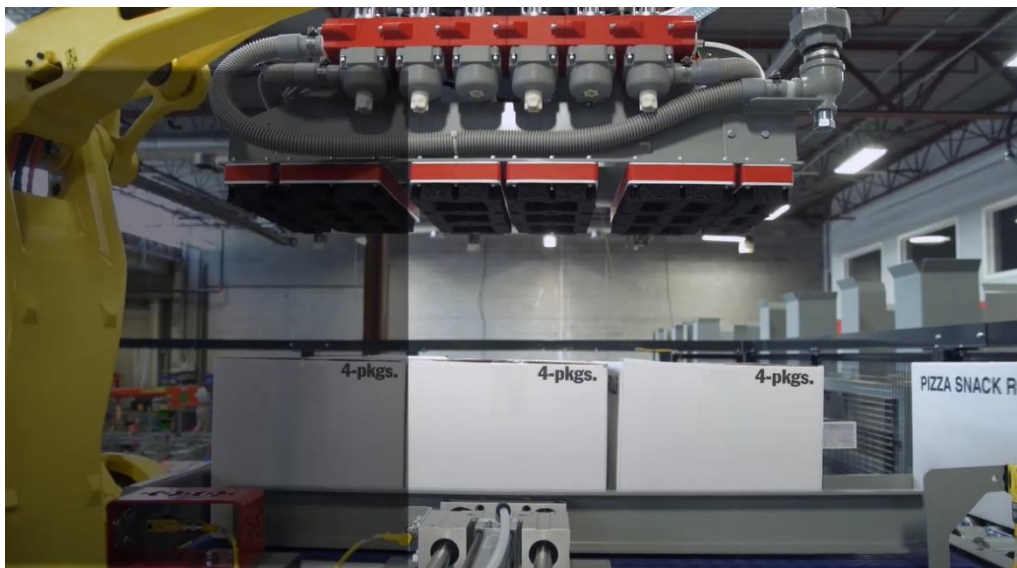


Fig. 34 View of the effector present in the application for the diploma project

7. Conclusions

In conclusion, the realization of a robotic cell is a process that requires a lot of attention, from the choice of components, to their location in the cell.

Also, some elements, such as the box alignment system because no 3D models were found from the manufacturer, had to be modeled based on the documentation provided.

Another contribution is the found documentation of the robot, without which it would not have been possible to make the execution drawings with the internal structure of the robot. The supplier only specified the components used, but assembling them in the execution drawing was his own contribution.

8. Bibliography

- 1) A. Nicolescu - Course "General IR Architectures"
- 2) A. Nicolescu - Course "THE UNITARY SYSTEMIC CONCEPT OF INDUSTRIAL ROBOT INTEGRATED IN THE TECHNOLOGICAL ENVIRONMENT"
- 3) Fundamental film- "<https://www.youtube.com/watch?v=9t1CKtgYOts>"
- 4) Cristina Pupaza - Computer Assisted Engineering Course 1 (2021-2022)
- 5) Cristina Pupaza - Computer Assisted Engineering Course 2 (2021-2022)

DEVELOPMENT OF A MODULAR AXIS STRUCTURE FOR THE PURPOSE OF ATTAINING SEVERAL ROBOTIC ARCHITECTURES

MUREȘAN Ștefan-Claudiu¹, MOROȘAN Teodor, S.I. PhD. Eng. CRISTOIU Cozmin Adrian, S.I. PhD. Eng. IVAN Andrei Mario

This paper has the objective to present the benefits of developing and implementing a series of translation axes into various robotic architectures, as well as to present the prototype that was built in order to study and research the performances it is capable of reaching outside virtual simulations. Further on, the process designing and manufacturing the series of axes is listed, which are then assembled together to achieve the structure of a 3-DoF Tripteron Cartesian parallel robot, one the configurations that these axes can be installed in.

Keywords: Prototype, translation axis, modularity, educational, Tripteron.

1. Introduction

Industrial robots, although versatile, a limit is set to the range of operations they are capable of doing by their very construction. Therefore, a robot that can change its structure is bound to have an increased number of applications that it can do efficiently, when compared to the usual industrial robots available on the market.

For the purpose of developing such a robot, a compact structure of modular translation axis proved to be the most efficient way when considering a price-performance ratio, on top of having relatively less complex kinematics. In order to achieve such a goal, it was essential to produce a prototype in order to predict the behaviour of future, improved versions of this modular axis, that could be assembled to create the previously mentioned versatile robot.

2. Designing the axis

The first aspect to consider when thinking about the design of the axis is how it is going to be assembled together with other axes in various positions, considering this is the fundamental quality of the axis, but also how it is going to be as compact as possible.

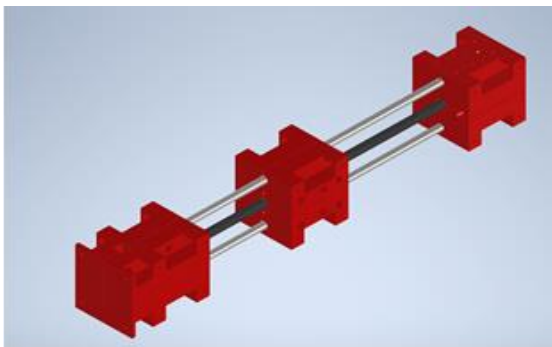


Fig. 1. 3D of the exterior of the axis prototype

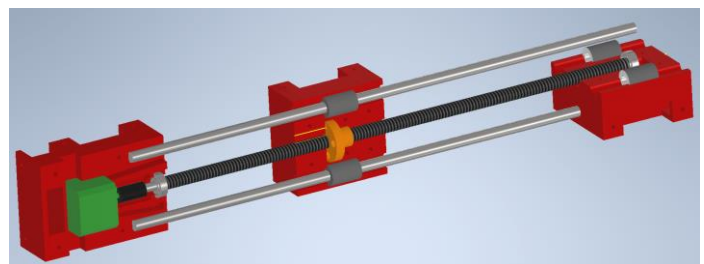


Fig.2. 3D of the interior of the axis prototype

¹ Faculty: Industrial Engineering and Robotics, Specialization: Robotics, year of study: II, e-mail: stefanclaudiu2812@gmail.com

Another aspect that has to be mulled over is about anticipating exactly how many architectures the combined axis is able to be integrated in. The conclusion we came to this far is that the axis is able to be implemented the following robots: Tripteron, Reversed Delta robots with 3,4 or 6 axes, Simple and Double gantry robots. Stewart platform, XY-Theta parallel robot, column robot.

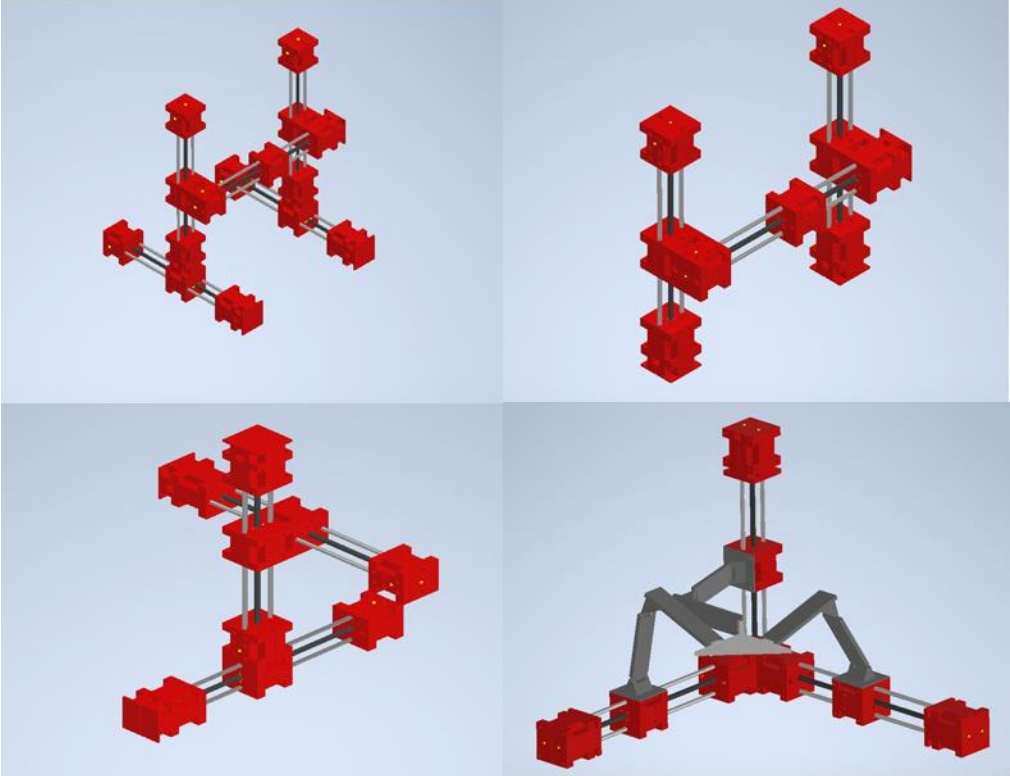


Fig.3. Some of the possible configurations that can be obtained (top left – double gantry robot, top right – simple gantry robot, bottom left – Column, bottom right – Tripteron)

For the design part of the axis and the robots, the software used was Inventor Profession from Autodesk, used for the design, animation and finite element analysis (possible due to Autodesk’s partnership with Ansys, from which they developed a patch).

3. Tripteron

Tripteron is a unique robot configuration, a three or four axis parallel cartesian robot with position command, with applicability in numerous domains, such as 3D printing, pick and place operations, cinematography etc. For the first prototype we built, we chose this architecture.

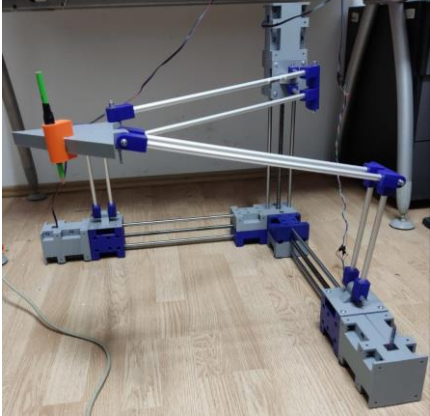


Fig.4. The built tripteron prototype

4. Manufacturing

As far as the process of manufacturing the cases goes, what we used was a 3D printer from Creality (CR-V 10S) and PLA as the filament. In order to obtain the least number of waste pieces, the CAD stage included a part of tolerances analysis. Due to the usage of a 3D printer however, the corresponding tolerances could not be obtained, so that the main aspect taken into consideration was the precision of the printed layer. Therefore, after several tests, the most optimal solution was to have an increase of 0.2 mm for every functional dimension, in order to make up for the errors of the printer. The parts that were meant to be assembled into the cases were fitted with a press-fit type of fastening. Although the procedure of calculating the tolerances could be considered vague, the results turned out to be more than promising, obtaining the respective lot of housings with the least possible amount of waste parts.

The specific settings for the process of 3D printing with PLA were the nozzle temperature of between 190 and 220 degrees Celsius, the bed temperature between 40 and 50 degrees Celsius, according to the specific characteristics provided by the manufacturer. For the infill amount of 20% Gyroid-type, due to its excellent strength-quantity ratio.



Fig.5. Resulted 3D printed parts with components slotted in

5. Computer Aided Engineering

For the finite element analysis we studied the axis behaviour under torsion, compression and bending stress with an equivalent force of 1000N and a torque of 10000Nm, obtaining maximum stress values of 2192,38 MPa (developed on the XX axis at bending) and maximum displacement values in module of 1,809 mm (obtained on the X axis at bending).

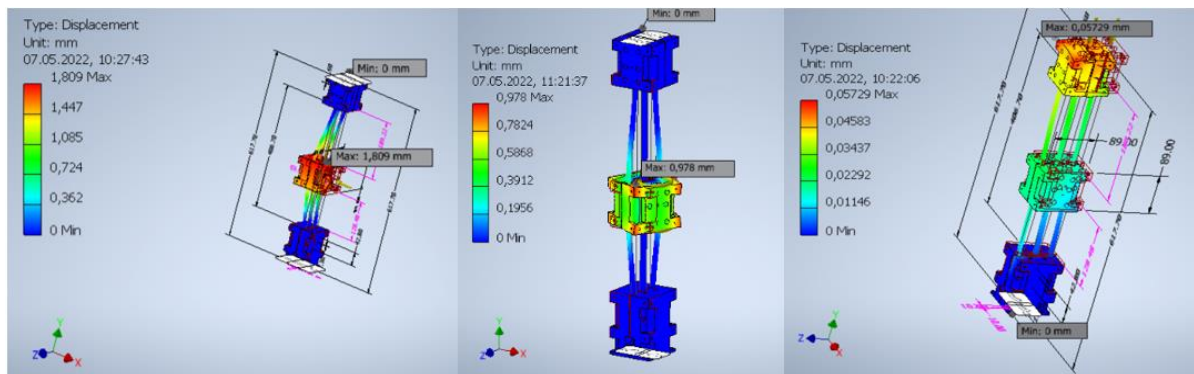


Fig.6. Finite element analysis results for displacement extracted from the report (left – bending, middle – torsion, right – compression)

6. Electrical command and control

As far as the electrical and command side of things is concerned, we used an Arduino UNO R3 development board, and since we used a NEMA 17HS4401 stepper motor, we also paired it with a A4988 stepper motor driver. The driver is connected to a 12V source which is more than enough to power the stepper motor.

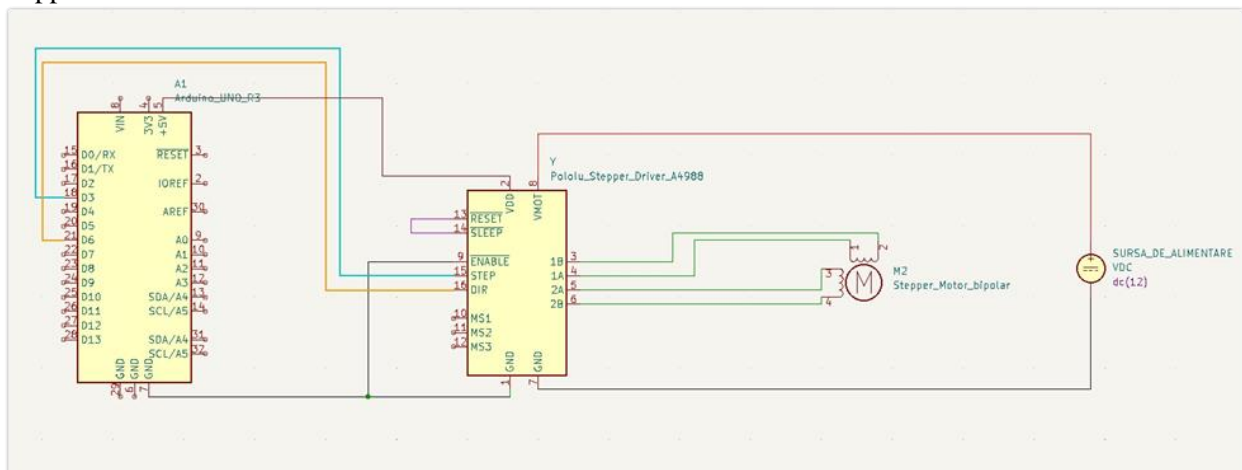


Fig.7. Electrical diagram for one axis

For the tripteron, the firmware on the Arduino we used GRBL, on top of which we used Universal G-code Sender (UGS) that acts as a Graphical User Interface (GUI) but also sends the G-code necessary to drive the mechanism.

7. Conclusions and future work

In this paper are presented the results of our analysis on reasons as to why we developed modular translation axis which can be assembled to form various architectures of robots. These results proved to be fruitful, as we think this subject is worth to be researched further. As a consequence, we decided to design and manufacture a prototype that can be studied upon.

Therefore, the benefit of constructing a prototype comes in the form of discovering issues that occurred due to several reasons, including the ones that appeared as a result of the fabrication process used for the housings, in our case, due to the 3D printing. This, in turn helps us gather information that is necessary to optimize the said fabrication process. In the future, we plan on changing the materials used for the construction of the axis, from PLA (which is comparably cheaper, but possesses lower qualities) to ones with better qualities, suited for industrial use, as well as switching to fabrication processes other than 3D printing. Improvements can be also made by replacing the current motors with ones that have greater

torque, to not only extend the range of applications that the robot is capable of doing, but also improve their quality, by also adding a closed-loop control system. Another aspect that can be polished up on is the modularity of the axes, as to allow future such improvements to be easier to implement and raise the degree of universality of the axis. Further improvements must be considered in more detail, in order to satisfy the condition of having a relatively low cost but high performance.

In the future, the prototype can also be used in education. In this way, students to study the discrepancies between a 3D model and the real, physical version of such a mechanism as well as to learn about the different types of architectures that it can achieve, and more. Going further, this can be a good method of collecting functional feedback on simulating processes similar to the ones in the industry, as we plan on further testing its capabilities. In this way, we can further discover the limitations of such a design and improve on it with the feedback that we received.

8. Bibliography

- [1]. Peter Mckinnon (2012), *Robotics: Everything You Need to Know about Robotics from Beginner to Expert*, Createspace Independent Publishing Platform, 240 pag., ISBN 9781523731510;
- [2]. Larry T. Ross, Stephen W. Fardo and Michael F. Walach (2017), *Industrial Robotics Fundamentals: Theory and Applications*, Goodheart – Wilcox Publisher, 480 pag., ISBN 9781631269417;
- [3]. Bruno Siciliano and Oussama Khatib (2008), *Springer Handbook of Robotics*, Springer Science & Business Media, 1611 pag., ISBN 9783319325507;
- [4]. Bruno Siciliano, Lorenzo Sciavicco, Luigi Villani and Giuseppe Oriolo (2010), *Robotics: Modellingm Planning and Control*, Springer Science & Business Media, 632 pag., ISBN 9781846286414;
- [5]. Guruprasad K. R.(2019), *Robotics Mechanics and Control*, PHI Learning, 244 pag., ISBN 9789388028615;
- [6]. Drăghici, G. (1999). *Ingineria integrată a produselor*, Eurobit, ISBN 973-96065-7-1, Timișoara;
- [7]. *** COSMOS/M – Finite Element System, User Guide, 1995.
- [8]. Ștefan I. Maksay and Diana A. Bistriian (2008). *Introducerea in Metoda Elementelor Finite*, CERMI, ISBN 978-973-667-324-5, Iași;
- [9]. William Bolton (2018), *Mechatronics: Electronic Control Systems in Mechanical and Electrical Engineering*, 688 pag., Pearson Education 7th edition, ISBN-13 978-129-225-097-7;
- [10]. John Craig (2021), *Introduction to Robotics*, Global Edition 4th edition, 448 pag., Pearson Education, ISBN-13 978-129-216-493-9;
- [11]. Oleksandr Stepanenko https://www.youtube.com/watch?v=MvEpi4FDhuI&list=PLUb-vZlf8Y40hHA_D_AWWIaXbTFFewU_M

NUMERICAL CONTROL MACHINE TOOL FOR MILLING AND 3D PRINTING

TURTUREA Petre-Gabriel, CULA Ștefan, Andrei Mario IVAN, Cozmin CRISTOIU
Faculty: Industrial Engineering and Robotics, Specialization: Robotics, Year of study: II, e-mail:
petre.turturea@stud.fiir.upb.ro
Scientific Mentor: PhD Ing. Andrei Mario IVAN, PhD Ing. Cozmin CRISTOIU

1. Introduction

The project's main focus is the rehabilitation, improvement and perfecting a Computerized Numerical Control machine by implementing a modern control module, performant driver modules and extending its functionality with an additional tridimensional printing using Fused Deposition Modeling. At the same time, it was proposed to strengthen the constructive structure of the CNC machine in favor of increasing the milling resolution.

2. Current state

In the current state, the CNC machine was designed, assembled and optimized in Fusion360.

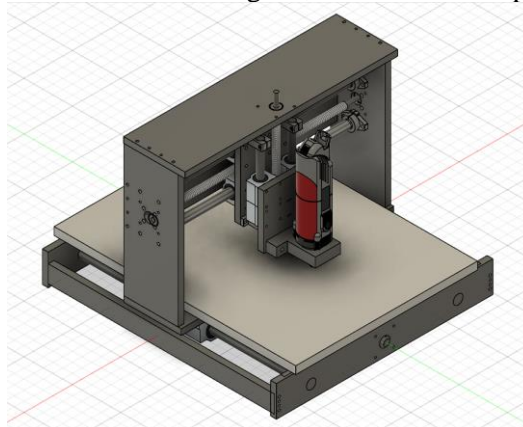


Fig. 1. Overall assembly model

The central processing unit of the machine was replaced with an integrated circuit from Espressif called ESP32. The new IC is faster and more efficient due to its 160MHz clock frequency, 32-bit memory addresses, enhanced flexibility provided by the fast GPIO pin matrix.



Fig. 2. Espressif ESP32 microcontroller [1]

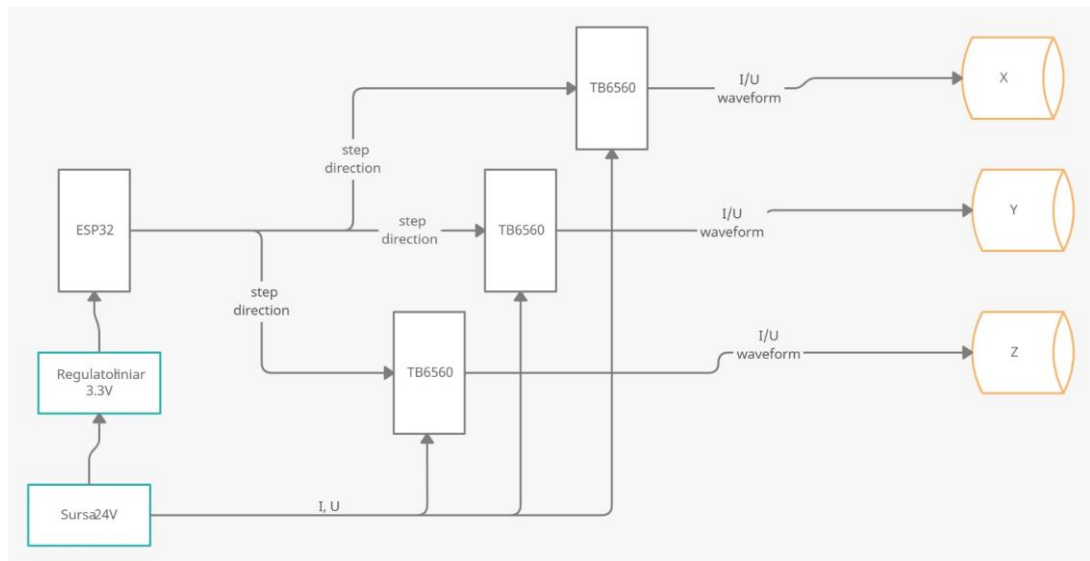
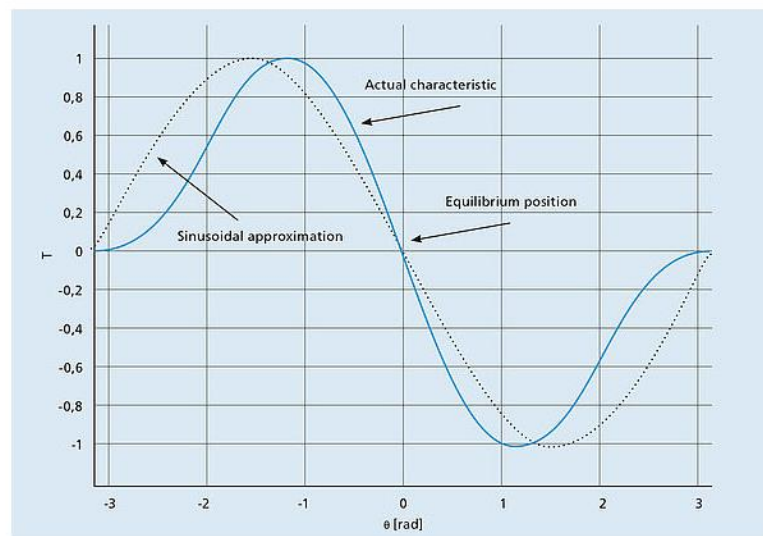


Fig. 3. Electrical block diagram

In regards to the stepper motor control subsystem they have been separated from the main control board with the discrete power drivers TB6560 [5]. These are capable of providing necessary electrical amperage to the NEMA 23 stepper motors which have a 1.8° angular step in 50% decay mode (mixed decay) thus assuring an adequate breaking force while still providing low current ripple and an accurate sine wave to the motor [6][7][8].

Torque vs. shaft position



Dotted line: Suitable response for precise microstepping positioning. Blue line: Distorted curves.

Fig. 4. Sine wave approximation by stepper drivers [3]

As for the used firmware, FluidNC is designed to be implemented on ESP32 having the ability to exploit every subsystem made for actuating the stepper motors [2]. Alongside the out-of-the-box compatibility, it implements a wireless interface which enables real-time calibration and the transmission of G-Code commands, including files.

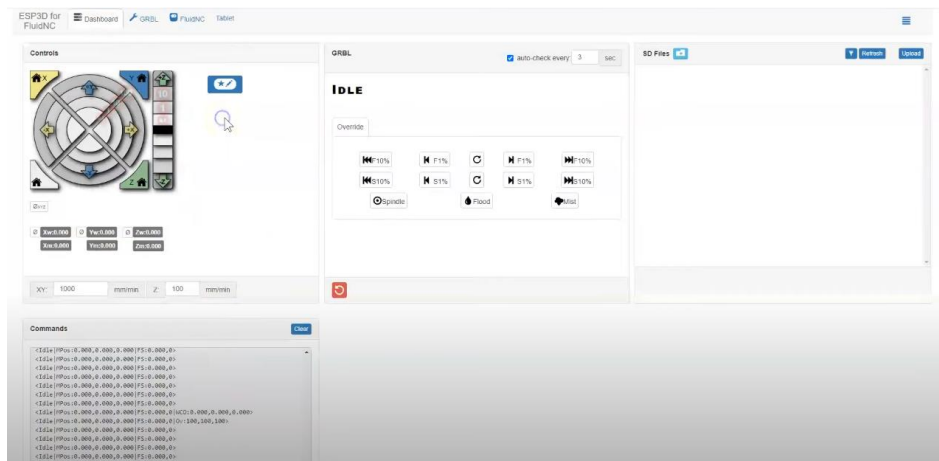


Fig. 6. FluidNC web interface [2]

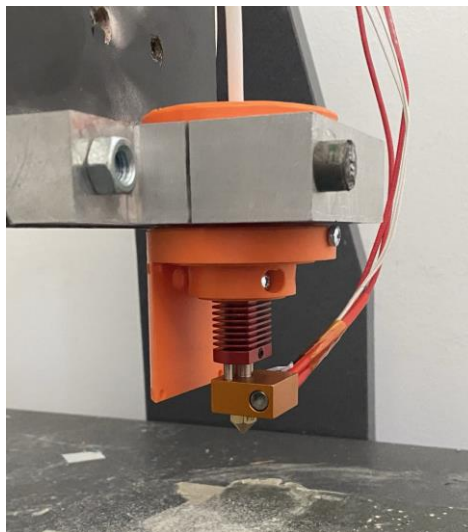


Fig. 5. Adaptor module with hot-end installed

On the subject of 3D printing, an adaptor module was designed to make the current flange compatible with a FDM print hot-end[4]. Paired with this is an aluminum plate fitted with a spring-nut leveling mechanism which serves as a bed.



Fig. 6. Leveling bed

3. Conclusions

As for the conclusions, the robotics club now has a CNC machine with the ability to mill and 3D print which can be used in further projects. The machine can now be operated wirelessly using a friendly web interface or third-party programs.

In regards to the improvements that can be made, there is the possibility to design an adaptor for laser engraving, the addition of an auto-leveling system, a software change to compensate for the backlash of the material and encoders for the backlash of the cinematic chain.

4. Bibliografie

- [1]. docs.espressif.com. (n.d.). ESP-IDF Programming Guide - ESP32 - — ESP-IDF Programming Guide latest documentation. [online] Available at: <https://docs.espressif.com/projects/esp-idf/en/latest/esp32/> [Accessed 19 April 2022]
- [2]. bdring (2022). bdring/FluidNC. [online] GitHub. Available at: <https://github.com/bdring/FluidNC> [Accessed 19 April 2022]
- [3]. www.faulhaber.com. (n.d.). Stepper Motor Tutorial - Microstepping Myths and Realities. [online] Available at: <https://www.faulhaber.com/it/support/technical-support/motors/tutorials/stepper-motor-tutorial-microstepping-myths-and-realities/> [Accessed 2 May 2022]
- [4]. Wikipedia Contributors (2019). Fused filament fabrication. [online] Wikipedia. Available at: https://en.wikipedia.org/wiki/Fused_Filament_Fabrication. [Accessed 5 April 2022]
- [5]. Datasheet-TB6560 3Axis Stepper Motor Driver. (n.d.). [online] Available at: https://www.allelectronics.com/mas_assets/media/allelectronics2018/spec/SMC-5.pdf [Accessed 16 March 2022]
- [6]. Electrical specifications General specifications Insulation Resistance (M) 80 Max (rated current 2 phase on). (n.d.). [online] Available at: https://components101.com/sites/default/files/component_datasheet/NEMA23%20Stepper%20Motor.pdf [Accessed 20 March 2022]
- [7]. datasheetpdf.com. (n.d.). NEMA23 motor Datasheet pdf - stepper motor. Equivalent, Catalog. [online] Available at: <https://datasheetpdf.com/pdf/1276820/Schneider/NEMA23/1> [Accessed 22 March 2022].
- [8]. ResearchGate. (n.d.). Fig. 7: Voltage Waveform for Full Stepping Mode. [online] Available at: https://www.researchgate.net/figure/Voltage-Waveform-for-Full-Stepping-Mode_fig7_269611096 [Accessed 22 March 2022].

CARTON BOX PALLETIZATION CELL, INTEGRATING AN INDUSTRIAL ARTICULATED ARM ROBOT

COTOILĂ Mihail-Constantin, Ș.l. dr. ing. Andrei Mario IVAN

Faculty: Industrial Engineering and Robotics, Specialty: Robotics, Year of study: 4

e-mail: cotoilamihail@outlook.com

Scientific leader: Ș.l. dr. ing. Andrei Mario IVAN

The study consists in the presentation of a flexible manufacturing cell in which a palletizing operation of several types of boxes is performed. The application has 4 inputs and 4 outputs, with 4 different types of boxes and 4 piles. The application integrates the industrial robot MOTOMAN GP225 with an articulated arm architecture and 6 degrees of freedom, which is equipped with a vacuum effector with the role of making piles. The functional working scheme of the robot being the alternative arrangement of the boxes according to the bar code printed on them.

1. Introduction

The study highlights the structure of the flexible cell, along with certain changes to eliminate the need of a human operator and to fully automate the process of making piles. The cell started from a reference film with the following main elements:



Fig. 1 The highlight of the main elements in the cell

In the reference film, you can see the operation cycle starting with the input of the boxes on a belt conveyor, and then they are diverted according to the barcode printed on them to a roller conveyor using a roller deflection system. When a box reaches the end of the stroke (at the end of the roller conveyor), the box is taken over by the industrial robot which will make the pile. The pallets on which the piles are made are introduced into the cell by a human operator and are centered with the help of some metal corners. The evacuation of a complete pile is done with the same human operator who takes the pile with a lysis and transports it to a storage area.

2. The preparation of the assembly

The GP225 industrial robot is integrated in the cell and is located on an elevation system for the robot base (which can also be seen in the structural kinematic diagram). It is a 6-axis robot for general purpose used due to its large reach of 2702 mm, a maxim payload of 225 kg and a repeatability of ± 0.05 mm.

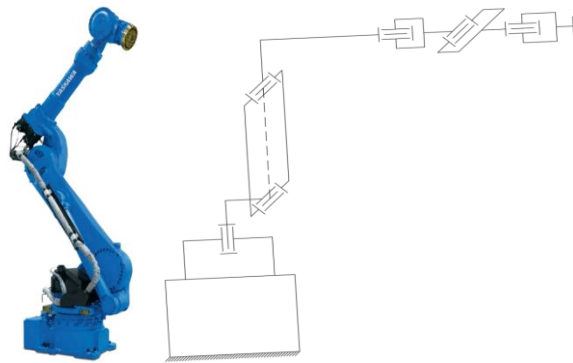


Fig. 2 The robot model with his structural kinematic scheme

For the robot orientation system, we have a mixed drive motors allocation with 3 motors located in the immediate vicinity of the driven elements for the first 3 axes and the last 3 motors are located at the end of the last segment of the robot for the last 3 axes.

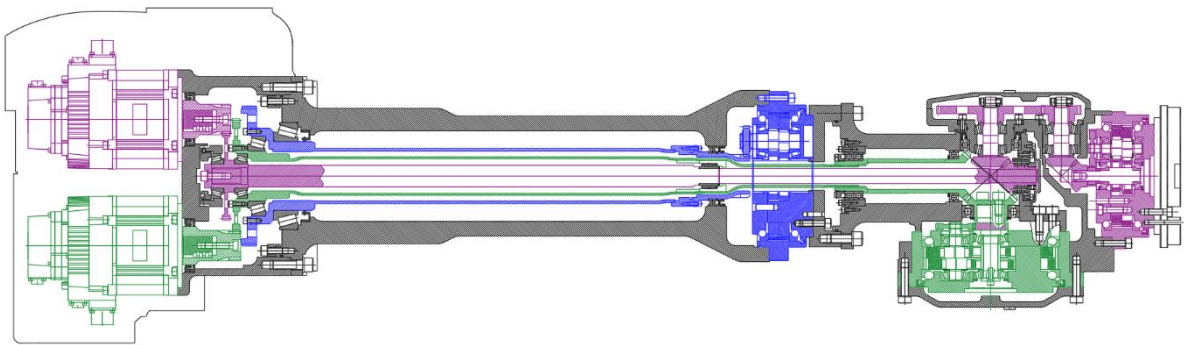


Fig. 3 A section through the orientation system

The section through the orientation system highlights in full the drive for axes 5 and 6 and partially for the axis 4. In the figure 2.3 we can see partially the structure in 3D format without motors.

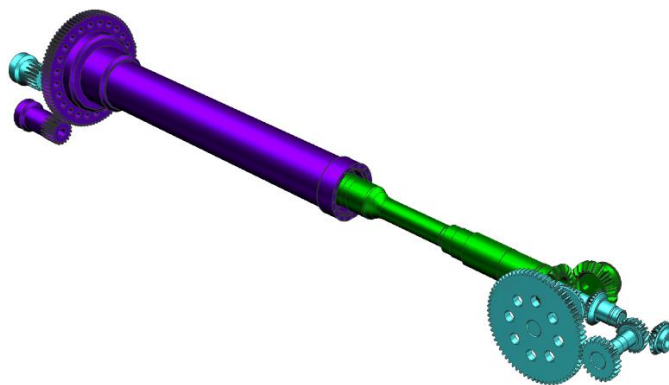


Fig. 4 The 3D structure of the orientation system realized in NX

The effector with which the robot is equipped is designed by me to be as close as possible to the one in the reference film, using standardized elements such as:

- A pneumatic island made with elements from Festo;
- Vacuum modules from Piab;
- Aluminum profiles from the company 80/20;

- The part of the hoses and cables were made in the Routing Electrical module of NX;
- An adapter plate between the robot flange and the rest of the effector which was modeled in the Modeling module in NX.

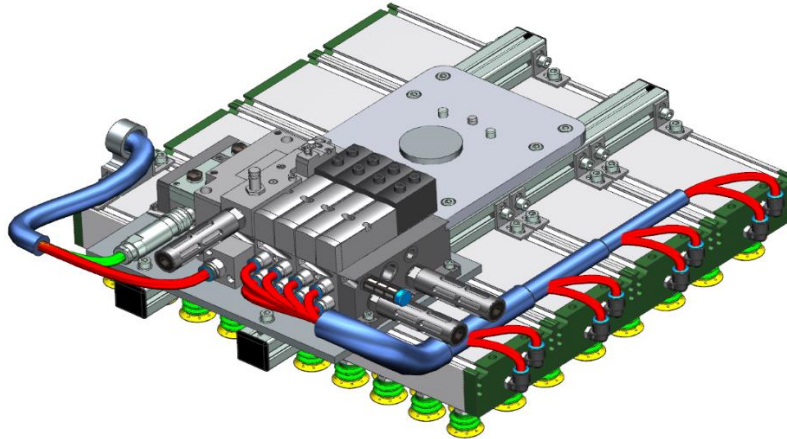


Fig. 5 The vacuum effector assembled in NX

Next, I made the execution drawing and the technological film for the adapter plate between the robot flange and the effector.

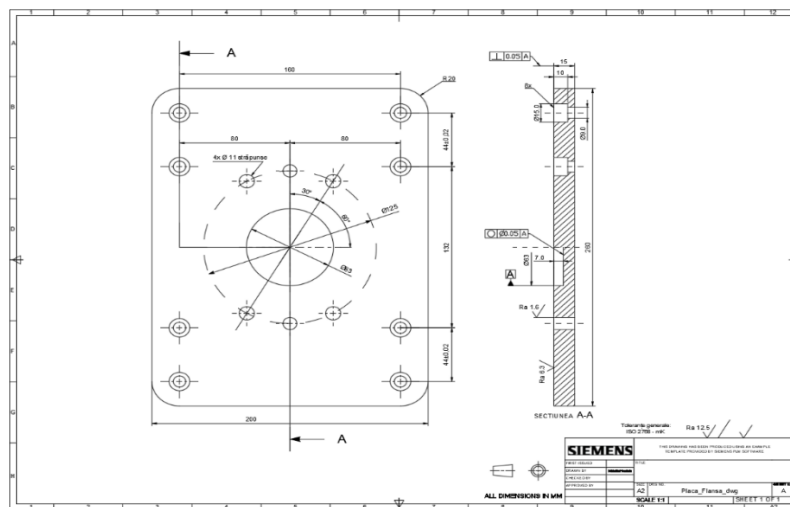


Fig. 6 The execution drawing for the adapter plate

For the technological film, I assumed the realization of the piece on a CNC machining center in 3 axes using the following operations with the specified tools:

- The orientation and fixing of the blank product after cutting to close dimensions on a universal with 3 jaws;
- The milling of the upper face done with a face milling cutter from Sandvik Coromant (CoroMill 245);
- The holes drilling using drills (CoroDrill 860 and CoroDrill 880 for different diameters)
- The reorientation of the blank product by rotating the part with 180° on the X axis and the fixing;
- The contour processing with a mill (CoroMill R215.H4);
- The milling of the lower face done with a face milling cutter (CoroMill 245);
- The detachment of the blank product;

- The final inspection done with a caliper;
- The preservation and the storage of the final product.

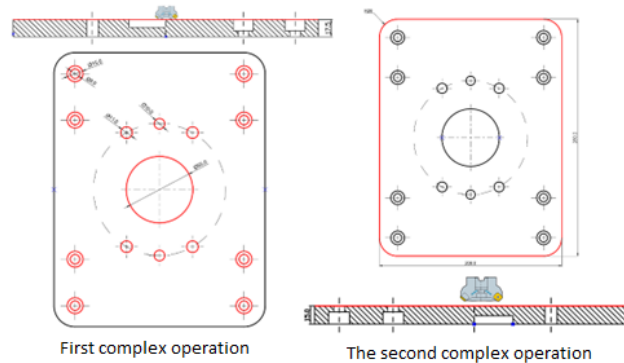


Fig. 7 The machined surfaces of the blank part

Below is the execution drawing of an elevation system made by me based on several similar systems from ABB Group and FANUC.

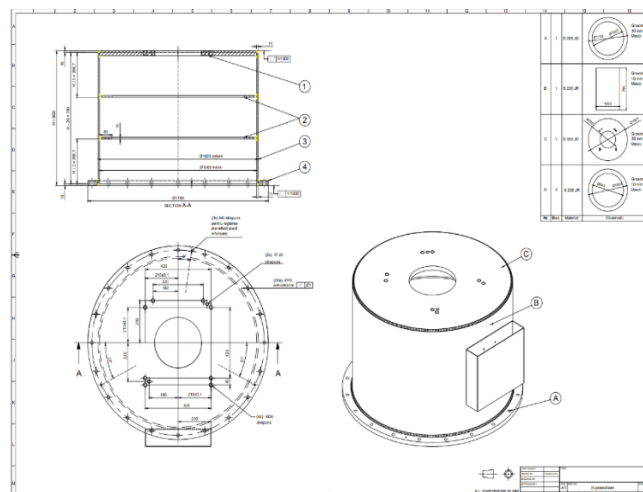


Fig. 8 The execution drawing of the elevation system

The changes to the cell are represented by some chain conveyors with the role in transporting the pallets from a pallet distributor, which is fed automatically by a guided vehicle, to the working points where the pallets are centered and fixed, and finally the complete piles are evacuated from the cell by another automatically guided vehicle.

The elements made by me using standardized elements, different from those in the reference film are:

- The robot base elevation system;
- The centering and fixing system of the boxes before being taken over by the robot;
- The centering and fixing systems for pallets in working points;
- Pallets and piles lifting systems;
- The conveyor assembly for evacuating piles from the cell;
- The pneumatic island corresponding to all the elements whose actuation is pneumatic in the cell.

Finally, the final variant of the cell is presented using the input part of the boxes according to the reference film and the input part of the pallets and piles evacuation made by me together with the preliminary version of the cable channel with plugs, cables, hoses and connectors for each element.

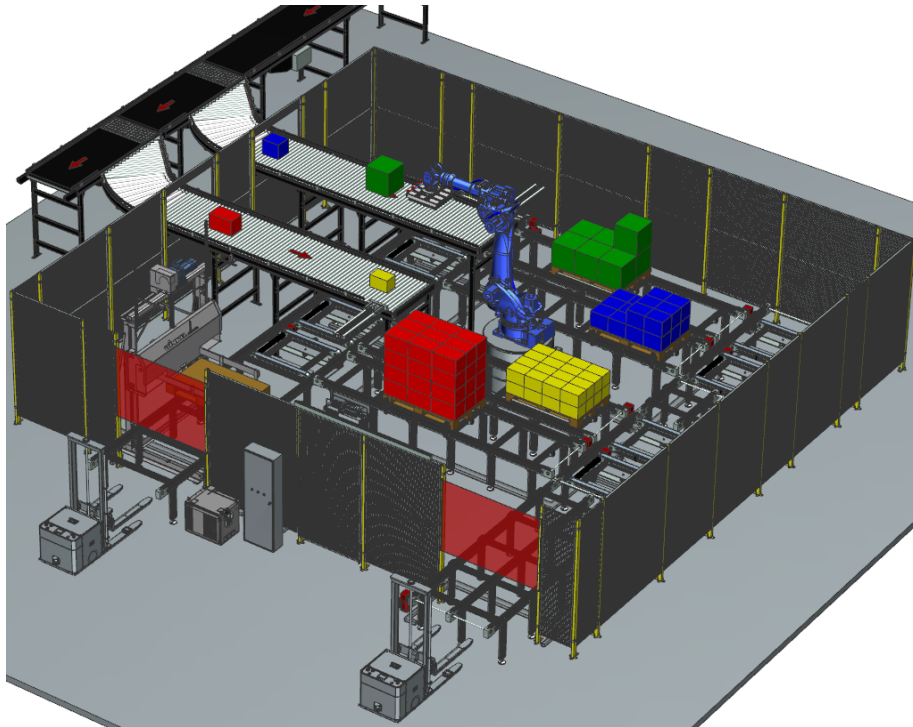


Fig. 9 The final version of the cell assembled in NX

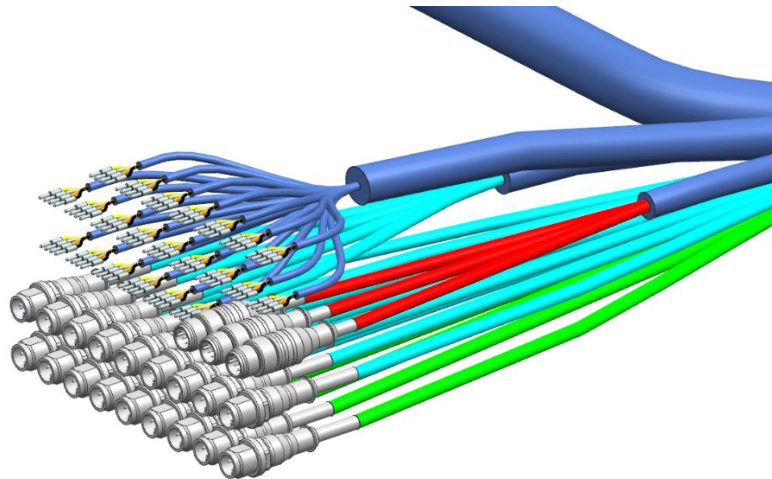


Fig. 10 Plugs from Sick and cables realized in NX

Along with the things presented above, I also performed a simulation in Tecnomatix 16.1 (Process Simulate) in which the work cycle of the cell is highlighted.



Fig. 11 The simulation realized in Process Simulate

3. Conclusions

To complete the study are also required:

- A section in which the actuation of axis 4 will be visible;
- The realization of a section view for the axis of rotation of the base of the robot together with the calculations of choice for the reducer and the drive motor;
- The completion of the internal structure of the robot;
- The completion of cables and hoses for each system in the cell.

4. Bibliography

- [1]. Bucuresteanu A. (2013), Elemente și sisteme pneumatice pentru acționarea roboților industriali, Editura Printech, Bucuresti, ISBN 978-606-23-0081-4
- [2]. Cristoiu C. A. și Nicolescu A. F. (2020), NX CAD-Basic - Proiectare asistată de calculator, 96 pag., Ed. Politehnica Press, ISBN 978-606-515-914-3
- [3]. Dobrescu T. (1998), Bazele Cinematicii Roboților Industriali, Ed. Bren, București, ISBN-973-9427-02-2
- [4]. Ivan M. (2020), Proiectare asistată de calculator pentru sisteme de prindere modulare, course notes and laboratory support, UPB
- [5]. Gheorghita M. (2021), Tehnologia Fabricării Componentelor Roboților Industriali, course notes, UPB
- [6]. Nicolescu A. și Coman C. (2018) - Robotică 2 și Robotică 3, course notes and applications, UPB
- [7]. Nicolescu, A. F. (2021), Concepția și Exploatarea Sistemelor de Producție Robotizate, course notes and design methodologies, UPB
- [8]. Nicolescu A. F. și Cristoiu C. A. (2020), Implementarea roboților industriali în sistemele de producție. Îndrumar de laborator și proiect, 75 pag., Ed. Politehnica Press, ISBN 978-606-515-915-0
- [9]. Companies from which standardized elements were taken - Interroll, Phd, mK North America, Festo, Winkel, Troax, Sick, Motorman, Piab, 8020, Sandvik Coromant.

DEVELOPMENT OF CONTROL AND IMAGE PROCESSING FIRMWARE FOR ARTICULATED ROBOT ARM EQUIPPED WITH ADDITIONAL TRANSLATION AXIS

ANASTASIU Alexandru-Ioan

Faculty: Industrial Engineering and Robotics, Specialization: Robotics, Year of study: 1 ; E-mail: a.anastasiu@outlook.com

Scientific mentors: PhD Ing. Cozmin CRISTOIU, Conf. Florea Dorel ANANIA

SUMMARY: The project's end goal was to develop firmware equivalent to the industry standard for an educational 5 axis robot, replicating functionality of a Teach-Pendant and offering the possibility of programming, either by manually writing programs, or by utilizing third-party software, such as RoboDK. Additionally, steps were taken in order to fully utilize available hardware.

Keywords: Robot, Programming, Hardware instructions

1. Introduction

Thanks to the growing availability of such kits, it is becoming increasingly easy for students and hobbyists alike to gain access to the world of robotics. This is helpful in understanding the key concepts behind such machines, without the need to work inside an industrial environment or access cost-prohibitive hardware. By using one such robot kit, a scaled-down but otherwise analogous in function 5 axis robot arm was programmed.

2. Current stage

Current industries are moving more and more towards automation. This can perhaps best be seen in assembly lines, with factories all around the world utilizing industrial robots in order to streamline construction and reduce running costs. Historically, such robots have been kept closed source, with all aspects, hardware and software, intellectual property of the manufacturer. This makes it difficult for those who wish to learn exactly how to utilize such a robot (in the case of students, for example). By using an open platform (such a robot kit available for purchase), coupled with open-source software, students can gain access to these robots with ease.

3. Hardware

The hardware structure was chosen for its simplicity and robustness. The manipulator is constructed from pressed and bent aluminum sheets, alongside absolute position encoders (of the resistive type) mounted to servomotors. The controller is a raspberry pi, mounted to a driver board for the motors. Documentation for the kit was limited, but it was used as a starting point for the reverse-engineering process required to build the software. The firmware was written from the ground up, using no components from the original.

4. The Teach Pendant

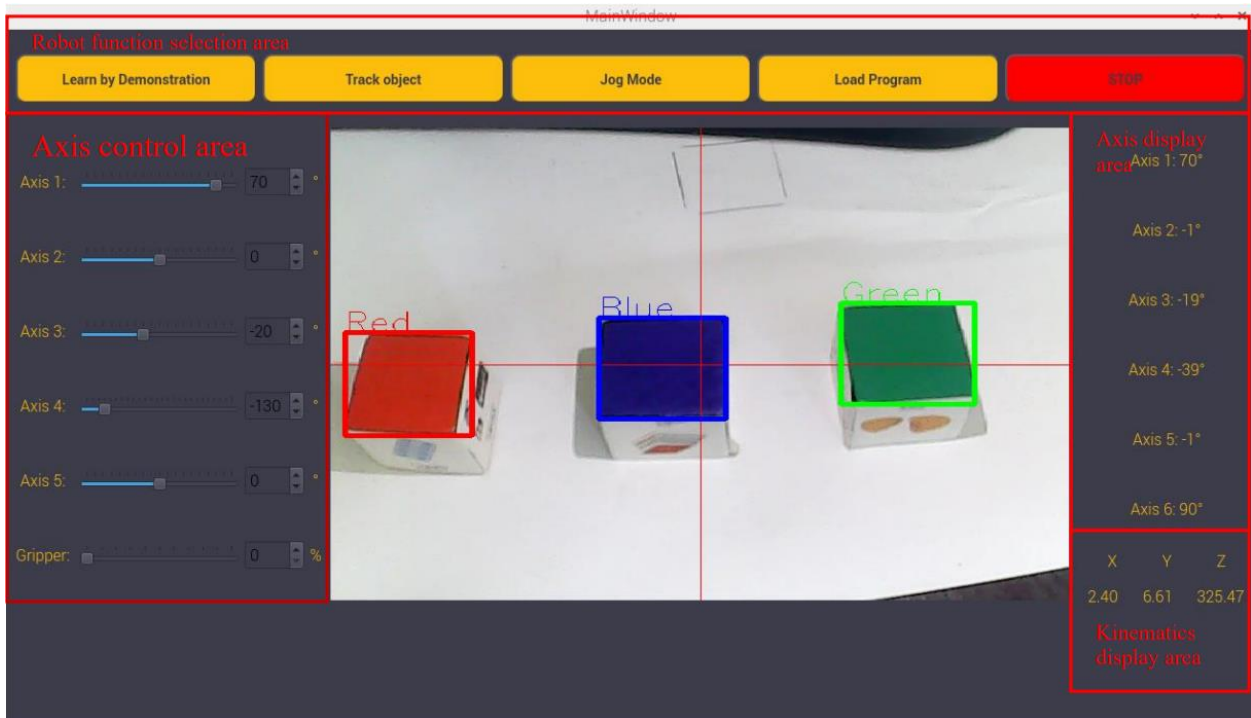


Fig. 1 The robot's graphical user interface

The Teach pendant is the main human-machine interface, allowing full control of the robot. It is designed to run on a computer attached to the robot, allowing a user to individually control the axes, to read information about current position of the robot, and to access the different operation modes. The position of the end-effector is calculated using a process called direct kinematics, transforming joint angles into XYZ coordinates, relative to the robot's base.

The different working modes can be divided into "Teach-in", or direct programming, "Object tracking", where the robot will automatically seek and follow an object of a selected color, "Free movement", or jog mode, where an operator can freely move the robot and "Program cycle", where the robot will follow a given program.

Teach-in allows the operator to program the robot directly, wherein the robot may be moved using the joystick, much like actual industrial robots. An operator can click a button to record a target once a specific position and orientation have been established. Upon running the cycle, it will subsequently proceed along the predetermined course while adhering as closely as possible to the coordinates specified.

Object tracking is done on a color basis, using an algorithm known as "Thresholding". This is done by filtering out every color that is not the one being searched for. This results in an image that only has non-black pixels in the areas colored with the value required. A bounding box can be drawn to contain all these pixels, resulting in a rectangle. By aligning the center of the viewfinder with the center of the box, tracking is achieved.

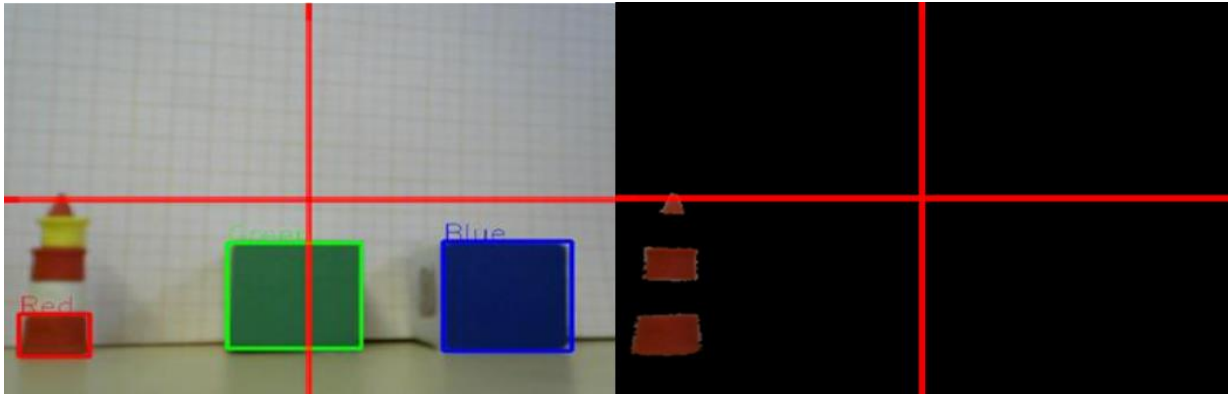


Fig. 2 Reference image

Fig. 3 Thresholding using red



Fig. 4 Thresholding using green

Fig. 5 Thresholding using blue

5. Programmability

In order to fully achieve the goal of being a scaled-down industrial robot, the possibility of off-line programming must be added. This entails the need to create an instruction set, somewhat similar to G-Code. Branded as RASM (Robot Assembly), it has a vaguely ARM assembly-like syntax and can read and carry out 17 particular opcodes (instructions) pertaining to the manipulator's spatial movement. This makes it possible for the robot to be fully programmed, including logic and arithmetic operations (addition, subtraction, multiplication, with variable support, if, else, rudimentary branching support by means of goto-like instructions).

RASM is a hybrid language, a crossover between the statically typed, compiled languages such as C and the dynamically interpreted ones such as Python. This means that, while the code does not run directly on given hardware, necessitating an interpreter to translate generic instructions into robot-specific commands, preprocessing is done in order to greatly speed up execution. For example, while variable names are important for humans to read code, a machine is more likely to find a numeric value in an array than it is to find an alphanumeric (containing numbers and letters) one. This means that variable names can be optimized out and replaced with numbers, the optimization being offset at the assembler level.

Generally speaking, the program runs in the same manner as an x86 or arm program, with instructions being laid out in an array called the program stack. Traversing this stack is a program pointer, an index that increases, indicating which instruction should be executed. Jump instructions manipulate this program pointer, changing it to whatever value is necessary.

In order not to write code by hand (which would be difficult to maintain and do), a postprocessor for RoboDK was created, which is able to generate RASM instructions from a set of point coordinates and orientations.

```

NME Prog1
// Program generated by RoboDK v5.4.2 for My Mechanism on 12/05/
// Using nominal kinematics.
ANGS 0.000 -0.000 0.000 -0.000 -0.000
ANGS 0.000 59.182 32.491 -1.683 0.000
ANGS 0.000 60.025 37.162 -7.196 0.000
// Attach to TCP_CLESTE
ANG 50
ANGS 0.000 59.182 32.491 -1.683 0.000
ANGS 45.000 59.180 32.490 -1.680 -0.000
ANGS 45.000 67.931 43.366 -21.308 0.000
// Detach from TCP_CLESTE
ANG 0
ANGS 45.000 59.180 32.490 -1.680 -0.000
ANGS 0.000 59.182 32.491 -1.683 0.000
ANGS 0.000 67.933 43.364 -21.306 -0.000
// Attach to TCP_CLESTE
ANG 50
ANGS 0.000 59.182 32.491 -1.683 0.000
ANGS 45.000 59.180 32.490 -1.680 -0.000
ANGS 45.000 60.023 37.164 -7.197 0.000
// Detach from TCP_CLESTE
ANG 0
ANGS 45.000 27.427 86.403 -23.840 -0.000
ANGS 45.000 22.236 72.361 -4.606 -0.000
ANGS 0.000 -0.000 0.000 -0.000 -0.000
END

```

Fig. 6 Example code generated by RoboDK

6. Direct kinematics optimization using ARM NEON

Direct kinematics is the process by means of which the position and orientation of an end-effector are calculated. This is done using a method called “The universal approach”, by utilizing a rotation matrix coupled with a translation vector combined into a 4x4 matrix. Each joint can therefore be described by such a matrix. Multiplying them results in the final one being the position and orientation of the end-effector. In a conventional approach, this is done the same way it is taught in school, by multiplying and adding each element. This method has the main drawback of speed, as it entails a large number of calculations being necessary, resulting in the processor needing to utilize more clock cycles. A better approach is to utilize SIMD (single instruction, multiple data) built-in to the ARM architecture. This allows 4x4 matrix multiplication to effectively be done in 4 clock cycles, resulting in a speedup of almost 3x over the conventional way.

This leverages the fused-multiply-accumulate function, which, as the name implies, implements multiplication and addition in the same clock cycle. At a silicon level, processors work on what are called registers, small (64 bit) memory locations used to store numerical values, used in arithmetic and logical operations. ARM NEON allows combining 4 such registers into what are called quadword registers, wherein they behave like a vector, with the added benefit of being able to do arithmetic instructions on them directly (vector addition, for example, is done by element, in parallel). The end benefit is being able to spend less time processing kinematics, allowing for faster response times to an operator’s requests.

8. The base translation axis

In order to allow the robot to achieve global movement (from one machine tool to another, for example), it is equipped with a base translation axis. Using a screw and two guiding rails, a steel platform is driven by a stepper motor. Control is done in an open loop, using an additional Arduino Nano microcontroller. The robot sends position commands to the axis controller, which then replies only when it has finished travelling. Live reporting cannot be done, due to the reduced clock speed of the Arduino. In essence, stepper control is generated by quickly pulsating the “step” pin of a driver module, each pulse causing the motor to turn 1.8°. Each operation to send data to the Serial port (the communication method

between Arduino and Raspberry Pi) consumes a certain number of clock cycles, reducing the overall speed at which the step pin can be pulsed.

Calibration is done at power-up, with the axis automatically moving to the reference point, where a limit switch indicates that it has been reached.

8. References

- [1] ARM Architecture Reference Manual, 2022 Arm Limited, <https://developer.arm.com/documentation/ddi0487/latest>
- [2]. Basic Thresholding Operations, https://docs.opencv.org/3.4/db/d8e/tutorial_threshold.html
- [3]. Cozmin CRISTOIU, Adrian NICOLESCU, “New approach for forward kinematics modeling of industrial robots with closed kinematic chain”, 2017
- [4]. Alexandru-Ioan ANASTASIU, Cozmin CRISTOIU, Florea Dorel ANANIA, “Educational 5 axis robot controller optimization using arm hardware instructions”
- [5]. Dobrescu, Tiberiu Gabriel & Dorin, Alexandru & Nicoleta-Elisabeta, Pascu & Ivan, Ioana. (2011). CINEMATICA ROBOTILOR INDUSTRIALI.
- [6]. Blanchette, Jasmin, and Mark Summerfield. C++ GUI programming with Qt 4. Prentice Hall Professional, 2006.

DESIGNING A SMALL SCALE FUNCTIONAL ARTICULATED ROBOT MOTOMAN MODEL

GUȚU Marius¹, NICOLESCU Adrian²

¹Faculty: FIIR, Specialization: Robotics, Year of Study: Masters I, e-mail: marius.gutu98@yahoo.com

²Professor PhD, Faculty: FIIR, Dept. Robots and Manufacturing Systems

Coordinator: Prof. dr. Ing. **Adrian NICOLESCU**

Abstract: The present study describes the internal structure of an articulated industrial robot, more specifically the robot's orientation system and one joint from the positioning system. The reference model is produced by the company Motoman, specifically Motoman MH215II. Among the items shown are 2 of the 4 gearboxes designed, one of which is of hollow shaft construction to allow the intermediate drive shafts of the numerically controlled axes 5 and 6 to pass through. The working environment used was Siemens NX. The construction is designed to allow the robot to be manufactured using additive manufacturing technology (3D printing).

Key words: Motoman, Robot, 3D Printing, Articulated robot, Cycloidal gearbox,

1. Introduction

The idea behind the work came from the desire to fill a void, to satisfy a need. Designing a small-scale robot that follows the mechanical construction solutions used in industrial robots to be used as an educational model for student training. For this reason, a model produced by Motoman [1] was chosen because of its complex mechanical design. The positioning system uses a distributed drive scheme, the motor is connected to the cycloidal gearbox which drives the moving element. The orientation system uses a centralized drive scheme. All the motors are mounted at the end of the robot's second segment. The motion is being transferred using intermediary shafts, gear assemblies and cycloidal drive.[2]

Most of the robot's components will be 3D printed using FDM or SLS technology.



Fig. 1 Reference Model - Motoman MH215II

2. Current Status

The first revision of the articulated robot was designed and manufactured during the diploma work project, more specifically the numerically controlled axes 5 and 6 were completed, these also being the most complex [2], [3]. The designed robot had several issues which have been corrected in the present version. In order to highlight the changes made to the 3D CAD assembly, a comparison between the previous and the present constructive solution was made [3].

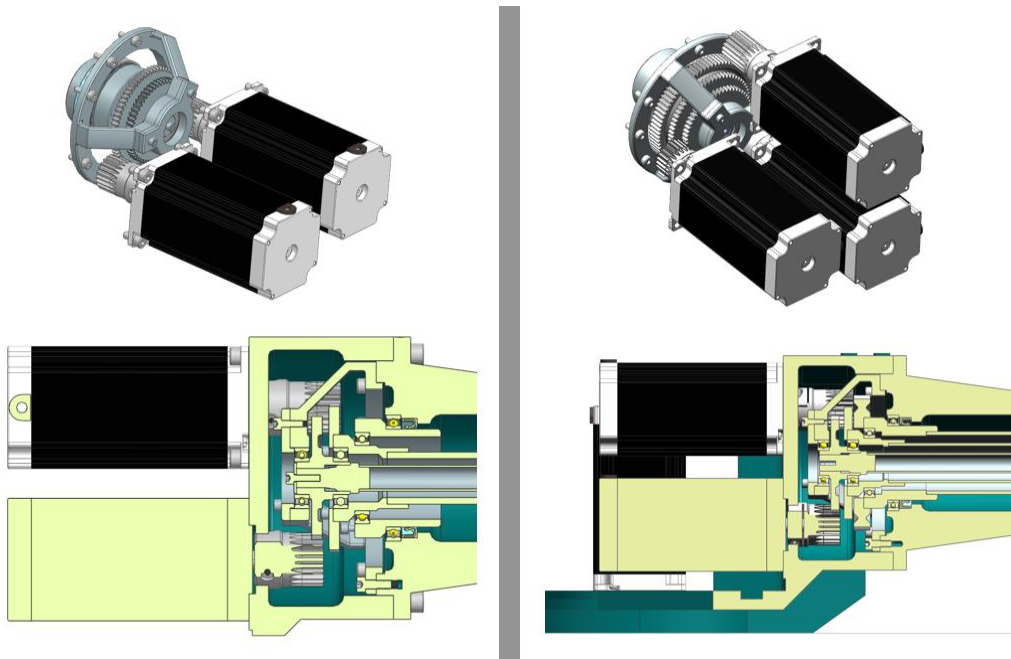


Fig. 2 Drive area for the orientation system

To drive the numerically controlled axes 4, 5 and 6 which materialize the robot's orientation system, NEMA stepper motors [4] will be used for two reasons. Simplicity of control and low price. Each motor has a pinion attached to the output shaft, which in the current solution uses a split bushing design for mounting, compared to the first solution where 3 set screws were used to secure the pinion to the shaft. The problem with the previous solution was vibrations. During operation the vibrations generated by the mechanical structure caused the set screws to unscrew. Thus, the motor shaft would rotate freely in the pinion bore. The previous assembly was completed. The motor for 4th joint and the gear assembly required to transfer the movement from the motor to the intermediate shaft were added. Nevertheless, there is still room for improvement. The sealing solutions used for the motor and pinion assembly needs to be added in order to prevent lubricant leaks.

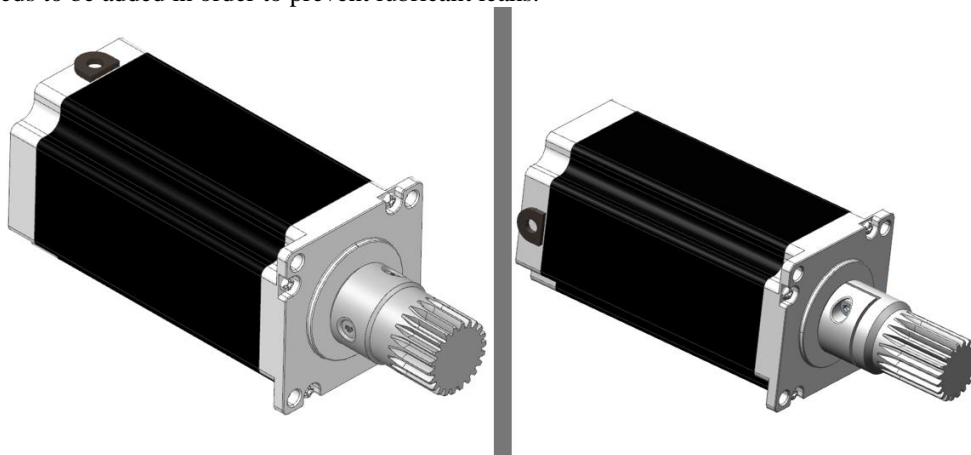


Fig. 3 Motor assembly

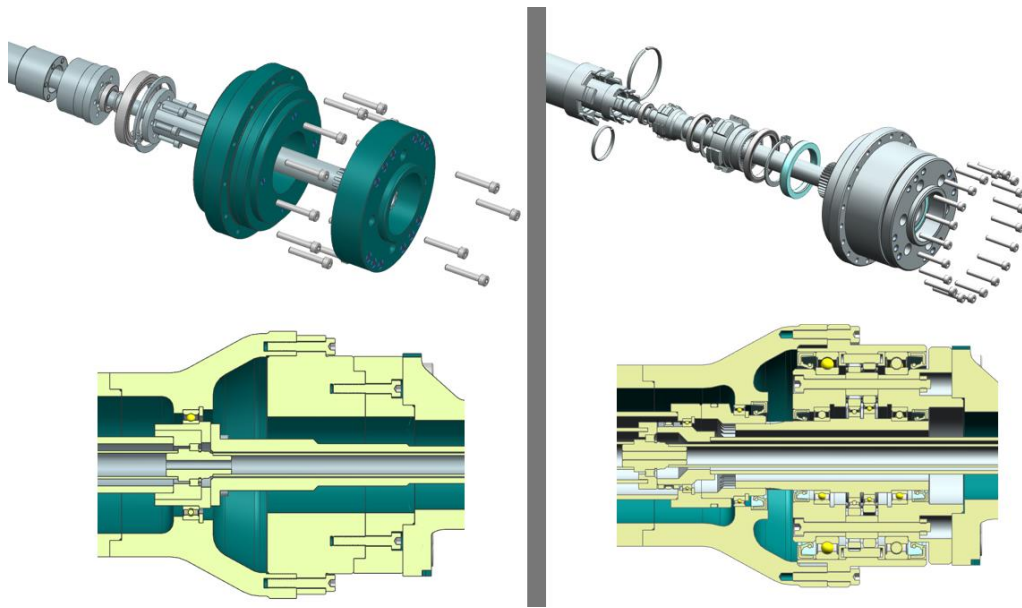


Fig. 4 4th joint and intermediate shafts assembly

The robot's second segment central area has been completely redesigned. To this end, a 1/42 transmission ratio cycloidal gearbox in hollow shaft construction has been designed to allow the intermediate shafts required to transmit motion to axes 5 and 6 to pass through.[3], [5]

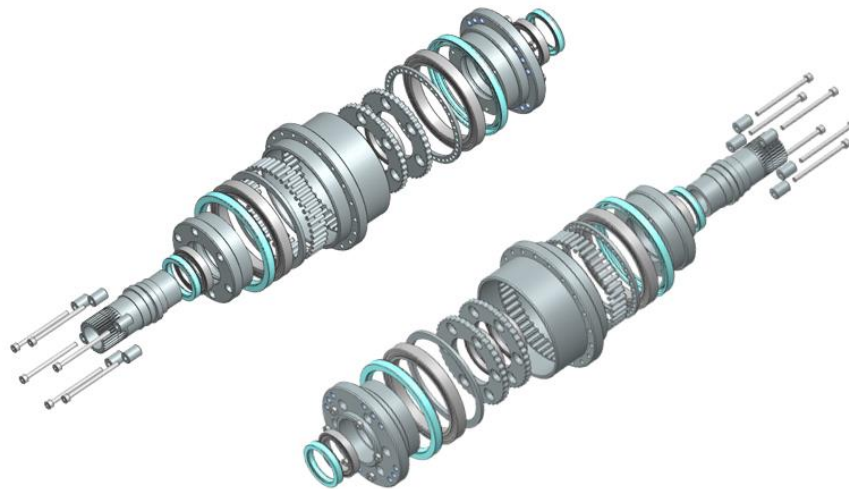


Fig. 5 Exploded view – Hollow shaft cycloidal shaft

Designing such a gearbox comes with several challenges. [3] The biggest challenge being limited space. In the current version, Rotary oil seals are used to seal the gearbox (colored blue in the image above) but considering the geometrical accuracy that can be achieved through additive FDM manufacturing, this is not the best solution. For this reason, two other constructive solutions will be explored, the first being the use of O rings for sealing the system. The limitations of using such a solution are the low peripheral speed of the shaft and the very low surface roughness. The surface on which the Oring is mounted must be polished to prevent damage to the seal. The second solution is the use of felt rings. They are a cheap and reliable sealing solution.

Another aspect to consider is the output flange of the gearbox. [3] Because of the robot's wrist weight and the positions of its center of gravity, the flange is subjected to high bending moments. For this reason, simply 3D printing the part is not a viable solution. Two solutions are presented: using metal inserts to increase the part's mechanical properties or manufacturing the part from aluminum or a composite material made from resin and fiberglass.

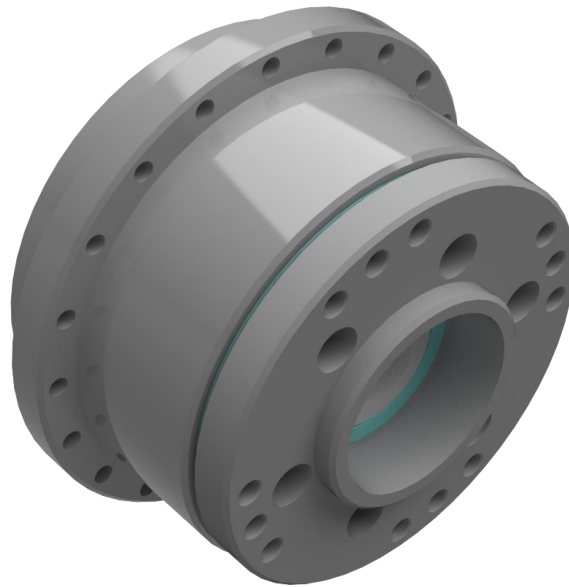


Fig. 6 Isometric View – Hollow Shaft cycloidal drive

As for the intermediate shaft assembly, each of the 3 shafts has a bearing mounted on them. To allow such a design, the shafts for the 4th and 5th joints were split in two parts and assembled by means of a jaw coupler integrated in the flanges of the two parts. An elastic ring is used to axially secure the two parts.

In order to maintain low production cost and to achieve high mechanical properties the main body for each of the shafts will be made from aluminum tubing. At each end 3d printed flanges will be attached.

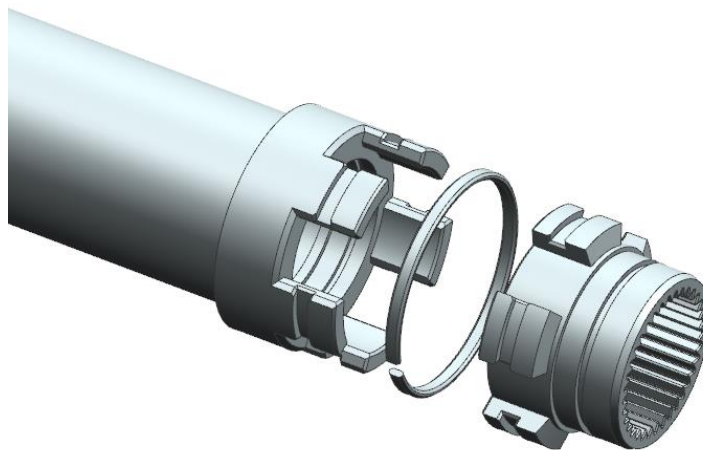


Fig. 7 4th joint intermediary shaft – Jaw coupler

The robot's wrist has not undergone major changes. Several windows have been added to allow viewing of the gear assemblies. The cycloidal drives for the 5th and 6th joints have been completely redesigned. The main problem regarding the 6th joint gearbox was the poorly designed cycloidal discs. At the slightest load the discs would slip because of their geometrical shape. The system has been redesigned. In order to define the shape of the new cycloidal discs mathematical equations were used that take into account the modulus, the number of teeth and the tooth height reduction coefficient. The current gearbox transmission ratio is 1/27.

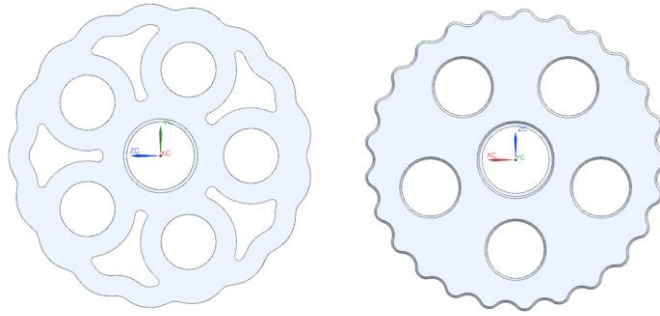


Fig. 8 Cycloidal Discs - 1st revision and 2nd revision

The 5th joint cycloidal drive has been updated. The pins that were originally modeled into the housing body were replaced with DIN 7 pins. Small changes were made to the output pins, the cycloidal discs were redesigned. The current transmission ratio is 1/69.

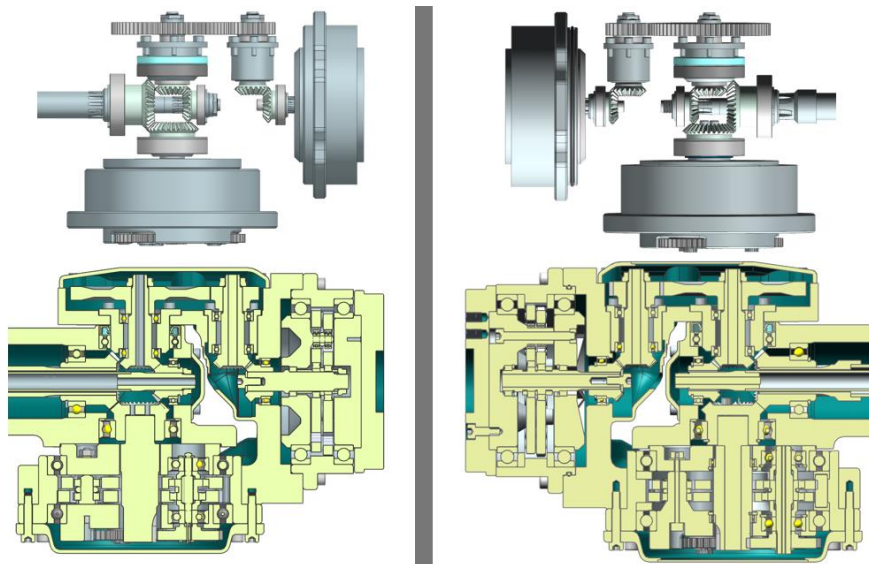


Fig. 9 Articulated robot wrist

The construction of the 3rd numerically controlled axis is much simpler compared to those previously presented. It includes only the drive motor, the cycloidal gearbox and the driven element.

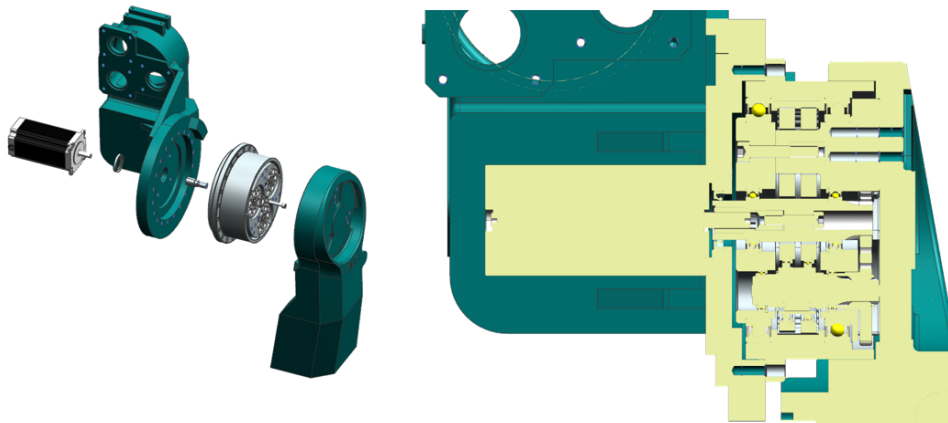


Fig. 10 3rd Joint mechanical structure

Of all the cycloidal drives presented in the current paper, the 3rd joint's gearbox is the most complex. [5] The larger size allows for a different solution to be adopted.

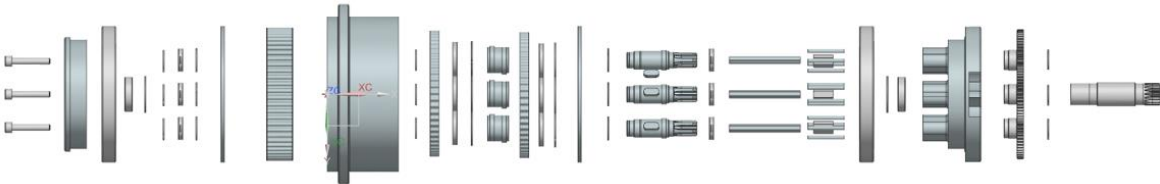


Fig. 11 3rd Joint Gearbox – Exploded View

Motion is transmitted from the main shaft to the three planetary shafts via a gear assembly with 1/3 transmission ratio. To withstand the shear and torsional stresses each of the 3 shafts has a hexagonal metal core. Motion transfer from the shafts to the cycloidal discs is achieved by means of eccentric bushings. These are mounted on the shaft by means of parallel keys and are secured axially between a shoulder and a retaining ring.

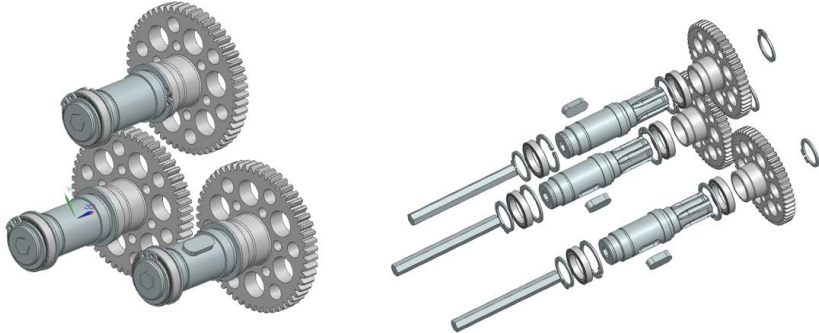


Fig. 12 Intermediary Shafts assembly

The cycloidal discs meshes with the pins mounted inside the housing. They are secured in the housing by means of two supporting rings. In order to achieve high life service life, the supporting ring will be manufactured from steel or another wear-resistant material like IGUS Iglidur.

The oscillating movement of the cycloidal disc will be transferred to the output shaft by means of 3 trapezoidal section pins. Such a design reduces the number of components of the assembly.



Fig. 8 Housing and Output Flanges Assembly

3. Conclusions

In conclusion, the present study details the improvements to the articulated robot. The mechanical structure of the guidance system has been defined. Work is currently underway to define the specific mechanical structure of the positioning system. Compared to the initial structure, the cycloidal gearboxes have been optimized, the orientation system has been completed with the 4th joint. The next step of the project is defining the sensors for the orientation system, followed by the start of the prototyping process. The next challenging task will be designing the 1st segment of the robot. Because of the high bending moment, steel inserts will need to be added.

4. References

- [1]. *** MH215II_MH250II Robot Datasheet (2017), Yaskawa America Inc. https://www.motoman.com/getmedia/71c07c7b-f918-454a-b80b-51fa333679b2/MH215II_MH250II.pdf.aspx
- [2] Nicolescu A. F., (2020). Design and operation of industrial robots. Calculus algorithms for industrial robots optimum design and operation conditions checking (in Romanian). Politehnica Press, ISBN 978-606-515-916-7, CIP BNR 2020-14500, Bucharest
- [3] Gutu M., (2021). Robotic cell with complex automation for machining parts with revolute surfaces (in Romanian). Diploma work, FIIR, Politehnica University of Bucharest.
- [4] *** Superior Electric and Danaher Motion Stepper Motors, Danaher Motion GmbH & Co. KG. <https://users.obs.carnegiescience.edu/crane/pfs/man/Electronics/Superior-StepMotors.pdf>
- [5] *** Precision Reduction Gear RVTM, Nabtesco Precision Europe GmbH. <https://precision.nabtesco.com/en/member/download/f/catalog/33319>

PROGRAMMING AND SIMULATION OF A ROBOTIC CELL FOR DEPALETIZING SUPPORT TRAYS WITH CHOCOLATE PRODUCTS

MARIN Roxana-Ioana

Faculty of Industrial Engineering and Robotics, Master program: Robotics, First Year
e-mail:roxanaioanamarin@yahoo.com

Scientific coordinator: Prof.dr.ing. **Cristina PUPĂZĂ**

ABSTRACT: The aim of the paper is to prepare the offline simulation for a depalletizing application employed in food industry. The 3D assembly was created in CATIA V5. After the design stage, the entire cell was exported in Process Simulate where the off line programming and simulation will be performed. Another stage of the research was to identify all the sensors present in the robotic cell. In terms of including intelligent algorithms in the virtual model, the current paper illustrates the preparation of the data sets.

KEYWORDS: Process Simulate, sensors, mapping, flowchart.

1. Introduction

This paper aims to present the first stages of an offline simulation approach in Process Simulate environment, namely: the specific sensors of the depalletizing cell together with their detailed presentation. The sensors mapping represents their assignment in the application, where they have to be placed. In order to have an overview of the whole approach, the flowchart must be created with all the processes and their relationships.

Following a market study in the chocolate industry, the links between buyers and products were identified. In terms of intelligent algorithms, the data sets (customers + ingredients) were also created employing the information available on the net regarding customer preferences, which will be further used of intelligent model training. The advantages and drawbacks of the Machine Learning procedure, as well as the main stages to solve the learning problem are illustrated in Fig. 1.

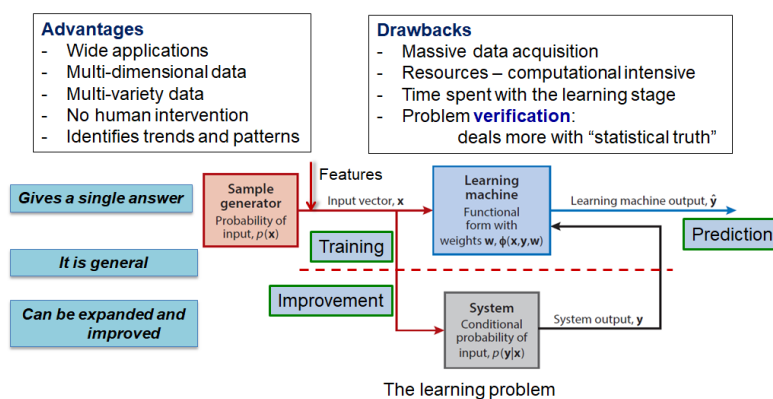


Fig. 1 – Machine learning general strategy

2. State of art

At present Artificial Intelligence (AI) is very popular in industry, especially in food industry. It helps producers to sort the ingredients, to ensure the supply chain, to generate information about the market and consumers, the management of the warehouse, including the development of new products. [1] AI enters the picture and transforms the old products by understanding consumer preferences from datasets. These include preferences about aromas, texture, and flavor, which help to improve chocolates sales on the market or any other food item. [2] Although attempts have already been registered, this work is original in the sense of implementing advanced algorithms in a classical robotic cell for the chocolate industry.

3. 3D CAD description of the cell in the virtual environment devoted to offline programming and simulation

The 3D assembly of the cell was created in the CATIA V5 software. The assembly was then exported, component by component, with the .jt extension to be compatible with the Process Simulate environment (Fig. 2 and Fig. 3).

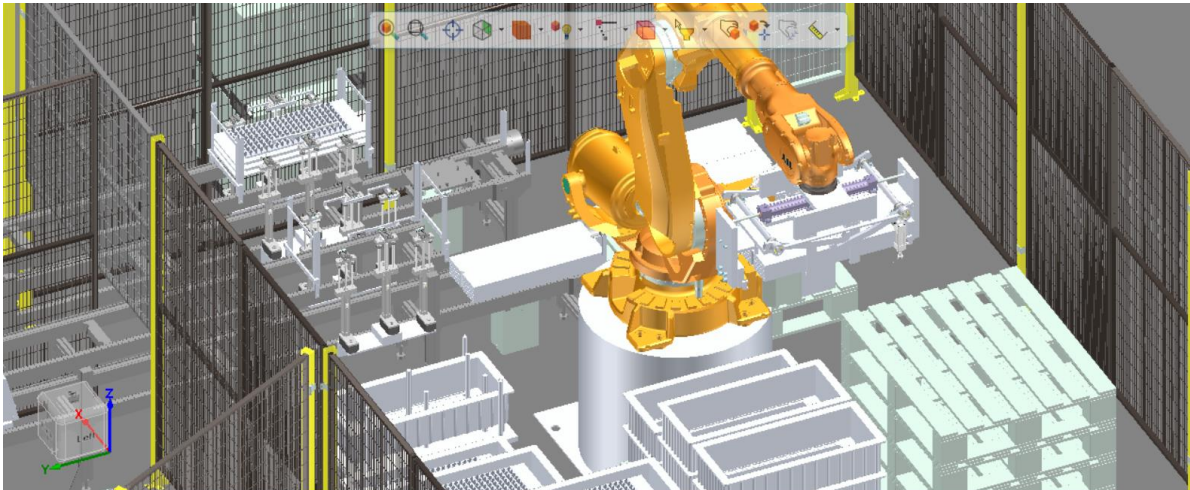


Fig. 2 – 3D model of the main cell in Process Simulate

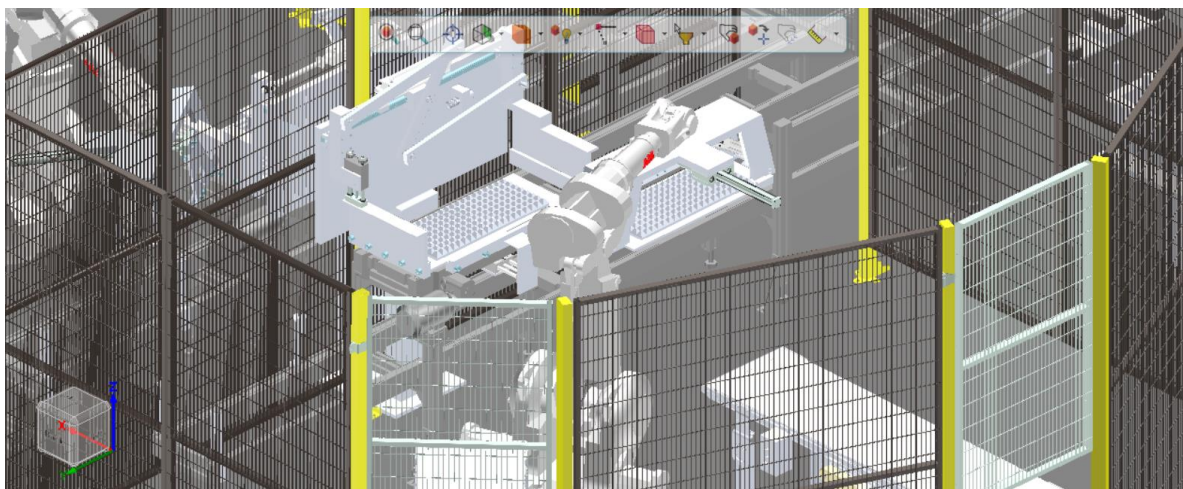


Fig. 3 – 3D model of the secondary cell in Process Simulate

In order to include all the elements in Process Simulate we need to specify what type of element they are. For fixed elements EquipmentPrototype was chosen, while for mobile devices - Device, for robots - Robot and conveyors – Conveyers (Fig. 4).

sysroot			
adaptor_conveior	PartPrototype	opritor_conveior	EquipmentPrototype
bomboane	EquipmentPrototype	paleti	EquipmentPrototype
carton	EquipmentPrototype	picior_gard	EquipmentPrototype
CELULA		picior_gard2	EquipmentPrototype
conevior_role	Conveyer	podea	EquipmentPrototype
controller	EquipmentPrototype	robot	Robot
conveioare_banda	Conveyer	robot2	Robot
conveioare_nivel	Conveyer	robot2_copie	Robot
cutii	EquipmentPrototype	sistem_impingere	Device
depunere_placi	PartPrototype	sistem_impingere_copie	Device
fixare_motoare	EquipmentPrototype	sistem_sustinere_distribuire	Device
gard1	EquipmentPrototype	sistem_sustinere_distribuire_copie	Device
gard2	EquipmentPrototype	stiva_bomboane	EquipmentPrototype
gard3	EquipmentPrototype	stiva_lazi	EquipmentPrototype
gard4	EquipmentPrototype	stiva_tavite	EquipmentPrototype
gard5	EquipmentPrototype	stiva_tavite_singra	EquipmentPrototype
gard6	EquipmentPrototype	suport_scos_tavite	EquipmentPrototype
lazi_tavite	EquipmentPrototype	suport_suprainaltare	EquipmentPrototype

Fig. 4 – Elements defined in the Simulation environment

After inserting all the cell's components, the mechanisms are built. This is done by defining the fixed elements in a link and the mobile elements in different links. They are connected by a rotational of translational axis (Fig. 5).

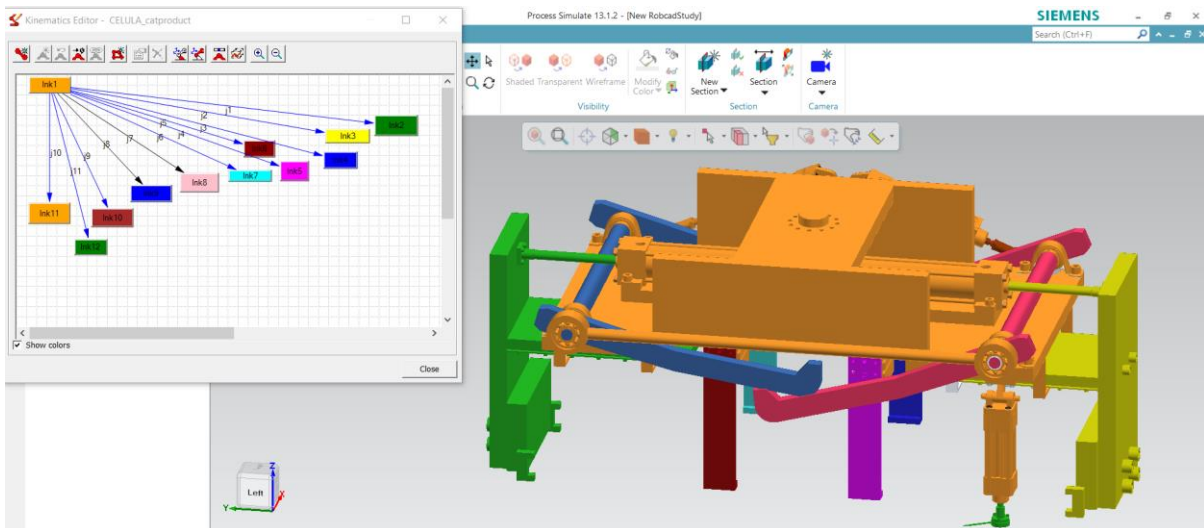


Fig. 5 – Definition of the effector kinematics

On Fig. 5 for each pair (link) a color is assigned both in the tree and on the 3D model. For example, orange color shows the fixed elements, while the moving elements are represented by the different colors. All couplings start from link1 because there are fixed elements and all other couplings depend on link1. All the links are prismatic since all the movements are linear.

4. Operational flowchart

In order to have an overview of the whole process, the flowchart must be designed. This is a sequential diagram of people or things actions involved in a complex system or activity.

Fig. 6 illustrates the process flowchart with the following symbols:

- rectangles - processes;

- rhombuses - sensorial elements;
- parallelograms - input / output data.

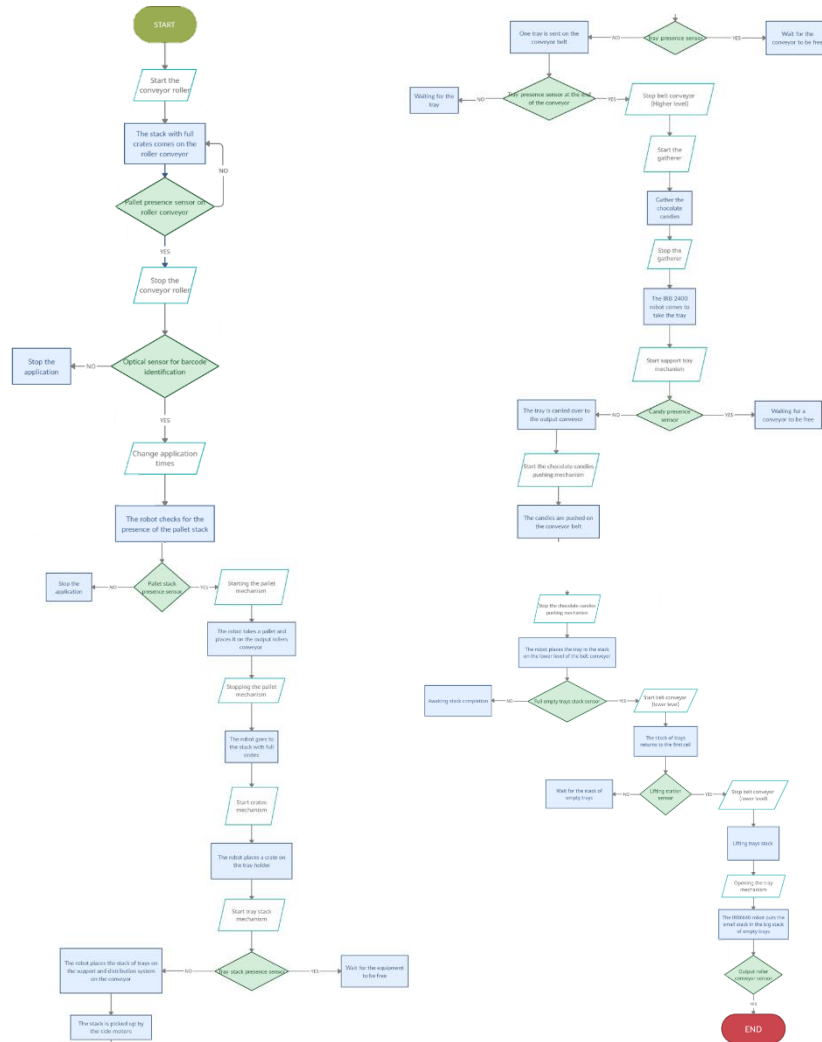


Fig. 6 – Flowchart of the process

The ABB IRB 6640 robot takes a pallet from the pallet stack and places it on the output conveyor. Then it takes the crates containing the trays together with the chocolate candies and place them on the tray support to remove the stack of chocolate trays from the crates. The chocolate together with the trays are lifted by the robot using another type of mechanism and placed on the support and distribution system with the role of sending them one by one, on the upper level of the belt conveyor. The now empty crate is placed on the output pallet, on top of the others. The final step is to put the pallet on which the crates arrived in the pallet stack. This last operation is performed with a claw gripper.

After the chocolate candies are removed from the belt conveyors in the first cell, they end up in a second cell where they are stacked by a special system to be picked up by an ABB IRB 2400 robot and pushed from the trays on two belt conveyors. They exit the system and move to the packing station.

It is easy to follow the programming steps on the flowchart because it clear which activities are done in parallel and what condition are needed to start/stop specific actions.

5. Sensor mapping

Sensors are vital elements in a robotic cell. They help to run the process accurately, without accidents and with a high productivity. Because the robotic cell is devoted to the food industry in which no metallic materials are allowed, the sensors that detect the presence of the objects have to be capacitive sensors. Most of the sensors need only two logic values (1 or 0). These values are of digital type. The only sensor that requires continuous electrical signals is the camera, since it has to recognize all the crates barcodes.

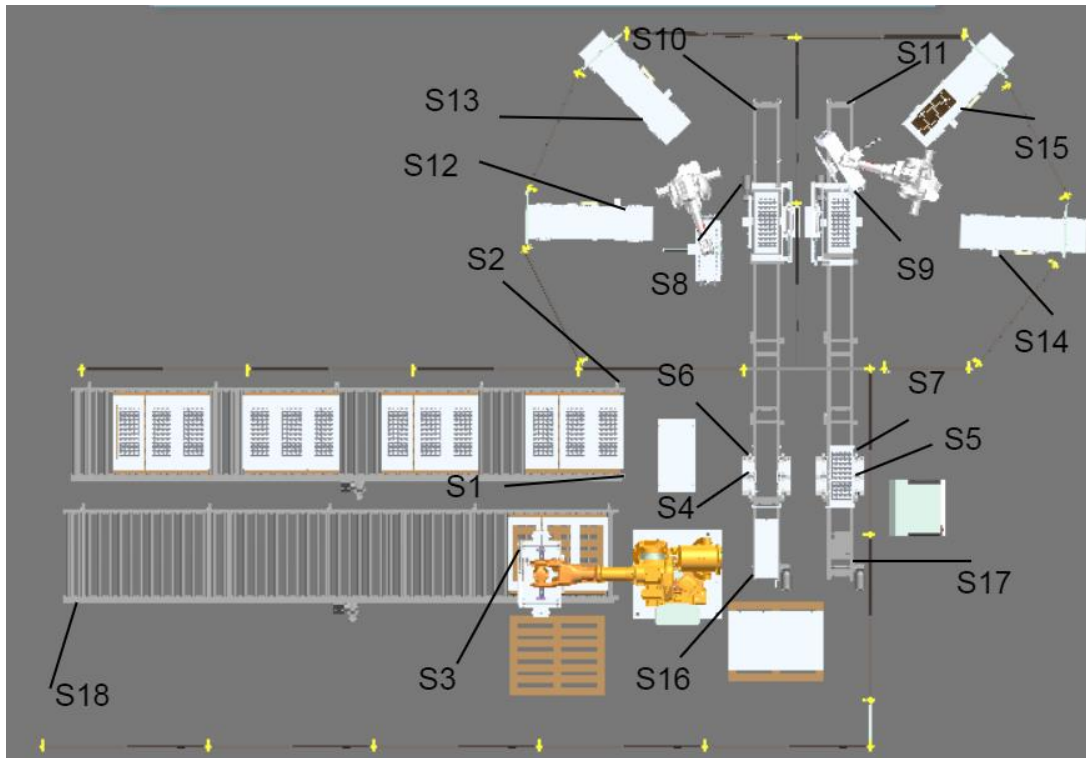


Fig. 7 – Sensor mapping

Table 1 describe each sensor type and the corresponding logical function. Analog Sensors **measure the external parameters and give an analog voltage as an output**. They produce a continuous output signal or voltage which is proportional to the quantity being measured.

Table 1 - Sensors

Nr.	Sensor type	Signal type	Logical function
S1	optical	analog	identifies the barcode specific to each type of chocolate candy
S2	capacitive	digital	stops the roller conveyor
S3	force	digital	detects the presence of the pallets
S4,S5	force	digital	detects the presence of the stack of trays
S6,S7	capacitive	digital	detects the presence of the tray start the side motors in the distributor to place one tray on the conveyor
S8,S9	capacitive	digital	detects the presence of the tray start the squeezing mechanism

S10,S11	capacitive	digital	detects the completion of the stack of empty trays start the belt conveyor (lower level)
S12,S13,S14,S15	capacitive	digital	detects the presence of candies on the output conveyors let the robot know if it can put the chocolate candies on the conveyor
S16,S17	weight	digital	detects the stack of empty trays reached start the lift system announces the robot to take the stack
S18	capacitive	digital	detects the empty pallet stack; stops the output conveyor

6. Datasets

To use a Machine Learning procedure in order to make original and customized recipes, a set of input data is needed. These are represented by two tables: customers and ingredients. The principle is to get new recipes knowing the type of chocolate and the favorite ingredient of each customer.

The “group” column was employed to sort the ingredients of the same type, so that not to put more ingredients in the same category. The data was generated randomly in Excel software, but it follows real-life studies found on the web [1],[2],[3].

gender	age	chocolate type	ingredient	name	associated chocolate	grup
1	32	milk	caramel	potato chips	black	1
2	26	black	caramel	almonds	black	1
2	22	milk	simple	peanuts	black	1
2	39	black	hazelnut	pretzels	black	1
2	29	white	hazelnut	goat cheese	black	2
2	17	white	caramel	parmesan	black	2
2	42	black	hazelnut	blue cheese	black	2
1	24	milk	orange	raspberries	black	3
2	16	milk	caramel	grapes	black	3
2	26	milk	hazelnut	strawberries	black	3
1	16	white	caramel	bananas	black	3
2	15	milk	caramel	peppers	black	4
1	41	white	orange	pumpkin	black	4
2	18	white	almonds	fennel	black	4
2	32	milk	hazelnut	walnuts	milk	5
2	18	milk	almonds	hazelnuts	milk	5
2	32	black	hazelnut	pecans	milk	5
1	26	milk	hazelnut	Gruyere cheese	milk	6
2	23	milk	almonds	Asiago cheese	milk	6
2	26	milk	hazelnut	coconut	milk	7
2	17	black	hazelnut	orange	milk	7
1	26	milk	hazelnut	apples	milk	7
1	27	black	simple	cherries	milk	7
2	39	milk	almonds	peanut butter	milk	8
2	20	black	caramel	honey	milk	8
1	15	white	caramel	caramel	milk	8
2	28	milk	caramel	blackberries	white	9
2	26	white	caramel	blueberries	white	9
2	25	black	hazelnut	lemon	white	9
1	19	black	simple	lime	white	9
2	44	black	caramel	Macadamia nuts	white	10
2	24	black	hazelnut	cashews	white	10
1	29	milk	hazelnut	caviar	white	11
2	39	black	caramel	matcha	white	12
2	32	black	caramel	cardamom	white	12
1	32	milk	caramel	saffron	white	12

Fig. 8 – Ingredients (left) and customer (right) datasets

The formulae (1), (2), (3) and (4) are based on the RAND function that generates numbers between (0;1), which can be interpreted as percentages. A similar function is RANDBETWEEN which generates a number between a given interval. Both this functions are integrated in an IF function that makes the program respect the conditions given by the operator.

An example is the “gender” column: the formula shows that there are 67% female costumers, while only 23% are male costumers. From this formula, it is also revealed that the chocolate is most popular with the young adults with the ages between 25–34. For the most popular chocolate receipt, it is shown that the women and men prefer the milk chocolate more then other chocolate types. The favorite ingredient is peanuts with a 37% of fans between the costumers.

$$Gender = IF(RAND()<0,67;RANDBETWEEN(2;2);RANDBETWEEN(1;1)) \quad (1)$$

$$Age = IF(RAND()<0,03;RANDBETWEEN(45;90);(IF(RAND()<0,17;RANDBETWEEN(35;44);(IF(RAND()<0,49;RANDBETWEEN(15;24);RANDBETWEEN(25;34)))))) \quad (2)$$

$$Chocolate\ type = IF(A2:A37=1;(IF(RAND()<0,18;"black";(IF(RAND()<0,56;"white";"milk"))));(IF(RAND()<0,2;"white";(IF(RAND()<0,55;"black";"milk")))) \quad (3)$$

$$Favorite\ ingredient = IF(RAND()<0,02;"portocale";(IF(RAND()<0,12;"migdale";(IF(RAND()<0,39;"caramel";(IF(RAND()<0,76;"alune";"simplă")))))) \quad (4)$$

6. Conclusion

The robotic cell is ready for the simulation and offline programming. Future work will focus to include the sensors in Process Simulate environment and link the mechanisms. Regarding the intelligent recipes, the generated data sets are prepared for including them in the Learning model, improving and smart predictions attempts that will allow to tune the simulation events with the manufacturing times required by the smart recipes.

Bibliography

- [1] <https://drchockenstein.com/blogs/chocolate-blog/how-artificial-intelligence-is-changing-the-confectionery-business>
- [2] <https://medium.com/mutualmobile/the-golden-ticket-ai-in-the-chocolate-industry-b40cf95a5aed>
- [3] <https://www.heraldopenaccess.us/openaccess/chocolate-consumption-and-health-beliefs-and-its-relation-to-bmi-in-college-students>
- [4] <https://moonstruckchocolate.com/tasting-pairing>
- [5] <https://snapcart.global/indonesian-chocolate-consumption/>

AUTOMATION OF A MANUFACTURING PROCESS USING RSLOGIX 5000 AND FACTORY TALK VIEW – AUTOMATIZAREA PROCESULUI DE FABRICATIE FOLOSIND RSLOGIX 5000 SI FACTORY TALK VIEW

ICA Sebastian-Ionuț¹, NICOLESCU Adrian²

Faculty: IIR, Specialization: Robotics, Year of study: Masters II, e-mail: icasebastian@gmail.com,

²Professor PhD, Faculty: FIIR, Dept. Robots and Manufacturing Systems

Coordinator: Prof. dr. Ing. **Adrian NICOLESCU**

Abstract: Will be studied the automation process of a continous manufacturing flow which will integrate various devices created in Factory I/O simulation software. The application will be linked with a virtual programmable logic computer which will run the ladder program for the used devices using Allen-Bradley software such as RSLogix/Studio 5000, Factory Talk View and Factory Talk Linx.

Key words: Studio 5000, Factory Talk View, Factory I/O, Allen-Bradley, PackML

1. Introduction

Industrial automation[1] is an interdisciplinary domain between mechanical and electrical engineering, as part of engineering science, which is using different methods which are leading to the automation of machines and/or industrial processes for independent work, without human intervention. The complexity and independency of the machines defines their difficulty for automation.

Allen-Bradley is a company which is specialized in producing equipments specific for automation, owned today by Rockwell Automation. The company produces industrial components such as programmable logic controllers (PLCs), Human-Machine interfaces (HMIs), sensors and transducers, different safety systems and components, frequency drives as well as softwares for each individual part.

Studio 5000 Logix Designer is the software where the PLC logic is produced. It is used to define industrial logic of different manufacturing processes and is the main link between the PLC and the other devices which are used for automation.

Studio Logix Emulate is a PLC emulator used to validate, test and optimize the control logic without the need of a physical controller.

FactoryTalk View ME (machine edition) is a software for creating and commissioning the human machine interface display for Allen-Bradley hardware.

Factory I/O is an educational software which creates a virtual industrial control system for industrial programming. You can create different working scenes of different complexities which can be automatized later on using an emulated or real PLC.

2. Developing and configuration of a manufacturing process using Factory/IO software.

A manufacturing flow have been created which includes a rejection zone of raw parts, a processing station and a transfer station to a packing line. (which needs additional development)



Figure 1. The virtual prototype of the manufacturing flow

The rejection zone is integrated in the entrance of the raw materials. The objects are scanned by a Vision camera which will send the result to the programmable logic controller for interpretation. If the objects are considered to be scrap they will be removed from the line by the sorting 3-way roller conveyor.

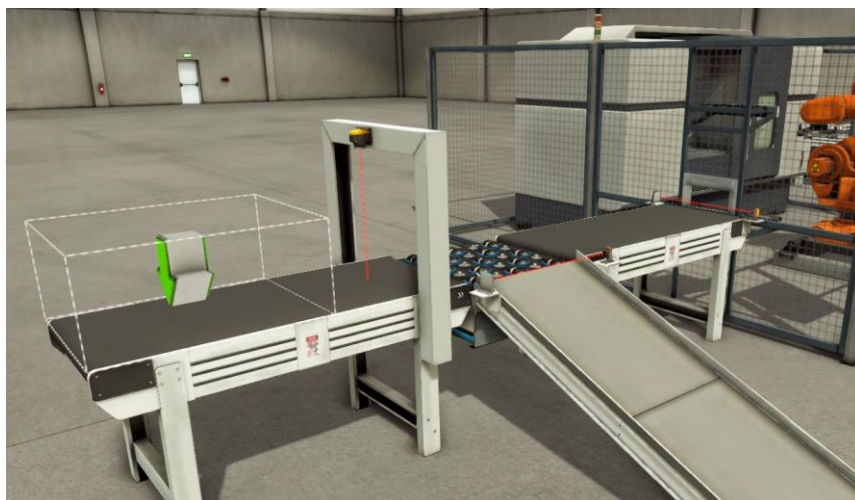


Figure 2. The rejection zone of the raw-parts

The processing CNC center is a working station used to manufacture finished products from the raw materials. The articulated arm robot is waiting for the raw parts in the pick-up area and feed the CNC machine with it. After the milling process is done the robot will take the finished product from the lathe machine and will place it in the exit conveyor.



Figure 3. Processing centre

After the finished products are made it is necessary to get them to a packing zone by a transfer station. For this task it is used a cartezian robot with 2 programmable axis, X and Z. The robot will take with the pneumatic end-effector the finished products and will place them in a box which comes from a roller conveyor. After the robot is creating a 3 pieces stack the roller conveyor will take the box away to a packing area.



Figure 4. Transfer station

2.1 How Factory I/O scenes are configured to create an automation process ready to be programmed.

All the instances which can be created in Factory I/O [2] have attached at least one digital or analogic signal that can be used in the PLC logic. The device signal will appear in the I/O tree. Every signal is configurable so it gives the programmer flexibility. For example a retro-reflexive barrier sensor is standard configured as having a normally open behavior but it's signal can be also transformed into a normally closed one.



Figure 5. Assembly of the manufacturing line

Down are summed up the following devices used for the automation process:

1. Roller and belt conveyors (Equipped later-on with guidance systems for the flow parts)

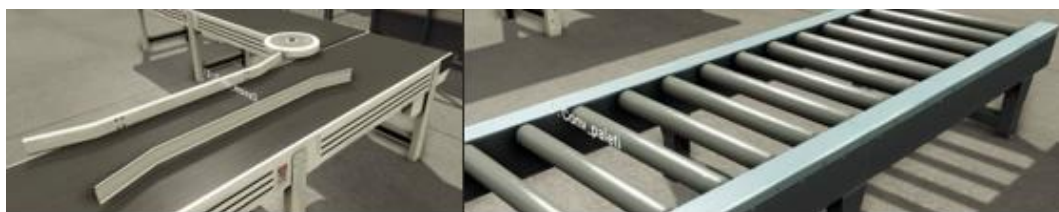


Figure 6. Types of conveyors used in project

They will generate inside the I/O tree 2 BOOL outputs which can be programmed in the PLC logic. (DO – Move forward ; DO – Move reverse)

2. Retro-reflexive barriers

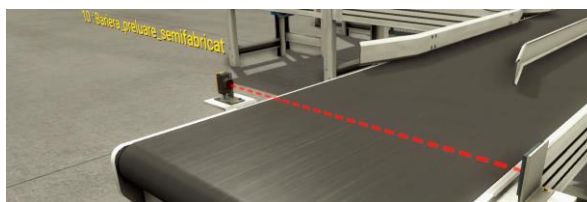


Figure 7. Barrier type sensor

It will send only one BOOL signal to the PLC. It is a digital input default defined as a normally opened sensor. (DI – Part is present)

3. Capacitive sensor

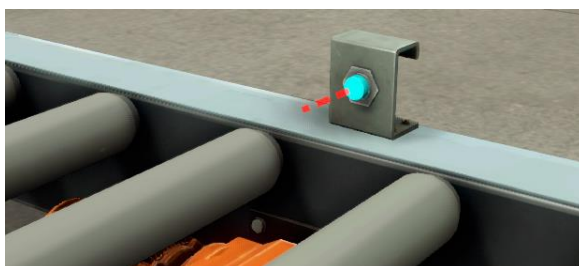


Figure 8. Capacitive sensor

Similar to the retro-reflexive barrier but different by functionality. This sensor is not based on the reflector, it will work by sensing different material objects placed within 20cm from it's emitter.

4. Cartezian robot



Figure 9. Cartezian robot

The cartesian robot have 6 digital signals from which 3 are inputs and the others are outputs. (DO – Axis Z movement / DI – Axis Z Feedback ; DO – Axis X movement / DI – Axis Z feedback; DO – Vacuum gripper actuate / DI – Vacuum gripper actuated feedback)

5. Visioin camera

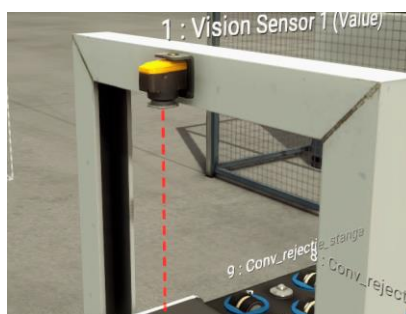


Figure 10. Vision camera

The vision camera have been configured to send to the PLC the numerical value of 1 for the scrap parts and 4 for the good parts. (Operating range is 30-200cm)

6. Sorting conveyor (used for rejection)

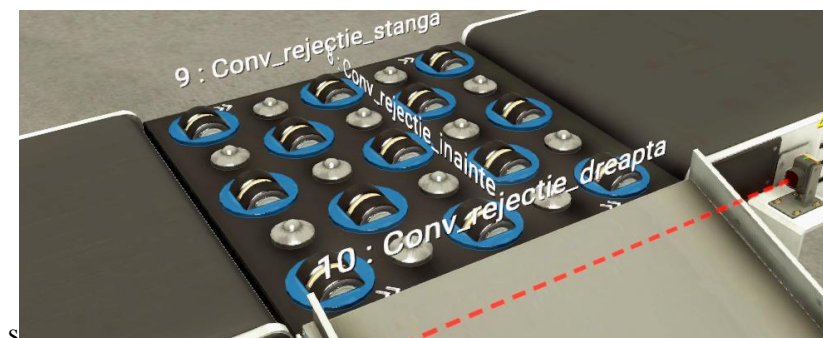


Figure 11. Sorting conveyor

The sorting conveyor have 3 digital outputs and it is used to reject the scrap parts out of the manufacturing process. (3 x DO – Forward / Left / Right)

7. Processing center



Figure 12. Lathe machine with industrial robot

The centre have 3 digital outputs and 3 digital inputs. (3 x DO – Start/Stop/Reset ; 3 x DI – Busy/Error/Opened)

8. InFeeders / OutFeeders

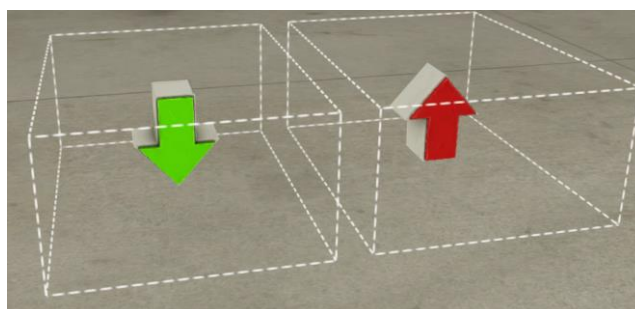


Figure 13. Infeeder/Outfeeder

With the configuration of an infeeder (green arrow) we can bring different materials into our flow at a defined amount of time. With the outfeeders (red arrow) we can erase parts out of the processing flow. (For example full pallets or scrap parts)

3. Configuring the communication between the used softwares. (Studio 5000 – FactoryTalk View – Factory I/O – Studio Logix Emulate)

The programs[3] need to communicate to each other for a successful simulation between the running ladder program developed in Studio 5000, the HMI created in FactoryTalk View ME as well as making the all the machines move in Factory I/O. To make this possible we will use FactoryTalk Linx, a communication software developed by Rockwell Automation used to link all the programs and to access the virtual PLC created in Logix 5000 emulate.

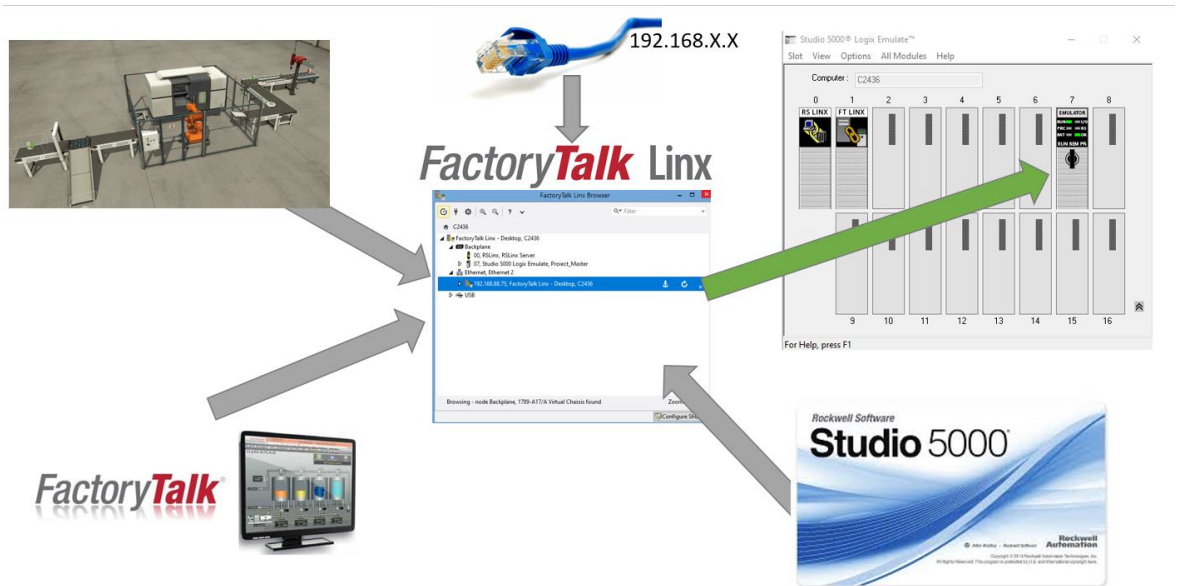


Figure 14. Communication diagram

1. Creating the PLC in Studio Logix Emulate on a virtual backplane.

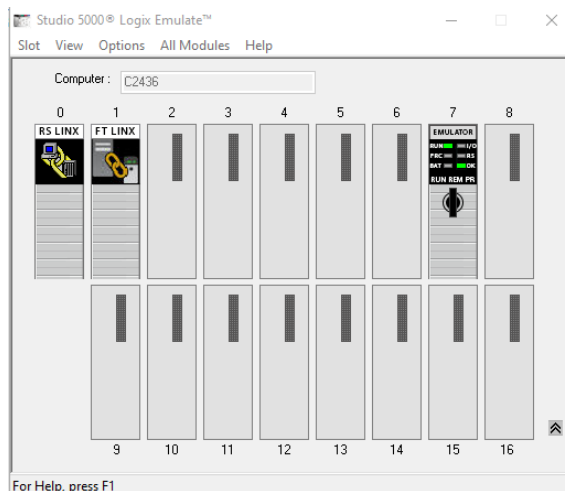


Figure 15. The virtual PLC on the 7th slot of the rack

2. Linking the PLC program with the emulated PLC. At this point the program can be downloaded and run online.

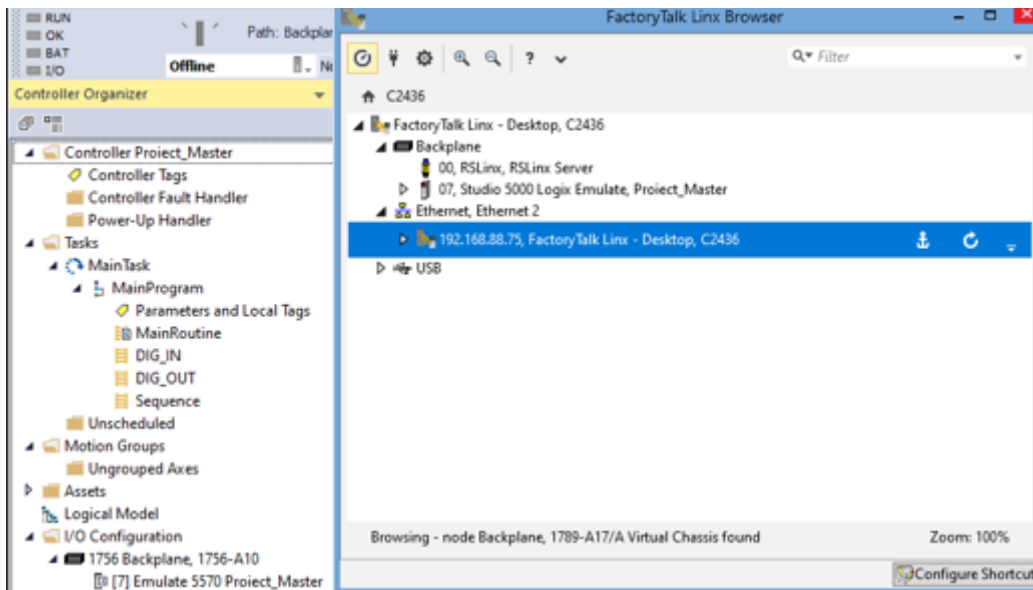


Figure 16. Establishing communication between Studio 5000 and FTLinx

3. Assigning a topic in FactoryTalk View ME which will be linked to the 7th slow of the previously created virtual backplane. At this point the HMI will communicate with the PLC.

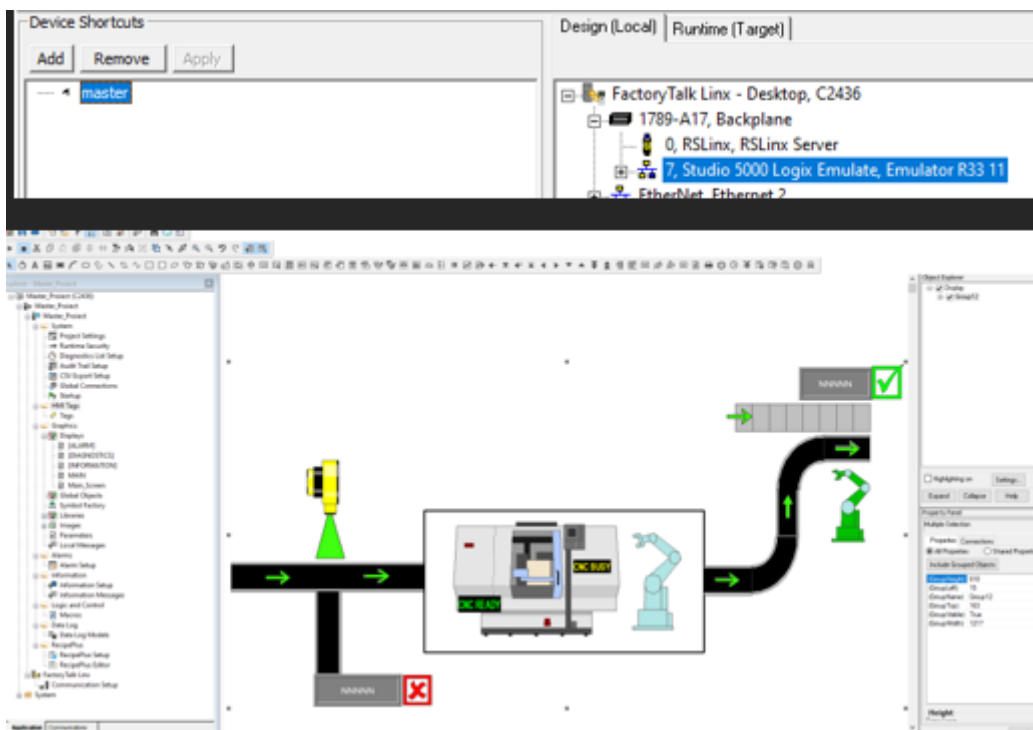


Figure 17. Communication between Studio 5000 and FactoryTalk View

4. Configuration of the Logix 5000 module in Factory I/O and assigning tags to the PLC.

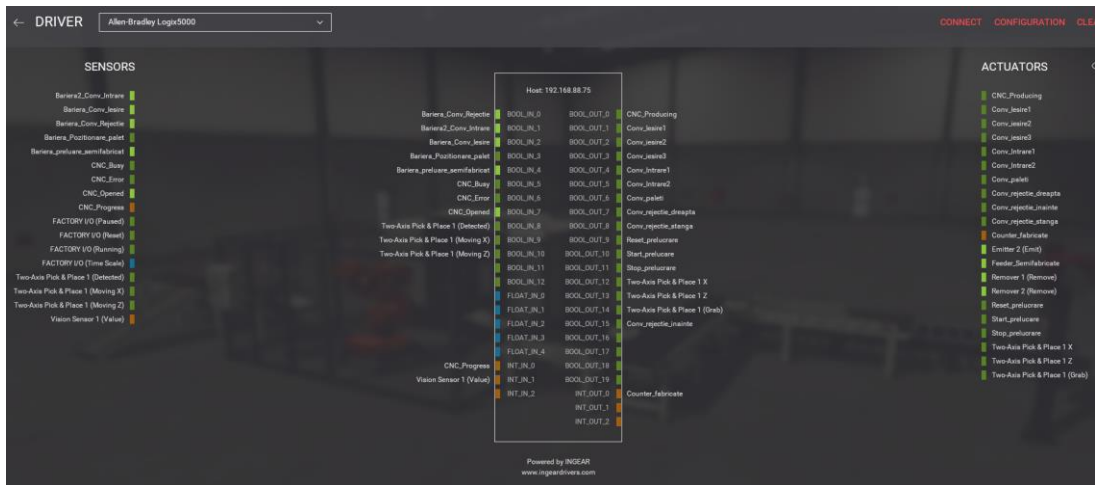


Figure 18. I/O mapping between Factory I/O and PLC

3.1 Programming approach in ladder language of the manufacturing process in Studio 5000.

A good practice[4] at a start of a project is to structure everything in routines. For the studied project will exist 3 routines: DIG_IN (where digital inputs will be mapped) ; DIG_OUT (where digital outputs will be mapped) ; Sequence (where the process automation logic will execute).

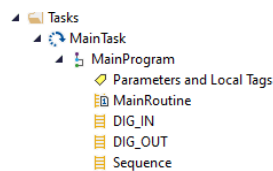


Figure 19. Routines structure

Assigning digital inputs to local bits for easy use.

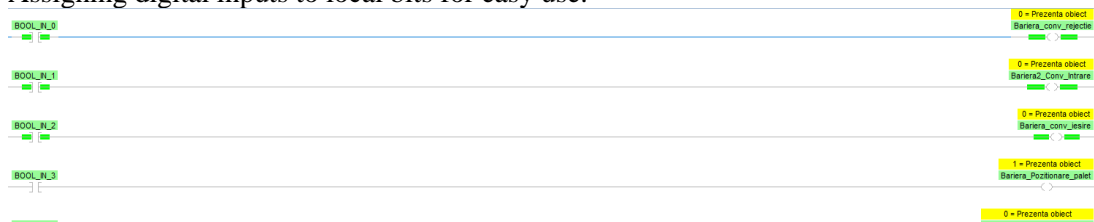


Figure 20. DIG_IN routine

Assigning local bits to digital outputs towards Factory I/O.

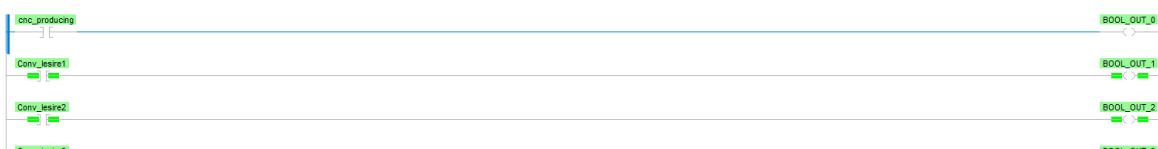


Figure 21. DIG_Out routine

Process sequence was created in a single routine named “Seq” in which is running the logic for rejection, manufacturing and transfer.

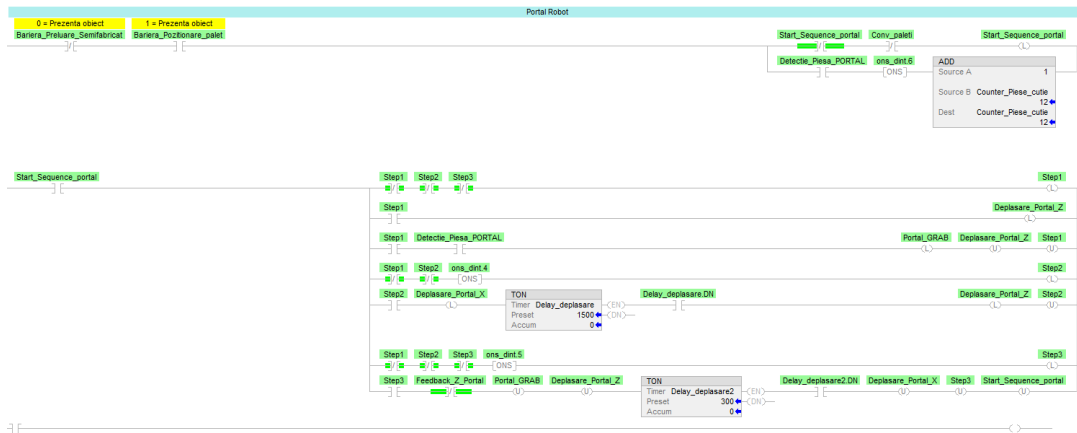


Figure 22. Logic for the transfer station

3.2 HMI application approach

Symbol Factory was used to create the objects in the HMI application. It is a library incorporated in FactoryTalk Machine edition full of industrial components ready to be linked to an application. Visualization for the following components have been created:

- Identification of a good and a scrap part
- Counter for scrap parts
- Counter complete pallets
- Feedback for the conveyors movements
- Status of the processing center
- Status of the cartesian robot

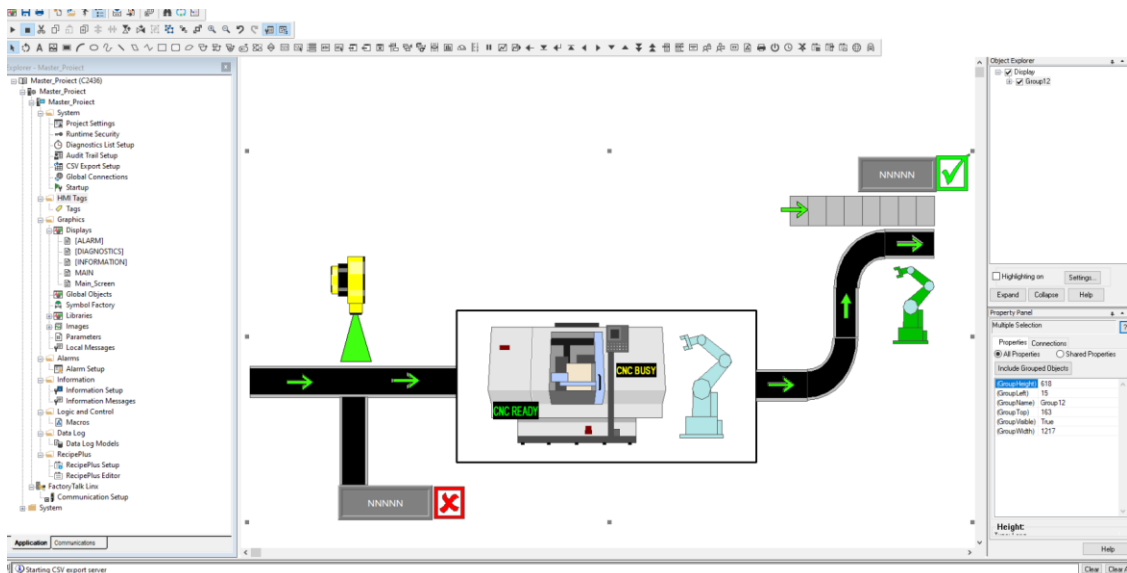


Figure 23. Application in FactoryTalk View

3.3 Introduction in the PackML , a packing machines software developed by OMAC

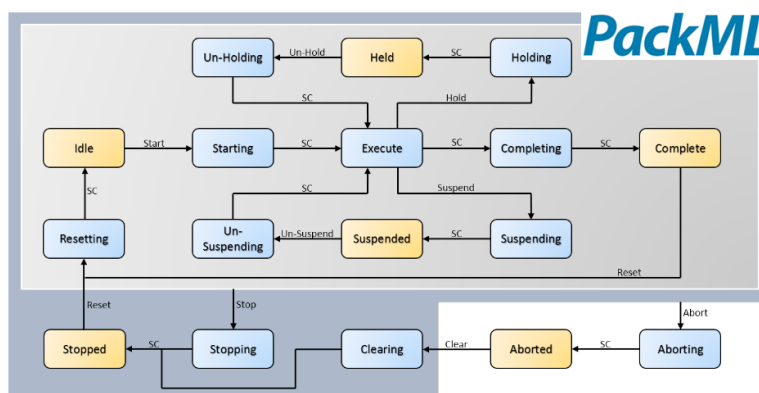


Figure 24. PackML standard with the symbolic 17 machine states

PackML (Packaging machine language) is a programming standard developed for machines used in packing lines which includes PLC logic as well as HMI interfaces. It was created by OMAC (Organization for machine automation) in collaboration with strong names from the industry such as Siemens, Rockwell, Omron and Schneider.

The programming of the machine is made by following 17 states which are attributed to the machine's behavior in a complete working cycle. By complexity of the machine we can use all the states provided or we can team up only with 4 main states which are Idle, Execute, Stopped and Aborted.

3.3 OEMs and packing lines

An OEM (Original equipment manufacturer) is a patented machine created by a vendor. Many times this type of machines are complex, unique and mainly programmed in the vendor's local programming standard.



Figure 25. OEMs

The integration[5] for such machines can get very difficult because of it's diversity in programming and HMI visualization. By this means an international client will always request from a vendor standardization in a packing/macking software which their company is familiar with.

3.4 Developing and programming of cartesian palletizer using PackML

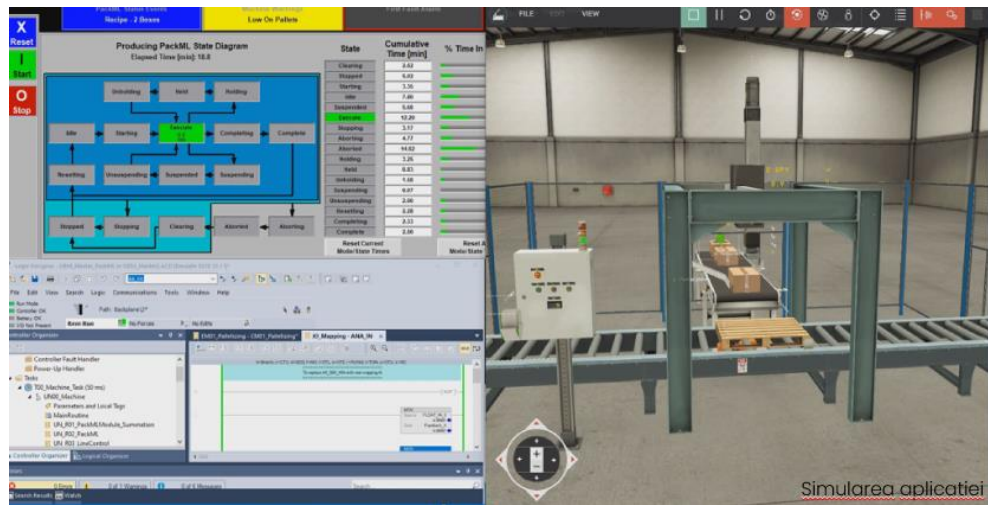


Figure 26. The palletizer running online with the HMI interface and PLC program

In order to create an effective and intuitive program we need to answer to the following questions corresponding to each machine state[6]:

- Idle – How can we say that the equipment is ready to run?
- Stopped – What happens when we stop the machine?
- Resetting – How the equipment gets ready to produce?
- Running – What the equipment is doing to produce?
- Holding – How can we pause the production without making scrap?
- Held – How do we know the equipment is paused?
- Restarting – What the equipment needs to do to get back from a temporary stop?
- Complete – How to you know the equipment finished the ordered product?
- Stopping – What happens at a normal stop with the equipment?
- Aborting – What happens at an emergency stop with the equipment?
- Aborted – How do we know if the equipment if safely stopped?

By answering these questions we can create a basic PackML flowchart from which a programmed can start building the ladder program.

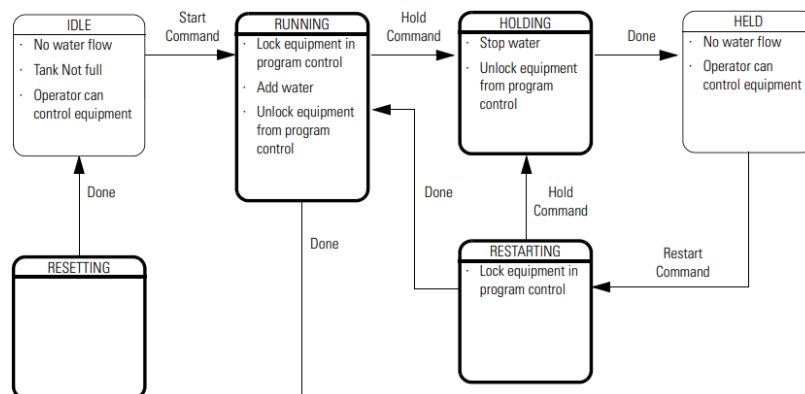


Figure 27. PackML FlowChart

4. Conclusions and future plans

1. The development and complete simulation of an industrial process using Factory I/O linked with Allen-Bradley/Rockwell software have been successful. A training zone can be created for students with will for automation learning. (Studio 5000, FactoryTalk ME, Studio Logix Emulate, FactoryTalk Linx)

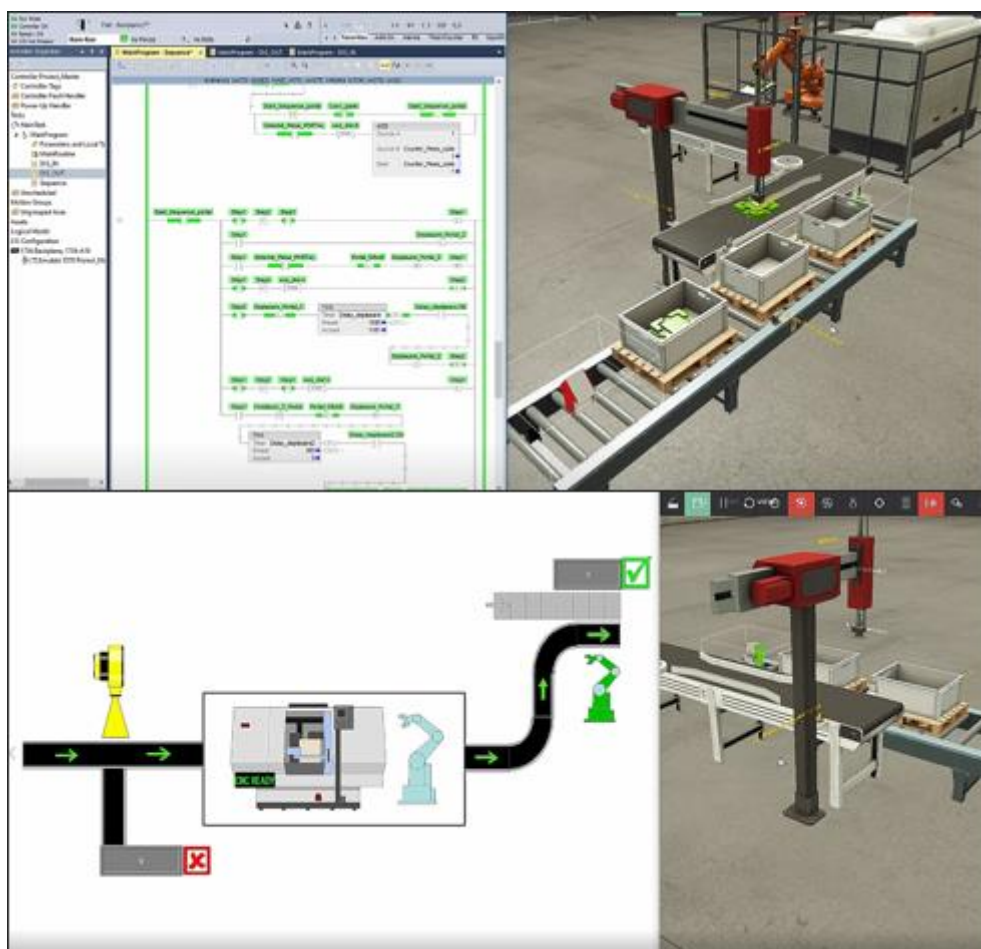


Figure 28. The complete application running

2. Factory I/O is an educational software very useful for teaching the automation principles and to create an overview of an automation process.

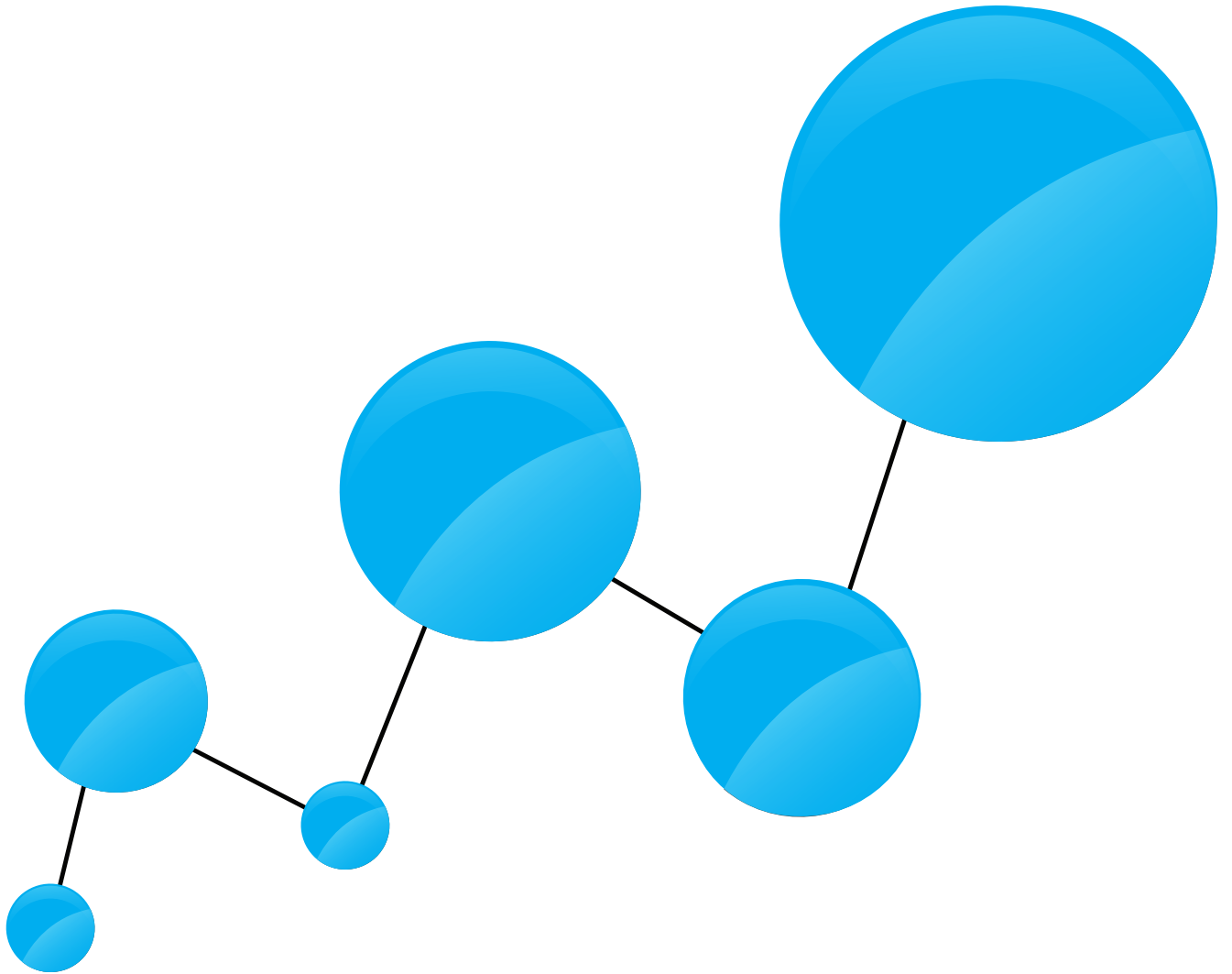
3. Creating this working scene, HMI application as well as developing a standard program serves as a solid point to further develop the manufacturing process by including a sorting warehouse zone based on RF/ID system.

4. Because there were only Allen-Bradley softwares used into this study it is fair to create an analytical point of view as well as a comparison with it's direct competitor Siemens by using Tia Portal to replicate the manufacturing flow and to point the advantages and disadvantages of both platforms.

5. The implementation of the PackML standard was adopted. A successful packing machine based on a cartesian application have been developed. In the future it is planned to implement PackML on the whole manufacturing line.

6. References

- [1]*** Robotic process automation. https://en.wikipedia.org/wiki/Robotic_process_automation
- [2]*** Sensors and equipment. <https://docs.factoryio.com/manual/parts/sensors/>
- [3]*** ControlLogix Control Systems. <https://www.rockwellautomation.com/en-us/products/hardware/allen-bradley/programmable-controllers/large-controllers/controllogix.html>
- [4]*** IO Buffering best practices for PLC inputs & outputs. <https://class.solisplc.com/courses/460200/lectures/10298223>
- [5]*** What is PackML?. <https://www.omac.org/packml>
- [6]*** PLC ladder programming <http://www.plctalk.net/Ladder>



www.fir.pub.ro

ISSN 2601-5471

ISSN-L 2601-5471